Mapping the Ubiquitin Ligase Interaction Landscape at the Endoplasmic Reticulum Membrane

Emma J Fenech



This thesis is submitted in fulfilment of the requirements for the degree of

Doctor of Philosophy

St Cross College

Ludwig Institute for Cancer Research

Nuffield Department of Clinical Medicine

University of Oxford

Trinity 2018

Declaration

I declare that this thesis has never been submitted, either in the same or a different form, to this or another University for a degree or other qualification. The work presented in Chapter 3 is a product of shared work between myself and Federica Lari (FL), a DPhil student in Dr.John Christianson's lab, with whom I was sharing the project at the time. Cell line generation and testing was shared equally between myself and FL, whereas I contributed more to testing the consequences of overexpression and to the optimisation of the LC-MS/MS sample preparation protocol. A list of figures which appear in FL's thesis are detailed on a separate sheet, as requested. The analysis of the LC-MS/MS data was mainly carried out by myself, with essential input from Dr Philip Charles (Kessler lab, TDI, Oxford), who wrote the code for the data analysis and generated figures in R for chapter 4 (clearly indicated in figure legends). The Nanostring™ experiment in chapter 4 was also shared between myself and FL. Chapter 5 is entirely the product of my own work, although Dr Katrin Bagola (Gyrd-Hansen lab, Ludwig Institute for Cancer Research, Oxford) provided help with Figures 5.3 and 5.4. The work in this thesis was carried out during my time as a DPhil student at the Ludwig Institute for Cancer Research, under the supervision of Dr. John Christianson.

Approx. word count: 41,000

Emma Fenech 10/08/2018

Abstract

The Endoplasmic Reticulum (ER) is the entry-point of the secretory pathway and is responsible for coordinating essential cellular functions, including ER-associated degradation, calcium flux and sterol homeostasis. These processes are regulated by a common post-translational mechanism: the ubiquitination of target substrates by RING-domain E3 ubiquitin ligases (E3s) resident in the ER membrane. At least 25 different transmembrane domain-containing E3s are reported to be ER-localised. However, despite the indication that select E3s control specific ER and cellular functions, few have been extensively characterised. Since E3 function is determined by the complexes it forms with specific cofactors, as well as interactions with the substrates it regulates, the primary objective of this project was to map the interaction networks of these E3 ligases. To this aim, mass spectrometry coupled with comparative proteomic profiling was employed to identify high-confidence interacting proteins (HCIPs) for the ER-resident E3 family. Using this approach, 226 HCIPs were discovered for 21 E3s, which represent novel potential cofactors and substrates, and implicate the ER-resident E3s in multiple homeostatic, metabolic and regulatory processes. A subset of HCIPs were validated as *bona fide* E3 interactors, including the RNF26 interactors TMEM43, TMED1 and ENDOD1. These largely uncharacterised membrane-embedded proteins were found to contribute to the role of RNF26 in regulating STING-dependent innate immune signalling, which orchestrates a protective response against pathogenic DNA viruses. Therefore, these data provide a comprehensive collection of E3 interaction networks at the ER membrane, which serves as a discovery platform to enable the characterisation of ER-resident E3 complexes and their functions.

Acknowledgements

I would like to thank my supervisor, Dr. John Christianson, first of all for selecting me as a DPhil candidate in his lab, and also for giving me such an interesting and challenging project to work on. I am very grateful to have had the privilege to present my work at several international conferences, help review papers and collaborate with many different groups. I would like to take this opportunity to acknowledge my co-supervisor, Professor Mads Gyrd-Hansen, for his time, support and scientific input into my project, and Professor Benedikt Kessler, for overseeing the mass spectrometry component of this project, and for being so enthusiastic and involved in this work. Finally, I also want to thank my future supervisor, Professor Maya Schuldiner, for her optimism and confidence in me.

Although I am the last member of John's lab here at the Ludwig, the previous students, post-docs and visiting scientists have all been remarkable people without whom this work would have been impossible. There is no thank you big enough to my 'partner in crime', Fede. We started the E3 project together, making and testing so many cell lines, sharing crazy days preparing mass spec and Nanostring samples (at the same time!), and although we did not finish the project together, it would be so far behind without you. Of course both the good and difficult times were shared with Norbert, Dönem, Jasmin, Steph, Markus and Seb, who all made the lab a great place to work, learn, laugh (and complain, of course!). And I could not forget my summer students: Ying, Kota, Rike and Ely, from whom I learned so much.

Apart from being John's student, I was really made to feel part of several other labs, and was (unofficially) granted 'honorary' member status to Dr. Sarah DeVal's lab as well as Professor Skirmantas Kriaucionis' lab. A special thanks to both Sarah and Skirmantas for listening, and to their lab members who are amazing friends and scientists. Alice, Sophie (my personal proofreader), Svanhild and Kira - you have always been there for me and made me smile (and I'm not sure I could ever have a more wonderful person than Kira to share my desk space with!). Martin (another proofreader) and Sophie K, for always motivating me to carry on, and Hiromi (XBPBP) for being a human encyclopedia of solutions to a range of problems, including how to get people to reply to your emails!

A special shout out to past and present members of Mads' group, in particular Katrin, Berthe and Lisa, and also to members of Professor Colin Goding's lab: Paola, Yure, Richard and Katie. All of this work would of course not have been possible without the expert help from Benedikt's group at the TDI. A huge thank you to Phil for all your help in analyzing the LC-MS/MS data, and to Roman and Marie for their support with sample preparation and instrumentation.

Of course, I owe everything to my family. You have all done so much for me that words cannot express. Thank you Mum, for all your advice and courage, Dad, for your continuous support, and Clare, for being the best sister ever. And finally, Mike. Your love, kindness, laugh, bread, pizza, cappuccino, aubergine curry, and all the other things you do for me got me through every second of this marathon and inspired me every step of the way. I couldn't end without saying thanks to Mike's parents, Sue and Dave, for giving me a second home and so many mangoes!

This thesis is dedicated to my lovely Nanna, Jean Fenech, who passed away in January, 2018.

Table of Contents

Chapter 1 Introduction 21

1.1 An overview of ER structure and function 22

1.2 The secretory pathway 23

1.3 Protein synthesis, quality control and ER homeostasis 24

1.3.1 Early biogenesis of secretory pathway proteins 24

1.3.2 Protein folding in the ER lumen 26

1.3.3 ER stress and the unfolded protein response 30

1.3.4 ER-associated degradation 34

1.3.5 The Hrd1 complex in UPR-driven ERAD 44

1.3.6 Maturation of secretory proteins 46

1.4 Lipid biogenesis 47

1.4.1 Regulation of lipid metabolism by E3 ubiquitin ligases 50

1.5 Calcium signalling 52

1.5.1 Control of Ca^{2+} metabolism by RNF170 53

1.6 The ER-resident E3 family: an overview 54

1.7 Aim of the study 63

Chapter 2 Materials and Methods 64

2.1 Lists of materials 65

2.2 Protocols 75

2.2.1 Cell culture methods 75

2.2.2 Protein biochemistry methods 78

2.2.3 Molecular biology - methods for DNA and RNA 90

2.2.4 Molecular biology – methods in cloning 93

2.2.5 Imaging 97

2.2.6 Data Analysis 98

Chapter 3 Development of cellular resources and proteomics protocols to generate E3 ligase interaction networks 100

3.1 Rationale 101

3.2 Results 102

3.2.1 Generation of Flp-In293 stable cell lines expressing FH-tagged E3s .. 102

3.2.2 Testing FH-tagged E3 protein expression and localisation 103

3.2.3 Monitoring ER stress upon FH-tagged E3 overexpression 106

3.2.4 Comparing endogenous and exogenous Hrd1 complexes 107

3.2.5 Optimisation of LC-MS/MS sample preparation for discovering novel E3 interactors 109

3.2.6 Sample preparation of E3 protein complexes for LC-MS/MS 111

3.2.7 LC-MS/MS troubleshooting: undetectable and anomalous E3s..... 114

3.3 Discussion 118

Chapter 4 Protein-protein interaction landscapes of ER-resident ubiquitin ligases…… 126

4.1 Introduction and rationale..... 127

4.2 Results 130

4.2.1 Identification of High-Confidence Interacting Proteins (HCIPs) using a cross-correlative, intensity-based methodology..... 130

4.2.2 Overview and topology of the E3 interaction landscape 137

4.2.3 Placement of HCIPs within ER functional modules 141

4.2.4 Identification of unique interactors by Spectral Index Quantitation (SINQ)……..163

4.3 Discussion 176

Chapter 5 Towards functional cofactors: the role of RNF26 and its interactors in regulating the innate immune response..... 185

5.1 An introduction to immune signalling at the ER membrane..... 186

5.1.1 Modulation of the immune response by E3s 189

5.2 Rationale 192

5.3 Results 194

5.3.1 Characterisation of the catalytic-inactive RNF26^{Y432A} mutant 194

5.3.2 Characterisation of an RNF26-containing protein complex 198

5.3.3 The role of RNF26 interactors in innate immune signaling regulation.. 207

5.4 Discussion 215

Chapter 6 Concluding remarks and future perspectives 225

Supplementary data..... 234

Bibliography..... 244

List of Figures

Figure 1.1: Protein folding mechanisms in the ER 29

Figure 1.2: The signalling branches of the mammalian UPR 33

Figure 1.3: The sequence of events in ERAD 34

Figure 1.4: Ubiquitination by RING and HECT E3s 40

Figure 1.5: The cholesterol biosynthetic pathway 49

Figure 1.6: Schematic of ER-resident E3 topology 55

Figure 3.1: Generation of stable Flp-In293 cell lines encoding FH-tagged E3s 103

Figure 3.2: Testing FH-tagged E3 protein expression by DOX titration 104

Figure 3.3: Testing FH-tagged E3 localisation by immunofluorescence 105

Figure 3.4: Monitoring ER stress upon FLAG-HA-tagged E3 expression..... 106

Figure 3.5: Comparing endogenous and exogenous Hrd1 interactions 108

Figure 3.6: Comparing endogenous and exogenous Hrd1 complex assembly 109

Figure 3.7: Venn diagrams of proteins identified by LC-MS/MS following either SDS or peptide elution 110

Figure 3.8: Basic workflow of the sample preparation protocol for LC-MS/MS of E3 complexes..... 111

Figure 3.9: Protein expression levels of FH-tagged E3s submitted for LC-MS/MS (1st batch)..... 112

Figure 3.10: Silver stain of LC-MS/MS sample eluates (1st batch)..... 113

Figure 3.11: RNF26 topology and testing protein expression of WT and mutant FH-RNF26 115

Figure 3.12: Monitoring ER stress upon FH-tagged E3 expression (2nd batch)..... 116

Figure 3.13: Silver stain of LC-MS/MS samples (2nd batch)..... 116

Figure 4.1: Box-and-whisker plot of log_2 mean abundance for each protein identified per sample 131
Figure 4.2: Plot of log_2 Standard deviation (SD) of protein abundances against SD rank..... 132
Figure 4.3: Box-and-whisker plot of the normalised log_2 mean abundance..... 133
Figure 4.4: Box-and-whisker plot of the fold-changes calculated using the BSCG method..... 134
Figure 4.5: Criteria imposed on all identified proteins to define HCIPs specific to each E3 ligase. 135
Figure 4.6: Plot of log_2(normalised E3 abundance) against the number of E3 HCIPs 136
Figure 4.7: Heatmap generated by hierarchical clustering of the all HCIPs and baits for the 21 WT E3 samples. 138
Figure 4.8: Pie charts showing HCIP frequency and topology 139
Figure 4.9: Interactions found in this study and reported on BioGRID 140
Figure 4.10: Heatmap of the Panther GO-Slim Biological Process terms associated with HCIPs and baits for the 21 WT E3 samples 141
Figure 4.11: Heatmap of ERAD components identified as HCIPs from the FH-E3 LC-MS/MS screen 142
Figure 4.12: Fold-change of E3 transcripts upon Tunicamycin treatment 145
Figure 4.13: Fold-change of E3 transcripts upon $SubtilaseAB_5$ treatment 145
Figure 4.14: Transcriptional fold-change of ERAD components identified as HCIPs upon Tunicamycin treatment 146
Figure 4.15: Heatmap of non-ERAD PQC components identified as HCIPs from the FH-E3 LC-MS/MS screen 147
Figure 4.16: Heatmap of lipid regulatory proteins identified as HCIPs from the FH-E3 LC-MS/MS screen..... 152

Figure 4.17: Heatmap of ion, fatty acid (FA) and amino acid (AA) transporters/channels identified as HCIPs from the FH-E3 LC-MS/MS screen..... 155
Figure 4.18: Endogenous Evi interacts with CGRRF1-FH 157
Figure 4.19: Heatmap of HCIPs involved in protein trafficking identified in the FH-E3 LC-MS/MS screen..... 160
Figure 4.20: Interaction networks for ER E3s 165

Figure 5.1: The cGAS-STING signalling cascade..... 188
Figure 5.2: WT and mutant RNF26 pulse-chase 194
Figure 5.3: WT and mutant RNF26 TUBE pull-downs 195
Figure 5.4: WT and mutant RNF26 *in vitro* ubiquitination assay 196
Figure 5.5: Venn diagram demonstrating the overlap between the WT FH-RNF26 and FH-RNF26^{Y432A} HCIPs..... 198
Figure 5.6: Validating FH-RNF26^{Y432A} HCIPs by reciprocal-tagging 200
Figure 5.7: The effect of different solubilisation conditions on FH-RNF26^{Y432A} interactions 201
Figure 5.8: Recapitulating interactions using WT FH-RNF26 202
Figure 5.9: Sucrose gradient sedimentation profile of FH-RNF26 and its endogenous interactors..... 204
Figure 5.10: Perinuclear co-localisation between FH-RNF26^{Y432A} and S-TMEM43.. 205
Figure 5.11: Reduced cGAMP-induced *IFIT1* upregulation upon RNF26 knockdown or expression of FH-RNF26^{Y432A}..... 208
Figure 5.12: The effect on cGAMP-induced *IFIT1* upregulation upon depletion of RNF26 interactors..... 209
Figure 5.13: Knockdown of AUP1 and UBXD8 has no effect on cGAMP-induced *IFIT1* upregulation..... 210
Figure 5.14: RNF26 interactor depletion does not effect FH-RNF26 turnover 211

Figure 5.15: Changes in basal STING levels upon RNF26 interactor knockdown . 212
Figure 5.16: Changes in cGAMP-induced STING levels following depletion of RNF26 interactors 213
Figure 5.17: A summary of the influence of RNF26 interactors on STING signalling downstream of its activation by cGAMP 220

List of Tables

Table 1.1: Evidence of E3 ligase activity, chain-linkage, and known substrates 58

Table 1.2: Evidence for ER and alternative localisations for each E3 62

Table 3.1: DOX concentrations used for the specified Flp-In293 cell lines 104

Table 4.1: Localisation and general function of lipid regulatory HCIPs identified from the FH-E3 LC-MS/MS screen..... 151

Table 4.2: Localisation and general function of HCIPs identified as transporters or channels from the FH-E3 LC-MS/MS screen 154

Table 4.3: Localisation and general function of HCIPs identified as trafficking components from the FH-E3 LC-MS/MS screen 159

Table 5.1: List of -log (*p-values*) and raw abundances for RNF26 HCIPs chosen for validation by reciprocal tagging. 199

Abbreviations

Acetyl-CoA	Acetyl-CoenzymeA
ALDH3A2	Fatty aldehyde dehydrogenase
AMFR/gp78	Autocrine motility factor receptor/glycoprotein 78
ATF4	Activating transcription factor 4
ATF6	Activating transcription factor 6
Atg9a	Autophagy-related protein 9a
ATP	Adenosine triphosphate
AUP1	Ancient ubiquitous protein 1
AVRD5	Arrhythmogenic right ventricular cardiomyopathy type 5
BCAP31	B-cell receptor-associated protein 31
BFAR	Bifunctional apoptosis regulator
BiP	Binding-immunoglobulin protein
BSCG	Bait-specific control group
bZip	Basic leucine zipper
C12E8	Octaethylene glycol monododecyl ether
Cdc48	Cell division control protein 48
CFTR	Cystic fibrosis transmembrane conductance channel
cGAS	Cyclic GMP-AMP synthase
CGRRF1	Cell growth regulator with RING finger domain protein 1
CHOP	CCAAT/enhancer-binding protein homologous protein
CHX	Cyclohexamide
CNX	Calnexin
COPE	Epsilon-coat protein
COPI/II	Coat protein complex I/II
CPY	Carboxypeptidase
CRIPR	Clusters of regularly interspaced short palindromic repeats
CRT	Calreticulin
Cymal-5	5-cyclohexpentyl β-D-maltoside
DDM	Dodecyl β-D-maltoside
DHCR24	24-dehydrocholesterol reductase
DHCR7	7-dehydrocholesterol reductase
DM	Decyl β-D-maltoside
DMNG	Decyl maltose neopentyl glycol

DNAJB11	DNAJ homologue subfamily B member 11
DNAJB12	DNAJ homologue subfamily B member 12
DNAJB6	DNAJ homologue subfamily B member 6
DNAJC13	DNAJ homologue subfamily C member 13
DNAJC16	DNAJ homologue subfamily C member 16
DNAJC18	DNAJ homologue subfamily C member 18
DOX	Doxycycline
dsDNA	Double-stranded DNA
DUB	De-ubiquitinating
EDEM1-3	ER degradation enhancing α-mannosidase-like protein 1-3
EDMD7	Emery-Dreifuss muscular dystrophy 7
eIF2α	Eukaryotic initiation factor 2 (alpha subunit)
EMC1	ER membrane protein complex subunit 1
ENDOD1	Endonuclease domain-containing protein 1
ER	Endoplasmic reticulum
ERAD	ER-associated degradation
ERdj1-7	ER-resident DnaJ-like 1-7
ERES	ER-exit site
ERFAD	ER flavoprotein associated with degradation
ERGIC-53	ER-Golgi intermediate compartment 53 kDa
ERLIN1	ER lipid raft-associated protein 1
ERLIN2	ER lipid raft-associated protein 2
ERMan1	ER α-1,2 mannosidase I
ERMES	ER-mitochondria encounter structure
ERMIONE	ER-mitochondria organising network
ERp57	ER-resident protein 57
ERp90	ER-resident protein 90
EST1	Synaptotagmin-1
Evi	Evenness interrupted homolog
FH	FLAG-HA
FRT	Flp recombination target
GADD34	Growth arrest and DNA damage-inducible protein 34
Glc	Glucose
GlcNAc	*N*-acetylglucosamine
GPCR	G protein-coupled receptor
GRP94	94 kDa Glucose-regulated protein

HADH	3-hydroxyacyl-CoA dehydrogenase type-2
HCIP	High-confidence interacting protein
HECT	Homology to E6Ap C terminus
HEK293	Human embryonic kidney 293
Herp1	Homocysteine-responsive ER stress-inducible ubiquitin-like domain member 1 protein
Herp2	Homocysteine-responsive ER stress-inducible ubiquitin-like domain member 2 protein
HMCV	Human cytomegalovirus
HMGCoA	3-hydroxy-3-methylglutaryl-CoA
HMGCR	HMGCoA reductase
Hrd1	HMGCoA reductase degradation 1
Hsp40	Heat-shock protein 40
Hsp70	Heat shock protein 70
Hsp90	Heat shcok protein 90
HSV-1	Herpes simplex virus 1
IB	Immunoblot
IF	Immunofluoresence
IFN	Interferon
IL-33	Interleukin-33
IL-6	Interleukin-6
IL-8	Interleukin-8
IMM	Inner mitochondrial membrane
INM	Inner nuclear membrane
Insig-1	Insulin-induced gene 1
Insig-2	Insulin-induced gene 2
IP	Immunoprecipitation
IP_3	Inositol-1,4,5-triphosphate
IP3R	IP_3 receptor
IRE1	Inositol-requiring protein 1
IRF3	Interferon regulatory factor 3
JNK	C-Jun N-terminal kinase
KLHL12	Kelch-like protein 12
KO	Knockout
LC-MS/MS	Liquid chromatography tandem mass spectrometry
LD	Lipid droplet

LMAN2L	Lectin mannose-binding 2-like
LMNG	Lauryl maltose neopentyl glycol
LRRFIP2	Leucine-rich repeat flightless-interacting protein 2
LTP	Lipid-transfer protein
MAM	Mitochondria-associated membrane
Man	Mannose
Man1C1	Mannosyl-oligosaccharide 1,2-alpha-mannosidase IC
MARCH6	Membrane-associated RING-finger protein 6
MCS	Membrane contact site
MDA5	Melanoma differentiation-associated protein 5
MEF	Mouse embryonic fibroblasts
MHC	Major histocompatibility complex
MIC60	MICOS complex subunit MIC60
MICOS	Mitochondrial contact site and cristae organising system
MRH	Mannose-6-phosphate receptor homology
mRNA	Messenger ribonucleic acid
MTX2	Metaxin2
MW	Molecular weight
NBD	Nucleotide-binding domain
NE	Nuclear envelope
NF-κB	Nuclear factor-kappa beta
NHK	Null Hong Kong
Npl4	Nuclear protein localisation homologue 4
OGNG	Octyl glucose neopentyl glycol
OMM	Outer mitochondrial membrane
ONM	Outer nuclear membrane
ORF	Open reading frame
OS-9	Osteosarcoma-9
OST	Oligosaccharyltransferase
PC	Phosphatidylcholine
PDI	Protein disulphide isomerase
PE	Phosphatidylethanolamine
PERK	Protein kinase RNA (PKR)-like endoplasmic reticulum kinase
PI	Phosphatidylinositol
PLC	Phospholipase C
PM	Plasma membrane

PP1	Protein phosphatase 1
PQC	Protein quality control
PRDX6	Peroxiredoxin-6
PS	Phosphatidylserine
PTK7	Protein-tyrosine kinase 7
PUB	Peptide N-glycosydase/ubiquitin-associated
PUL	PLAA, Ufd3 and Lub1
RAB11FIP1	Rab11 family-interacting protein 1
RAB5C	Ras-related protein Rab-5C
RBR	RING-between-RING
RIDD	Regulated Ire1-Dependent Decay
RING	Really interesting new gene
RNase	Endoribonuclease
RNC	Ribosomal-nascent chain complex
RNF	RING-finger protein
RNFT1	RING finger and transmembrane domain-containing protein 1
Rpn1/10/13	Regulatory particle non-ATPase 1/10/13
S1P	Site-1 protease
S2P	Site-2 protease
SAM	Sorting and assembly machinery
SAMM50	Sorting and assembly machinery component 50 homologue
SAR1	Secretion-associated Ras-related 1
SBD	Substrate-binding domain
SCAP	SREBP cleavage-activating protein
SCD1	Stearol-CoA desaturase 1
SD	Standard deviation
SDS	Sodium dodecyl sulphate
SDS-PAGE	SDS-polyacrylamide gel electrophoresis
SEC23IP	Sec23-interacting protein
SEL1L	Suppressor/Enhancer of Lin-12-like
SERCA	Sarco(endo)plasmic reticulum calcium ATPase
Shh	Sonic hedgehog
shRNA	Short hairpin RNA
SLC1A5	Solute carrier family 1 member 5
SLC27A3	Solute carrier family 27 member 3
SLC38A2	Solute carrier family 38 member 2

SOCE	Store-operated calcium entry
SP	Signal peptide
SPC	Signal peptidase complex
SQLE	Squalene epoxidase
SQSTM1	Sequestosome-1
SREBP	Sterol regulatory element-binding protein
SRP	Signal recognition particle
STIM1	Stromal interaction molecule 1
STING	Stimulator of interferon genes
TAG	Triacylglycerol
TBK1	TRAF family member-associated NFκB activator (TANK)-binding kinase 1
TGN	Trans-Golgi network
TLR9	Toll-like receptor 9
TMBIM6	Transmembrane Bax inhibitor motif-containing protein 6
TMCO1	Transmembrane and coiled-coil domain-containing protein 1
TMD	Transmembrane domain
TMED1	Transmembrane emp24 domain-containing protein 1
TMED10	Transmembrane emp24 domain-containing protein 10
TMEM129	Transmembrane protein 129
TMEM33	Transmembrane protein 33
TMEM43	Transmembrane protein 43
TMUB1	Transmembrane and ubiquitin-like domain-containing protein 1
TMUB2	Transmembrane and ubiquitin-like domain-containing protein 2
TMX(1-3)	Thioredoxin-related transmembrane protein 1-3
TNFRSF10B	Tumour necrosis factor receptor superfamily member 10B
TRAF2	Tumour necrosis factor receptor stress-induced apoptosis factor 2
TRIM	Tripartite motif
TTR	Transthyretin
TUBE	Tandem ubiquitin-binding element
TXNDC15	Thioredoxin domain-containing protein 15
TXNRD1	Thioredoxin reductase 1
Ubc6	E2 ubiquitin-conjugating enzyme 6
Ubc7	E2 ubiquitin-conjugating enzyme 7
UBD	Ubiquitin-binding domain
UBE2G2	Ubiquitin-conjugating enzyme E2 G2

UBE2J1	Ubiquitin-conjugating enzyme E2 J1
UBX	Ubiquitin regulatory X
UBX-L	UBX-like
UBXD8	UBX-domain containing protein 8
Ufd1	Ubiquitin fusion degradation 1
UGGT1	UDP-glucose:glycoprotein glucosyltransferase 1
UPR	Unfolded protein response
UPS	Ubiquitin-Proteasome system
USP21	Ubiquitin carboxyl-terminal hydrolase 21
UTR	Untranslated region
VAMP7	Vesicle-associated membrane protein 7
VBM	VCP-binding motif
VCP/p97	Valosin-containing protein
VDAC	Voltage-dependent anion channel
VIM	VCP-interaction motif
VIMP	VCP-interacting membrane protein
WB	Western blot
WCL	Whole-cell lysate
WT	Wild-type
XBP1	X-box-binding protein 1
XTB3-P	Transactivated protein B
Ypf1	Yeast presenilin fold 1
Zrt1	Zinc-regulated transporter 1

Chapter 1

Introduction

1.1 An overview of ER structure and function

The endoplasmic reticulum (ER) is a large, dynamic, interconnected network, capable of occupying almost the entirety of the cytoplasm. It is continuous with the outer nuclear membrane (ONM) and historically was divided into 'rough' (ribosome-studded) and 'smooth' (ribosome-free) ER. The ER is additionally classified into cisternae and tubules. Cisternae are most often adjacent to the nuclear envelope (NE), and have a larger volume and higher ribosomal concentration compared to the tubular structures, which dominate the ER periphery (Shibata et al., 2006). Remarkably, the ER is composed of a single, continuous lipid bilayer, which encapsulates its lumen. The ER membrane forms contact sites with the plasma membrane (PM) and several organelles including the Golgi apparatus, mitochondria, lipid droplets, endosomes and peroxisomes (reviewed in (English and Voeltz, 2013)). The distinct domains formed by the ER reflect its key functions. Representing the entry-point to the secretory pathway, it accommodates folding and quality control of secretory proteins. However it is also the primary site for sterol biosynthesis, and is the largest cellular calcium store (Schwarz and Blower, 2016). Throughout this thesis, I will discuss the diverse functions of the ER, and how ER-resident E3 ubiquitin ligases interact with them.

1.2 The secretory pathway

The secretory pathway describes a specific route taken by approximately a third of the eukaryotic proteome (Ghaemmaghami et al., 2003). Secretory proteins include those delivered to the extracellular environment, as well as integral membrane proteins and luminal proteins of the ER and Golgi. These proteins all mature through a determined series of modifications, quality control checkpoints, and transport to ensure they are deployed to their required location in their native, functional structure. The translocation of secretory polypeptides into the ER lumen marks the start of their journey along the secretory pathway. The ER lumen is optimised for protein folding, and has specialised machinery to distinguish between partially-folded, fully-folded and misfolded protein states. This enables natively structured proteins to mature to the Golgi apparatus via coat protein complex (COP)II vesicles, whereas aberrant forms are targeted for degradation. ER-lumenal proteins, such as chaperones, are retrieved by retrograde transport via the COPI system. Proteins are further modified in the different compartments of the Golgi and finally shuttled towards the PM (reviewed in (Barlowe and Miller, 2013)). The details of secretory protein biogenesis in the ER are discussed below.

1.3 Protein synthesis, quality control and ER homeostasis

1.3.1 Early biogenesis of secretory pathway proteins

A newly synthesized polypeptide entering the ER lumen is subject to a plethora of modifications. These ensure it attains its correct conformation required for eventual release from the ER, and subsequent maturation along the secretory pathway. The discovery that secretory proteins encode amino-terminal, short, cleavable sequences signified a landmark in our understanding of secretory protein biogenesis (Blobel, 1975). In a mechanism known as co-translational insertion, this 'signal peptide' (SP) targets ribosomal-nascent chain complexes (RNCs) to the signal-recognition particle (SRP) (Walter and Blobel, 1980), which in turn docks onto the ER-membrane-embedded SRP-receptor (SR) (Gilmore, 1982a; Gilmore, 1982b). The RNC is then transferred onto the Sec61 translocon by conformational changes within the SRP complex (Halic et al., 2004). The specific sequence of the SP determines both the efficiency of nascent chain translocation into the ER, as well as the timing of its cleavage. SP cleavage is executed by the ER membrane-embedded signal peptidase complex (SPC) and is generally thought to occur co-translationally (reviewed in (Braakman and Hebert, 2013)).

Decoration of the nascent polypeptide chain with a glycan structure can also take place co-translationally, with 12 amino acids being the minimum number of residues required to be translocated into the ER lumen prior to glycosylation (Nilsson and Heijne, 1993). Oligosaccharides consisting of two *N*-acetylglucosamine (GlcNAc), nine mannose (Man), and three glucose (Glc) molecules, are transferred onto a nucleophilic asparagine (Asn/N) residue within the consensus sequence (Asn-X-Ser/Thr), by the hetero-oligomeric membrane protein complex oligosaccharyltranferase (OST) (Breitling and Aebi, 2013). The mammalian OST was described to have two isoforms, distinguished by containing either the STT3A or the STT3B component (Kelleher et al., 2003). It was later determined that the isoforms were necessary for co- and post-translational *N*-linked glycosylation, respectively (Ruiz-Canada et al., 2009), with the two processes ensuring maximum glycosylation of the polypeptide. Thermodynamic and kinetic analyses revealed *N*-linked glycosylation to increase stability and decrease activation energy required for folding (Hanson et al., 2009). Additionally, the *N*-glycan has broader functions in secretory protein biogenesis by recruiting chaperones to assist with folding, as discussed in the following section.

1.3.2 Protein folding in the ER lumen

The ER lumen is a unique environment enriched with chaperones and foldases, poised to assist newly synthesized polypeptides attain their native three-dimensional structure (Figure 1.1). Chaperones can be categorised into two sub-groups: the 'classical' chaperones belonging to the heat-shock protein (Hsp) family; and the 'carbohydrate-binding' chaperones (also known as lectins).

Binding of lectins to nascent proteins is promoted by trimming of the glycan structure on the polypeptide. The 14-subunit glycan is first processed by glucosidase I, generating a diglucosylated form which associates with the carbohydrate chaperone malectin (Schallus et al., 2008). Further trimming by glucosidase II generates a monoglucosylated intermediate, which was shown to favourably complex with the calcium-binding, soluble protein, calreticulin (CRT) (Peterson et al., 1995), and its membrane-bound homologue, calnexin (CNX) (Hammond et al., 1994; Hebert et al., 1995). By inhibiting glucosidases, thus depleting monoglucosylated polypeptide species, it was demonstrated that the model substrate haemagglutinin (HA) oligomerised prematurely and aggregated prior to degradation (Hebert et al., 1996). Removal of the final glucose residue terminates polypeptide-lectin binding (Hebert et al., 1996; Hebert et al., 1995). However, incompletely-folded polypeptides can be recycled to the CNX/CRT pathway, courtesy of the UDP-glucose:glycoprotein glucosyltransfrase 1 (UGGT1), which facilitates the re-addition of a glucose unit to the unglucosylated form (Sousa and Parodi, 1995).

Termed a ‘master regulator’ of the ER, binding-immunoglobulin protein (BiP) is an Hsp70 ER luminal chaperone, which recognises extended, hydrophobic patches within its substrates (Blond-Elguindi, 1993). As with all Hsp70 members, it contains an N-terminal nucleotide-binding domain (NBD) and a C-terminal substrate-binding domain (SBD), which encapsulates its client proteins through conformational changes induced by ATP hydrolysis (Mayer and Bukau, 2005). Co-chaperones belonging to the Hsp40 (J-domain protein) family assist BiP function by enhancing its ATPase activity. (Braakman and Hebert, 2013). ER-resident DnaJ-like (ERdj)1 is a membrane-embedded J-protein, which bridges the interaction between the translating ribosome and BiP, thus positioning the chaperone for immediate folding of the incoming nascent chain (Dudek, 2002). Similarly, ERdj2 was discovered as a translocon- and BiP-binding transmembrane domain (TMD) J-protein (Tyedmers et al., 2000), however little is known about its specific function. ERdj3 is known to deliver unassembled polypeptides, such as immunoglobulin heavy chain, to BiP (Shen and Hendershot, 2005). ERdj4, ERdj5 and ERdj6 have all been shown to interact with both misfolded proteins and BiP, with a proposed role in ER-associated degradation (ERAD) for the former two members (Dong et al., 2008). The functional manifestation of ERdj6 and misfolded protein interaction is not understood (Petrova et al., 2008), and the predicted membrane-bound ERdj7 remains completely uncharacterised. Although BiP is a promiscuous chaperone, the ERdj co-chaperones are likely to impart some client specificity (Behnke et al., 2016).

Glucose-regulated protein (GRP)-94 is one of the most abundant ER luminal proteins, and is a member of the Hsp90 chaperone family. Like all family members, it is composed of: an N-terminal domain which, like BiP, harbours the NBD; a linker domain; a middle domain; and a C-terminal domain required for dimerization (Eletto et al., 2010). The linker domain was verified to support ATPase activity and co-chaperone binding in Hsp90 (Hainzl et al., 2009). Despite this, GRP94-specific co-

chaperones have remained elusive. The discovery of an interaction between GRP94 and the lectin OS-9, which is required for the degradation of misfolded luminal proteins, raised the possibility of a GRP94 function in ERAD with OS-9 as its co-chaperone (Christianson et al., 2008). However, it is now evident that OS-9 is required for the turnover of non-natively folded GRP94 (Dersh et al., 2014), leaving the question of how GRP94 promotes folding and quality control largely unanswered. It is known that GRP94 has a more restricted client specificity compared to BiP (Marzec et al., 2012), with known substrates including procollagen (Ferreira et al., 1994), Toll-like receptors (TLRs), and integrins (Randow and Seed, 2001).

Despite the activity of the above-described chaperones, ER protein folding would be too inefficient without protein disulphide isomerases (PDIs), and polypeptides would misfold and aggregate. PDIs, often referred to as foldases, promote the formation of covalent disulphide bonds between proximal cysteine residues in the client protein (Ellgaard and Ruddock, 2005). Formation of the correctly folded secretory protein structure relies on the reduction of PDI itself, by oxidative substrate disulphide bond formation, and the reduction of disulphides that form throughout the folding process, but that must be broken for the final native structure to be achieved (Jansens, 2002). PDI, the 'founder' of the PDI class, is the best-characterised member, and is unique as it contains both oxidoreductase and chaperone activity (Klappa et al., 1995). Another member, ER-resident protein (ERp)57, possesses only foldase capacity, however it recruits chaperone activity through its interaction with CNX and CRT (Oliver, 1997). Additionally, the BiP co-chaperone, ERdj5, was found to have reductase activity crucial for the retrotranslocation and subsequent degradation of the model ERAD substrate α1-antitrypsin (null Hong Kong (NHK) variant) (Ushioda et al., 2008). This study highlights that these enzymes are able to interact with both folding and degradative branches of the ER quality control system.

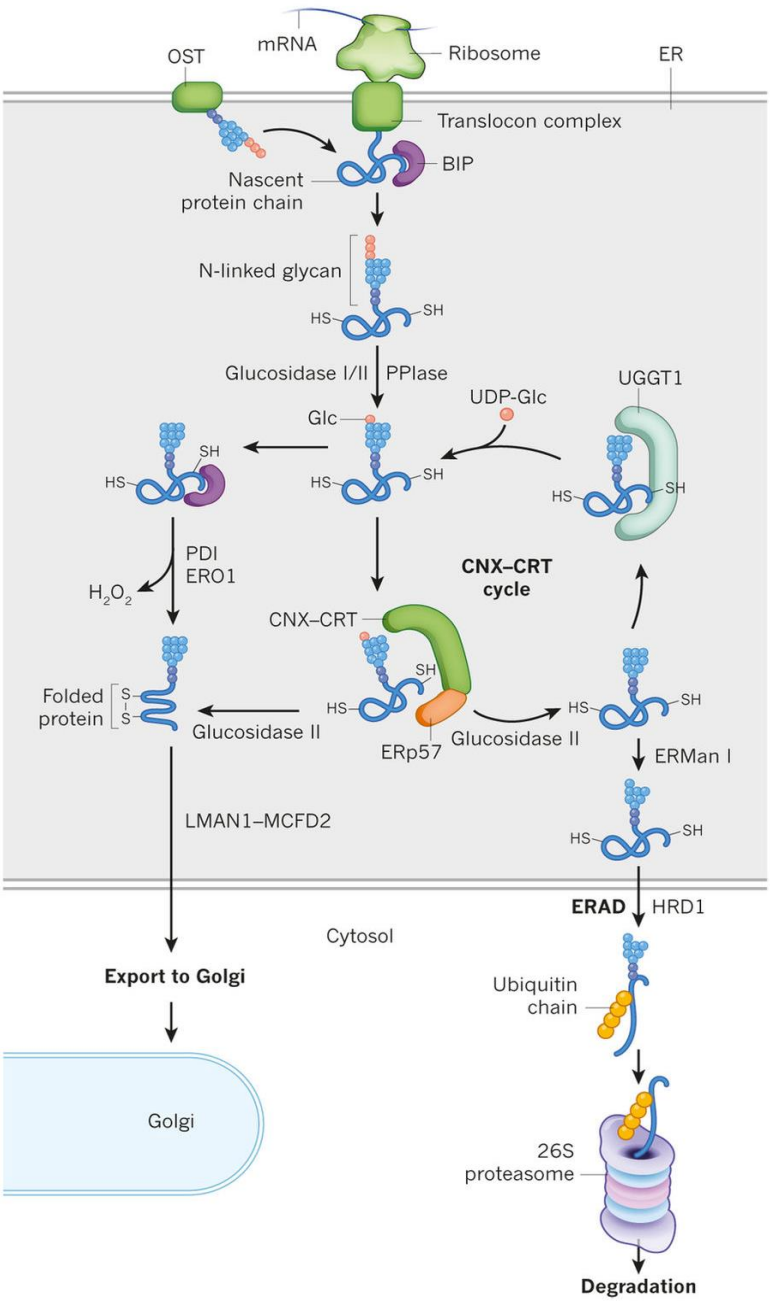

Figure 1.1: Protein folding mechanisms in the ER. Nascent polypeptide chains inserted into the ER through the Sec61 translocon commonly undergo glycosylation by oligosaccharyltransferase (OST). Protein folding is orchestrated by several different chaperones and foldases including: the Hsp70 chaperone BiP; the lectin-binding chaperones calnexin (CNX) and calreticulin (CRT), which together with UGGT1 perform several cycles of folding; and the protein disulphide isomerase (PDI) class of foldases. Correctly folded secretory proteins are exported from the ER to the Golgi (see section 1.3.6), whereas folding-incompetent or misfolded proteins are degraded by ER-associated degradation (ERAD) (see section 1.3.4). Figure from **(Wang and Kaufman, 2016)**.

1.3.3 ER stress and the unfolded protein response

A sudden influx of newly synthesized polypeptides results in the augmentation of unfolded proteins in the ER. Proteins can also become misfolded due to genetic mutation (Silverman et al., 2013), amino acid misincorporation (Patil et al., 2012), or inefficient folding (Dimcheff et al., 2004). Unfolded or misfolded protein accumulation causes ER stress, a condition also triggered by environmental changes such as hypoxia, nutrient deprivation, pathogenic infection, and calcium efflux from the ER (Rao and Bredesen, 2004). The loss of proteostatic fidelity with aging means that ER-stress is a common feature of several age-related pathologies, such as Alzheimer's disease, Parkinson's disease and cancer (Urra et al., 2016; Yoshida, 2007).

ER stress activates a pathway called the unfolded protein response (UPR) (Walter and Ron, 2011). The UPR consists of a transcriptional and translational program designed to restore homeostasis, and, in cases where this is unachievable, to initiate programmed cell death. The mammalian UPR signals through three ER membrane-embedded transducers: inositol-requiring enzyme 1 (IRE1), protein kinase R (PKR)-like ER kinase (PERK) and activating transcription factor 6 (ATF6) (Figure 1.2). The IRE1 branch is the most ancient of the three, present in all eukaryotes and plants. IRE1 is a type 1 transmembrane protein with an N-terminal luminal domain and a cytosolic C-terminus, which harbours both endoribonuclease (RNase) and kinase domains (reviewed in (Schröder and Kaufman, 2005)). Under basal conditions BiP interacts with the N-terminus of IRE1 (Todd-Corlett et al., 2007). However, upon accumulation of misfolded proteins, BiP is titrated away from IRE1, which in turn has been shown to directly interact with misfolded proteins (Gardner and Walter, 2011). IRE1 first dimerises and then oligomerises into foci, triggering the activation of its RNase and kinase domains (Korennykh et al., 2008; Lee et al., 2008). The active

RNase excises a 26-nucleotide intron from the X-box binding protein 1 (*XBP1*) transcript, generating spliced *XBP1* (*XBP1s*) (Yoshida et al., 2001). XBP1s translocates to the nucleus, upregulating pro-survival foldases (PDI), chaperones (BiP), and components of the ERAD machinery (Lee et al., 2003; Shoulders et al., 2013; Travers et al., 2000). IRE1 can also cleave a subset of mRNAs docked to the ER membrane, in a process known as Regulated IRE1-Dependent Decay (RIDD) (Hollien et al., 2009). These mRNAs encode both secretory and membrane proteins, and therefore their degradation presumably lowers the influx of nascent proteins into the ER, thus contributing to alleviating ER stress.

Unlike its RNase activity, the IRE1 kinase domain largely promotes pro-apoptotic signalling. To date, IRE1 is the only known substrate of its kinase activity. Its auto-phosphorylation plays a role in its disassembly from oligomeric structures, and hence its deactivation (Rubio et al., 2011). Additionally, phospho-IRE1 interacts with the adaptor protein tumour necrosis factor receptor stress-induced apoptosis factor 2 (TRAF2), which recruits and activates C-Jun N-terminal kinase (JNK) at the ER membrane (Urano et al., 2000). Activation of JNK is associated with ER stress-induced cell death, although the mechanism through which this is achieved remains to be determined.

PERK shares several features with IRE1, including an N-terminal luminal domain, capable of binding BiP, and a cytosolic C-terminal kinase domain. Upon detection of misfolded proteins, BiP dissociates from PERK, which oligomerises and auto-phosphorylates (Ma et al., 2002). PERK also phosphorylates the serine51 residue of the translation complex subunit, eukaryotic initiation factor 2α (eIF2α). Phosphorylation of eIF2α stalls general protein translation, providing the ER with more time to clear misfolded proteins (Harding et al., 1999). However, phospho-eIF2α actually promotes the translation of transcripts that contain at least two

upstream open reading frames (ORFs) (Jackson et al., 2010), such as *ATF4* (Vattem and Wek, 2004). ATF4 upregulates genes involved in amino acid transport and that confer resistance to oxidative stress (Harding et al., 2003), as well as the pro-apoptotic gene, CCAAT/enhancer-binding protein homologous protein (*CHOP*) (Harding et al., 2000). CHOP creates a redox imbalance in the ER, whilst upregulating growth arrest and DNA damage-inducible (*GADD34*) transcription (Marciniak et al., 2004). GADD34 is the regulatory subunit of protein phosphatase 1 (PP1), which catalyses the dephosphorylation of phospho-eIF2α, thus re-initiating protein translation (Novoa et al., 2001). Therefore, prolonged activation of the PERK branch is considered to commit the cell to a pro-apoptotic fate.

ATF6 is a type II transmembrane domain ER-stress transducer. The accumulation of unfolded proteins is thought to promote its activation through the dissociation of BiP (Shen et al., 2002; Shen and Hendershot, 2005). During ER stress, it trafficks to the Golgi apparatus, where it is cleaved by site-1 and site-2 proteases (S1P and S2P) (Haze et al., 1999). Cleavage releases the N-terminal fragment, ATF6(f), which is a basic leucine-zipper (bZIP) transcription factor. ATF6(f), like XBP1s, induces the transcription of a plethora of ER quality control genes (Adachi et al., 2008).

UPR activation therefore restores ER homeostasis through pro-survival ATF6, IRE1-RNase, and initial PERK responses, however a cell death route is promoted through the IRE1-kinase and long-term PERK activation.

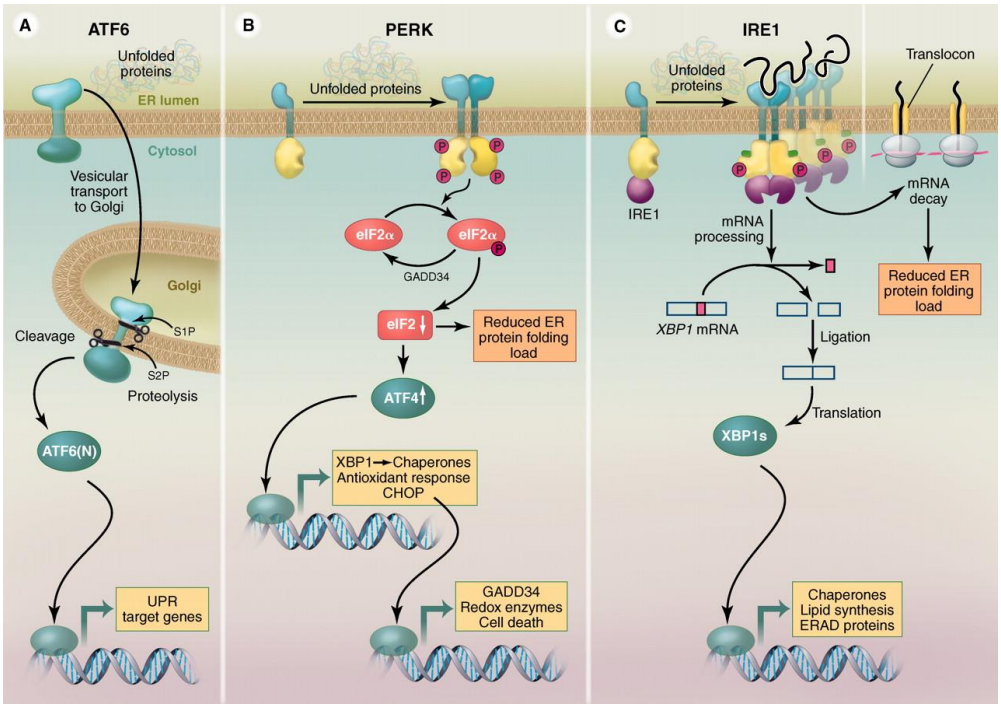

Figure 1.2: The signalling branches of the mammalian UPR. Unfolded or misfolded protein accumulation activates the three signalling branches of the UPR: ATF6, PERK and IRE1. ATF6 translocates to the Golgi apparatus where it is cleaved to release the active N-terminal transcription factor, ATF6(f). PERK dimerises, auto-phosphorylates, and stalls protein translation through the phosphorylation of eIF2α. Translation of ATF4 upregulates pro-apoptotic targets, CHOP and GADD34. IRE1 oligomerises, activating its RNase and kinase domains. RNase activity is responsible for RIDD and XBP1 splicing, which generates the XBP1s transcription factor. IRE1 kinase activity is required for auto-phosphorylation and apoptotic signalling (not shown). Figure from **(Walter and Ron, 2011)**.

1.3.4 ER-associated degradation

The relationship between the UPR and ERAD was demonstrated at the turn of the century (Travers et al., 2000). ERAD components are upregulated by ER stress to execute the degradation of potentially toxic misfolded proteins. However, it is also required to turnover unassembled subunits from within the ER lumen (Bonifacino et al., 1991; Christianson and Green, 2004; Tyler et al., 2012). ERAD is a multi-step process, which culminates in the destruction of the target substrate by the ubiquitin-proteasome system (UPS). The process of ERAD describes: (1) recognition of the substrate; (2) dislocation into the cytoplasm; (3) substrate ubiquitination by E3 ubiquitin ligases; and (4) extraction and 26S proteasomal degradation (Olzmann et al., 2013a), summarised in Figure 1.3.

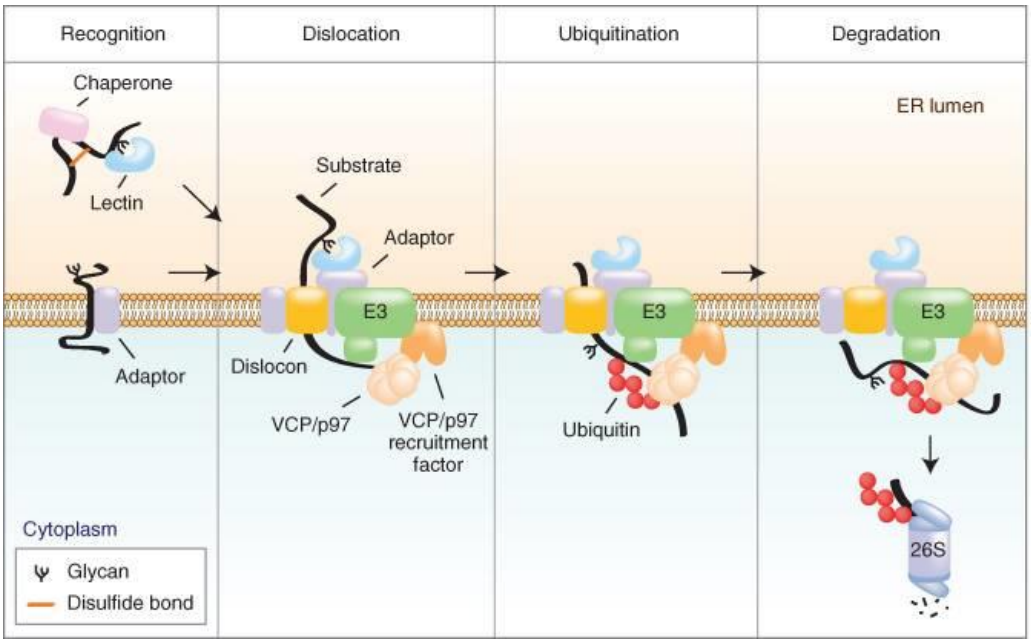

Figure 1.3: The sequence of events in ERAD. Incorrectly folded client proteins are recognised by chaperones and lectins resident in the ER lumen. Recognition complexes bind adaptor proteins in the ER membrane, which form part of a macromolecular complex, consisting of E3 ubiquitin ligases and retrotranslocation machinery. The substrate is translocated across the lipid bilayer using energy derived from the AAA ATPase, VCP/p97. It is then polyubiquitinated by E3 ligases, fully extracted from the membrane, and degraded by cytosolic 26S proteasomes **(Olzmann et al., 2013a)**.

1.3.4.1 Substrate recognition

As previously discussed, the CNX/CRT cycle provides glycoproteins with sufficient time to correctly fold. However, if glycoproteins are unable to achieve their native conformation, then they must be diverted towards degradation. This is predominantly achieved by the action of ER-resident demannosylation enzymes. The first mannosidase identified was ER α-1,2 mannosidase I (ERManI) (Gonzalez et al., 1999), followed by ER degradation enhancing α-mannosidase-like protein (EDEM)1 (Olivari et al., 2006), EDEM3 (Hirao et al., 2006), Golgi-resident α-1,2 mannosidase IC (ManIC1) (Hosokawa et al., 2007), and most recently, EDEM2 (Ninagawa et al., 2014). EDEM2, previously thought to be enzymatically inactive, was demonstrated to perform the first mannose trimming step, with subsequent trimming carried out preferentially by EDEM3, then EDEM1 (Ninagawa et al., 2014). Of note, in EDEM1/2/3-triple knockout cells, the long-term degradation kinetics of the glycosylated α1-antitrypsin (NHK variant) were remarkably similar to the wild-type (WT) cells, suggesting severely misfolded glycoproteins can be degraded by a currently unidentified non-EDEM-requiring route (Ninagawa et al., 2015).

The functional consequence of demannosylation is that the misfolded substrate is precluded from re-glucosylation by UGGT1, and hence can no longer enter the CNX/CRT folding cycle (Ferris et al., 2014). Demannosylated substrates are instead recognised by lectins containing the mannose-6-phosphate receptor homology (MRH) domains (Lederkremer, 2009). Two such lectins are osteosarcoma-9 (OS-9) and transactivated protein B (XTP3-B), both of which were found to promote the degradation of the misfolded glycoprotein NHK (Bernasconi et al., 2008; Christianson et al., 2008; Hosokawa et al., 2008a). Contrary to prediction, the MRH domain of either lectin was dispensable for substrate binding. Instead, it was necessary for interaction with suppressor/enhancer lin12 1-like (SEL1L), a

transmembrane adaptor protein which mediates the interaction between the substrate and the Hrd1 E3 ubiquitin ligase in the ER membrane (Christianson et al., 2008). The two lectins appear to be redundant, at least for certain luminal substrates, since only their combined depletion retarded degradation of the soluble BACE467Δ substrate (Bernasconi et al., 2010).

Although the majority of secretory proteins are glycosylated, terminally-misfolded non-glycosylated proteins must also be degraded by the UPS. One possible mechanism for oligosaccharide-free structures to be targeted for degradation is by post-translational glycosylation. This was demonstrated for the non-glycosylated mutant of transthyretin (TTR), the unfolded structure of which was glycosylated by a STT3B-containig OST complex, allowing subsequent recognition by EDEM3 (Sato et al., 2012). Alternatively, XTP3-B and OS-9 have been shown to bind misfolded proteins lacking *N*-glycans (Bernasconi et al., 2008; Christianson et al., 2008). Both lectins form a complex with BiP and the SEL1L-Hrd1 membrane-spanning subunit, leading to the hypothesis that chaperone-lectin complexes recognise misfolded, unglycosylated substrates and deliver them to Hrd1 for ubiquitination (Christianson et al., 2008; Hosokawa et al., 2008b).

Evidence has also been growing for a role of EDEMs in non-glycosylated substrate recognition. EDEM1 was validated to bind the non-glycosylated version of NHK with SEL1L (Cormier et al., 2009). Recent studies suggest that EDEM1 and EDEM2 bind hydrophobic patches within misfolded proteins, as mutation of BACE457 into a less hydrophobic form impaired interaction with both mannosidases, and was rendered completely stable (Sokołowska et al., 2015). EDEM2 has also been recently implicated in the XTP3-B-independent degradation of non-glycosylated mutant sonic hedgehog (Shh) (Tang et al., 2014). Therefore, although EDEMs and lectins clearly

function in luminal substrate recognition, the precise mechanisms and additional players in this process await discovery.

Less still is understood about the recognition of membrane substrates. Transmembrane domains of Hrd1 were demonstrated to selectively identify misfolded clients of the ERAD-M (membrane) pathway in yeast (Sato et al., 2009). Additionally, the integral membrane protein (IMP), Derlin-1, was shown to retain a mutant form of cystic fibrosis transmembrane conductance regulator (CFTR) in the ER (Younger et al., 2006), and was proposed to recognise this misfolded membrane substrate (Sun et al., 2006).

1.3.4.2 Retrotranslocation into the cytosol

26S proteasomes are found throughout the cytoplasm and nucleoplasm, however the ER is devoid of such degradative machinery. Hence, luminal and membrane substrates must be retrotranslocated out of the ER into the cytosol for degradation. Apart from delivering substrates to Hrd1 via its interaction with OS-9 and XTP3-B (discussed above), SEL1L also scaffolds IMPs including Derlin-1, Derlin-2, ancient ubiquitous protein 1 (AUP1), ubiquitin regulatory X (UBX)-domain containing protein 8 (UBXD8), homocysteine-responsive ER stress-inducible ubiquitin-like domain membrane proten1 (Herp1) and valosin-containing protein (VCP)-interacting membrane protein (VIMP) (Iida et al., 2011; Mueller et al., 2006; Mueller et al., 2008). Several of these IMPs recruit the cytosolic AAA ATPase, VCP/p97, to the ER membrane, which provides the energy for substrate extraction (see section 1.3.4.4). Despite the fact that most of these components are involved in retrotranslocation, the identity of the physical protein-conducting pore has largely remained elusive.

The Sec61 translocon was the first proposed dislocation channel (Wiertz et al., 1996), and it appeared to be required in yeast for the export of misfolded carboxypeptidase (CPY*) from the ER to the cytosol (Plemper et al., 1997). However, retrotranslocation out of the ER involves substrates that are likely to be structurally incompatible with the Sec61 translocon, as evidence suggests ERAD substrates may not be fully unfolded prior to extraction (Tirosh et al., 2003). While there is data to support that disulphide bond reduction by PDI members ER flavoprotein associated with degradation (ERFAD) and ERp90 occurs prior to dislocation (Riemer et al., 2009; Riemer et al., 2011), de-glycosylation is not a requirement for retrotranslocation (Blom et al., 2004). Folded, sugar-modified substrates would not be able to pass through the narrow Sec61 pore, and hence other membrane-embedded proteins have been proposed to function as the dislocon.

Experiments in yeast have provided evidence that Hrd1 is the protein-conducting channel. The E3 ligase Hrd1p has been suggested to be the protein-conducting channel in yeast. Using site-specific photocrosslinking, an interaction between the retrotranslocating substrate and Hrd1 was detected (Carvalho et al., 2010). Additionally, Usa1p (the yeast homologue of Herp (Yan et al., 2014)), was demonstrated to promote Hrd1p oligomerisation, which was required for luminal substrate dislocation (Carvalho et al., 2010). Apart from assembly into oligomers, recent evidence suggests that Hrd1p auto-ubiquitination of its RING-domain is necessary for substrate extraction, presumably by inducing a conformational change within the dislocon (Baldridge and Rapoport, 2016).

The Hrd1 interactor, Derlin-1 was proposed as the dislocon in 2004 (Lilley and Ploegh, 2004; Ye et al., 2004). Very recent data from yeast supports a model where misfolded integral membrane proteins are dependent on Dfm1 (homologue of Derlin-

1) for retrotranslocation (Neal et al., 2018). Derlin-1 and Hrd1 have six and eight TMDs, respectively (Greenblatt et al., 2011; Schoebel et al., 2017), and one can envisage how multiple TMDs, and assembly of these, could create a pore with a diameter sufficient for the dislocation of ERAD substrates. However, greater advances in membrane protein microscopic and crystallographic techniques will ultimately be required to definitively identify the elusive ERAD dislocon.

1.3.4.3 Ubiquitin conjugation

Ubiquitination of substrates at the ER membrane is required to target them for degradation. Ubiquitin is a 76 amino acid protein conserved throughout eukaryotes. E3 ubiquitin ligases (E3s) conjugate ubiquitin onto substrate lysine (Lys/K) residues, and subsequently onto any of the seven Lys residues on the surface of ubiquitin to generate K6, L11, K27, K29, K33, K48 and K63 linkage types. Poly-ubiquitin chains can be composed of a single linkage type (homotypic) or mixed linkages (heterotypic). The combination of different chain types together with their post-translational modifications (PTMs) creates an expansive 'ubiquitin code' specifying the destiny of the substrate (Swatek and Komander, 2016).

The human genome encode more than 600 E3 ubiquitin ligases (Li et al., 2008), which can be broadly divided into three subcategories: **r**eally **i**nteresting **n**ew **g**ene (RING)-domain E3s, **h**omology to **E**6Ap **C t**erminus (HECT)-domain E3s, and **R**ING-**b**etween-**R**ING (RBR) E3s. Independent of the E3 type, ubiquitination begins with an E1-activating enzyme forming a thioester linkage with the C-terminus of ubiquitin in an ATP-dependent reaction. In a transthioesterification reaction, the E1 transfers ubiquitin onto the active site cysteine within the E2-conjugating enzyme, generating an E2-ubiquitin thioester intermediate. RING-domain E3s catalyse the transfer of ubiquitin from the E2 to the appropriate lysine residue on the substrate, by binding

both simultaneously. HECT-E3s, on the other hand, undergo another round of thioester transfer to yield an E3-ubiquitin thioester intermediate, which then binds and ubiquitinates the substrate (reviewed in (Berndsen and Wolberger, 2014) and summarised in Figure 1.4).

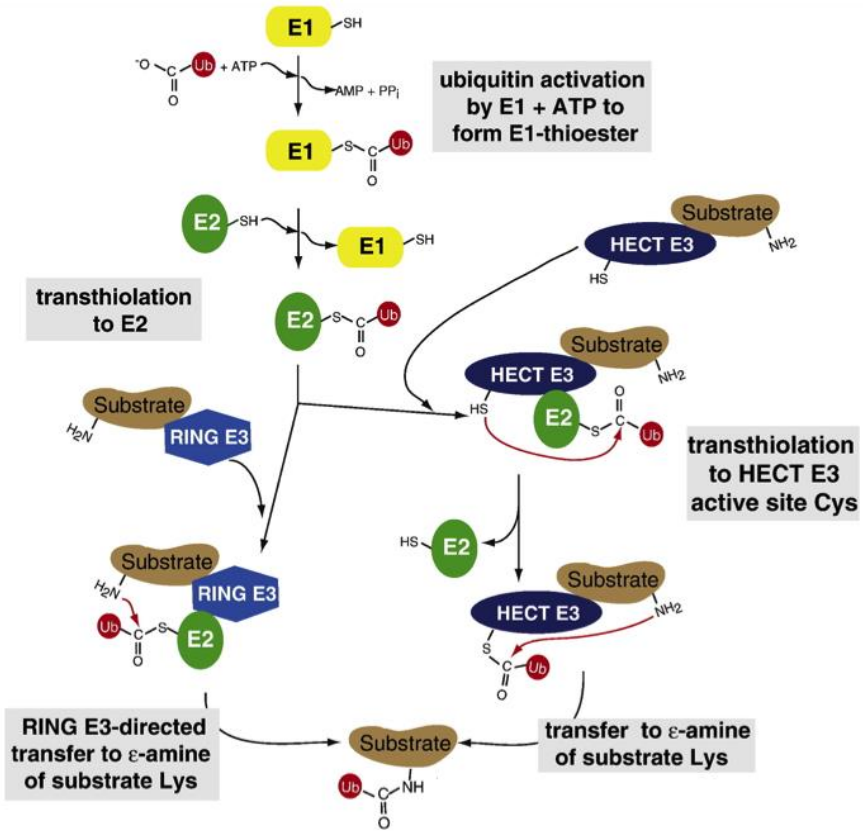

Figure 1.4: Ubiquitination by RING and HECT E3s. Ubiquitin is activated by an E1 in an energy-dependent process. The thioester bond between the E1 and ubiquitin is then transferred onto the active-site cysteine of the E2 (transthiolation). Another transthiolation reaction occurs to transfer ubiquitin onto the active site cysteine of HECT E3s, prior to substrate ubiquitination. RING-type E3s instead mediate ubiquitin transfer from the E2-ubiquitin intermediate to the substrate. Ubiquitination most frequently occurs on the primary amine of substrate lysine residues. Figure adapted from **(Metzger et al., 2014)**.

The E3s embedded in the ER membrane, which have been validated to play a role in ERAD, all belong to the RING-E3 family. Most of what we know about the mammalian ERAD pathway has been derived from studies on two E3s: autocrine motility factor receptor/glycoprotein 78 (AMFR/gp78) (Fang et al., 2001); and Hrd1 (Kikkert et al., 2004; Nadav et al., 2003), both orthologues of the yeast ERAD E3, Hrd1p. These ligases principally utilize ubiquitin-conjugating enzyme E2 (UBE2) G2 and UBE2J1, respectively (Burr et al., 2011; Fang et al., 2001), to conjugate K48-linked poly-ubiquitin chains onto substrates, hence targeting them for degradation by 26S proteasomes (Chau et al., 1989; Thrower, 2000). K11-linked Ub chains can also lead to proteasomal degradation, although they are less common (Xu et al., 2009). Hrd1 is strongly upregulated by the UPR (Travers et al., 2000), and degrades both misfolded proteins (Burr et al., 2011; Christianson et al., 2008; Wang et al., 2011) and unassembled protein subunits (Kikkert et al., 2004; Tyler et al., 2012). The role of the Hrd1 complex in ERAD is the focus of section 1.3.5. Other ER-resident E3s have been shown to take part in ERAD, including RING-finger protein (RNF)5, RNF139/Trc8 and membrane-associated RING-finger protein 6 (MARCH6) (Nakamura, 2011). The role of the ER-resident E3s in ubiquitination and degradation at the ER membrane is discussed later in this chapter.

1.3.4.4 Extraction and proteasomal degradation

Proteins ubiquitinated by ER-resident E3 ubiquitin ligases are extracted from the ER and subsequently degraded by 26S proteasomes. The energy for extraction is provided by VCP/p97, a member of the AAA-ATPase family, which commonly execute their functions by remodelling client substrates (Erzberger and Berger, 2006). VCP/p97 is a hexamer of protomers, each containing D1 and D2 ATPase domains forming two stacked rings encompassing a central pore (DeLaBarre and Brunger, 2003). The alternation of ATP hydrolysis between the D1 and D2 domains is critical for the extraction of polypeptides from the ER to the cytosol (Ye et al., 2003). Central pore residues within the VCP/p97 D2 pore were known to be required for substrate interaction (DeLaBarre et al., 2006) and it has recently been shown that polypeptide chains pass directly through the pore of this AAA-ATPase (Bodnar and Rapoport, 2017).

VCP/p97 was first demonstrated to extract misfolded major histocompatibility complex (MHC) Class I heavy chains from the ER with its cytosolic cofactors ubiquitin fusion protein 1(Ufd1) and nuclear protein localisation homologue 4 (Npl4) (Ye et al., 2001). K48-poly-ubiquitin chains conjugated to the substrate were recognised by p97 itself, and a ubiquitin-binding domain on the N-terminus of Ufd1 (Ye et al., 2003). However, how VCP/p97 was recruited to the ER membrane remained unclear. It later emerged that ER-resident E3s can directly bind VCP/p97. The E3 ligase AMFR has been shown to link VCP/p97 to the ER membrane via its VCP-interaction motif (VIM) domain (Ballar et al., 2006). An unspecified region in the cytosolic C-terminal tail of Hrd1 also proved sufficient to interact with VCP/p97 (Ye et al., 2005), and was later defined as a VCP-binding motif (VBM) domain (Morreale et al., 2009).

VIMP, an ER transmembrane protein, interacts with VCP/p97 through its VIM-domain, and simultaneously mediates interaction between VCP/p97 and Derlin-1 (Ye et al., 2004). Derlin-1 and Derlin-2 are rhomboid pseudoproteases which are components of the Hrd1 and AMFR membrane protein complexes (Lilley and Ploegh, 2005; Ye et al., 2005). Derlin-1 was demonstrated to promote export of MHC Class I molecules from the ER (Lilley and Ploegh, 2004; Ye et al., 2004) and has more recently been implicated in the degradation of potassium and sodium channels (Wang et al., 2012; You et al., 2017). NHK extraction was also shown to depend on WT Derlin-1 (Greenblatt et al., 2011), however, these findings are contradicted by a later study which claims degradation of both glycosylated and non-glycosylated NHK is specifically dependent on Derlin-2 (Huang et al., 2013). Importantly, both Derlins recruit VCP/p97 to the ER-membrane via their C-terminal SHP domains (Greenblatt et al., 2011). Membrane-tethered UBXD8 also promotes VCP/p97 dislocation through interaction with its UBX domain (Suzuki et al., 2012). In summary, VCP/p97 is scaffolded to the ER membrane by resident proteins containing distinct VCP/p97-adaptor domains.

VCP also interacts with the de-glycosylating enzyme peptide *N*-glycanase (PNG1) (Kim et al., 2006; Li et al., 2006) and deubiquitinating enzymes Ataxin-3 and YOD-1 (Liu and Ye, 2012), which collectively promote dislocation and degradation of misfolded secretory proteins. The dislocated proteins are finally shuttled to the 26S proteasome, where they are recognised by the ubiquitin receptors regulatory particle non-ATPase (Rpn)1, Rpn10 and Rpn13 in the 19S regulatory particle (Fu et al., 1998; Husnjak et al., 2008; Shi et al., 2016). The polypeptide is subsequently deubiquitinated, unfolded and transferred into the barrel-shaped 20S core particle, where it is proteolytically degraded by tryptic, chymotryptic and caspase-like activities, releasing short 8-10 amino acid sequences into the cytosol (Livneh et al., 2016).

1.3.5 The Hrd1 complex in UPR-driven ERAD

Hrd1 was previously introduced as a RING domain ubiquitin ligase with a key role in ERAD. It is a polytopic E3 ligase, and is one of two E3s conserved in *Saccharomyces cerevisiae*. Yeast Hrd1p mediates ERAD of misfolded lumenal and membrane substrates (Carvalho et al., 2006), and was originally identified to be upregulated downstream of UPR activation (Travers et al., 2000). It was subsequently confirmed to be upregulated in human cells by both XBP1 and ATF6 transcriptional branches (Kaneko et al., 2002). Overexpression of WT Hrd1, but not the inactive Hrd1 RING-mutant, protected cells from ER stress-induced cell death (Kaneko et al., 2002). Consistently, MEFs cultured from *Hrd1*$^{-/-}$ mouse embryos were more susceptible to apoptosis following treatment with either Tunicamycin or Thapsigargin, two ER stress-inducing agents (Yagishita et al., 2005). The *Hrd1* knockout has an embryonic lethal phenotype, indicating its importance.

As previously discussed, SEL1L is a crucial adaptor protein, which nucleates a complex of recognition factors and dislocation machinery around the Hrd1 ubiquitin ligase. It also coordinates interaction between Hrd1 and the E2-conjugating enzyme UBE2J1 (Mueller et al., 2008). Tail-anchored UBE2J1 is necessary for Hrd1-mediated ubiquitination and degradation of misfolded MHC Class I heavy chains (Burr et al., 2011), and like Hrd1 is upregulated by ER stress (Christianson et al., 2012).

Knockout of SEL1L is also embryonic lethal and *Sel1l*$^{-/-}$ mouse embryos were found to have developed systemic ER stress by embryonic day 12.5. Furthermore, *Sel1l*$^{-/-}$ MEFs were demonstrated to be sensitised to ER stress-inducing agents and were impaired in ERAD of misfolded, soluble substrates (Francisco et al., 2010). The luminal cofactors of SEL1L, OS-9 and XTP3-B, are both required for Hrd1-specific

disposal of luminal, misfolded substrates (Bernasconi et al., 2010), and are upregulated by the ATF6 and XBP1 pathways, respectively (Shoulders et al., 2013). Herp1, an ER-transmembrane protein, directly interacts with Hrd1 (Schulze et al., 2005), and is activated by all three branches of the UPR (Ma and Hendershot, 2004). Herp1 and related protein Herp2, are both required for Hrd1-dependent substrate degradation, along with the Derlin family members (Huang et al., 2014; Okuda-Shimizu and Hendershot, 2007). Both Derlin-1 and Derlin-2 are targets of the UPR (Christianson et al., 2012), and knockout of Derlin-2 constitutively activates ER stress (Dougan et al., 2011).

Although Hrd1 degrades both unassembled and misfolded proteins (see section 1.3.4.3), its most recently discovered endogenous substrate was identified as the ER stress-transducer, IRE1α, which is degraded under basal conditions, but not during ER stress (Sun et al., 2015). Collectively, the data argue that Hrd1 forms a macromolecular membrane protein complex specialising in misfolded protein degradation and maintenance of ER proteostasis. However, several other ligases have been shown to be upregulated as a consequence of UPR activation (Kaneko et al., 2016). The contribution of the ER-resident E3 ligase family to ER stress resolution is explored and discussed in Chapter 4.

1.3.6 Maturation of secretory proteins

Proteins that have correctly folded and escaped ERAD are allowed to mature along the secretory pathway. Secretory cargo is trafficked from the ER membrane in COPII-coated vesicles, which fuse with acceptor regions on the Golgi apparatus. The COPII coat is composed of five cytosolic subunits: secretion-associated Ras-related 1 (SAR1), Sec23, Sec24, Sec13 and Sec31 (Barlowe, 1994). Sec24 is the adaptor protein of the coat, harbouring distinct regions capable of selecting and interacting with different cargo (Miller et al., 2003). For soluble proteins incapable of accessing the cytoplasmic coat proteins, cargo receptors, which bridge the luminal and cytosolic space, are used. One of the most well-characterised of these is ER-Golgi intermediate compartment (ERGIC)-53 (Schweizer, 1988), which binds soluble glycoproteins in the ER lumen and Sec23-Sec24 components with its cytosolic tail (Appenzeller et al., 1999; Kappeler et al., 1997). Some secretory proteins are modified with a lipid moiety (glycosylphosphotidylinositol (GPI)-anchor), which embeds them in the ER membrane. These proteins use the p24 family as cargo receptors for COPII transport (Takida et al., 2008).

Both ERGIC-53 and p24 proteins require relocalisation to the ER membrane to enable further anterograde cargo trafficking. This is achieved by COPI vesicles, which mediate the retrograde transportation of ER-exit proteins as well as immature proteins which escaped the quality control mechanisms in the ER (reviewed in (Gomez-Navarro and Miller, 2016)). Secretory proteins that successfully reach the Golgi undergo further modification and eventual export to the plasma membrane by clathrin-coated vesicles.

1.4 Lipid biogenesis

Lipids are essential to life, forming plasma and organelle membranes, and serving as energy storage molecules. The ER membrane houses many of the enzymes responsible for the production of the majority of cellular lipids. Phospholipids, sphingolipids and cholesterol are all manufactured at the ER. Cholesterol can be converted to cholesterol ester, which along with triacylglycerol (TAG), is packaged into energy-storing lipid droplets (LDs), which bud off the ER membrane. Many lipids are distributed along the secretory pathway by vesicle trafficking. In addition, lipid transport is mediated lipid-transfer proteins (LTPs), which are thought to work at membrane contact sites (MCSs) (reviewed in (Jacquemyn et al., 2017)).

Fatty acids, which form the hydrophobic tails of phospholipids, are also synthesized at the ER membrane. In general, enzymes involved in fatty acid and phospholipid biosynthesis are upregulated by the transcription factor sterol regulatory element-binding protein 1 (SREBP-1) (Amemiya-Kudo et al., 2002). Phosphatidic acid, the simplest phospholipid, is *de novo* synthesized at the ER and is the precursor used to generate phosphatidylcholine (PC), phosphatidylethanolamine (PE), and the less common phosphatidylserine (PS) and phosphatidylinositol (PI) (Hermansson et al., 2011). These phospholipids, along with sphingolipids and cholesterol, are incorporated into individual membranes at different ratios, given them unique biochemical and biophysical properties that support their specific functions.

Cholesterol biosynthesis is achieved through a multi-step process, beginning with the activation of acetyl-coenzymeA (acetyl-CoA) at the start of the mevalonate pathway, and ending with either the Bloch or Kandutsch-Russell pathway. 3-hydroxy-3-methylglutaryl-CoA (HMGCoA) is converted to mevalonic acid (MA) by HMGCoA reductase (HMGCR) in a rate-limiting step. Squalene epoxidase (SQLE) acts downstream of the isoprenoid branch, and is therefore required specifically for sterol synthesis (Figure 1.5) (Goldstein and Brown, 1990). Transcription of sterol-biosynthetic enzymes is generally under the control of SREBP-2, which forms part of a feedback response. In homeostatic conditions, SREBP-2 is bound in a complex with SREPB cleavage-activating protein (SCAP), Insig-1, and Insig-2 at the ER membrane (Hua et al., 1996; Yabe et al., 2002; Yang et al., 2002). Depletion of sterols induces a conformational change with SCAP (Brown et al., 2002), which causes the uncoupling of Insigs. This allows the translocation of the SREBP-2-SCAP complex to the Golgi, where site-proteases cleave SREPB-2, generating the active transcription factor (Rawson, 2003). Conversely, sterol accumulation results in the proteasomal degradation of cholesterol-biosynthetic machinery by ER-resident E3 ubiquitin ligases (discussed in the next section). In summary, the ER is the primary site for *de novo* lipid synthesis, and contains both biosynthetic and regulatory machinery to ensure lipid homeostasis is maintained.

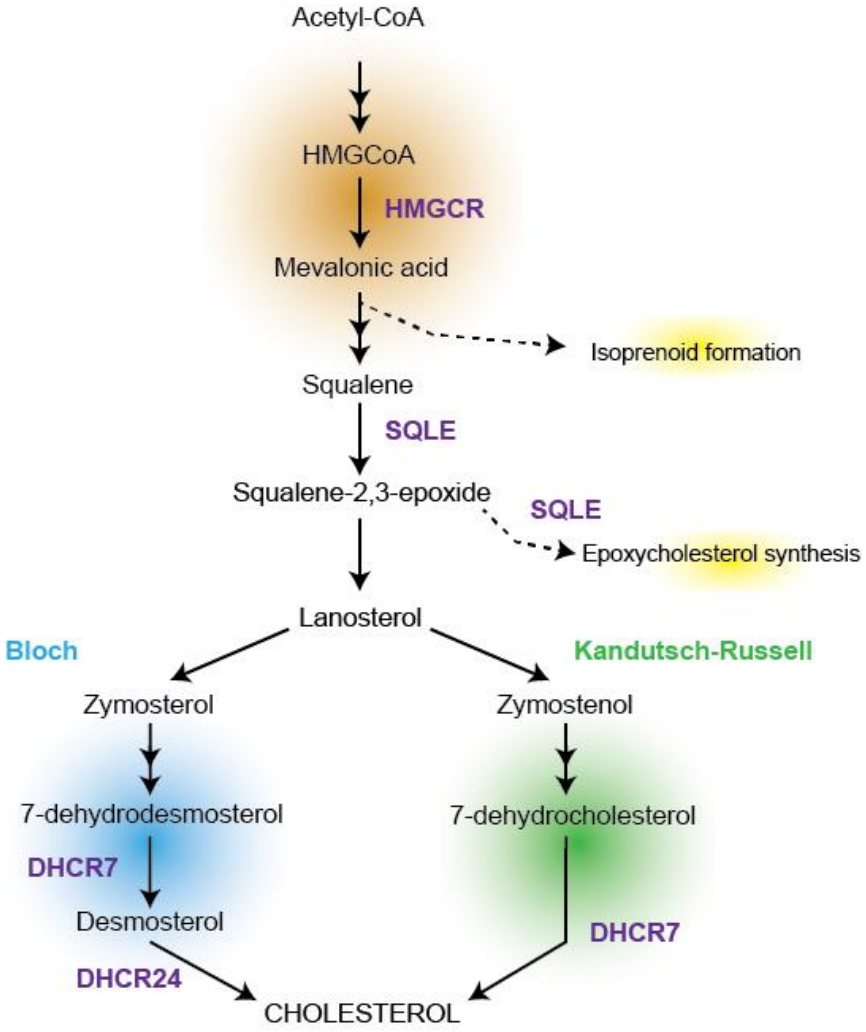

Figure 1.5: The cholesterol biosynthetic pathway. The mevalonate pathway begins with the conversion of Acetyl-CoA into HMGCoA. The subsequent reaction, which generates MA is a rate-limiting step carried out by the ER-resident HMGCR. SQLE is required to convert squalene to squalene-2,3-epoxidase. Lanosterol is the final product of the mevalonate pathway, which can enter either the Bloch or the Kandutch-Russell pathway to generate cholesterol. The intermediate structures, MA and squalene-2,3-epoxidase, can be used to generate isoprenoids and epoxysterols, respectively. Enzymes highlighted in purple are discussed in greater detail in section 1.4.1 and in Chapter 4.

1.4.1 Regulation of lipid metabolism by E3 ubiquitin ligases

As discussed above, the conversion of HMGCoA to mevalonate by the ER-resident enzyme, HMGCR is a rate-limiting step, which is precisely regulated to ensure lipid homeostasis is maintained (Burg and Espenshade, 2011). An accumulation of sterols triggers the proteasomal degradation of HMGCR and this process was shown to be controlled by yeast orthologues of Hrd1 (**H**MGCoA **r**eductase **d**egradation 1: named from this study) and SEL1L (Gardner et al., 2001; Hampton et al., 1996). However, we now understand that in mammals, HMGCR turnover is mediated by two polytopic E3s, AMFR and RNF139 (Jo et al., 2011a). AMFR had initially been demonstrated to promote ubiquitination at the ER membrane, with its cognate E2, UBE2G2 (Fang et al., 2001). Around the same time, polytopic ER proteins Insig-1 and Insig-2 were discovered to interact with HMGCR and promote its ubiquitination and degradation in the presence of sterol intermediates (Sever et al., 2003). It was subsequently established that Insig-1 recruits AMFR to ubiquitinate and hence target HMGCR for VCP/p97-dependent proteasomal degradation (Song et al., 2005). The observation that AMFR depletion did not completely rescue HMGCR from degradation, and the fact that another ER-resident ligase, RNF139, had been shown to interact with both Insig members (Lee et al., 2010), lead to the discovery that AMFR and RNF139 cooperatively degrade HMGCR in a sterol-dependent manner (Jo et al., 2011a). The same group later elucidated that ERLIN2 is recruited to AMFR by transmembrane and ubiquitin-like domain-containing protein 1 (TMUB1), and that both ER membrane embedded cofactors were required for HMGCR degradation (Jo et al., 2011b). Importantly however, the Weissman group demonstrated that the high concentration of siRNA used to target AMFR may be responsible for off-target effects which contributed to the observed HMGCR stabilisation (Tsai et al., 2012). Therefore, additional studies are required to definitively conclude how E3s and their interactors regulate HMGCR levels.

SQLE is another ER-resident enzyme which catalyses the rate-limiting conversion of squalene into 2,3-oxidosqualene, in a reaction required for sterol biosynthesis. Unlike HMGCR, its sterol-dependent degradation is controlled by the same basic mechanism in yeast and mammals (Foresti et al., 2013; Zelcer et al., 2014). MARCH6, or Doa10 in yeast, is a 14 TMD ER-resident E3 ligase. It was found to ubiquitinate Erg1 (yeast orthologue of SQLE) on one lysine residue, prompting its proteasomal degradation. Depletion of Doa10, cell division control protein 48 (Cdc48, the yeast orthologue of VCP/p97), Npl4 and E2 ubiquitin-conjugating enzymes Ubc6 and Ubc7, all lead to the stabilisation of Erg1 (Foresti et al., 2013).

The ER is the primary site for lipid metabolism and transport and several enzymes involved in these pathways are known to be ER-resident. With E3s and their cofactors clearly critical for the post-translational regulation of both HMGCR and SQLE, the question over which other enzymes are controlled in this manner remains unanswered.

1.5 Calcium signalling

Calcium is a secondary messenger that regulates a variety of functions including muscle contraction, gene transcription, secretion and cell death (Berridge et al., 2000). Although both the mitochondria and lysosomes are calcium-storage organelles, the ER represents the largest cellular calcium store (Raffaello et al., 2016). Rapid calcium release from the ER ensures the increase of cytosolic calcium levels required for specific functions. The process of calcium release is initiated at the plasma membrane (PM), where ligand binding of G protein-coupled receptors (GPCRs) and activation of phospholipase C (PLC) leads to the release of inositol-1,4,5-triphosphoate (IP_3) from the PM. IP_3 subsequently binds the tetrameric IP_3 receptor (IP_3R) in the ER membrane, triggering the release of calcium into the cytosol (Raffaello et al., 2016). IP_3Rs can also transfer calcium to the mitochondria through an interaction with the mitochondrial voltage-dependent anion channel (VDAC) (Szabadkai et al., 2006). A novel ER-resident calcium channel, transmembrane and coiled-coil domain-containing protein 1 (TMCO1), was recently described, which releases calcium into the cytosol upon ER calcium overloading (Wang et al., 2016).

For the ER to sustain calcium flux into the cytosol, a process named store-operated calcium entry (SOCE) is engaged. This involves the translocation of ER-resident stromal interaction molecule 1 (STIM1) to ER-PM contact sites, where it can interact with the PM calcium channel, ORAI1, hence promoting calcium influx into the ER (Feske et al., 2006; Vig et al., 2006). Sacro(endo)plasmic reticulum calcium ATPase (SERCA) pumps import calcium into the ER across an electrochemical gradient in an ATP-dependent process (Vandecaetsbeek et al., 2011). By mediating the uptake of calcium into the ER, the resting cytosolic calcium concentration can be restored.

Several ER-resident chaperones, including BiP, CNX, CRT and GRP94 are calcium-dependent, with BiP alone storing as much as 25% of the ER calcium pool (Lièvremont et al., 1997). It is therefore unsurprising that the loss of calcium from the ER can lead to the accumulation of misfolded proteins and downstream activation of the UPR. Hence the tight regulation of ER calcium concentration by the various channels and pumps is required not only to control cytosolic calcium levels, but also to maintain the specialised folding environment of this organelle (Carreras-Sureda et al., 2018).

1.5.1 Control of Ca^{2+} metabolism by RNF170

Upon GPCR activation at the plasma membrane, IP_3Rs embedded in the ER membrane are activated and immediately become substrates of ERAD (Wojcikiewicz, 2004). Early experiments demonstrated the downregulation of these calcium channels coincided with rapid ubiquitination, followed by degradation by 26S proteasomes (Oberdorf et al., 1999; Wojcikiewicz et al., 2003). IP_3R ubiquitination was later found to be dependent on the E2-conjugating enzyme, UBE2G2 (Webster et al., 2003), an adaptor protein already known to play a role in ERAD of other substrates (Biederer et al., 1997). VCP/p97 and two of its associated cofactors, Ufd1 and Nlp4, were also shown to be necessary for delivery of this substrate for proteasomal degradation (Alzayady et al., 2005). An siRNA-based screen later identified ERLIN2 (SPFH2) (Pearce et al., 2007), and ERLIN1 (SPFH1) (Pearce et al., 2009) as integral membrane complex components, responsible for the recruitment of the E3 ligase, RNF170 (Lu et al., 2011), required for substrate ubiquitination. Collectively, these studies demonstrate a complex centred around the ER-resident E3 ligase RNF170, which cooperatively degrade the IP_3R to limit calcium efflux from the ER after GPCR activation.

1.6 The ER-resident E3 family: an overview

Representing the entry-point to the secretory pathway, the primary function of the ER is to accommodate folding and quality control of secretory proteins (see section 1.3 and (Schwarz and Blower, 2016)). It is also involved in essential cellular pathways, including calcium homeostasis (Carreras-Sureda et al., 2018), and lipid biogenesis (Blom et al., 2011). As highlighted in sections 1.3.5, 1.4.1 and 1.5.1, a common feature of all of these functions is their regulation by the covalent modification of target substrates by ubiquitin (Ub), mediated by RING-domain E3 ubiquitin ligases resident in the ER membrane (Nakamura, 2011). Furthermore, the relatively well-characterised E3s discussed above demonstrate that the formation of multi-component complexes is an absolute requirement for correct functional execution.

However, including the E3s already explored in this chapter, there are 25 RING domain-containing proteins documented to localise to the mammalian ER membrane. The majority of this family was found in a study by Neutzner *et al*., (2011), in which the 49 predicted transmembrane RING-E3s encoded by the human genome were tagged with YFP and studied by immunofluorescence. This revealed a total of 23 ER-resident E3s (Neutzner et al., 2011). In addition, RNF103 and transmembrane protein 129 (TMEM129) were independently validated as ER-embedded ligases (Maruyama et al., 2008; van de Weijer et al., 2014). All 25 members of this family have a RING domain orientated towards the cytoplasm and collectively represent a topologically diverse group of enzymes, with some E3s spanning the membrane only once, and others possessing up to 14 TMDs (Figure 1.6).

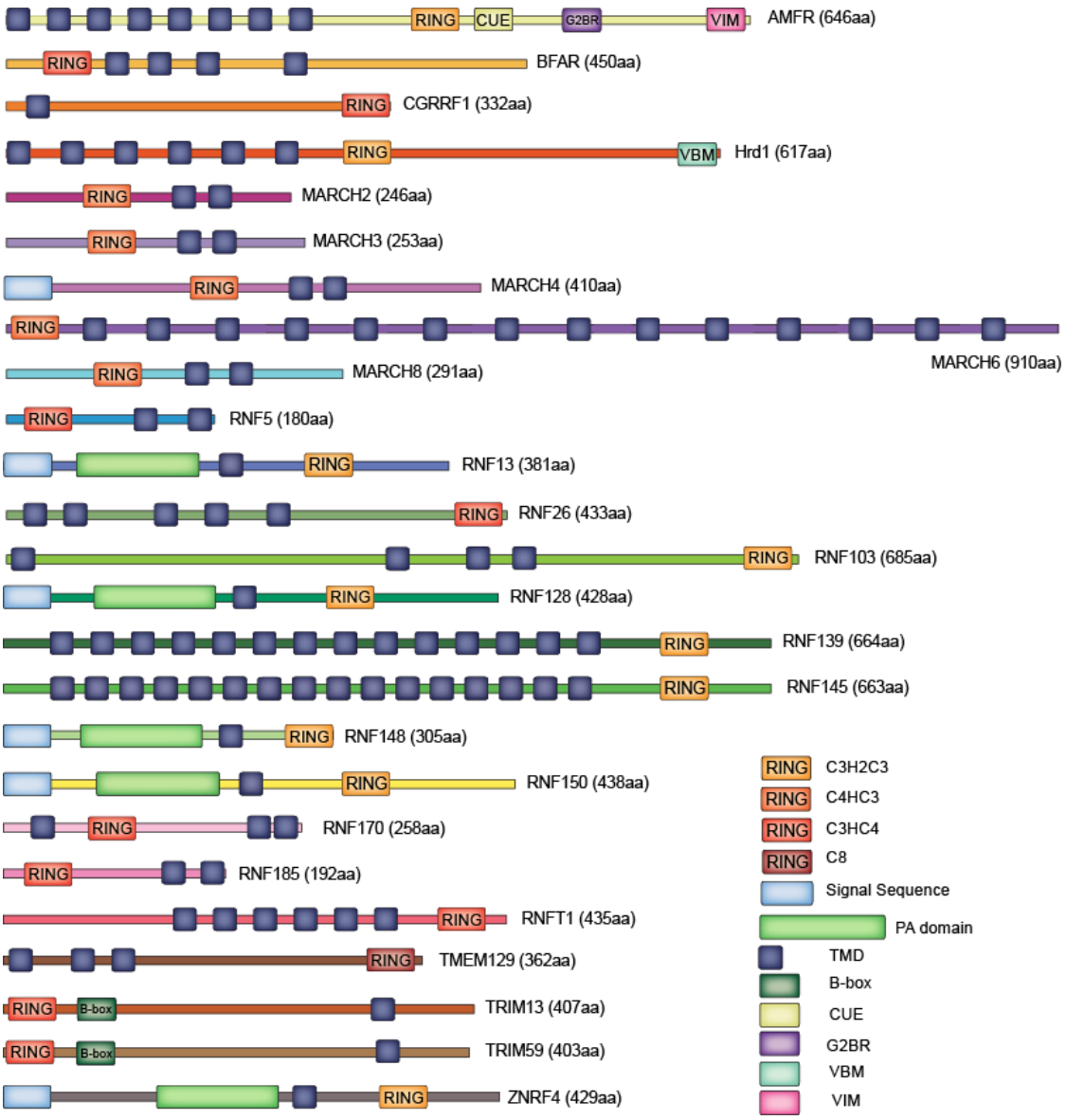

Figure 1.6: Schematic of ER-resident E3 topology. Length and different domains of each of the 25 mammalian ER-resident E3 ubiquitin ligases. C3H2C3, C4HC3, C3HC4, and C8 represent the different types of RING domain. Signal sequences, protease-associated (PA) domains, transmembrane domains (TMDs), B-box, CUE, G2BR, VCP-binding motifs (VBM), and VCP-interacting motifs (VIM) are all colour-coded. BFAR - bifunctional apoptosis regulator, CGRRF1 - cell growth regulator with RING finger domain protein 1, RNFT1 – RING finger and transmembrane domain-containing protein 1.

The first-discovered ER-resident E3, Hrd1p, was characterised by genetic screens in the model organism *Saccharomyces cerevisiae.* It was initially found to ubiquitinate and degrade HMGCR, thus post-translationally regulating sterol biosynthesis (Gardner et al., 2001; Hampton et al., 1996). However, it soon became apparent that it was required for the ERAD of misfolded ER luminal and membrane proteins (Bordallo et al., 1998) and its importance in maintaining ER homeostasis was further highlighted by the discovery that it was a principal target of the UPR (Travers et al., 2000).

The other RING-E3 in the yeast ER membrane is Doa10, which was initially described as promoting ERAD of the soluble transcription factor, Matα2 (Swanson et al., 2001). Further studies on both yeast E3s have led to the current general consensus that both Hrd1p and Doa10 complexes control ERAD of misfolded proteins, with Doa10 mediating ERAD of cytosolic clients, and Hrd1p preferentially degrading misfolded luminal and membrane substrates (Carvalho et al., 2006).

Yeast Hrd1p is structurally and functionally related to two E3s in mammals: Hrd1 (Kikkert et al., 2004; Nadav et al., 2003) and AMFR (Fang et al., 2001). Both ligases have been instrumental in our understanding of the mammalian ERAD system. They form large macromolecular complexes with their cofactors and are necessary for the K48-mediated degradation of a wide range of substrates. Their known substrates are summarised in Table 1.1. Other ER-embedded E3 complexes were later discovered to play a role in mammalian ERAD, including: the mammalian homologue of Doa10, MARCH6 (Hassink et al., 2005); RNF5 (Younger et al., 2006); RNF170 (Lu et al., 2011); RNF139 (Stagg et al., 2009); and TMEM129 (van de Weijer et al., 2014; van den Boomen et al., 2014).

It was initially suggested that these ligases might have a more restricted client range than Hrd1 and AMFR, and that their functions could be more specialised (Olzmann et al., 2013a). While this may be the case for some E3s, such as the RNF170-mediated degradation of IP_3 receptors (Lu et al., 2011), other ligases such as RNF5 have been implicated in regulating multiple substrates (see Table 1.1). Apart from its wide substrate range, RNF5 also cooperates with other E3s. It has been proposed to function upstream of AMFR in a coordinated process where RNF5 initially ubiquitinates mutant CFTR-ΔF508 and AMFR subsequently extends the ubiquitin chain, acting as an E4 ligase (Morito et al., 2008). In addition, RNF5 is suggested to function alongside its related ER-resident E3 ligase, RNF185, which also contributes to mutant CFTR degradation (Khouri et al., 2013). The diversification of ER-resident E3s in mammals, and the evidence of cooperation between them, reflects the increased complexity of the mammalian system relative to yeast.

As highlighted in Table 1.1, a number of substrates have been reported for the ER-resident E3s, suggesting these enzymes may be broadly involved across multiple cellular processes. Most have been linked with K48-linkages that promote proteasomal degradation. However, AMFR, BFAR, RNF5, RNF26, RNF128, RNF185 and TRIM13 appear to promote the formation of non-K48-linked poly-ubiquitination, with K11, K27, K29 and K63 chain-types being suggested. Conventionally, K48-linked ubiquitination was considered the primary linkage for proteasomal degradation although it is now generally acknowledged that all chain types, with the exception of K63, are able to target proteins to 26S proteasomes (Xu et al., 2009). Importantly, other functions outside degradation have been attributed to different chain linkages, including endocytosis, protein recruitment, and signalling cascade regulation for K11, K27 and K63 chains, respectively (reviewed in (Swatek and Komander, 2016)). This reflects the range of roles for E3s in both degradation and non-ERAD related processes.

E3	Active?	Ub chain	Substrates	References
AMFR	Y	K48, K27	CD3-δ, A1AT, ApoB, SOD1, ATXN3, CFTR, Insig-1, HMGCR, STING	(Fang et al., 2001; Jo et al., 2011a; Lee et al., 2006; Liang et al., 2003; Morito et al., 2008; Shen et al., 2006; Wang et al., 2014; Ying et al., 2009)
BFAR	Y	K48, K63	Auto-, BI-1	(Rong et al., 2011)
CGRRF1	Y	K48	Evi	(Glaeser et al., 2018) *
HRD1	Y	K48	Auto-, TCRα, CD3-δ, A1AT, BACE457, MHC-I, Nrf1, CD147, APP, HTT, PaelR, IRE1α	(Amano et al., 2003; Bernasconi et al., 2010; Burr et al., 2011; Christianson et al., 2008; Kaneko et al., 2010; Kikkert et al., 2004; Omura et al., 2006; Steffen et al., 2010; Sun et al., 2015; Tyler et al., 2012; Yang et al., 2007)
MARCH2	Y	ND	-	(Bartee et al., 2004)
MARCH3	ND	ND	ND	-
MARCH4	Y	ND	MHC-I, CD4	(Bartee et al., 2004)
MARCH6	Y	ND	SQLE, DIO2	(Foresti et al., 2013; Zavacki et al., 2009; Zelcer et al., 2014)
MARCH8	Y	K48	CD98, TFRC, MHC-II, IL1RAP, TRAIL-R1, DR4	(Ablack et al., 2015; Bartee et al., 2004; Chen et al., 2012; Fujita et al., 2013; Ohmura-Hoshino et al., 2006; van de Kooij et al., 2013; Wang et al., 2017a)

Table 1.1: Evidence of E3 ligase activity, chain-linkage, and known substrates. All papers referenced show either ubiquitination capacity and/or ubiquitination of the substrate, or in the case of a few ERAD substrates, pulse-chase/cycloheximide experiments. Y - Yes, ND - not determined, Auto- refers to auto-ubiquitination, * refers to a substrate of CGRRF1 found in this project. (Continued overleaf).

E3	Active?	Ub chain	Substrates	References
RNF5	Y	K48, K63	Auto-, STING, JAMP, SLC1A5, SLC38A2, Paxillin, SopA, ATG4B, CFTR	(Didier et al., 2003; Huang et al., 2018; Jeon et al., 2015; Kuang et al., 2012; Morito et al., 2008; Tcherpakov et al., 2009; Zhang et al., 2005; Zhong et al., 2009)
RNF13	Y	K29	Snapin	(Zhang et al., 2008)
RNF26	Y	K11	STING, SQSTM1	(Jongsma et al., 2016; Qin et al., 2014)
RNF103	Y	ND	ND	(Maruyama et al., 2008)
RNF128	Y	K48, K63	CD63, CD81, CD151, ARPC5, COR1A	(Ichikawa et al., 2011; Lineberry et al., 2008; Nurieva et al., 2010)
RNF139	Y	ND	Insig-1, MHC-I, uXBP1	(Chen et al., 2014; Lee et al., 2010; Stagg et al., 2009)
RNF145	Y	ND	SCAP, HMGCR	(Jiang et al., 2018; Zhang et al., 2017)
RNF148	ND	ND	ND	-
RNF150	ND	ND	ND	-
RNF170	Y	ND	IP_3 receptor	(Lu et al., 2011)
RNF185	Y	K27, K63	cGAS, CFTR, Dvl2, BNIP1	(Khouri et al., 2013; Tang et al., 2011; Wang et al., 2017b; Zhou et al., 2014)
RNFT1	ND	ND	ND	-
TMEM129	Y	ND	Auto-, MHC-I	(van de Weijer et al., 2014; van den Boomen et al., 2014)
TRIM13	Y	K29	Auto-, AKT1, MDM2, TRAF6	(Huang and Baek, 2017; Joo et al., 2011; Lerner et al., 2007)
TRIM59	ND	ND	ND	-
ZNRF4	Y	ND	Calnexin	(Neutzner et al., 2011)

Table 1.1 (continued)

As reviewed above, E3s embedded in the ER membrane orchestrate ERAD of misfolded proteins, cholesterol biosynthetic machinery, and ER-resident calcium channel. In addition to these functions, ERAD can also control the expression of plasma membrane proteins that traffic along the secretory pathway, thus regulating nutrient uptake into the cell. This was elegantly demonstrated in yeast, where the high-affinity zinc-regulated transporter 1 (Zrt1) was proteolytically cleaved by presenilin fold 1 (Ypf1) and subsequently degraded following ubiquitination by Doa10 (Avci et al., 2014). In a similar process, mammalian RNF5 has recently been shown to mediate the degradation of two glutamine transporters, solute carrier (SLC)1A5 and SLC38A2 (Jeon et al., 2015).

As well as regulating the strict metabolic, signalling, and quality control demands of the cell, ERAD can be hijacked by pathogenic machinery. Human cytomegalovirus (HCMV) components US2 and US11 have been demonstrated to engage ER-resident RNF139 and TMEM129, which ubiquitinate and destroy host MHC class I molecules. This downregulates antigen presentation, thereby allowing HMCV to avoid detection by the host adaptive immune defence (Stagg et al., 2009; van den Boomen et al., 2014).

Independently of their roles in adaptive immunity, several ER-resident E3s have been implicated in regulating innate immune signalling. The cGAS-STING pathway is the principal route through which pathogenic DNA is recognised and a downstream protective response is elicited. AMFR, RNF5, RNF26 and RNF185 have all been demonstrated to ubiquitinate either cGAS or STING, thus modulating the downstream IFN response (see Chapter 5, section 5.1). Apart from RNF5, which is proposed to K48-poly-ubiquitinate STING, thus promoting its turnover (Zhong et al., 2009), the other ligases catalyse non-degradative ubiquitination in this pathway. There is evidence that RNF185 and AMFR modify cGAS and STING with K27-linked

ubiquitin chains, respectively (Wang et al., 2014; Wang et al., 2017b). RNF26, meanwhile, is proposed to mediate K11-linked ubiquitination of STING, thus blocking it from the addition of K48-linked chains by RNF5 and reducing STING degradation (Qin et al., 2014).

RNF26 has also been linked with endosomal sorting from the ER. Ubiquitination of sequestosome-1 (p62/SQSTM1) by RNF26 has been demonstrated to attract ubiquitin-binding domains (UBDs) of vesicle adaptor proteins through which endosomal positioning is controlled (Jongsma et al., 2016). Other examples of E3s that mediate non-ERAD functions from the ER membrane include TRIM13 and MARCH8. TRIM13 is suggested to modify TRAF6 by K29-linked ubiquitination, which in turn potentiates nuclear factor-kappa beta (NF-κB) signalling (Huang and Baek, 2017). Catalytically-active MARCH8 promotes lysosomal turnover of the transferrin receptor (TFRC) (Fujita et al., 2013), which is responsible for the endocytosis of the iron-transferrin module from the plasma membrane. Interestingly, MARCH8 is localised to the endosomal compartments as well as the ER. Indeed, eight of the 25 E3s are proposed to also localise to different organelles or membranes (see Table 1.2). It is therefore important to consider that although this E3 family is resident in the ER, some members may have alternative localisations, and consequently their functions may not be exclusive to the ER.

E3	Location	References
AMFR	ER	(Fang et al., 2001)
BFAR	ER	{(Rong et al., 2011; Roth et al., 2003)
CGRRF1	ER	(Glaeser et al., 2018; Kaneko et al., 2016)
HRD1	ER	(Kikkert et al., 2004)
MARCH2	ER, endosome	(Bartee et al., 2004; Han et al., 2012; Nakamura et al., 2005)
MARCH3	ER, endosome	(Fukuda et al., 2006)
MARCH4	ER, Golgi	(Bartee et al., 2004)
MARCH6	ER	(Hassink et al., 2005)
MARCH8	ER, endosome, PM	(Bartee et al., 2004; Chen et al., 2012)
RNF5	ER, Mitochondria	(Tcherpakov et al., 2009; Zhong et al., 2009)
RNF13	ER	(Arshad et al., 2013)
RNF26	ER	(Jongsma et al., 2016)
RNF103	ER	(Maruyama et al., 2008)
RNF128	ER, PM	(Lineberry et al., 2008)
RNF139	ER	(Gemmill et al., 2002)
RNF145	ER	(Graham et al., 2015; Jiang et al., 2018; Zhang et al., 2017)
RNF148	ER	Predicted SP and glycosylation sites
RNF150	ER	Predicted SP and glycosylation sites
RNF170	ER	(Lu et al., 2011)
RNF185	ER, Mitochondria	(Kaneko et al., 2016; Khouri et al., 2013; Tang et al., 2011)
RNFT1	ER	(Kaneko et al., 2016)
TMEM129	ER	(van de Weijer et al., 2014; van den Boomen et al., 2014)
TRIM13	ER, NE	(Lerner et al., 2007)
TRIM59	ER	(Kondo et al., 2012)
ZNRF4	ER	(Neutzner et al., 2011)

Table 1.2: Evidence for ER and alternative localisations for each E3. The evidence is provided in addition to that in **(Neutzner et al., 2011)** and is based on immunofluorescence.

In summary, the 25 ER-resident E3s coordinate multiple essential cellular processes. Functions classically associated with the ER, such as quality control of secretory proteins, calcium signalling, and lipid production, are all regulated by E3s in the context of ERAD. However, these enzymes also control other functions including immune signalling, lysosomal degradation and vesicular trafficking. Despite the functional significance of these ligases, relatively little information is available on the complexes they form with cofactors, with some ligases remaining completely uncharacterised in terms of both cofactors and substrates.

1.7 Aim of the study

The human ER accommodates at least 25 different E3 ligases (Maruyama et al., 2008; Neutzner et al., 2011; van de Weijer et al., 2014), yet despite their significance in maintaining both ER and cellular homeostasis, most are either partially or poorly characterised. E3 function is strictly dependent on the interactions it forms with both cofactors and substrates. Therefore, the principal aim of this project is to define the interaction networks of this ligase family. FLAG-HA(FH)-tagged E3-expressing cells lines were generated to enable liquid-chromatography tandem mass spectrometry (LC-MS/MS) on immunoprecipitated FH-E3 complexes. Comparative proteomic profiling is used to define the high-confidence interactors (HCIPs) for each E3. To gain insight into the functional significance of individual E3 networks, the interaction data is mapped to known ER functions. Furthermore, the contribution of these E3 ligase complexes to resolving ER stress is established by merging the proteomic dataset with transcriptional analyses, which determine E3 expression changes in response to different ER stress-inducing agents. Finally, several HCIPs are validated as *bona fide* interactors by a reciprocal tagging strategy, and a novel RNF26-containing complex is characterised both biochemically and functionally. Collectively, these data describe a comprehensive collection of ubiquitination networks at the ER membrane, whilst demonstrating the utility of comparative proteomics as a discovery platform to characterise ER-resident E3 complexes and their functions.

Chapter 2

Materials and Methods

2.1 Lists of materials

2.1.1 List of compounds

Compound	Abbreviation	Solvent	Source
Cyclic [G(2',5')pA(3',5')p]	cGAMP	H_2O	Invivogen
Cycloheximide	CHX	DMSO	Abcam
Dimethyl sulfoxide	DMSO	-	Sigma-Aldrich
Dithiothreitol	DTT	H_2O	Sigma-Aldrich
Doxycycline	DOX	DMSO	Sigma-Aldrich
Iodoacetamide	IAA	H_2O	Roche
MG132	-	DMSO	Merck Millipore
N-Ethylmaleimide	NEM	Ethanol	Acrose organics
NMS-873	-	DMSO	Sigma-Adrich
SubtilaseAB$_5$	SubAB$_5$	50% glycerol in PBS	J. Paton (University of Adeleide)
Tunicamycin	TM	DMSO	Sigma-Aldrich

2.1.2 List of plasmids used in this study

Plasmid name	Description	Vector	Source
pFL001	FRT/TO vector encoding N-terminal FLAG-HA	pcDNA™5/FRT/TO	Lab stock
pFL002	FRT/TO vector encoding C-terminal FLAG-HA	pcDNA™5/FRT/TO	Lab stock
S-tag pcDNA3.1(+)	Vector encoding N-terminal S-tag	pcDNA™3	Lab stock
S-tag pcDNA3.1(-)	Vector encoding C-terminal S-tag	pcDNA™3	Lab stock
S-AUP1 pcDNA3.1(+)	Vector encoding N-terminal S-tagged AUP1	pcDNA™3	Lab stock
EMC1-S pcDNA3.1(-)	Vector encoding C-terminal S-tagged EMC1	pcDNA™3	Lab stock
ERLIN2-S pcDNA3.1(-)	Vector encoding C-terminal S-tagged ERLIN2	pcDNA™3	Lab stock
UBXD8-S pcDNA3.1(-)	Vector encoding C-terminal S-tagged UBXD8	pcDNA™3	Lab stock

2.1.3 List of oligonucleotides

2.1.3.1 List of primers for qRT-PCR

F/R	Ref seq	Protein Name	Supplier	Sequence
F	NM_032015.4	RNF26	IDT	GAATCCCCTCCTACCCCTGT
R				GAGGAGAGCCCACAGCAAAT
F	NM_018126.2	TMEM33	IDT	CCCAGCGCTGACGTTTTCT
R				GCTGCTTCATGCAACCCAAG
F	NM_001101.3	Actin	IDT	GAGGCACTCTTCCAGCCTT
R				AAGGTAGTTTCGTGGATGCC

2.1.3.2 List of primers used for amplifying E3 ORFs

Name	Sequence	Description	To generate
oFL035	AATAAGCTTGCCACCATGCCGCTGCTCTTCCTCGA	AMFR HindIII F	AMFR-FH
oFL036	TTGAATATTACCGGTGGAGGTCTGCTGCTTCTGAA	AMFR AgeI R	AMFR-FH
oFL059	AATGCTAGCGCCACCATGGAGGAACCTCAGAAAAG	BFAR NheI F	BFAR-FH
oFL060	TTGAATATTGGATCCCAACACCTGGGTTTCCAGCC	BFAR BamHI R	BFAR-FH
oFL101	AATATACCGGTGAGGAACCTCAGAAAAGCTA	BFAR AgeI F	FH-BFAR
oFL102	CTTGCGGCCGCTCACAACACCTGGGTTTCCA	BFAR NotI R	FH-BFAR
oFL037	AATAAGCTTGCCACCATGGCTGCGGTGTTTCTGGT	CGRRF1 HindIII F	CGRRF1-FH
oFL038	TTGAATATTACCGGTAAGAGTCTTCGGTTTGTCTT	CGRRF1 AgeI R	CGRRF1-FH
oFL063	AATAAGCTTGCCACCATGTTCCGCACGGCAGTGAT	Hrd1 HindIII F	Hrd1-FH
oFL064	TTGAATATTACCGGTGTGGGCAACAGGAGACTCCA	Hrd1 AgeI R	Hrd1-FH
oFL049	AATAAGCTTGCCACCATGACGACGGGTGACTGCTG	MARCH2 HindIII F	MARCH2-FH
oFL050	TTGAATATTACCGGTTACTGGTGTCTCCTCTGCCA	MARCH2 AgeI R	MARCH2-FH
oFL051	AATAAGCTTGCCACCATGACAACCAGCCGCTGCAG	MARCH3 HindIII F	MARCH3-FH
oFL052	TTGAATATTACCGGTAACAACTGTCTCCTTTGAGT	MARCH3 AgeI R	MARCH3-FH
oFL053	AATAAGCTTGCCACCATGCTGATGCCCCTGTGTGG	MARCH4 HindIII F	MARCH4-FH
oFL054	TTGAATATTACCGGTCACTGTCGTGACTCTCATGA	MARCH4 AgeI R	MARCH4-FH
oFL021	AATATACCGGTGACACCGCGGAGGAAGACAT	MARCH6_AgeI F	MARCH6-FH
oFL022	CTTGCGGCCGCTTATTCTTGGGATGACTGTG	MARCH6 NotI R	MARCH6-FH
oFL090	AATAAGCTTGCCACCATGGACACCGCGGAGGAAGA	MARCH6 HindIII F	FH-MARCH6
oFL091	TTGAATATTACCGGTTTCTTGGGATGACTGTGGAG	MARCH6 AgeI R	FH-MARCH6
oFL039	AATAAGCTTGCCACCATGAGCATGCCACTGCATCA	MARCH8 HindIII F	MARCH8-FH
oFL040	TTGAATATTACCGGTGACGTGAATGATTTCTGCTC	MARCH8 AgeI R	MARCH8-FH
oFL031	AATATACCGGTGCAGCAGCGGAGGAGGAGGA	RNF5 AgeI F	FH-RNF5
oFL032	CTTGCGGCCGCTCAAATACTGAGCAGCCAAA	RNF5 NotI R	FH-RNF5
oFL027	AATATACCGGTCTGCTCTCCATAGGGATGCT	RNF13 AgeI F	FH-RNF13
oFL028	CTTGCGGCCGCTCAAACAGTATTTGCTATGT	RNF13 NotI R	FH-RNF13
oFL094	AATAAGCTTGCCACCATGCTGCTCTCCATAGGGAT	RNF13 HindIII F	RNF13-FH
oFL095	TTGAATATTACCGGTAACAGTATTTGCTATGTTGT	RNF13 AgeI R	RNF13-FH
oFL057	AATAAGCTTGCCACCATGGAGGCAGTGTACCTGGT	RNF26 HindIII F	RNF26-FH
oFL058	TTGAATATTACCGGTGAGGTAGACATTGAGGGTCT	RNF26 AgeI R	RNF26-FH
oFL109	AATATACCGGTGAGGCAGTGTACCTGGTAGT	RNF26 AgeI F	FH-RNF26
oFL110	CTTGCGGCCGCTCAGAGGTAGACATTGAGGG	RNF26 NotI R	FH-RNF26
oFL111	CTTGCGGCCGCTCAGAGTGCGACATTGAGGG	RNF26 NotI R (M)	FH-RNF26^{Y432A}
oFL067	AATATACCGGTTGGCTGAAGCTTTTTTTCTT	RNF103 AgeI F	FH-RNF103
oFL068	CTTGCGGCCGCTTAAGATGGGACATCATTTG	RNF103 NotI R	FH-RNF103
oFL096	AATGCTAGCGCCACCATGTGGCTGAAGCTTTTTTT	RNF103 NheI F	RNF103-FH
oFL097	TTGAATATTGGTACCAGATGGGACATCATTTGACA	RNF103 KpnI R	RNF103-FH

oFL025	AATATACCGGTGGGCCGCCGCCTGGGGCCGG	RNF128 AgeI F	FH-RNF128
oFL026	CTTGCGGCCGCTTAAGATTTAATTTCTCGAA	RNF128 NotI R	FH-RNF128
oFL082	AATGCTAGCGCCACCATGGGGCCGCCGCCTGGGGC	RNF128 NheI F	RNF128-FH
oFL083	TTGAATATTGGATCCAGATTTAATTTCTCGAACAG	RNF128 BamHI R	RNF128-FH
oFL043	AATGCTAGCGCCACCATGGCGGCCGTGGGGCCCCC	RNF139 Nhe1 F	RNF139-FH
oFL044	TTGAATATTGGATCCGTCAGTATCATCATTAAATT	RNF139 BamHI R	RNF139-FH
oFL033	AATATACCGGTGCTGCAAAGGAGAAACTGGA	RNF145 AgeI F	FH-RNF145
oFL034	CTTGCGGCCGCCTAGGCTGATTCAACAGGAT	RNF145 NotI R	FH-RNF145
oFL045	AATAAGCTTGCCACCATGAGCTTCCTTAGAATTAC	RNF148 HindIII F	RNF148-FH
oFL046	TTGAATATTACCGGTAGTTTTCAGGATGTCACACT	RNF148 AgeI R	RNF148-FH
oFL029	AATATACCGGTGCAATGTCTCTCATCCAAGC	RNF150 AgeI F	FH-RNF150
oFL030	CTTGCGGCCGCTCAAGATTTCACTTCTTCAC	RNF150 NotI R	FH-RNF150
oFL047	AATAAGCTTGCCACCATGGCCAAATATCAAGGTGA	RNF170 HindIII F	RNF170-FH
oFL048	TTGAATATTACCGGTACCTGAGAACCAAAGGATGG	RNF170 AgeI R	RNF170-FH
oFL055	AATAAGCTTGCCACCATGGCAAGCAAGGGGCCCTC	RNF185 HindIII F	RNF185-FH
oFL056	TTGAATATTACCGGTGGCAATCAGGAGCCAGAACA	RNF185 AgeI R	RNF185-FH
oFL065	AATAAGCTTGCCACCATGCCGCTGTTCTTGCTGTC	RNFT1 HindIII F	RNFT1-FH
oFL066	TTGAATATTACCGGTATATATTTGAAGGTGTGATG	RNFT1_AgeI_R	RNFT1-FH
oFL088	AATATACCGGTCCGCTGTTCTTGCTGTCGCT	RNFT1 AgeI F	FH-RNFT1
oFL089	CTTGCGGCCGCTTAATATATTTGAAGGTGTG	RNFT1 NotI R	FH-RNFT1
oFL092	AATAAGCTTGCCACCATGGACAGCCCCGAGGTGAC	TMEM129 HindIII F	TMEM129-FH
oFL093	TTGAATATTGGATCCGCGCACGGTGCACACATCCA	TMEM129 BamHI R	TMEM129-FH
oFL061	AATAAGCTTGCCACCATGGAGCTGCTTGAAGAAGA	TRIM13 HindIII F	TRIM13-FH
oFL062	TTGAATATTACCGGTTAATAGTTTATATTTGCACA	TRIM13 AgeI R	TRIM13-FH
oFL023	AATATACCGGTCACAATTTTGAGGAAGAGTT	TRIM59 AgeI F	FH-TRIM59
oFL024	CTTGCGGCCGCTCAATGGGAAACTATTTTCC	TRIM59 NotI R	FH-TRIM59
oFL086	AATAAGCTTGCCACCATGCACAATTTTGAGGAAGA	TRIM59 HindIII F	TRIM59-FH
oFL087	TTGAATATTACCGGTATGGGAAACTATTTTCCACA	TRIM59 AgeI R	TRIM59-GH
oFL041	AATAAGCTTGCCACCATGCCGCTCTGCCGTCCGGA	ZNRF4 HindIII F	ZNRF4-FH
oFL042	TTGAATATTACCGGTCTGACCAGGGGCCTCAGGAG	ZNRF4 AgeI R	ZNRF4-FH

2.1.3.3 List of primers used to amplify HCIP ORFs

Sequence	Description	To generate
AATATACCGGTGAGCTCGAAGTCCGGCGGGT	ALDH3A2 Age1 F	S-ALDH3A2
AATTCTAGATTATCTCTGCTTACTGGACC	ALDH3A2 Xba1 R	S-ALDH3A2
AATGCTAGCGCCACCATGGAAGTGAGAAAGTTGAG	DNAJC16 Nhe1 F	DNAJC16-S
TTGAATATTGGTACCGTCTAGTTCAGGCCATGATG	DNAJC16 Kpn1 R	DNAJC16-S
AATTCTAGAGCCACCATGGGCACCGCGCGCTGGCT	ENDOD1 XbaI F	ENDOD1-S
ATATTGAATTCGATAACTCCCCAGAATTGTCAA	ENDOD1 EcoRI R	ENDOD1-S
AATATACCGGTGAGGGAGGTTTGGCAGATGG	OSBPL8 Age1 F	S-OSBPL8
AATTCTAGACTACTTGAACATGAAGTTTA	OSBPL8 Xba1 R	S-OSBPL8
AATTCTAGAGCCACCATGGCTGCCGAGGATGTGGT	PGRMC1 Xba1 F	PGRMC1-S
TTGAATATTGGTACCATCATTTTTCCGGGCACTCT	PGRMC1 Kpn1 R	PGRMC1-S
AATATACCGGTGCGACGGCGGCCTACGAGCA	SACM1L Age1 F	S-SACM1L
AATGCTAGCTCAGTCTATCTTTTCTTTCT	SACM1L Nhe1 R	S-SACM1L
AATTCTAGAGCCACCATGGGGACTGTGCACGCCCG	SAMM50 Xba1 F	SAMM50-S
TTGAATATTGGATCCCAGGAACCTTATCCCAGCTC	SAMM50 BamHI R	SAMM50-S
AATTCTAGAGCCACCATGCCGGCCCACTTGCTGCA	SCD1 Xba1 F	SCD1-S
TTGAATATTGGTACCGCCACTCTTGTAGTTTCCAT	SCD1 Kpn1 R	SCD1-S
AATTCTAGAGCCACCATGATGGCGGCCGGCGCGGC	TMED1 Xba1 F	TMED1-S
TTGAATATTGGTACCCGTGGGCACCGGGCGCTTGT	TMED1 Kpn1 R	TMED1-S
AATTCTAGAGCCACCATGTCTGGTTTGTCTGGCCC	TMED10 Xba1 F	TMED10-S
TTGAATATTGGTACCCTCAATCAATTTCTTGGCCT	TMED10 Kpn1 R	TMED10-S
AATTCTAGAGCCACCATGAAGCTCTTATCTTTGGT	TMEM9 Xba1 F	TMEM9-S
TTGAATATTGGTACCGCTGAGCATCTTGTGCCGAT	TMEM9 Kpn1 R	TMEM9-S
ATTCTAGAGCCACCATGGCAGATACGACCCCGAA	TMEM33 Xba1 F	TMEM33-S
TTGAATATTGGTACCTGGAACTGTTGGTGCCAA	TMEM33 Kpn1 R	TMEM33-S
AATATACCGGTGCAGATACGACCCCGAAC	TMEM33 Age1 F	S-TMEM33
AATTCTAGACTATGGAACTGTTGGTGCCA	TMEM33 Xba1 R	S-TMEM33
AATATACCGGTGCCGCGAATTATTCCAGTAC	TMEM43 Age1 F	S-TMEM43
AATTCTAGATTACTCCAACTTTTTGGCTG	TMEM43 Xba1 R	S-TMEM43
AATTCTAGAGCCACCATGTCGGAGCACGTGGAGCC	TMEM259 Xba1 F	TMEM259-S
TTGAATATTGGTACCTGGAATGCGCAGCCAATGCC	TMEM259 Kpn1 R	TMEM259-S
AATATACCGGTACCCTGATTGAAGGGGTGGG	TMUB1 Age1 F	S-TMUB1
AATTCTAGACTACGGGCGGTACATGGCAA	TMUB1 Xba1 R	S-TMUB1
AATATACCGGTGAGCTCTCTGATGTCACCCT	TMUB2 Age1 F	S-TMUB2
AATTCTAGATTATCGTCCATACATCCCAA	TMUB2 Xba1 R	S-TMUB2

2.1.4 List of siRNAs

oligo#	Uniprot ID	Protein Name	Supplier	Catalog #	target site
1	Q9BTV4	TMEM43	Sigma	SASI_Hs01_00130391	301
2				SASI_Hs01_00130393	591
3				SASI_Hs01_00130395	1168
4				SASI_Hs01_00130397	569
1	O94919	ENDOD1	Sigma	SASI_Hs02_00346845	936
2				SASI_Hs02_00346846	1173
1	Q96CS3	UBXD8	Sigma	SASI_Hs01_00205252	357
2				SASI_Hs01_00205253	787
3				SASI_Hs01_00205254	273
4				SASI_Hs01_00205256	747
1	P57088	TMEM33	Sigma	SASI_Hs01_00209910	967
2				SASI_Hs01_00209911	505
1	Q13445	TMED1	Sigma	SASI_Hs01_00021210	453
2				SASI_Hs01_00021211	546
1	Q9Y679	AUP1	Sigma	SASI_Hs02_00370182	1228
2				SASI_Hs01_00193155	862
3				SASI_Hs01_00193156	1322
4				SASI_Hs02_00370183	880
1	Q9BY78	RNF26	Sigma	SASI_Hs01_00160403	2028
2				SASI_Hs01_00160405	2062
siNTC	-	-	Sigma	SIC001	-

2.1.5 List of Nanostring® Codeset

Gene Name	Target ID	Gene Name	Target ID
AMFR	NM_001144.4	SEL1L	NM_005065.5
MARCH6	NM_005885.2	FAM8A1	NM_016255.2
RNF103	NM_005667.3	HERP	NM_014685.3
RNF139	NM_007218.3	ERdj5	NM_018981.2
RNF170	NM_001160223.1	GRP94	NM_003299.2
RNF185	NM_152267.3	AUP1	NM_181575.3
RNF5	NM_006913.3	VIMP	NM_203472.1
SYVN1	NM_032431.2	VCP/p97	NM_007126.3
TRIM13	NM_001007278	CPVL	NM_031311.3
BFAR	NM_016561.2	DERLIN1	NM_024295.5
CGRRF1	NM_006568.2	DERLIN2	NM_016041.3
MARCH2	NM_016496.4	DERLIN3	NM_001135751.1
MARCH3	NM_178450.3	ERLIN1	NM_006459.3
MARCH4	NM_020814.2	ERLIN2	NM_007175.6
MARCH8	NM_001002265.1	UBAC2	NM_001144072.1
RNF128	NM_194463.1	EDEM1	NM_014674.2
RNF13	NM_007282.4	EDEM2	NM_018217.2
RNF145	NM_001199380.1	EDEM3	NM_025191.3
RNF148	NM_198085.1	UBXD8	NM_014613.2
RNF150	NM_020724.1	ERFAD	NM_024955.5
RNF26	NM_032015.4	TXD16/ERp90	NM_020784.2
RNFT1	NM_016125.3	PDIA6	NM_005742.2
TRIM59	NM_173084.2	UBE2J1	NM_016021.2
ZNRF4	NM_181710.3	UBE2G2	NM_003343.5
KIAA0090	NM_015047.2	ATF6	NM_007348.3
C15ORF24	NM_020154.2	PERK	NM_004836.5
MMGT1	NM_173470.1	IRE1	NM_001433.3
TMEM85	NM_016454.2	ATF4	NM_001675.2
TMEM93	NM_001014764.1	CHOP	NM_001195053.1
C14ORF122	NM_016049.3	XBP1	NM_005080.3
COX4NB	NM_006067.4	OS9 exon11	NM_006812.3
TTC35	NM_014673.3	OS9 exon13	NM_006812.3
C19ORF63	NM_206538.2	MT1X	NM_005952.3
TMEM111	NM_018447.2	MT1H	NM_005951.2
CANX	NM_001746.3	ACTB	NM_001101.2
BiP/HSP5A	NM_005347.4	GAPDH	NM_002046.3
OS9	NM_006812.3	TUBB	NM_178014.2
XTP3B	NM_015701.4		

2.1.6 List of primary and secondary antibodies

Antigen	Host	Source	Product #	Use	Dilution
Primary					
AUP1	Rb pAb	Atlas Antibodies	HPA007674	WB	1:1000
CD147	Ms mAb	Santa Cruz	sc-25273	WB	1:1000
CNX	Rb pAb	Enzo Life Sciences	ADI-SPA-860-D	IF	1:400
Derlin1	Rb pAb	Gift from Y.Ye (NIH, Bethesda)	-	WB	1:5000
ENDOD1	Rb pAb	Abcam	ab121293	WB	1:1000
FAM8A1	Rb pAb	Purified serum	-	WB	1:10000
FLAG	Ms mAb	Sigma	F3165	WB/IF	1:2000/1:400
FLAG	Rb pAb	Sigma	F7425	WB/IF	1:2000/1:400
HA	Rb mAb	Cell Signaling	3724	WB	1:2000
Herp1	Rb pAb	Abcam	ab150424	WB	1:10000
Hrd1	Rb pAb	Bethyl	A302-946A	WB	1:2000
KDEL	Rb pAb	Abcam	ab176333	IF	1:200
OS-9	Rb pAb	Purified serum	-	WB	1:3000
S-tag	Ms mAb	Thermo Scientific	MA1-981	WB/IF	1:1000/1:200
SEL1L	Gt pAb	Santa Cruz	sc-48081	WB	1:2000
STING	Rb mAb	Cell Signaling	D2P2F	WB	1:1000
TMED1	Rb pAb	Abcam	ab224411	WB	1:500
TMEM43	Rb mAb	Abcam	ab184164	WB	1:1000
Tubulin	Ms mAb	Sigma	T6074	WB	1:10000
UBE2J1	Rb pAb	Abcam	ab39104	WB	1:5000
Ubiquitin	Ms mAb	Cell Signaling	P4D1	WB	1:1000
Ubiquitin	Rb pAb	Cell Signaling	3933	WB	1:1000
UBXD8	Rb pAb	Proteintech	16251-1-AP	WB	1:1000
Secondary					
α-Rb IgG HRP	Goat	Bio-Rad	170-6515	WB	1:10000
α-Ms IgG HRP	Goat	Santa Cruz	sc-2005	WB	1:10000
α-Gt IgG HRP	Donkey	Santa Cruz	sc-2020	WB	1:10000
Alexa Fluor® 488 α-Rb IgG	Goat	Thermo Scientific	A11008	IF	1:400
Alexa Fluor® 568 α-Ms IgG	Goat	Thermo Scientific	A11031	IF	1:400

2.1.7 List of solutions and buffers

Solution	Component	Concentration
LMNG lysis buffer	Tris-HCl, pH 7.4	50 mM
	NaCl	150 mM
	EDTA	5 mM
	LMNG	1% (w/v)
	Protease inhibitor cocktail	1 x
	NEM	2 mM
RIPA lysis buffer	Tris-HCl, pH 7.4	50 mM
	SDS	0.1% (w/v)
	Sodium deoxycholate	1% (w/v)
	NP-40	1% (v/v)
	EDTA	2 mM
	NaCl	150 mM
	Protease inhibitor cocktail	1 x
	NEM	2 mM
Triton-X-100 lysis buffer	Tris-HCl, pH 7.4	50 mM
	NaCl	150 mM
	EDTA	5 mM
	Triton-X-100	1% (w/v)
	Protease inhibitor cocktail	1 x
	NEM	2 mM
TUBE lysis buffer	Sodium phosphate, pH 7.5	20 mM
	EDTA	2 mM
	NP-40	1% (v/v)
	DTT	1 mM
	PhosSTOP	1 x
	Protease inhibitor cocktail	1 x
	NEM	50 mM

2.1.7 List of solutions and buffers (continued)

Solution	Component	Concentration
PFA	PFA	4% (v/v)
PBST	PBS	1 x
	Tween™ 20	0.1% (v/v)
Ponceau S	Ponceau S	0.5% (w/v)
	Acetic Acid	1% (v/v)
Transfer buffer	Tris, pH 8.3	25 mM
	Glycine	190 mM
	Methanol	20% (v/v)
SDS sample buffer (5x)	Tris-HCl, pH 6.8	312.5 mM
	Glycerol	50% (v/v)
	SDS	10% (w/v)
	DTT	60 mM
	Bromophenol blue	0.05% (w/v)
Deubiquitinating buffer	HEPES, pH 7.5	50 mM
	NaCl	100 mM
	DTT	2 mM
	$MnCl_2$	1 mM
	Brij-35	0.01% (w/v)
In vitro ubiquitination buffer	Tris-HCl, pH 7.5	50 mM
	$MgCl_2$	2.5 mM

2.2 Protocols

2.2.1 Cell culture methods

2.2.1.1: Maintenance of human cell lines

All cell lines were grown in a 37°C incubator with a humidified, 5% CO_2 atmosphere. Flp-In™ T-REx™ human embryonic kidney 293 cells (referred to as Flp-In293) were cultured in high glucose Dulbecco's Modified Eagle Medium (DMEM, Lonza, BE12-604F) supplemented with 10% (v/v) foetal bovine serum (FBS, Sigma, F4135), and 2 mM glutamine (Life Technologies). 100 µg/ml Hygromycin B Gold (Invivogen) was used to maintain selection pressure on cell lines containing a stably integrated gene of interest. Cells were maintained in 10 cm plates and passaged upon reaching ~90% confluency. To passage, cells were washed once with 10 ml of PBS prior to the addition of 1 ml warmed 0.25% trypsin-EDTA (Life Technologies). Cells were returned to the incubator for 2 min before being resuspended in 9 ml fresh medium. Cells were counted using the TC10™ Automated cell counter (Bio-Rad) and seeded according to experimental requirements. Maintenance plates were generally seeded between 10-20% confluency.

2.2.1.2: Cryopreservation of human cell lines

Cells grown in 10 cm plates were trypsinised and resuspended as described above. Resuspended cells were centrifuged at 1,250 g for 3 min at RT and the supernatant was removed. Cell pellets were subsequently resuspended in 2 ml 10% (v/v) DMSO/FBS and aliquoted into two cryovial tubes. Tubes were placed in a freezing container containing isopropanol (Nalgene), which was stored overnight at -80°C. Tubes were subsequently transferred to liquid nitrogen for long-term storage.

2.2.1.3 Stable cell line generation

Stable cell lines expressing each of the 25 documented E3 ligases were generated using Flp-In™ T-REx™ human embryonic kidney 293 cells (referred to as Flp-In293, Thermo Fischer Scientific). 1 x 10^6 Flp-IN293 cells were seeded per 10 cm plate. The following day, 3 µg of the FLAG-HA-E3 (pcDNA™5/FRT/TO) and 1 µg Flp recombinase (pOG44) were transfected into the cells using Lipofectamine™2000 according to manufacturer's instructions. 24 h after transfection, the cells were expanded to 10 cm plates and the following day 100 µg/ml hygromycin B (InvivoGen) was added to select positive clones. Only cells in which the pcDNA™5/FRT/TO plasmid was integrated would be resistant to hygromycin B treatment. Selection generally took between 2-3 weeks, after which the positive clones were expanded and frozen stocks were prepared as described above (2.2.1.2).

2.2.1.4 siRNA transfection (Sigma reagents)

200,000 Flp-In293 cells were seeded per well in a 12-well plate for transfection the following day. For each reaction, 2 µl RNAiMax transfection reagent (Thermo Scientific) was diluted in 125 µl OptiMEM (Thermo Scientific), and 0.5 µl of each 100 µM siRNA was diluted in 125 µl OptiMEM. After incubation at RT for 5 min, the diluted transfection reagent was mixed into the siRNA dilution and incubated for 20 min at RT. During this time, the medium on the cells was exchanged with 0.75 ml fresh medium per well. 250 µl of the transfection mixture was added dropwise to each well. The final concentration of individual siRNAs per well was 50nM. The cells were incubated at 37°C for 24 h, after which they were expanded to 6-well plates. Cells were harvested 24 h later (48 h post-transfection) and cell pellets were snap frozen and stored at -80°C until further processing. Cell numbers and reagent concentrations were proportionally scaled up according to the plate well area.

2.2.1.5: cGAMP transfection

200,000 Flp-In293 cells were seeded per well in a 24-well plate for transfection the following day. For each reaction, 1.25 µl cGAMP (2 mg/ml, Invivogen) was diluted in 48.75 µl DMEM (without FBS or glutamine), and 1 µl Lipofectamine2000 (Thermo Scientific) was diluted in 49 µl OptimMEM. The cGAMP:DMEM solution was vortexed to mix. After incubation at RT for 5 min, the diluted transfection reagent was mixed into the cGAMP dilution and incubated for 25 min at RT. During this time, the medium on the cells was exchanged with 400 µl fresh medium per well. 100 µl of the transfection mixture was added dropwise to each well. The final concentration of cGAMP per well was 5 µg/ml unless otherwise stated. Cells were harvested 6 h post-transfection and cell pellets were snap frozen and stored at -80°C until further processing. Cell numbers and reagent concentrations were proportionally scaled up according to the plate well area.

2.2.1.6:Transfection of S-tagged HCIPs

1 x 10^6 Flp-In293 cells were seeded per 6 cm plate for transfection the following day. For each reaction, 1 µg of pcDNA3.1 plasmid expressing the appropriate S-tagged HCIP was diluted in 250 µl OptimMEM, and 10 µl Lipofectamine2000 was diluted in 250 µl OptimMEM. The diluted plasmid was mixed into the Lipofectamine dilution and incubated for 5 min at RT. During this time, the medium on the cells was exchanged with 4.5 ml fresh medium per well. 500 µl of the transfection mixture was added dropwise to each well. 24 h post-transfection, the medium was exchanged with 5 ml fresh medium containing the required concentration of doxycycline. Cells were harvested after 18 h of doxycycline treatment and cell pellets were snap frozen and stored at -80°C until further processing.

2.2.2 Protein biochemistry methods

2.2.2.1 Preparation of whole-cell lysate

Cells were placed on ice, washed once in ice-cold PBS and then collected using a cell scraper (Greiner) in ice-cold PBS-EDTA. The cells were transferred to a 1.5 ml Eppendorf tube and were briefly spun down at 6,000 g, 2 min, 4°C. The supernatant was aspirated and the cell pellet was lysed in the according lysis buffer (List 2.1.7) and incubated on ice for 45 min. The lysate was cleared by centrifugation at 17,000 g, 30 min, 4°C. The supernatant was collected carefully and a Bradford assay (2.2.2.2) was carried out to determine protein concentration. After the concentrations of each sample were normalized, 5 x SDS sample buffer was added to the lysates and the samples were heated at 55°C for 10 min.

2.2.2.2: Determination of protein concentration

The concentration whole cell lysate was determined by the Bradford assay. The lysate was diluted 1:5 in water. 1 µl of the dilution was pipetted into a flat-bottomed 96-well plate and 200 µl of Bradford reagent (Bio-Rad) was added on top. All samples were prepared in duplicate and measured against a BSA standard curve ranging from 0 – 2 mg/ml. A microplate reader (Tecan Sunrise) was used to measure the absorbance at 570 nm.

2.2.2.3: SDS-polyacrylamide gel electrophoresis (PAGE)

Protein samples in 1 x SDS-sample buffer were heated briefly at 55°C prior to separation on 4-12% Bis-Tris pre-cast gels (NuPAGE™, Invitrogen). Typically, 30 µg of whole-cell lysate was used. Gels were run in MES buffer (Thermo Fisher Scientific) at 160 V for 1.5 h in a cooled environment. Precision Plus Protein™ All Blue Standards (Bio-Rad) was used as a molecular weight marker.

2.2.2.4: Western blotting and detection

PVDF membrane (Amersham Hybond, 0.45 µm pore size) was activated in 100% methanol for 1 min, and subsequently transferred to a tray containing 1 x transfer buffer (List 2.1.7). Whatman paper and sponges were also equilibrated in 1 x transfer buffer. The transfer 'sandwich' consisting of two Whatman papers, PVDF membrane, protein gel, and a further two Whatman papers was carefully assembled into a plastic cassette, ensuring no air bubbles were trapped between the gel and membrane. The cassette was transferred into an electrophoretic tank containing 1 x transfer buffer and an ice-pack and was run at 100 V for 1.5 h at 4°C. Ponceau staining was used to confirm even transfer of the protein onto the membrane. The membrane was immersed in blocking solution (5% (w/v) fat-free milk/PBST) either at RT for 1 h, or at 4°C, overnight. The membrane was incubated with primary antibody (List 2.1.6) diluted in blocking solution at RT for 1 h and subsequently washed for at least 3 x 5 min with 1 x PBST. It was then incubated with HRP-conjugated secondary antibody diluted in blocking solution at RT for 1 h. The membrane was finally washed in a tray for 5 x 5 min with 1 x PBST prior to incubation with ECL for 2 min at RT prior to being developed. The signal emitted was either detected by X-ray film (Fujifilm) or by the ChemiDoc™ MP Imaging System (Bio-Rad).

Membranes were often re-probed with a different primary antibody. In cases where the host of the second primary antibody matched that of the first primary antibody, the membrane was incubated in stripping buffer (Thermo Scientific) for 10 min at RT and subsequently washed for at least 3 x 5 min with 1 x PBST. The protocol described above was then followed from the blocking stage. When the host of the second primary antibody was different to that of the first primary antibody, the membrane was incubated with 5% sodium azide (w/v) solution in the dark, overnight at 4°C. After washing for at least 3 x 5 min with 1 x PBST, the protocol described above was followed from the primary antibody stage.

2.2.2.5: Densitometry

Images acquired on the ChemiDoc™ MP Imaging System were quantified using the Image Lab™ software (Bio-Rad). This was carried out for both STING and tubulin blots, both of which were confirmed to produce a linear, and therefore quantifiable, signal. The levels of STING were normalised to those of tubulin and then further normalised to the negative control to represent the amount of STING remaining in the samples in question.

2.2.2.6 Sucrose gradient sedimentation

Solution	5 M NaCl	1 M Tris pH 7.4	0.5 M EDTA	Sucrose	H_2O
5%	1.5 ml	2.5 ml	0.5 ml	2.5 g	35 ml
10%	1.5 ml	2.5 ml	0.5 ml	5 g	30 ml
30%	1.5 ml	2.5 ml	0.5 ml	15 g	10 ml
40%	1.5 ml	2.5 ml	0.5 ml	20 g	5 ml

Table 2.1: recipe for sucrose gradient solutions

Cells were disrupted in 1% LMNG lysis buffer and a Bradford assay was carried out to determine protein concentration. 5-30% or 10-40% sucrose solutions were prepared according to Table 2.1. Solutions were supplemented with 5 ml of 10% (w/v) LMNG and H_2O was added to achieve a final volume of 50 ml. Prior to use, 1 mM PMSF was added. To prepare the gradient solutions, the 'lighter' sucrose fraction was very carefully pipetted onto the 'heavier' fraction and continuous gradients were formed by following instructions in the Gradient Master 108™ (BioComp) manual (parameters for 5-30% sucrose: short, S1/1, time = 1.36, angle = 81.5°, rpm = 19; parameters for 10-40% sucrose: short, S1/1, time = 1.48, angle = 81.5°, rpm = 17). 1 mg whole lysate was added to the gradients and the tubes were gently lowered into SW41 swing buckets. Samples were centrifuged at 39,000 rpm for 16 h at 4°C. Following centrifugation, 13 fractions, each 940 µl, were collected from each gradient. Proteins were precipitated by addition of 190 µl 50% (v/v) TCA to each fraction and subsequent incubation on ice for 1 h. Samples were centrifuged at 17,000 g for 5 min at 4°C to pellet the protein and washed twice with 1 ml of ice-cold acetone. After air-drying, the pellets were resuspended by vortexing in 100 µl 2 x SDS-sample buffer. 1 M Tris (pH 9) was used to neutralise acidic samples. Samples were incubated at 56°C for 10 min and stored at -80°C until analysis by SDS-PAGE and Western blot.

2.2.2.7 Immunoprecipitation

Each specific immunoprecipitation protocol is described in detail below; however in general, the following protocol was used. Cells were lysed in either 1% (w/v) LMNG or 1% Triton-X-100 for 1 h at 4°C and then centrifuged at 17,000 g for 30 min at 4°C. The supernatant was used to carry out a Bradford assay (2.2.2.2) and prepare input samples (2.2.2.1). 40 µl FLAG-/HA/S-agarose beads were incubated with 1 mg whole-cell lysate for 2 h at 4°C. The beads were then briefly spun down, washed three times in basic lysis buffer (without detergent or protease inhibitors) and resuspended in 150 µl 2 x SDS-sample buffer, prior to being heated at 56°C for 10 min. Proteins were analysed by SDS-PAGE Western blot.

2.2.2.8 Immunoprecipitation of ubiquitinated proteins

FLAG-HA-RNF26 and FLAG-HA-RNF26^{Y432A} -expressing FlpIn293 cells were seeded in 10 cm plates and induced for 18 h with doxycycline. Proteasome inhibited samples were additionally treated with 10 µM MG132 for 2 h. Cells were ~80% confluent at the time of harvesting. Cells were harvested as described above and lysed in 600 µl TUBE lysis buffer (List 2.1.7) and incubated on ice for 20 min. Lysates were cleared by centrifugation at 15,000 g for 15 min at 4°C. Lysates were incubated with 15 µl magnetic GST resin (Thermo Fischer Scientific) conjugated to 50 µg 1xUBA-His6 binder (UBA derived from human Ubiquilin, isoform 3), overnight at 4°C under constant rotation. The following day, the resin was washed three times using TUBE lysis buffer, dividing the samples in two prior to the last wash. Samples were then subject to control or deubiquitinating treatment.

2.2.2.9 Deubiquitination assay

Bead-bound material from ubiquitin pulldowns was resuspended in 30µl deubiquitinating-buffer (List 2.1.7) without or with 0.5 µM USP21 (Ubiquigent). Samples were incubated for 1 h at 30°C in a thermoshaker set to 750 rpm, and subsequently denatured by incubation at 65°C for 20 min in 2 x SDS-sample buffer.

2.2.2.10 *In vitro* ubiquitination assay

FLAG-HA-RNF26 and FLAG-HA-RNF26^{Y432A} -expressing FlpIn293 cells were seeded, harvested and lysed as described above (2.2.2.8). Supernatants were incubated with 12 µl magnetic FLAG resin (M2, Sigma) for 3 h at 4°C under constant rotation. The resin was washed three times in TUBE lysis buffer, dividing the samples in two prior to the last wash. Samples were subsequently washed once with *in vitro* ubiquitination buffer (List 2.1.7). The resin was resuspended in 15 µl *in vitro* ubiquitination buffer (supplemented with 0.5 mM DTT, 10 µM ubiquitin (Boston Biochem), 150 nM E1 (Enzo), and 1 µM E2 (UbcH5c, Enzo)) with or without ATP (4 mM, pH 8.0, Sigma) and incubated for 15 min at 30 C in a thermoshaker set to 750 rpm. Samples were denatured by incubation at 65°C for 20 min in 2 x SDS-sample buffer.

2.2.2.11 LC-MS/MS sample preparation

FLAG-HA-E3-expressing Flp-IN293 cells were seeded in three 15 cm plates and treated with the appropriate concentration of doxycycline for 18 h. Cells were ~80% confluent at the time of harvesting. Prior to harvesting, the workstation was cleaned thoroughly with 70% EtOH and a clean perspex shield was set up to protect the samples from excessive keratin contamination. Growth medium was aspirated and cells were gently washed with 10 ml ice-cold PBS (0.2 µm sterile-filtered) prior to being collected with a clean cell scraper (Greiner) in 5 ml ice-cold 10 nM EDTA/PBS (0.2 µm sterile-filtered). The cell suspension was transferred into a 15 ml falkon tube (Corning). Samples were centrifuged at 1,200 rpm for 2 min at 4°C and the cell pellets were resuspended in 5 ml ice-cold PBS (0.2 µm sterile-filtered). Following centrifugation at 3,000 g for 2 min at 4°C, cell pellets were snap frozen in a methanol/dry ice bath and transferred to -80°C until further processing.

Pellets were resuspended in 2 ml 1% (w/v) LMNG lysis buffer (List 2.1.7, 0.2 µm sterile-filtered prior to the addition of detergent) containing protease inhibitors and briefly vortexed. Lysis took place under constant rotation for 1 h at 4°C. Lysates were cleared by centrifugation at 17,000 g for 30 min at 4°C, and the supernatant was further centrifuged using the same settings for 15 min. Supernatants were pre-cleared overnight under constant rotation using 100 µl washed CL-4B Sepharose beads (Pharmacia). Beads were precipitated the following day by centrifugation at 3,000 g for 2 min at 4°C, and protein concentration was determined by Bradford assay (2.2.2.2). 10 mg of whole-cell lysate (in a volume of 1.8 ml) was transferred to a fresh Eppendorf tube and FLAG-HA-E3 protein complexes were immunoprecipitated with 75 µl washed FLAG-agarose slurry (M2, Sigma) under constant rotation for 2 h at 4°C. During immunoprecipitation, left-over whole-cell lysate was used to prepare ‘input’ samples as described in (2.2.2.1).

Immunoprecipitated material bound to FLAG-agarose was precipitated by centrifugation at 5,000 g for 30 sec, at 4°C. The beads were washed twice in lysis buffer (0.2 µm sterile-filtered; without detergent), followed by another two washed with 1 x TBS (0.2 µm sterile-filtered). The beads were not completely dried after the final wash.

Bead-bound protein was eluted with 100 µl 2 x SDS sample buffer (containing 10% β-Mercaptoethanol; Sigma) at 95°C for 10 min. The beads were then collected by centrifugation at 5,000 g for 30 sec at RT, allowing the eluate to be carefully collected with a gel-loading tip. 8% of the eluate volume was saved for silver staining.

Eluate volume was increased to 175 µl using ddH_2O. 5 µl 200 mM DTT (in 0.1 M Tris buffer, pH 7.8) was added to each of the samples, which were vortexed briefly and reduced by incubation for 30 min at RT. Alkylation of the samples was carried out by addition of 20 µl 200 mM IAA (in 0.1 M Tris buffer, pH 7.8), followed by a brief vortex and incubation for 30 min at RT. The final volume of the sample was 200 µl.

To remove SDS used for sample eluation, double methanol-chloroform prepcipitation was carried out. 600 µl methanol (HPLC-grade) was added to each sample, followed by 150 µl chloroform (HPLC-grade). Samples were vortexed again before adding 450 µl ddH_2O and vortexing once more. Aqueous and organic phases were separated by centrifugation at 17,000 g for 2 min at 4°C. The upper aqueous phase was pipetted off, ensuring not to disturb the protein precipitate at the interphase. 450 µl methanol was added to each sample and then vortexed. All samples were centrifuged at 17,000 g for 5 min at 4°C. The supernatant was removed using a P1000 tip inserted into a gel loading tip, to dry the protein pellets. 200 µl of ddH_2O was added and the protocol was repeated from the addition of 600 µl methanol.

In cases where peptide elution (250 µg/ml) was performed, TCA precipitation was carried out as described in 2.2.2.6. Protein pellets were vortexed in 50 µl 6 M urea (in 0.1 M Tris buffer, pH 7.8) and subsequently placed in a bath-sonicator for 2 min to ensure the sample was fully resuspended. The samples were briefly spun down and 250 µl ddH_2O was added to reduce the urea concentration to 1 M. 2 µl sequencing-grade trypsin (Promega; in 0.1 M Tris buffer, pH 7.8) was added to each sample, which was gently pipetted up and down to mix. Proteins were digested overnight at 37°C in the dark, in a thermoshaker set to 300 rpm. Pure TFA was added at a final concentration of 1% (v/v) to each sample the following day, to fully deactivate the trypsin.

C18 Sep-Pak cartridges (Waters) were used to purify trypsinised peptides. 5 ml solution 'B' (65% (v/v) HPLC-grade acetonitrile, 0.1% (v/v) TFA) was used to equilibriate the columns. 10 ml solution 'A' (2% (v/v) HPLC-grade acetonitrile, 0.1% (v/v) TFA) was subsequently added to each column and the peptide samples were carefully layered on top. Samples were run slowly into the column and washed once with 10 ml Solution 'A'. Samples were eluted with 2 x 600 µl Solution 'B' and collected in 2 ml Eppendorf tubes prior to drying by speed-vac. Dried sample was resuspended by vortexing and sonication in 20 µl Solution 'A'. Finally, samples were transferred into a glass vial and placed at -20°C for long-term storage.

2.2.2.12 LC-MS/MS settings

2 µl of purified peptides were analyzed by tandem mass spectrometry (Q Exactive-HF, Thermo Fischer Scientific) coupled to an ultra-high performance liquid chromatography (Dionex Ultimate 3000 UHPLC, Thermo Fischer Scientific) using an Acclaim™ PepMap™ 100 C18 LC Column (3 µm, 100Å, 75 µm x 50 cm, Thermo Fischer Scientific). The samples were loaded in a 0.1% (v/v) TFA solution and analysed using a 1 h linear gradient at a flow rate of 250 nl/min. For peptide elution, the gradient started at 3 min with 2% buffer 'B' (0.1% (v/v) FA and 5% (v/v) DMSO in acetonitrile) increasing to 5% buffer 'B' by 6 min followed by an increase of up to 35% by 63 min. The column was washed for 5 then 6 minutes with 99% buffer 'B'. Each analytical run lasted 100 min, allowing for re-equilibration of the column. The data were acquired with a resolution of 70,000 full-width half maximum at mass/charge 400 with lockmass enabled (445.120025 m/z), Top 15 precursor ion selection, Dynamic Exclusion of 27 s, and fragmentation performed in Higher-energy C-trap dissociation (HCD) mode with Normalized Collision Energy of 28. All samples were run in technical duplicate.

2.2.2.13 Radiolabeling and pulse-chase

6 cm plates were coated with poly-L-lysine and 700,000 Flp-In293 cells were seeded per plate. The following day, cells were treated with doxycycline for 18 h. Radiolabeling and pulse-chase were conducted according to methods described previously (Christianson et al., 2008; Schulz et al., 2017). Briefly, cells were incubated in starvation medium (methionine/cysteine-free DMEM (Lonza) + 10% dialysed FBS + 2mM glutamine) for 10 min at 37°C and subsequently labelled using ^{35}S-methionine/cysteine (EXPRE^{35}S^{35}S Protein Labelling Mix (PerkinElmer) for 10 min at 37°C. The labelling medium was rapidly aspirated and the cells were washed once with ice-cold PBS and twice in chase medium (DMEM + 10% FBS + 2mM glutamine + 50 mM methionine + 50 mM cysteine). Cells were incubated for the required chase time-points and subsequently harvested. Cell lysates were prepared in 1% Triton-X-100 lysis buffer and subject to immunoprecipitation (2.2.2.14). Immunoprecipitated protein samples were separated by SDS-PAGE and gels were dried for 1 h at 80°C. A phosphoimager was used for visualization and Image Lab™ software was used for quantitation.

2.2.2.14 Immunoprecipitation of rabiolabelled protein lysate

^{35}S-labeled lysates were pre-cleared overnight by rotation with 80 µl of CL-4B sepharose beads (Pharmacia) at 4°C. The following day, samples were briefly centrifuged at 3,000 rpm for 1min at 4°C and the supernatant was carefully transferred to a fresh tube. 5 µl of purified HA antibody (12CA5 clone; lab hybridoma stock) was added to the lysate and rotated for 2 h at 4°C. 70µL of Protein G agarose (Roche) was then added to each sample and rotated for a further 1.5 h at 4°C. The supernatant was aspirated and the beads were washed in 1ml lysis buffer (without detergent). The wash step was repeated once using high salt lysis buffer and then once more with lysis buffer. The beads were resuspended by briefly vortexing in 40 µl 2 x SDS sample buffer and incubated at 65°C for 15 min.

2.2.3 Molecular biology - methods for DNA and RNA

2.2.3.1 RNA extraction

Cells were placed on ice, washed once in ice-cold PBS and then collected using a cell scraper (Greiner) in ice-cold PBS-EDTA. The cells were transferred to a 1.5 ml Eppendorf tube and were briefly spun down at 6,000 g, 2 min, 4°C. The supernatant was aspirated and the cell pellet was solubilized using buffer RLT + β-mercaptoethanol. The rest of the protocol followed manufacturer's instructions from the RNeasy kit (Qiagen). RNA was eluted from the column in 30 µl nuclease-free water.

2.2.3.2 cDNA synthesis

Using the QuantiTect Reserve Transcription kit (Qiagen), ~200 ng RNA was used for cDNA synthesis. The manufacturer's instructions were followed, however reaction volumes were halved to achieve a final volume of 10 µl. cDNA was diluted 1:10 using nuclease-free water.

2.2.3.3 qRT-PCR

The recipe for each PCR reaction was as follows: 5 µl 1:10 cDNA dilution; 7.5 µl GoTaq® qPCR Master Mix (Promega); 0.45 µl 10 µM forward primer; 0.45 µl 10 µM reverse primer; 1.6 µl sterile nuclease-free H_2O. An annealing temperature of 60°C was used for the designed primer pairs (List 2.1.3.1). Reactions were performed in a Rotor-Gene® Q Thermal Cycler (Qiagen). *Actin* was used as the housekeeping gene for normalization. The $\Delta\Delta C_t$ method was used to determine relative gene expression.

2.2.3.4 Taqman qRT-PCR

The recipe for each PCR reaction was as follows: 5 µl 1:10 cDNA dilution; 7.5 µl Taqman™ Universal PCR Master Mix (Thermo Fisher Scientific); 0.6 µl Taqman probe; 1.9 µl sterile nuclease-free H_2O. Pre-developed Taqman probes against human *GAPDH* (Hs02758991_g1, Life Technologies) and *IFIT1* (Hs03027069_s1, Life Technologies) were used. Reactions were performed in a 96-well plate format in a StepOnePlus™ Thermal Cycler (Thermo Fisher Scientific) using the standard 2 h program. *GAPDH* was used as the housekeeping gene for normalization. The $\Delta\Delta C_t$ method was used to determine relative gene expression.

2.2.3.5 XBP1 splicing assay

The recipe for each PCR reaction was as follows: 1 µl cDNA; 1 µl 20 µM *XBP1* forward primer; 1 µl 20 µM *XBP1* reverse primer; 12.5 µl MyTaq Red Mix, 9.5 µl nuclease-free H_2O. Primer sequences and details of the PCR program are from (Lin et al., 2007). The PCR products were run on a 2.5% (w/v) agarose gel.

2.2.3.6 NanoString® Assay

RNA was extracted using the RNeasy kit (Qiagen) according to manufacturer's instructions, ensuring to include the genomic DNA digestion step with DNaseI (Qiagen). 150 ng RNA was added to each hybridization reaction, composed of 10 µl hybridization buffer, 10 µl Reporter CodeSet, 10 µl Capture ProbeSet. Reactions were incubated in a thermocycler at 65°C for 18 h. Samples were subsequently loaded in the PrepStation according to manufacturer's instructions. During this stage, hybridized probe/target complexes were immobilized on the nCounter® Cartridge which was then imaged in the Ditigal Analyzer on the high-resolution setting. Data were analysed following user guidelines (NanoString® Technologies).

2.2.4 Molecular biology – methods in cloning

2.2.4.1 Restriction enzyme-based cloning:

The plasmids referred to as pFL001 and pFL002 are modified versions of the pcDNA™5/FRT/TO vector (Invitrogen) carrying the FLAG-HA-tag sequence in the multiple cloning site (MCS), for N-terminal and C-terminal tagging, respectively (List 2.1.2). ORFs for each E3 ligase (Table 2.2) were amplified with Phusion® High-Fidelity DNA polymerase (2.2.4.2) using primers with restriction site sequences at their 5' termini (List 2.1.3.2). The required plasmid and amplified ORF were subsequently digested using the same pair of restriction enzymes (2.2.4.5) and ligated using the T4 DNA ligase (2.2.4.8). Competent DH5α cells were transformed and incubated on ampicillin LB-plates overnight (2.2.4.9). Colonies were selected for culturing and the prepared plasmid DNA (2.2.4.10) was sent for sequencing (Source Bioscience/Eurofins). Sequences were verified using Serial Cloner software (version 2.6.1). Vectors pFL001 and pFL002 carrying E3 ORFs were used for stable cell line generation (2.2.1.3). The same workflow was employed for generating S-tagged HCIPs using the modified pcDNA3.1 vector (List 2.1.2). HCIP ORFs were all obtained from the Mammalian Gene Collection (MGC) and were amplified using primers in List 2.1.3.3. In this case, the resulting plasmids containing S-tagged HCIP ORFs were used for transient transfection (2.2.1.7). Detailed protocols for each of the cloning steps are described below.

ORF	Source
BFAR, CGRRF1, RNF103, RNF128, RNF145, RNF148, RNF185, RNFT1, TRIM13, TRIM59, ZNRF4	MGC (Mammalian Gene Collection)
AMFR	Thermo Fischer Scientific
Hrd1	Lab stock
MARCH2, MARCH3, MARCH4, MARCH8, RNF5, RNF139, TMEM129	Lehner lab (University of Cambridge)
MARCH6	Wiertz lab (UMC Utrecht)
RNF150	Neuroblastoma
RNF170	PlasmID repository (Harvard Medical School)

Table 2.2: Sources of E3 ORFs used to generate FLAG-HA-tagged E3 sequences.

2.2.4.2 Polymerase chain reaction

Target DNA (~100 ng) was amplified using Phusion® High-Fidelity DNA polymerase (NEB) in 50 µl reactions, according to manufacturer's instructions. If DMSO was not sufficient to enhance amplification, 1 M Betaine was used instead. Serial Cloner (version 2.6.1) was used to help determine the annealing temperatures for the specific primer pair. Reactions were performed in a C1000™ Thermal Cycler (Bio-Rad).

2.2.4.3 Agarose gel electrophoresis

1% (w/v) agarose was heated in 1 x TAE buffer (50 x stock, Thermo Scientific) and upon cooling, peqGREEN dye (VWR) was added at a concentration of 1:10,000 prior to the gel being cast. Gel Loading Dye (NEB) was added to purified PCR products, digested plasmids and 1 Kb Plus DNA Ladder (Thermo Fischer Scientific). Samples were loaded onto the gel, which was run at 120 V in 1 x TAE buffer, for the appropriate amount of time.

2.2.4.4 Purification of DNA from agarose

DNA separated by agarose gel electrophoresis was visualized by UV-light. The appropriate bands were excised with a clean scalpel and transferred into a clean 1.5 ml Eppendorf tube. DNA purification was carried out using the QIAquick Gel Extraction Kit (Qiagen) according to manufacturer's instructions. DNA was eluted in a volume of 30 µl.

2.2.4.5 Restriction enzyme digestion

Gel-extracted PCR products were incubated with 1 µl restriction enzyme (NEB) using the appropriate buffer (https://nebcloner.neb.com/#!/redigest) in a final volume of 50 µl, for 1 h at 37°C. For 1 µg plasmid DNA, 1 µl restriction enzyme was used in a final volume of 20 µl. Plasmid DNA was digested for 3 h at 37°C, and was subjected to agarose gel electrophoresis to determine digestion efficiency.

2.2.4.6 PCR product purification

The QIAquick PCR Purification Kit (Qiagen) was used for purification of PCR products and digested PCR products, following manufacturer's instructions. DNA was eluted in a volume of 30 µl.

2.2.4.7 Determination of nucleic acid concentration

NanoDrop™2000 spectrophotometer (Thermo Fischer Scientific) was used to measure absorbance at 260 nm and 280 nm, hence determining concentration and purity of both DNA and RNA samples.

2.2.4.8 DNA ligation

Ligation reactions took place between the digested, gel-purified plasmid, and the digested, purified PCR product, at a molar ratio of 1:3, using the T4 DNA Ligase (NEB) for 20 min at RT.

2.2.4.9 Transformation of competent *E.coli*

DH5α competent bacteria (lab stocks) were thawed on ice for 15 min. The entire ligase reaction was added to 100 µl bacterial suspension, which was then incubated on ice for a further 15 min. Bacteria were heated-shocked at 42°C for 45 sec, and then immediately placed on ice for 2 min. Since all plasmids used for transfection were ampicillin-resistant, the bacteria could be plated onto LB-agar + 100 µg/ml ampicillin and incubated for 18 h at 37°C. The following day, colonies could be selected for culture inoculation in 4 ml LB-broth + 100 µg/ml ampicillin for 18 h at 37°C.

2.2.4.10 Small-scale preparation of plasmid DNA

'Minpreps' were carried out using the PureYield™ kit (Promega), starting with 3 ml of overnight culture. Purified DNA was eluted in a volume of 30 µl.

2.2.5 Imaging

2.2.5.1 Immunofluorescence

170,000 Flp-IN293 cells were seeded in wells of a 12 well plate which contained PLL-coated 13 mm diameter cover slips. The following day cells were induced with doxycycline for 18 h. The cells were washed once in PBS and then fixed with 4% (w/v) PFA for 20 min at RT. After two washes in PBS the cells were then permeabilised with 0.2% (v/v) Triton-X-100 for 5 min at RT, and then washed twice more in PBS. Incubation with 0.2% (v/v) PBG for 30 min followed. The cells were incubated with 1° antibody (in 0.2% PBG) for 1 h at RT. The cells were washed twice in PBS and then incubated with Alexa-Fluor 2° antibody (in 0.2% PBG) for 1 h at RT, in the dark. The cells were washed once in PBS, and then once in ddH_2O, prior to incubation with DAPI (1:10,000 dilution in ddH_2O) for 10 min at RT, in the dark. The cells were finally washed twice in ddH_2O before mounting each cover slip onto ProLong® Gold antifade reagent (Life Technologies). The slides were left to dry overnight in the dark at RT, and the following day were sealed with clear nail polish and stored at 4°C in the dark. Images were acquired using a confocal microscope (Zeiss, 710) at 63 x magnification.

2.2.6 Data Analysis

2.2.6.1 Statistical analysis

Nanostring™ data was analysed using multiple t-tests (Holm-Sidak method, $\alpha = 0.05$) comparing untreated and Tunicamycin-treated (Tm, 500 ng/ml, 8 h)/SubtilaseAB$_5$-treated (10 ng/ml, 8 h) samples, to determine the statistical significance of the fold-change of E3 transcripts and selected ERAD components. All other data was analysed using a two-tailed paired t-test comparing non-targeting control siRNA (siNTC) to each siRNA target. All statistical analysis was carried on GraphPad Prism (Version 7.0).

2.2.6.2 LC-MS/MS data analysis

Over $1.5x10^6$ spectra were identified by LC-MS/MS. Chromatogram alignment and protein abundance was determined by uploading raw data files onto Progenesis QI (nonlinear Dynamics) and the SwissProt database was used to identify peptides. Using methods described in Keilhauer *et al*., 2015 (Keilhauer et al., 2015), a background proteome was defined and used to normalize the dataset to allow direct comparison between all samples. First, the mean intensity of each identified protein from both technical duplicates was calculated and logarithmized. The standard deviation (SD) of proteins found in all samples was calculated and plotted against the SD rank. The background proteome (BP) was defined as the bottom 90% percentile, with this cohort displaying the least variation between all samples. The BP was used to calculate the median intensity for each sample and this value was used for median normalization. The Cyclic-Loess method was then used to standardize sample distributions without forcing equal distribution. To define fold-changes, the intensity was divided by the mean intensity of that protein across all samples (referred to as the 'Bait-specific control group' in Keilhauer *et al*., 2015). Fold-changes were converted to *p-values* using MaxQuant Significance A (Cox and Mann, 2008). A series of filtration steps were imposed on the dataset to define high-confidence interactors (HCIPs). Firstly, a threshold of >0.05 was applied to the *p-value* scores. Subsequently, hits with negative fold changes and only identified by 1 peptide were removed. Finally, contaminants (defined as nuclear or cytoskeletal proteins) were also removed from the list (a detailed description of the analysis is provided in Chapter 4).

Using the MS/MS data, SINQ quantitation (Trudgian et al., 2011) was also carried out to identify interactors unique to one E3 only, which would not be assigned a *p-value* with the above-described comparative analytical method (see Chapter 4).

Chapter 3

Development of cellular resources and proteomics protocols to generate E3 ligase interaction networks

3.1 Rationale

For well-characterised E3s, such as Hrd1, it is evident that these enzymes form macromolecular complexes with cofactors. Components of these complexes can: deliver and mediate substrate interactions; contribute to substrate dislocation into the cytosol; control ubiquitination; and escort ubiquitinated species away from the ER. It is the interactions with both adaptor proteins (complex components) and substrates which define E3 function. However, most E3 ligases remain uncharacterised in terms of the interactions they form. Therefore, to discover and compare the interactions formed within this E3 family, an affinity-purification LC-MS/MS strategy was employed.

Initially, immunoprecipitation (IP) of each endogenous complex was considered, however there were two limiting factors to this approach. Firstly, there was a lack of antibodies available specifically for IP for several of the E3s, meaning an interaction network could not be produced for the whole E3 family. Secondly, the use of different antibodies would introduce significant variation between samples, making comparison of each E3 IP profile very challenging. Hence, each E3 ORF was instead engineered to have either an N- or C-terminal FLAG-HA (FH) tag. These constructs were used to generate stable cell lines using the Flp-In T-Rex HEK293 (Flp-In293) system. The Flp-In293 cells used were also doxycycline inducible, allowing the timing and amount of FH-tagged E3 gene expression to be controlled. IP of each E3 complex via the FH-tag would hence permit comparative proteomic profiling and subsequent determination of high-confidence interaction networks for each E3.

3.2 Results

3.2.1 Generation of Flp-In293 stable cell lines expressing FH-tagged E3s

To generate stable, inducible cell lines expressing epitope-tagged versions of each E3, the Flp-In recombination method was used. The plasmids referred to as pFL001 and pFL002 are modified versions of the pcDNA™5/FRT/TO vector (Invitrogen), which were engineered to carry the FH sequence in the multiple cloning site (MCS). The two plasmids were used for N-terminal and C-terminal tagging, respectively. Initially, the position of the epitope tag was based on predicted topology (in particular the presence of a signal sequence) and experimental localisation evidence from previous studies (Maruyama et al., 2008; Neutzner et al., 2011; van den Boomen et al., 2014). Hence, ORFs for each E3 ligase were subcloned into either the pFL001 or pFL002 vector and transfected into WT Flp-In293 cells along with another vector expressing the Flp recombinase. The latter promotes homologous recombination at the Flp recombination target (FRT) sites present in both the pcDNA™5/FRT/TO vector, and at a specific locus in the Flp-In293 genome. Cells in which this recombination took place were resistant to hygromycin treatment. Clones selected by this treatment were used to create a mixed population. Figure 3.1 below presents the workflow followed to construct these cell lines.

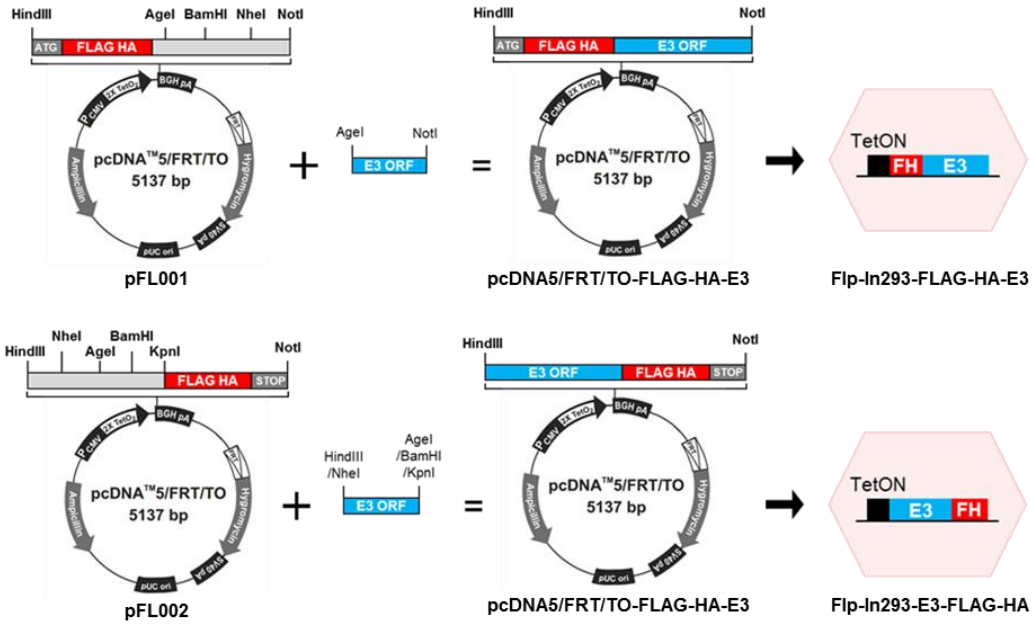

Figure 3.1: Generation of stable Flp-In293 cell lines encoding FH-tagged E3s. Illustration of the cloning procedure to create N- or C-terminally tagged E3 ORFs and subsequent Flp-In293 stable cell generation.

3.2.2 Testing FH-tagged E3 protein expression and localisation

To test epitope-tagged E3 protein expression, doxycycline (DOX) titrations were performed on each cell line. A range of DOX concentrations (1ng/ml, 10ng/ml, 100ng/ml and 1µg/ml) was used and in addition, a 1µg/ml DOX treatment was combined with MG132 (10µM) to inhibit proteasomal degradation and facilitate detection of unstable E3s. Anti-FLAG Western blots (WB) were carried out to analyse expression from whole-cell lysate (WCL). FH-tagged BFAR, MARCH6, RNF13, RNF103, RNF128, RNFT1 and TRIM59 were not detectable by WB, and therefore the tag on these E3 was re-located to the opposite terminus. New cell lines were generated for the 're-tagged' E3s, and subjected to the same DOX titration followed by anti-FLAB WB. Re-positioning the tag enabled detection of these E3s by WB. Of note, cell lines expressing FH-tagged RNF145 and RNF150 had not been generated at this stage, due to difficulties in cloning. Figure 3.2 shows the successful induction and detection of 23 FH-tagged E3s by DOX titration.

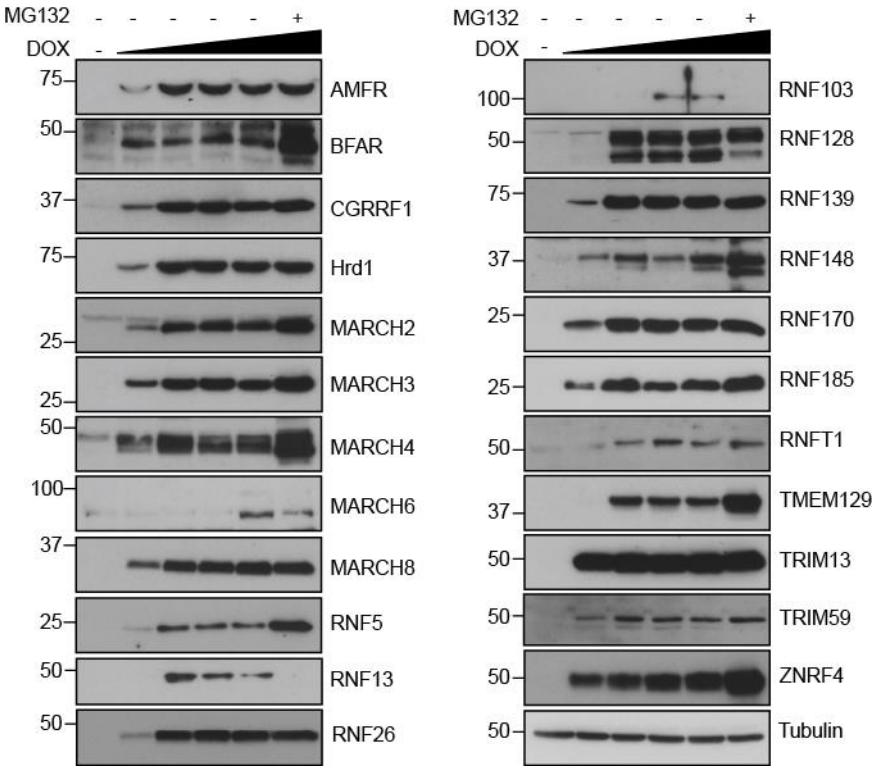

Figure 3.2: Testing FH-tagged E3 protein expression by DOX titration. Anti-FLAG WBs from WCL originating from Flp-In293 cells encoding FH-tagged E3s, subject to doxycycline titration (18h) and MG132 treatment (4 h). Panels show the strongest FLAG-positive signal at the expected molecular weight. Unstimulated cells were treated with DMSO. The tubulin blot serves as a loading control and is representative of each WB shown.

Based on these WBs, DOX concentrations were chosen to enable detectable expression of each E3, whilst attempting to limit overexpression. Table 3.1 shows the concentrations of DOX used for each cell line in the following experiments, and also illustrates the final tag position for each of the E3s.

E3	[DOX]	E3	[DOX]	E3	[DOX]	E3	[DOX]
AMFR-FH	1	MARCH4-FH	1	RNF103-FH	100	FH-RNFT1	10
FH-BFAR	1	FH-MARCH6	1000	RNF128-FH	10	TMEM129-FH	1
CGRRF1-FH	1	MARCH8-FH	1	RNF139-FH	10	TRIM13-FH	1
Hrd1-FH	1	FH-RNF5	10	RNF148-FH	1	TRIM59-FH	10
MARCH2-FH	10	RNF13-FH	1	RNF170-FH	1	ZNRF4-FH	1
MARCH3-FH	1	RNF26-FH	1	RNF185-FH	1		

Table 3.1: DOX concentrations used for the specified Flp-In293 cell lines. All DOX treatments were 18 h. The 'E3' column refers to the cell line expressing that particular tagged E3.

Using the cell lines and DOX concentrations from Table 3.1, immunofluorescence (IF) was carried out to determine that overexpression of the tagged-forms of each ligase did not result in mislocalisation from the ER (Figure 3.3). The ER-markers Calnexin (CNX) or KDEL were used to confirm co-localisation with the FH-tagged E3.

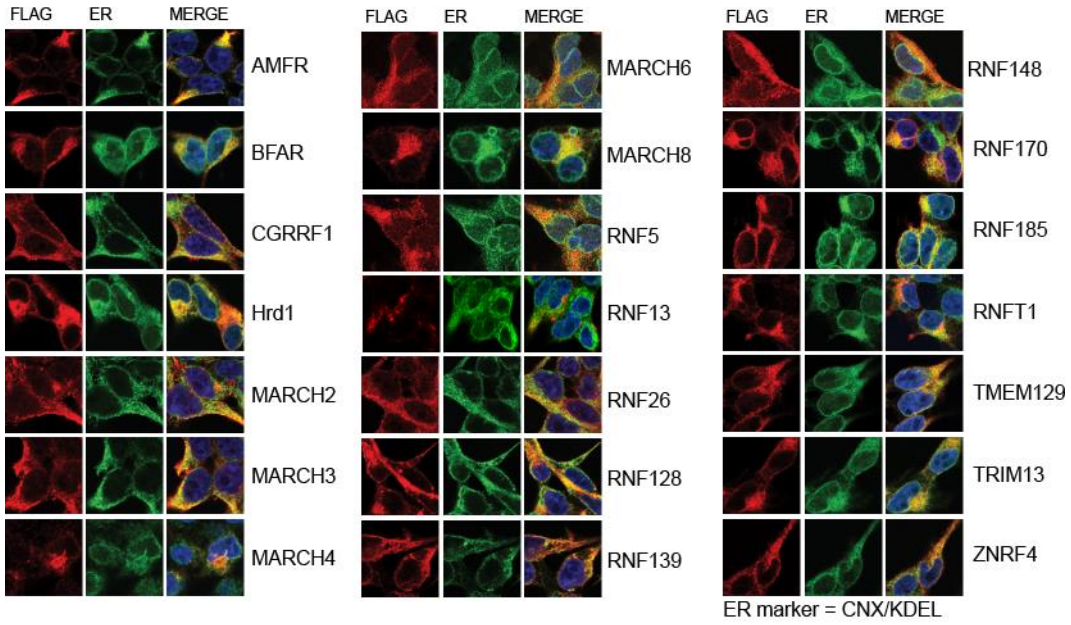

Figure 3.3: Testing FH-tagged E3 localisation by immunofluorescence. Immunofluorescence of DOX-induced Flp-In293 cell lines expressing FH-tagged E3s. Anti-FLAG (ms), anti-CNX/KDEL (Rb) and the corresponding Alexa-Fluor® secondary antibodies were used to stain E3s and the ER, respectively. Nuclei were stained using DAPI. ImageJ software was used to alter the contrast to generate images with a more comparable signal intensity.

RNF103-FH and TRIM59-FH were not detectable by IF, presumably due to low expression levels. All other tagged E3s were found to co-localise with the ER markers used. It is important to note that dense, concentrated areas of FLAG-positive signal were not observed in the cell lines imaged (with the exception of RNF13) indicating that overexpression of these FH-tagged E3s is unlikely to result in the formation of large, insoluble aggregates.

3.2.3 Monitoring ER stress upon FH-tagged E3 overexpression

Epitope-tagging proteins can alter their structure and thus cause them to misfold (Zordan et al., 2015). Misfolded proteins are less likely to form native interactions and would instead be susceptible to recognition by components of the ER quality control machinery. The accumulation of misfolded or unfolded proteins causes ER stress, which can be monitored by the splicing of the *XBP1* transcript (see Chapter 1, section 1.3.3). Therefore, to determine whether tagging or overexpression of this family of ligases caused ER stress, an *XBP1* splicing assay was performed on cDNA generated from each E3-expressing Flp-In293 cell line. Treatment with Tunicamycin (Tm), which causes ER stress by inhibiting *N*-linked glycosylation (Merlie et al., 1982), was used as a positive control (Figure 3.4).

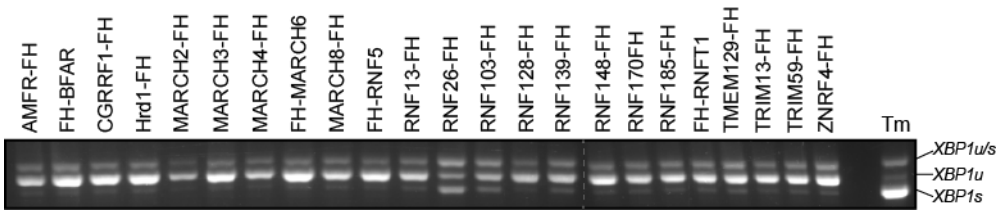

Figure 3.4: Monitoring ER stress upon FLAG-HA-tagged E3 expression. *XBP1* splicing assay on cDNA from DOX-induced Flp-In293 cell lines expressing FH-tagged E3s. Tunicamycin (Tm) (500 ng/ml, 8 h) was used on WT Flp-In293 cells as a positive control. The lower band shows spliced *XBP1*, the middle band is the unspliced form, whereas the top band is hybrid of both spliced and unspliced *XBP1* **(Lin et al., 2007)**.

Overexpression of all FH-tagged E3s did not cause *XBP1* splicing, with the exception of RNF26-FH, and to a much lesser extent RNF103-FH. The splicing caused by RNF26-FH overexpression was less than that observed as a result of Tm treatment, but more than the very mild stress response observed upon RNF103-FH overexpression. Overall, however, this result demonstrates that the tagged E3s are unlikely to accumulate as unfolded or misfolded forms in the ER.

3.2.4 Comparing endogenous and exogenous Hrd1 complexes

Since the main aim of the project was to discover interactions formed by the ER-resident E3s, different detergents were compared for their ability to preserve macromolecular membrane protein complexes. To do this, we took advantage of the well-characterised Hrd1 complex, carrying out SEL1L immunoprecipitations (IPs) from WT Flp-In293 cells solubilised in nine different detergents. SEL1L is the principal interactor of Hrd1 and therefore subsequent immunoblotting (IB) for the Hrd1 complex components (OS-9, Herp1, Fam8A1, Ube2j1) enabled the stringencies of each detergent to be compared. The IP profiles produced from Digitonin and lauryl maltose neopentyl glycol (LMNG) lysis were strikingly similar, with both preserving all tested interactions within the complex (Figure 3.5a). LMNG belongs to the group of recently developed MNG amphiphiles, which have been shown to preserve native membrane protein complexes and are compatible for use with LC-MS/MS (Chae et al., 2010).

To test whether E3 overexpression would drive non-native complex formation, the interaction profiles of endogenous and exogenous Hrd1 complexes were compared. Anti-FLAG and anti-Hrd1 IPs were performed on LMNG-solubilised lysate from DOX-induced Flp-In293-Hrd1-FH cells and WT Flp-In293 cells (Figure 3.5b).

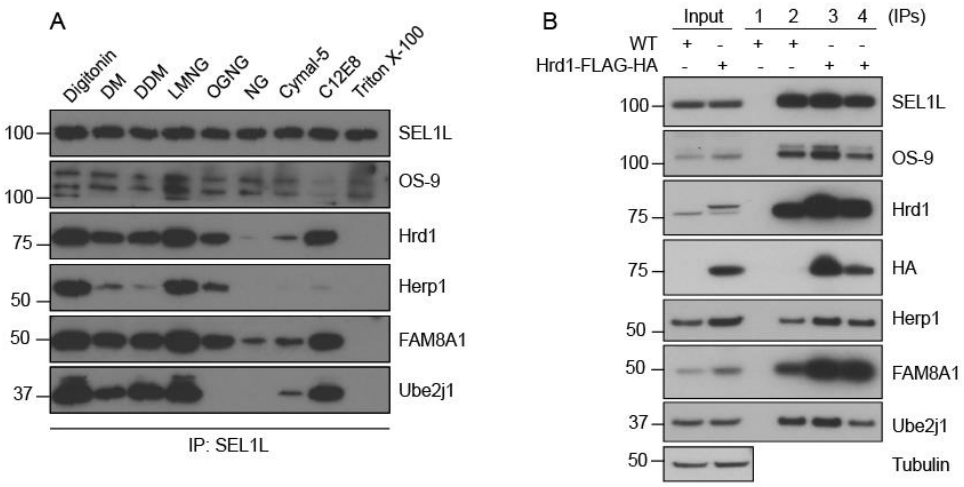

Figure 3.5: Comparing endogenous and exogenous Hrd1 interactions. (a) WT Flp-IN293 cells were solubilised in either: Digitonin, DM, DDM, LMNG, OGNG, DMNG, Cymal-5, C12E8, or Triton-X-100 (all 1% w/v). 500 µg WCL from each condition was used for anti-SEL1L IP, followed by SDS-PAGE and IB of the Hrd1 complex components. (b) DOX-induced Flp-In293-Hrd1-FH cells and WT Flp-In293 cells were solubilised in 1% LMNG. 500 µg WCL from either condition was used for both anti-FLAG and anti-Hrd1 IPs. 20% input (WCL) and IP samples were subject to SDS-PAGE and IB of the Hrd1 complex components. Lanes marked 1 and 3 are from FLAG IPs and lanes 2 and 4 are from Hrd1 IPs.

These results show that the IP profiles of both WT and overexpressed, tagged Hrd1 are highly comparable, and therefore demonstrate that exogenous Hrd1 is able to interact with its endogenous, native cofactors.

Following from these results, sucrose gradient sedimentation was employed to validate that overexpressed Hrd1-FH assembled into complexes akin to endogenous Hrd1. Figure 3.6 shows the sucrose sedimentation profiles of both WT and exogenous Hrd1 complexes. WT Hrd1 complex components co-sediment predominantly between fractions 5-8, which was also the case for the FH-tagged Hrd1 cofactors. It was noted that components of the tagged-Hrd1 complex did also migrate to the lower fractions, however this is likely to represent partially assembled complexes, that may arise if cofactors become limiting.

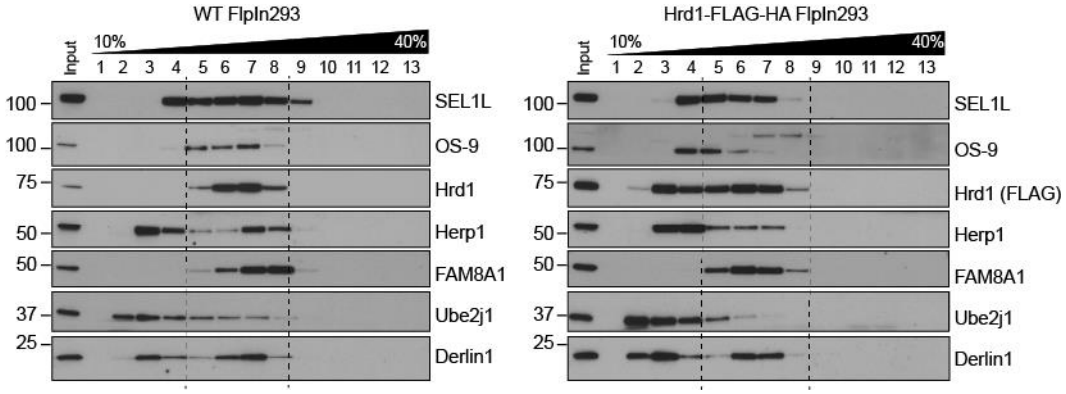

Figure 3.6: Comparing endogenous and exogenous Hrd1 complex assembly. DOX-induced Flp-In293-Hrd1-FH cells and WT Flp-In293 cells were solubilised in 1% LMNG. 500 µg WCL was loaded onto 10-40% sucrose gradients and sedimented by ultra-centrifugation. Collected fractions were TCA-precipitated. 20% input (WCL) and precipitated samples were subject to SDS-PAGE and IB of the Hrd1 complex components.

Collectively these data indicate that neither E3 overexpression nor tagging interferes grossly with the formation of protein-protein interactions or complex assembly, validating our approach for discovering novel E3 interactors.

3.2.5 Optimisation of LC-MS/MS sample preparation for discovering novel E3 interactors

Having selected LMNG to preserve E3 complexes, the next step to optimise was the elution of the complexes from the affinity matrix. Anti-FLAG covalently-linked to agarose beads were used for pulldown, and therefore the affinity-captured complexes could be eluted with either FLAG peptide, or more stringent reagents, such as sodium dodecyl sulphate (SDS) sample buffer. Elution with peptide results in the more specific release of protein complexes bound to the FLAG-antibody. However, the recovery of bead-bound material is often inefficient. SDS elution, on the other hand, is less selective, as it simply disrupts all protein-protein interactions by denaturation, including non-specific proteins captured within the affinity matrix. The advantage is that recovery is nearly 100% efficient.

To compare both types of elution, Hrd1-FH complexes were eluted from FLAG-agarose resin using either FLAG peptide or SDS sample buffer. WT Hrd1 complexes were used as a positive control, using anti-Hrd1/Protein G-agarose for pulldown, and either Hrd1 peptide or SDS sample buffer for elution. All samples were analysed by LC-MS/MS and the proteins identified were plotted in Venn diagrams (Figure 3.7).

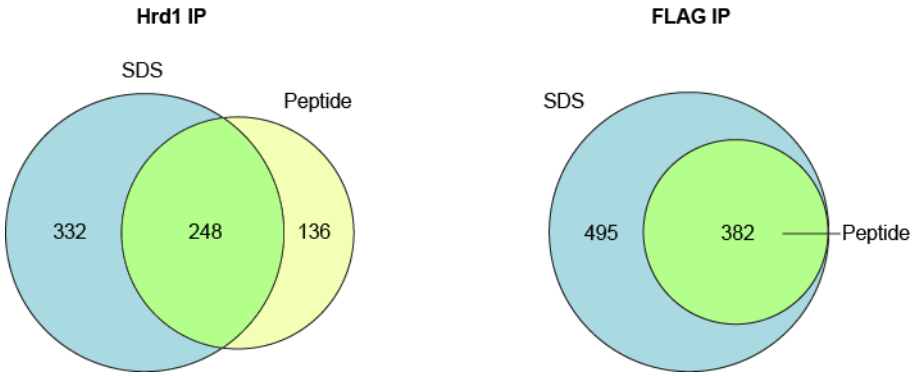

Figure 3.7: Venn diagrams of proteins identified by LC-MS/MS following either SDS or peptide elution. Samples were eluted from Hrd1 IP of endogenous Hrd1 complexes (left) and FLAG-IP of Hrd1-FH complexes (right). IPs were from 1 mg of WCL.

As expected, a greater number of proteins were identified following SDS elution compared with peptide elution. Importantly, Hrd1 cofactors (SEL1L, OS-9, XTP3-B, Herp1, FAM8A1, and Ube2j1) were detected in both elutions from either pulldown. It was reasoned that since SDS elution would increase the recovery of both specific and non-specific interactions, it would facilitate downstream data analysis by enabling normalisation of the proteomes associated with each FH-tagged E3 IP sample (discussed in greater detail later in this chapter and in chapter 4).

3.2.6 Sample preparation of E3 protein complexes for LC-MS/MS

Following optimisation of the solubilisation and elution conditions, the 23 cell lines were stimulated with the appropriate DOX concentration for 18 h (Table 3.1), and subsequently all simultaneously prepared for LC-MS/MS following the illustrated workflow (Figure 3.8). Briefly, all samples were lysed in 1% LMNG buffer, and 10 mg WCL was used for each of the 23 FLAG IPs. Immunoprecipitated material was eluted with SDS, then reduced and alkylated, prior to double-chloroform/methanol precipitation. Samples were finally digested with trypsin, purified on C18 columns and subject to LC-MS/MS (see Protocol 2.2.2.11 for detailed methodology).

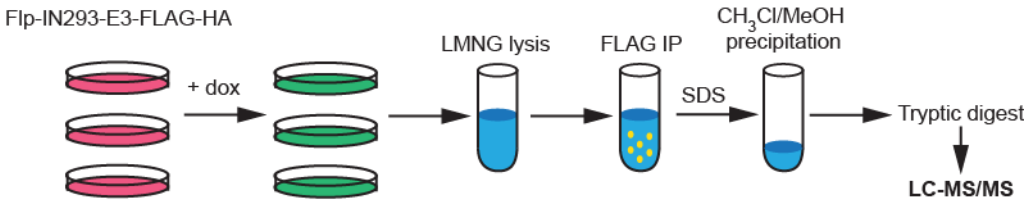

Figure 3.8: Basic workflow of the sample preparation protocol for LC-MS/MS of E3 complexes.

Throughout the workflow, WCL lysate from each sample was prepared for WB and ~8% of the SDS-eluted material was retained for analysis by silver stain. Analysis of WCL lysate by WB revealed a large range of steady-state expression levels between the different FH-tagged E3s (Figure 3.9).

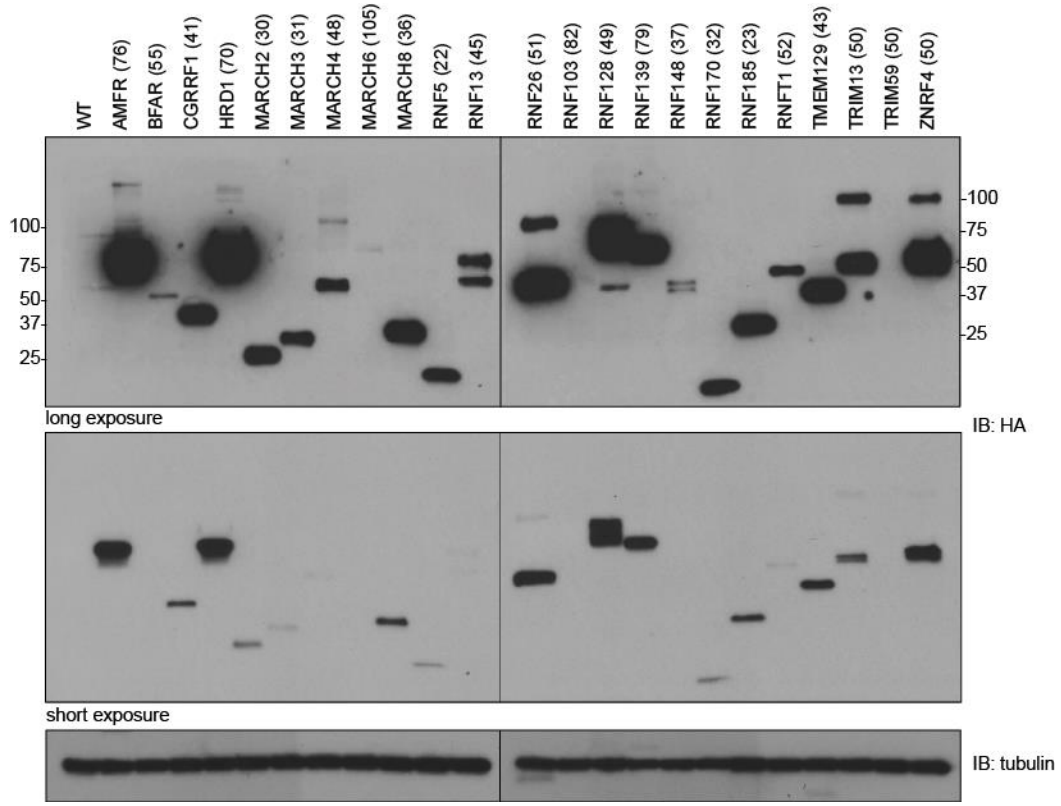

Figure 3.9: Protein expression levels of FH-tagged E3s submitted for LC-MS/MS (1st batch). 50 µg of WCL from each of the 23 Flp-In293 cell lines expressing FH-tagged E3s was subject to SDS-PAGE and HA IB. The expected MW is written in parenthesis above each E3 name. Tubulin was used as a loading control.

Despite earlier detection of FLAG-positive signal (Figure 3.2), RNF103 and TRIM59 were not detected by HA WB. The remaining 21 E3s were detected as a single band at the expected molecular weight (MW) with the exception of: RNF13; RNF26; RNF128; RNF148; TRIM13; and ZNRF4, all of which displayed two HA-positive bands. For RNF13, RNF128 and RNF148, the higher MW band most likely represents a glycosylated form. This agrees with published data for RNF13 (Zhang et al., 2008), and sequence predictions for RNF128 and RNF148 (Source: UniProt). The higher MW HA-positive band in RNF26, TRIM13 and ZNRF4, is roughly twice the size of the lower (expected) MW band, and therefore may represent SDS-resistant dimers. Of note, RNF170 was detected at a significantly lower MW than expected, although this is consistent with published results (Wright et al., 2015).

Despite the differences in steady-state expression levels between the family of ER-resident E3s, silver stain analysis of the eluate revealed highly comparable amounts

of total protein in each sample (Figure 3.10). The homogeneity observed at this stage is most likely due to the elution conditions and therefore the presence of a largely consistent population of non-specific 'background' proteins in each eluted sample.

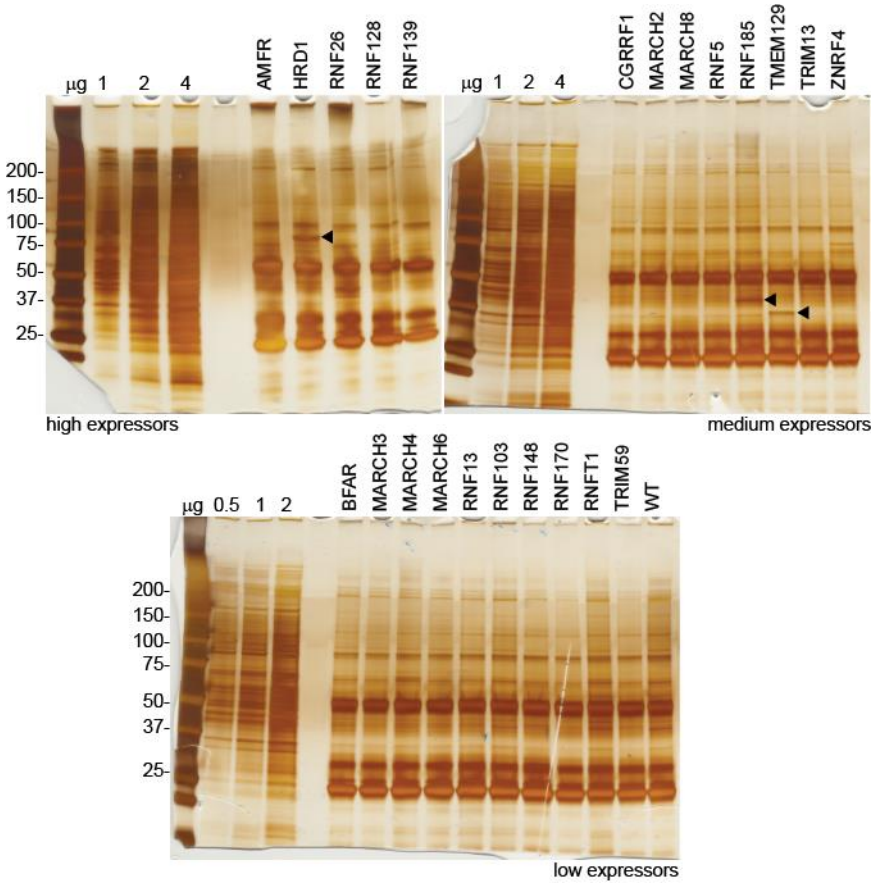

Figure 3.10: Silver stain of LC-MS/MS sample eluates (1st batch). SDS-PAGE gel loaded with 8% (volume) of the sample eluted from FLAG-agarose in SDS buffer. E3 complex samples were grouped into high- medium- and low-expressors, based on the results in Figure 3.9. The black arrows mark the band corresponding to the MW of the E3 in that sample. Between 0.5 and 4 µg of WCL from WT Flp-In293 cells was loaded as a reference for protein amount.

Following LC-MS/MS of the above 23 samples, chromatogram alignment was performed on Progenesis-QI software, followed by peptide identification using SwissProt. In total, over 2,000 individual protein signatures were identified, with approximately 1,600 proteins present in each E3 sample. This confirms that a large proportion of proteins are found in all samples, in agreement with a largely consistent background proteome across the dataset, and the results in Figure 3.10 above.

3.2.7 LC-MS/MS troubleshooting: undetectable and anomalous E3s

Using the visualisation tools on Progenesis-QI, it was immediately apparent that each E3 was strongly enriched in its corresponding sample, with the only exception being RNF13 (data not shown[1]). Although RNF13-FH was easily detectable by WB, it was not enriched relative to other samples and instead appeared to have near-uniform expression across the dataset (as would be expected for an abundant common contaminant). Additionally, despite TRIM59-FH being enriched in its appropriate sample, it was only identified by two unique peptides, which was much lower compared with all other E3 baits[1].

Interestingly, ATF6 was strongly enriched in the RNF26 sample (data not shown). This finding together with the *XBP-1* splicing observed downstream of RNF26-FH expression (Figure 3.4), raised the question of how RNF26 *bona fide* interactions would be discovered if ER stress was induced by RNF26-FH misfolding. Analysis of the RNF26 C-terminus revealed that the penultimate residue was a hydrophobic tyrosine (Y432, Figure 3.11a). The equivalent residue in the cytosolic ligase, RNF4, is crucial for maintaining the C-terminal RING-domain structure and coordinating its catalytic activity (Plechanovová et al., 2011). This led to the hypothesis that the C-terminal FH-tag may interfere with structure and/or function of RNF26. The FH-tag

[1] Refer to Supplementary data, Table S3.1

was therefore relocated to the N-terminus and a new Flp-In293 cell line encoding FH-RNF26 was generated. A stable cell line encoding the Y432A mutant of RNF26 (FH-RNF26^{Y432A}) was also generated, which based on its homology with RNF4, should be catalytic-inactive. DOX titrations carried out on the two new cell lines (as described for Figure 3.2) showed that FH-RNF26 steady-state levels were much lower relative to FH-RNF26^{Y432A}. Furthermore, FH-RNF26 was acutely sensitive to MG132, whereas the mutant, like RNF26-FH, was not (Figure 3.11b).

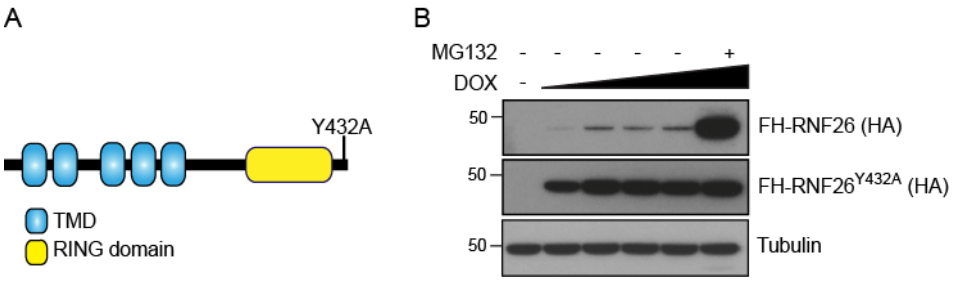

Figure 3.11: RNF26 topology and testing protein expression of WT and mutant FH-RNF26. (a) Schematic of the RNF26 topology, highlighting its TMDs, RING domain, and penultimate hydrophobic residue mutated to generate RNF26^{Y432A}. (b) Anti-HA WBs from WCL originating from Flp-In293 cells encoding FH-tagged WT and mutant RNF26, subject to DOX titration and MG132 treatment. Unstimulated cells are treated with DMSO.

Next an *XBP1* splicing assay was performed on cDNA generated from cells expressing FH-RNF26, FH-RNF26^{Y432A}, or RNF26-FH. Strikingly, neither of the N-terminally tagged forms caused ER stress relative to the C-terminally tagged form (Figure 3.12a).

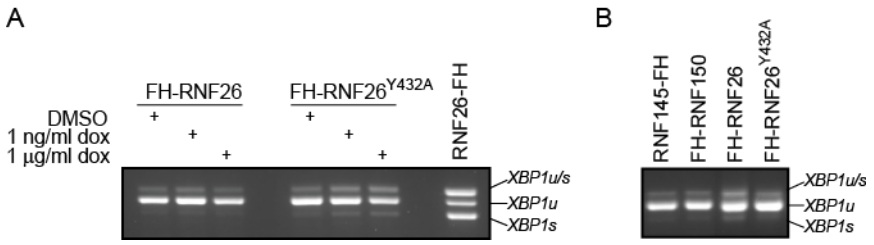

Figure 3.12: Monitoring ER stress upon FH-tagged E3 expression (2nd batch). *XBP1* splicing assay on cDNA from DOX-induced Flp-In293 cell lines expressing: (a) all three forms of RNF26 and (b) FH-tagged E3s form the four new cell lines generated for the second 'batch' of LC-MS/MS. The lower band shows spliced *XBP1*, the middle band is the unspliced form, whereas the top band is hybrid of both spliced and unspliced *XBP1* **(Lin et al., 2007)**.

Therefore, a second 'batch' of LC-MS/MS samples was prepared. This included: both FH-RNF26 and FH-RNF26^{Y432A}; new replicates of RNF13-FH and TRIM59-FH; and RNF145-FH and FH-RNF150, both of which had been successfully cloned and used to generate cell lines since the first LC-MS/MS run. Notably, neither RNF145-FH nor FH-RNF150 was detectable from WCL or by IF, however expression did not cause XBP1 splicing (Figure 3.12b). The silver stain from these six new LC-MS/MS sample preparations is shown in Figure 3.13.

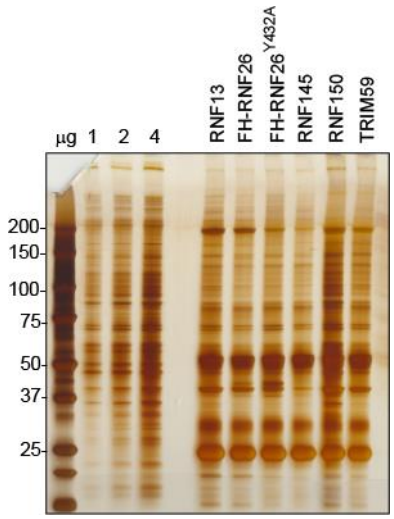

Figure 3.13: Silver stain of LC-MS/MS samples (2nd batch). Silver stain of SDS-PAGE gel loaded with 8% (volume) of the sample eluted off FLAG-agarose in SDS sample buffer. E3 complex samples represent the second LC-MS/MS 'batch'. From left to right, the DOX concentrations used for the respective cell lines was: 1 ng/ml, 1 µg/ml, 1 ng/ml, 1 µg/ml, 1 µg/ml, and 10 ng/ml.

Hrd-FH, RNF13-FH and ZNRF4-FH samples from the first LC-MS/MS ‘batch’ were re-run alongside the new samples to facilitate chromatogram alignment and downstream integration of the two datasets prior to analysis (see Chapter 4). RNF26 was strongly enriched in both WT and mutant samples. RNF145-FH, FH-RNF150 and TRIM59-FH were enriched in their appropriate samples, but only identifed by one or two unique peptides[1]. Combining this observation with the difficulty in detecting these proteins by WB, it was concluded that the expression of these E3s was insufficient to confidently discover interactors. Lastly, RNF13 still appeared evenly distributed across the dataset, indicating inadequate enrichment.

In summary, the LC-MS/MS of 21 out of the 25 ER-resident E3 was successfully completed. Comparative profiling analysis was then used to discover high-confidence interacting proteins (HCIPs) for each E3, which is the focus Chapter 4.

3.3 Discussion

Strategy, cell line generation and testing

The main objective of this project was to construct interaction networks of the E3s resident in the ER membrane. Antibodies available for IP of endogenous E3s were limited and therefore to capture and characterise each E3 complex, the 25 family members were epitope tagged with a FLAG-HA tag at their N- or C-terminus. This strategy ensures that each pulldown can be compared and cross-correlated with all other pulldowns, as the affinity of the FLAG antibody to each tagged E3 should be equal.

The FH-tagged E3 ORFs were used to generate stable, inducible Flp-In293 cell lines. The Flp-In system is designed to incorporate the gene of interest at a single, known locus by homologous recombination at the FRT sites present in the genome and in the vector carrying the required ORF. This prevents off-target effects associated with viral transfection, which can cause random and multiple integrations in the host genome. The tagged E3s were not constitutively overexpressed, as the Flp-In293 cells were also doxycycline-inducible, offering temporal control over gene expression.

Doxycycline (DOX) titrations were carried out on each of the cell lines generated. As can be seen from Figures 3.2 and 3.11b, there is not a linear relationship between DOX concentration and the amount of protein detected by WB. For most E3s, 1 ng/ml DOX was sufficient to induce protein expression, and although 10 ng/ml DOX did often result in higher steady-state levels, this generally did not increase further when DOX concentrations were increased up to 1 µg/ml. The DOX concentrations chosen for induction of E3 expression reflect a balance between detection and limiting overexpression, and can be found in Table 3.1 and Figure legend 3.13.

Auto-ubiquitination leading to degradation by 26S proteasomes is a hallmark of RING-E3s (Metzger et al., 2012). MG132 treatments (4 h, 10 µM) were hence included in the DOX titrations to inhibit proteasomal degradation and thus facilitate detection of E3s with high turnover rates. BFAR, MARCH4, RNF5, RNF26, RNF148, TMEM129 and ZNRF4 levels were all increased upon MG132 treatment, suggesting these E3s are proteasomally degraded. Indeed, BFAR and RNF5 have independently been shown to mediate their proteasomal degradation through auto-ubiquitination (Huang et al., 2018; Rong et al., 2011). MARCH2, MARCH3, and RNF185 were only very mildly sensitive to MG132 treatment. Unexpectedly, RNF128 (lower band), RNF13 and RNF103 expression was lost upon proteasomal degradation. One explanation could be that autophagy (which is upregulated by MG132 treatment (Ding et al., 2007)) can degrade these ligases, however this would have to be confirmed experimentally.

Having tested protein expression, it was subsequently verified that the over-expressed, tagged forms of these ligases are still targeted to the ER. To this end, IF was carried out on each of the cell lines. 21 of the 23 FH-tagged ligases were detectable by IF, and Figure 3.3 demonstrates that each of these E3s co-localises with ER-markers, with the exception of RNF13. RNF13 shows a punctate pattern,

indicative of aggregate formation, whereas all other ligases display a diffuse pattern. Although a clear ER localisation was observed for these E3s, other localisations were not tested. As reviewed in Table 1.2, some of these E3s co-localise with markers of different organelles, and therefore it must be acknowledged that not all of these E3s are likely to be exclusive to the ER.

By tagging proteins, there is always the risk of the structure being altered and the protein becoming misfolded. Alternatively, if the turnover rate of a protein is not very fast, then its overexpression may cause it to accumulate in the ER. The accumulation of either unfolded or misfolded proteins in the ER lumen causes stress, which activates the unfolded protein response (UPR). One of the first changes that can be monitored is the IRE1-mediated splicing of the *XBP1* transcript. By utilising this assay, it was shown that the DOX-induced expression of the tagged ligases did not induce ER stress, with the exception of C-terminally tagged RNF26, and to a lesser extent, RNF103 (Figure 3.4).

More detailed analysis of RNF26 showed it bears sequence similarity with the cytosolic RING-E3, RNF4, and in particular shares a penultimate hydrophobic tyrosine residue (for sequence alignment, see Supplementary data, Figure S3.1). RNF4 is a cytosolic, dimeric ligase, and evidence shows that its C-terminus, particularly its penultimate hydrophobic tyrosine residue, is critical for coordinating its structure and ubiquitination capacity (Plechanovová et al., 2011). Therefore, there were two possible hypotheses regarding why overexpression of RNF26-FH causes ER stress. The first was that C-terminal tagging causes structural disorder and misfolding which leads to UPR activation. Alternatively, RNF26 could have an uncharacterised role in maintaining ER homeostasis, and therefore by tagging its C-terminus, would be rendered catalytically inactive, giving rise to an ER stress phenotype.

To differentiate between these two scenarios, stable cell lines expressing N-terminally tagged WT RNF26 (FH-RNF26), and FH-RNF26^{Y432A} were generated. Based on what is known about RNF4, the RNF26^{Y432A} mutant was predicted to be catalytically inactive (see Chapter 5). DOX titrations on these two new cell lines, revealed that FH-RNF26 was acutely sensitive to MG132 treatment, and that its steady-state levels were much lower compared to the mutant. This indicates that WT RNF26 is rapidly turned over by the proteasome, and that this is most likely by auto-ubiquitination, since the mutant was insensitive to MG132 (Figure 3.11b). Furthermore, overexpression of either of the N-terminally tagged forms of RNF26 did not induce *XBP1* splicing.

Therefore, RNF26-FH is likely to be misfolded, and hence its expression leads to ER stress and downstream activation of the UPR. Intriguingly, the UPR sensor, ATF6, was strongly enriched in the RNF26-FH sample in the first batch of LC-MS/MS (data not shown). However, there is no published evidence of misfolded protein interaction with the luminal domain of ATF6, unlike with IRE1 and PERK (Gardner et al., 2013). To avoid conditions of ER stress, LC-MS/MS was therefore carried out on the N-terminally FH-tagged forms of RNF26.

LC-MS/MS sample preparation protocol optimisation

Having shown that the overexpressed, tagged, E3s were localised to the ER and were not misfolded, we next focused on optimising solubilisation conditions for the E3 complexes. Protein complexes are preserved by micelles, which are formed by detergents present in lysis buffers. The biochemical and biophysical properties of micelles are determined by the molecular structure of the specific detergent (Garavito and Ferguson-Miller, 2001). Detergents that form larger micelles are required to encapsulate large protein complexes, however they are also considered less stringent as they can also encompass additional non-specific interactions.

Nine different detergents were tested for their ability to preserve the interactions within the well-characterised Hrd1 complex. SEL1L, one of the principal interactors of Hrd1, was used to pulldown Hrd1 complexes from cells solubilised in the different detergents. Upon SDS-PAGE and immunoblotting (IB) for the different complex components, it was immediately apparent that Digitonin and LMNG were most able to preserve the interactions within this E3 complex. LMNG has a hydrophilic head group derived from maltose, and two 12-carbon chains. It forms very stable, large micelles (Hauer et al., 2015), and is a member of the MNG amphiphiles, which were originally synthesized for the stabilisation and solubilisation of membrane proteins for crystallography. They have also been shown to be compatible with mass spectrometry (Chae et al., 2010).

LMNG was subsequently used to compare endogenous and exogenous Hrd1 complexes by both IP and sucrose gradient sedimentation. The IP profiles from both WT and Hrd1-FH-expressing cells were essentially identical, with the only difference being the increased amount of FAM8A1 in the exogenous complex, an observation consistent with published data (Schulz et al., 2017). Sucrose gradient sedimentation

revealed that both WT and Hrd1-FH complexes co-migrate between fractions 5-8, however exogenous complex components did experience a shift to lower molecular weight (MW) fractions. This likely represents partially assembled protein complexes, which is an expected phenomenon considering only one of the complex components (Hrd1) was overexpressed, and therefore the stoichiometric ratio between Hrd1 and its interactors is altered (Hwang et al., 2017). Importantly, Hrd1 did not shift to higher MW fractions, which would be indicative of non-native and aggregated interactions.

The next stage of the LC-MS/MS sample preparation pipeline to be optimised was the elution of the complexes immunoprecipitated by FLAG agarose beads. Peptide elution selectively competes for interaction with the bead-bound FLAG antibody, however poor recovery could compromise interactor detection. Conversely, SDS is less specific, but is associated with high recovery.

Although counter-intuitive, non-specific background is advantageous to retain in the LC-MS/MS dataset as it enables normalisation and comparison between the different E3 bait samples, and subsequent discovery of ‘high-confidence interacting proteins’ (HCIPs). This is discussed in detail in Chapter 4. The combined use of LMNG, a detergent which forms comparatively large micelles, and elution with the anionic denaturing reagent, SDS, results in an increase in the number of non-specific, background binders.

LC-MS/MS of E3 complexes and concluding remarks

The optimised protocol was used to prepare each of the E3 complexes for LC-MS/MS. This was carried out in two batches, with the second batch including three samples from the first batch, to allow both datasets to be successfully merged. When preparing the majority of E3 complexes for the first LC-MS/MS run, a WB showing all E3s together showed a large heterogeneity in expression levels (Figure 3.9). This had been anticipated as each E3 is biochemically unique, and therefore intrinsic differences in both RNA and protein stability, translation rate, and folding efficiency means that steady-state amount of each E3 will be different.

Despite the differences in E3 protein expression, silver stain analysis revealed a uniformity across the IP samples (Figure 3.10), suggesting that the strategy aimed at enriching non-specific background in each sample had been successful. Downstream analysis of the LC-MS/MS data from the 25 E3 complexes revealed that 21 E3s were strongly enriched in their respective samples. Whilst RNF145, RNF150 and TRIM59 were enriched in their respective samples, they were only detected by one or two unique peptides, consistent with the difficulties detecting these proteins by WB and IF. One explanation for diminished detection of these specific E3s is that their overexpression may not be tolerated and thus they are instantly degraded. Alternatively, the proteins may be co-translationally degraded if they become misfolded during translation, or simply not produced in cases where transcript instability is high.

Although FLAG and HA positive bands were easily detectable for RNF13, it was not found to be enriched in the E3 LC-MS/MS dataset, and instead appeared to have a uniform expression across all samples. As previously discussed, RNF13 did exhibit certain anomalous features, such as expression being lost upon MG132 treatment (Figure 3.2), and forming punctate structures visible by IF (Figure 3.3). RNF13 may indeed form aggregates that are destroyed by autophagy upregulated by proteasomal inhibition. Since both RNF13 and TRIM59 were prepared for LC-MS/MS on two separate occasions, the likelihood of diminished detection being a product of sample preparation error is very low. If RNF13 is indeed aggregated then the most likely reason for its lack of detection is that the IP was unsuccessful as the antibody-antigen interaction was compromised.

To conclude this chapter, cell lines expressing FLAG-HA-tagged E3s were constructed and tested to confirm protein expression and ER localisation. It was also validated that the overexpressed E3s did not induce ER stress and assembled into native complexes, forming interactions with their endogenous cofactors. The sample preparation pipeline for the E3 complexes was optimised and LC-MS/MS was successfully performed on 21 of the ER-resident E3s. The next chapter discusses how HCIPs were identified for these 21 E3s and the biological significance of the ER E3 interaction landscape.

Chapter 4

Protein-protein interaction landscapes of ER-resident ubiquitin ligases

4.1 Introduction and rationale

Protein-protein interactions define cellular mechanisms and underpin all biological processes. The function of E3 ubiquitin ligases is dictated by interactions formed with both cofactors and substrates. Chapter 3 described the workflow developed to enable LC-MS/MS of ER-resident E3s and their interacting proteins. FH-tagging the E3s allowed equivalent FLAG IPs to be performed on each sample and facilitated parallel processing, minimizing variation between samples. The combination of using LMNG for solubilisation and SDS for elution maximized non-specific (background) interactions. LC-MS/MS was carried out for 32 samples run in two separate batches and resulted in the identification of over 2,000 unique proteins. Approximately 1,600 different proteins were present in each individual bait sample, signifying that every sample consisted largely of background binders. Of course, the principal aim of this project was to define putative interactions for each E3 with high confidence. Therefore, the challenge of the LC-MS/MS data analysis was to distinguish the likely *bona fide* interactors from the non-specific background.

The concept of exploiting non-specific interactions for identifying HCIPs of multiple bait proteins was used to develop the comparative analytical tool, CompPASS (Sowa et al., 2009). This software 'weights' proteins identified in each sample against each other to differentiate between non-specific proteins and candidate interactors. This approach has been used to discover HCIPs for the human deubiquitinating enzymes (Sowa et al., 2009), ERAD components (Christianson et al., 2012) and VCP/p97-adaptor proteins (Raman et al., 2015).

In LC-MS/MS, peptides generated by trypsin digestion are ionised and their intensity is measured, producing MS1 data. A pre-determined fraction of these peptide ions are fragmented and detected, generating MS2 data (spectral counts). MS2 data is used for peptide sequence identification and for spectral count-based quantitation. CompPASS uses total spectral counts to quantify protein levels (Sowa et al., 2009), however spectral counting is only a semi-quantitative estimation of protein abundance (Liu et al., 2004).

Therefore, to discover the HCIPs for each E3, I used a technique that, like CompPASS, is based on comparative proteomic analysis, but instead utilises peptide intensity rather than spectral counts to determine protein amounts. Due to recent major advances in both LC-MS/MS instrumentation and software development, the use of peptide intensity is considered a robust and accurate method of quantifying protein abundance (reviewed in (Nahnsen et al., 2013)).

The strategy used is based on the analytical methods described by Keilhauer and colleagues (Keilhauer et al., 2015). Initially, the background proteome (defined in section 4.2.1) is used to normalise the dataset. Individual bait sample proteomes can now be cross-correlated to derive fold-changes for each identified protein by using the **b**ait-**s**pecific **c**ontrol **g**roup (BSCG) method (Keilhauer et al., 2015). This is achieved by comparing the abundance of a protein found in a particular bait sample to the abundances of the same protein across different bait samples. The BSCG method therefore exploits the large sample size and non-specific interactions to create the largest possible control group for deriving fold-changes for each identified protein in every bait sample. Significantly enriched proteins in each bait sample can hence be classified as E3 HCIPs (described in detail in section 4.2.1). To explore the biological significance of this E3 interaction landscape and build a foundation to help characterise the function of these E3s, the HCIPs defined from this comparative

approach were subsequently mapped to different ER-related processes including ERAD, protein quality control (PQC), lipid biosynthesis and secretory protein trafficking.

Finally, although comparative proteomics was principally used to define putative E3 interactors, the classification of a protein as a HCIP by this method relies on the presence of this protein in at least one other sample, so as a fold-change can be generated. This is a concern for proteins highly abundant and present in only one sample, as they would likely represent *bona fide* interactors. Therefore, a spectral count-based method was used to identify proteins unique to one E3. Collectively, results from both methods were used to describe the interaction networks of the ER-embedded E3s.

4.2 Results

4.2.1 Identification of High-Confidence Interacting Proteins (HCIPs) using a cross-correlative, intensity-based methodology

To adjust for variation between different mass spectrometry runs, the chromatograms from each of the two LC-MS/MS 'batches' were aligned in Progenesis QI (Nonlinear Dynamics). This software uses peptide ion intensity to quantify the abundances of peptides. Peptide sequence information from the raw data files was simultaneously analysed using the Mascot search engine (V.2.5.1, Matrix Science) using the SwissProt *Homo sapiens* database as a reference. Abundances of peptides that can only have been derived from a single protein (unique peptides) were then used to infer the abundance of the corresponding protein. In total 2,274 proteins were identified across all 32 samples: 23 from the first 'batch', and nine from the second. Further analysis of the data was performed using R, where the two datasets were merged into a single matrix. Since each sample was resolved by LC-MS/MS in technical duplicate, the mean of the abundances was calculated for each identified protein. The $\log_2$-transformed mean abundance for each protein in each sample is shown in Figure 4.1.

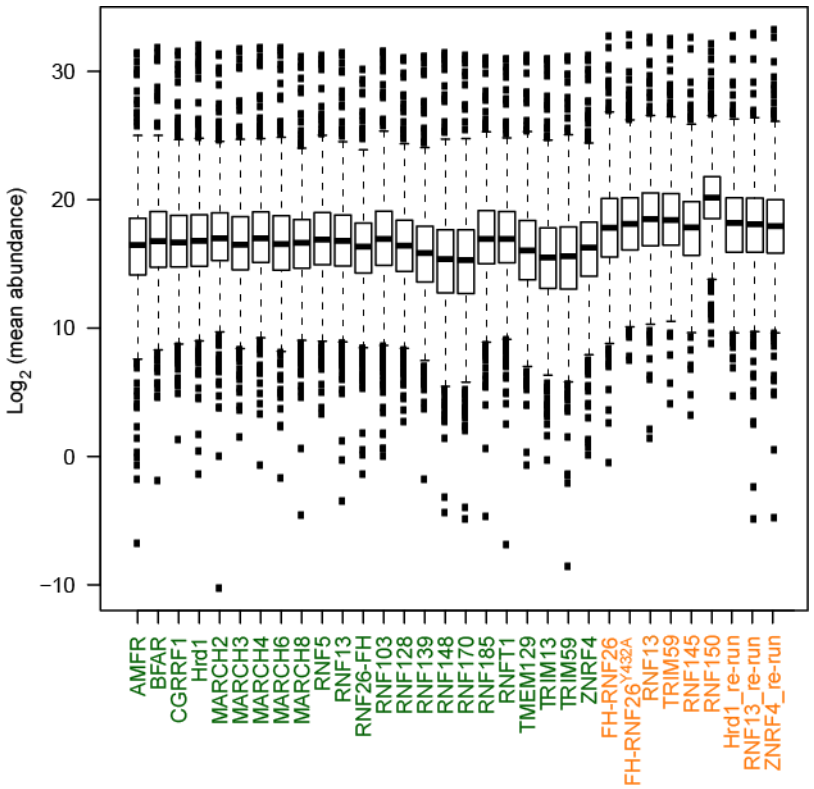

Figure 4.1: Box-and-whisker plot of log_2 mean abundance for each protein identified per sample. The black bar in each box shows the median abundance for proteins identified in the particular sample and the limits of the box show the interquartile range (75% of the data). The whiskers (dotted lines) extend 1.5 x the interquartile range above and below the main box. Dots represent outliers in the tails of each distribution. Figure generated in R.

To normalise this dataset, the 'background proteome' method described in **(Keilhauer et al., 2015)** was employed. This proteome consists of proteins identified in all samples and whose abundances varied the least between samples. They are therefore most likely to represent non-specific proteins trapped by LMNG micelles, or eluted by SDS from within the agarose bead matrix. To define the background proteome, the standard deviation (SD) of the abundances of proteins present in all samples was calculated, logarithmised and subsequently ranked from lowest (least variable) to highest (most variable). Plotting log_2(SD) against the SD-rank produces the sigmoidal curve shown below (Figure 4.2).

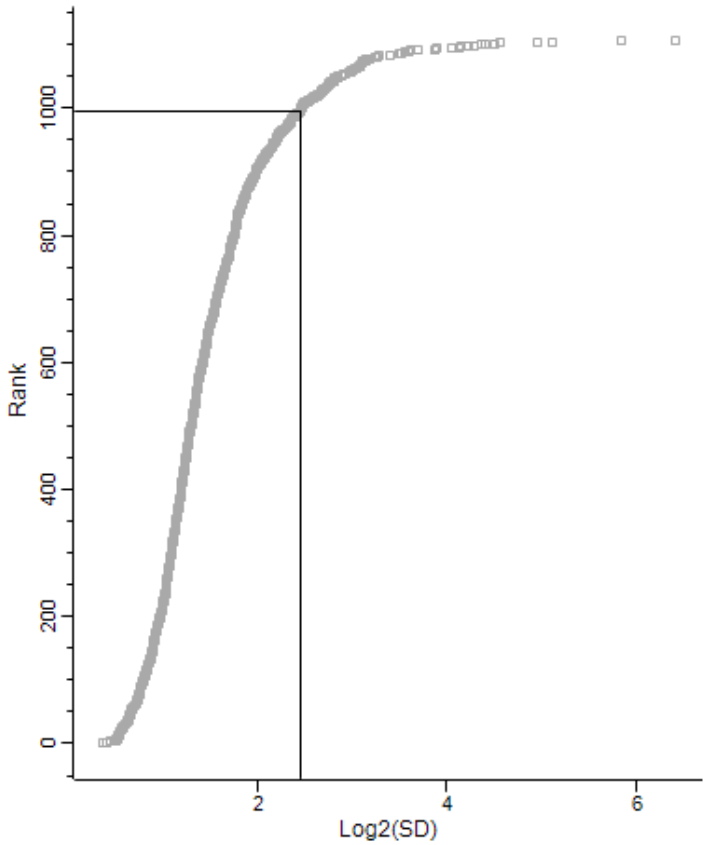

Figure 4.2: Plot of log_2 Standard deviation (SD) of protein abundances against SD rank. The plotted lines indicate the bottom 90th percentile of proteins ranked by SD. Image generated using Perseus software.

The background proteome was defined as the bottom 90th percentile of proteins ranked by SD (indicated on the graph in Figure 4.2). This protein cohort displays the least variation in intensity across the whole dataset, consistent with the observation that the 90% cut-off coincided with the point of inflection on the curve above. The median intensity of the background proteome in one bait sample was calculated and used as a normalisation factor for all of the proteins identified in that particular sample. This was repeated for each sample.

Following median normalisation, Cyclic Loess normalisation was additionally performed to ensure that the spread of the variance is consistent across the intensity ranges, without forcing equal distribution. The spread of intensities of the normalised dataset is depicted below (Figure 4.3).

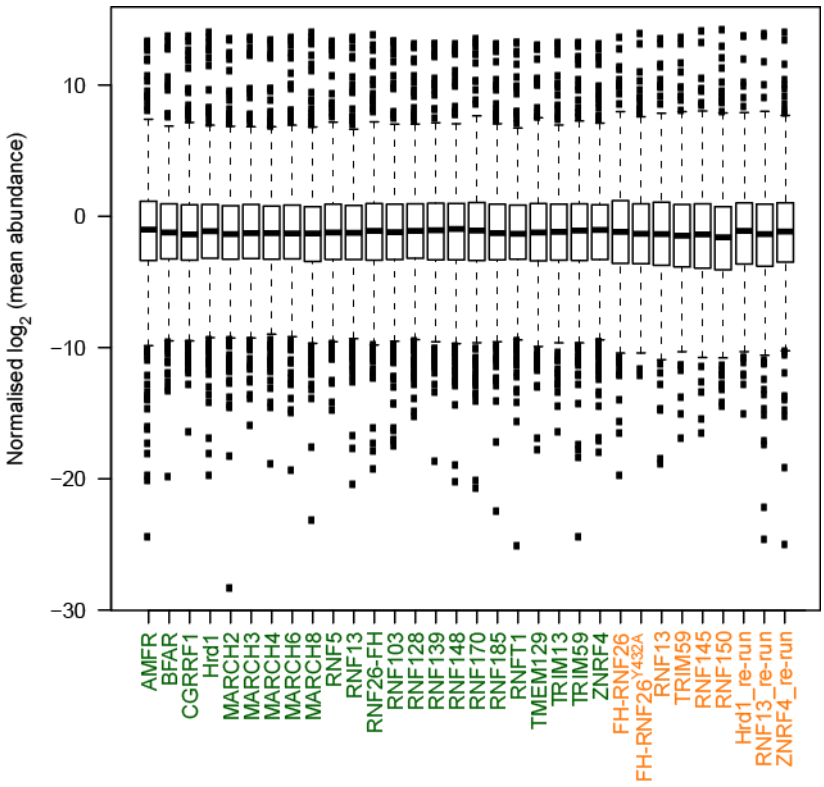

Figure 4.3: Box-and-whisker plot of the normalised log_2 mean abundance. The description of the components within the plot is as in the legend of Figure 4.1.

By comparing Figure 4.3 with Figure 4.1, one can appreciate that the dataset was successfully normalised, as the median abundance of each sample (represented by the black bar in each column) was nearly equal and centred around zero. Batch-specific effects present due to the fact that the samples were run in two separate batches were subsequently removed using a function of the Limma package (Ritchie et al., 2015).

At this stage, each sample could be compared to each other to identify proteins specifically enriched in each E3 sample. To do this, the BSCG method described in (Keilhauer et al., 2015) was utilised. The BSCG-method calculates the fold-change of each protein in every sample. This is achieved by dividing the intensity of a protein in one sample by the mean intensity of that protein in all remaining samples (Figure 4.4).

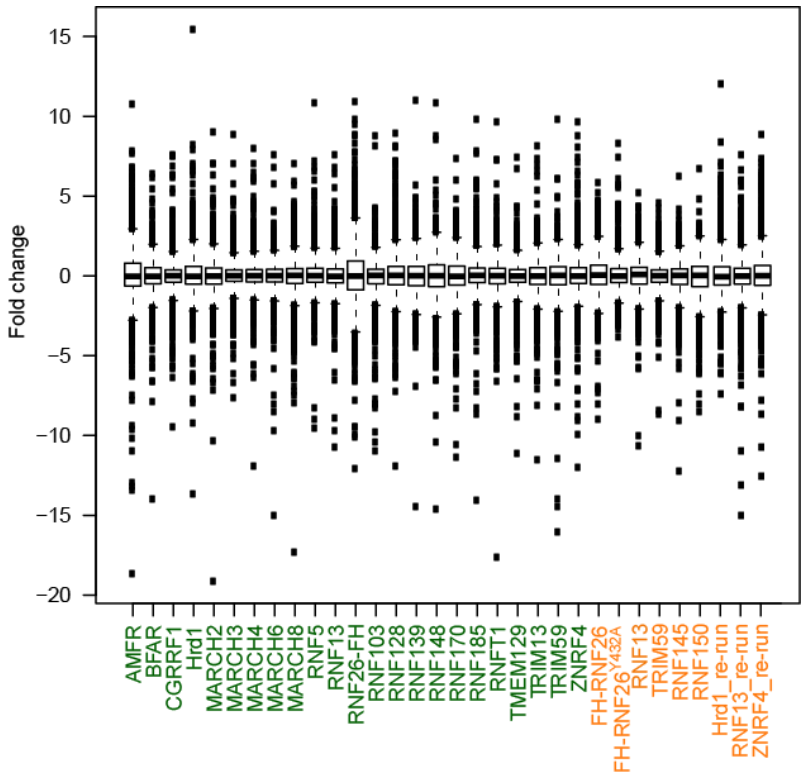

Figure 4.4: Box-and-whisker plot of the fold-changes calculated using the BSCG method. The description of the components within the plot is as in the legend of Figure 4.1.

The above figure shows both enriched (positive fold-change) and depleted (negative fold-change) proteins in each E3 sample. Fold-changes were subsequently used to generate *p-values* using the MaxQuant Significance A algorithm (Cox and Mann, 2008). The greater the fold-change of the protein, the lower the associated *p-value* (higher confidence). With the exception of RNF13, all of E3 baits were annotated with a high *p-value* indicating successful immunoprecipitation and enrichment.

To define **H**igh-**C**onfidence-**I**nteracting-**P**roteins (HCIPs) specific to each E3, a series of criteria were applied to the dataset (Figure 4.5). First, a *p-value* threshold of <0.05 was imposed on the data, to select proteins with a significant fold change. Secondly, proteins with a negative fold-change which were assigned *p-values* of <0.05 were removed from each E3 sample, as these represent proteins that are significantly depleted, rather than significantly enriched. Subsequently, proteins identified by <2 peptides were also removed as they were less likely to correspond to *bona fide* interactors. Lastly, any commonly reported contaminants, including keratins, cytoskeletal proteins, and nuclear proteins such as histone-binding proteins, were also excluded from the final E3 HCIP lists (Supplementary data, Table S4.1).

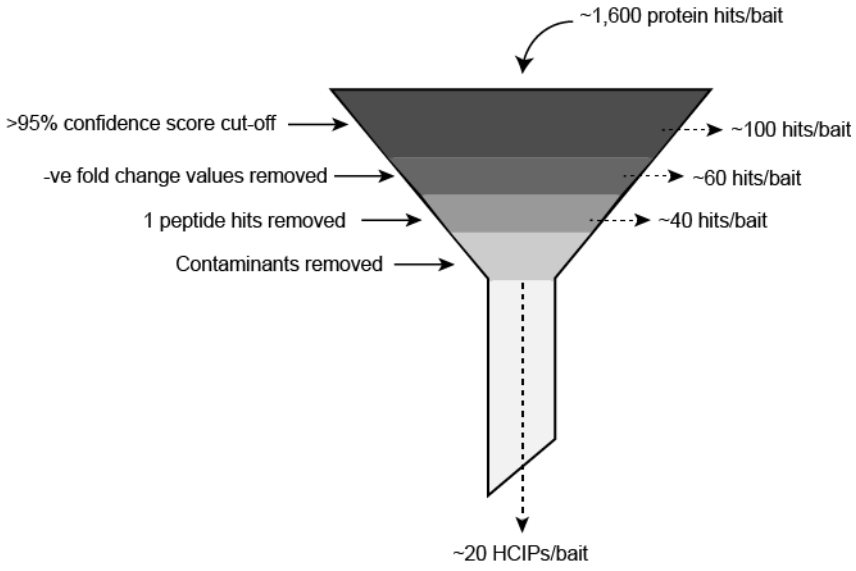

Figure 4.5: Criteria imposed on all identified proteins to define HCIPs specific to each E3 ligase.

Proteins that satisfied this scoring system were categorised as HCIPs. HCIPs are not reported for RNF145, RNF150 and TRIM59 as only 2 peptides were detected for these baits, which was deemed insufficient for adequate interactor enrichment. Additionally, although multiple peptides were detected for RNF13, it was not enriched in any of its corresponding IP samples (see Supplementary data, Table S3.1), and therefore no interactor data was derived. Finally, interactions are not reported for the C-terminally tagged form of RNF26, as this is most likely a misfolded protein unlikely to form native interactions (see Chapter 3).

An average of 20 HCIPs was identified for each of the E3 baits, ranging from four HCIPs for RNF148, to 36 HCIPs for RNF128. Despite the differences in FH-tagged E3 expression levels (Figure 3.9), there was no correlation between E3 normalised abundance and the number of HCIPs associated with each E3 (Figure 4.6). Not only does this demonstrate that the E3 abundance does not bias HCIP discovery, but also that HCIPs can be successfully discovered over a broad range of bait expression levels.

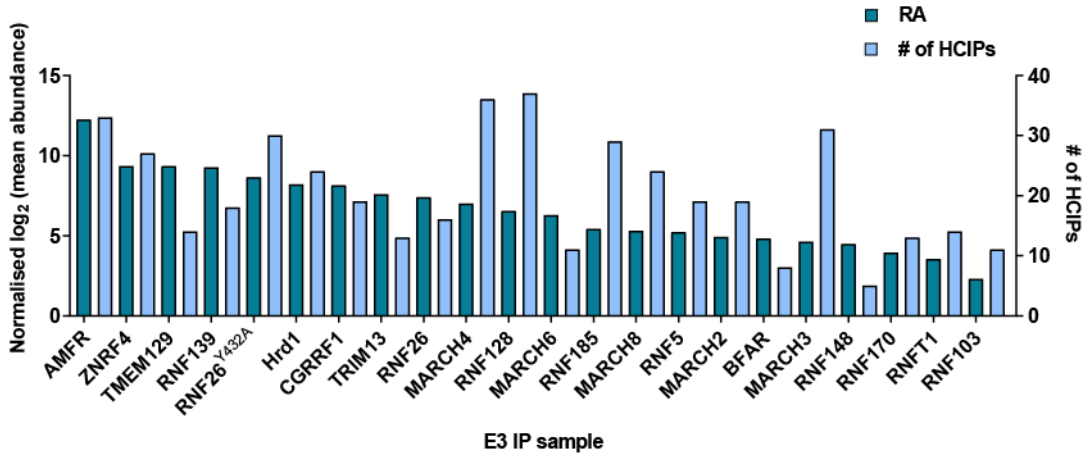

Figure 4.6: Plot of log_2(normalised E3 abundance) against the number of E3 HCIPs. E3s were ranked from by decreasing intensity from left to right.

4.2.2 Overview and topology of the E3 interaction landscape

In total, 218 HCIPs were identified for the 21 WT E3s. An additional 8 HCIPs were found exclusively in the RNF26^{Y432A} interaction network. Apart from HCIPs unique to one E3, some HCIPs were common to two or more E3 baits. Taking into consideration the shared HCIPs, the 226 HCIPs collectively form a total of 429 putative interactions. Figure 4.7 maps all interactions and includes hierarchical clustering of the E3 baits and their associated HCIPs based on the similarity between each E3 interaction network.

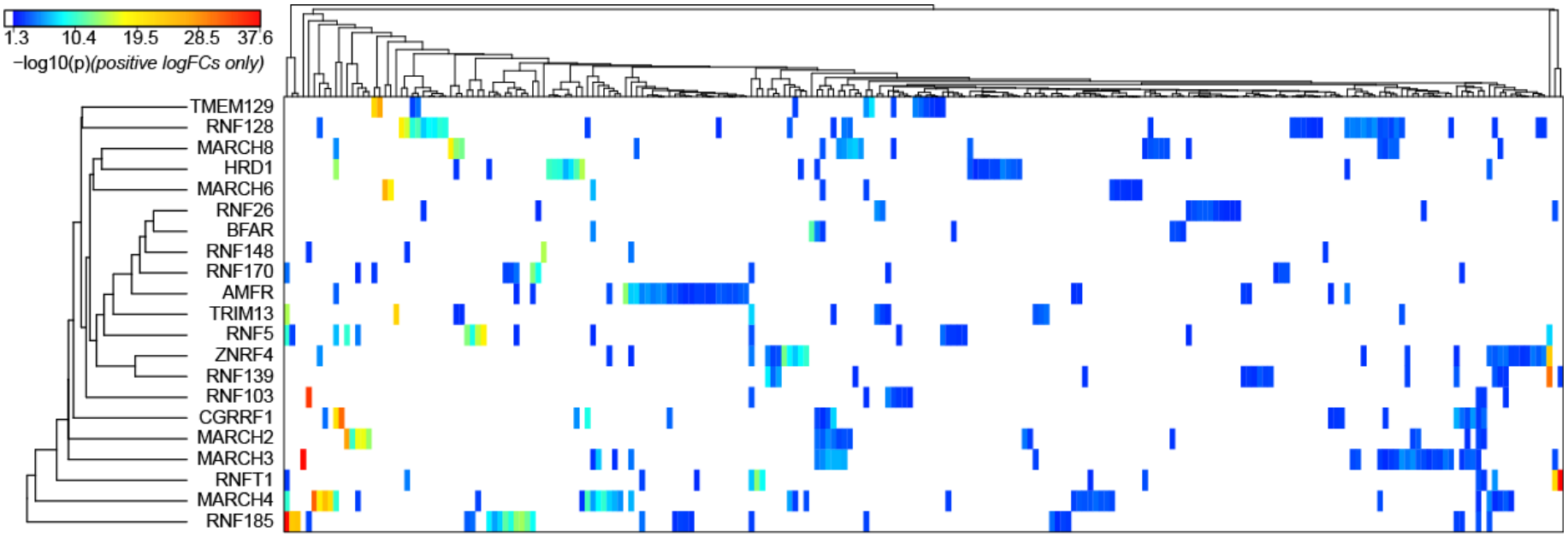

Figure 4.7: Heatmap generated by hierarchical clustering of the all HCIPs and baits for the 21 WT E3 samples. The colour of the square indicates the -$\log_{10}$ (*p-value*) of the interaction.

Putative shared interactors may represent components required for 'general' E3 function. Alternatively, it may indicate a level of cooperation between the E3 complexes. 21 HCIPs were shared between 4-7 baits, and 28 HCIPs were common to 3 baits. Less than a third of HCIPs were associated with two baits and almost 50% of HCIPs were unique to one E3 bait (Figure 4.8a), indicating the E3s are likely to form functionally distinct complexes.

To ascertain the overall topology of these protein-protein interactions, HCIPs were broadly categorised into ER/transmembrane proteins and cytosolic proteins. To classify HCIPs, the 'Retrieve/ID mapping' function (UniProt) was used to search for markers of proteins either targeted to or modified in the ER (predicted signal peptides, glycosylation sites, disulphide bonds) and transmembrane domains. Any HCIP that satisfied one or more of these criteria was assigned as an ER/membrane protein, whereas HCIPs that did not contain any of these features were deemed cytosolic. Using this strategy, only 80 of the 226 HCIPs were classified as cytosolic proteins, showing an overall enrichment for membrane-embedded and ER-localised proteins (Figure 4.8b).

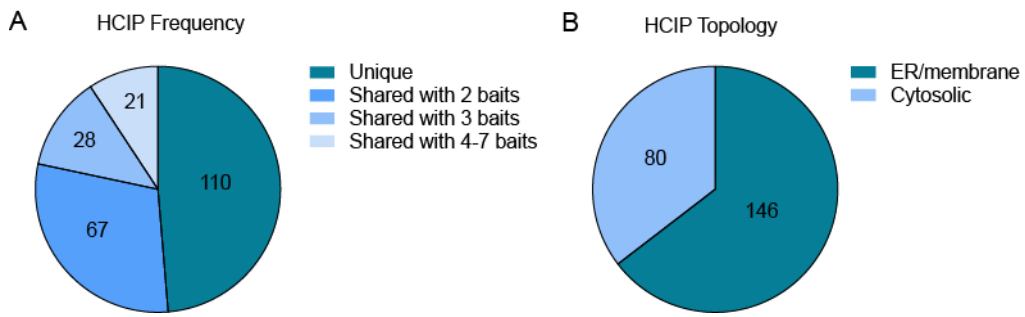

Figure 4.8: Pie charts showing HCIP frequency and topology. (a) Distribution of HCIPs unique to one bait or shared between two or more baits. (b) Proportion of HCIPs defined as either ER/membrane proteins, or cytosolic proteins. HCIPs were classified using the 'Retrieve/ID mapping' function (UniProt).

Finally, the interactions identified were compared against those reported in the online protein-protein interaction database, BioGRID (Stark, 2006) to identify the proportion of novel features discovered in this study. Only 31 of 429 interactions were found in BioGRID, with 18 of these associated with the well-characterised ligases, Hrd1 and AMFR (Figure 4.9). The latter two E3s serve as positive controls for both the LC-MS/MS sample preparation and the subsequent analytical approach.

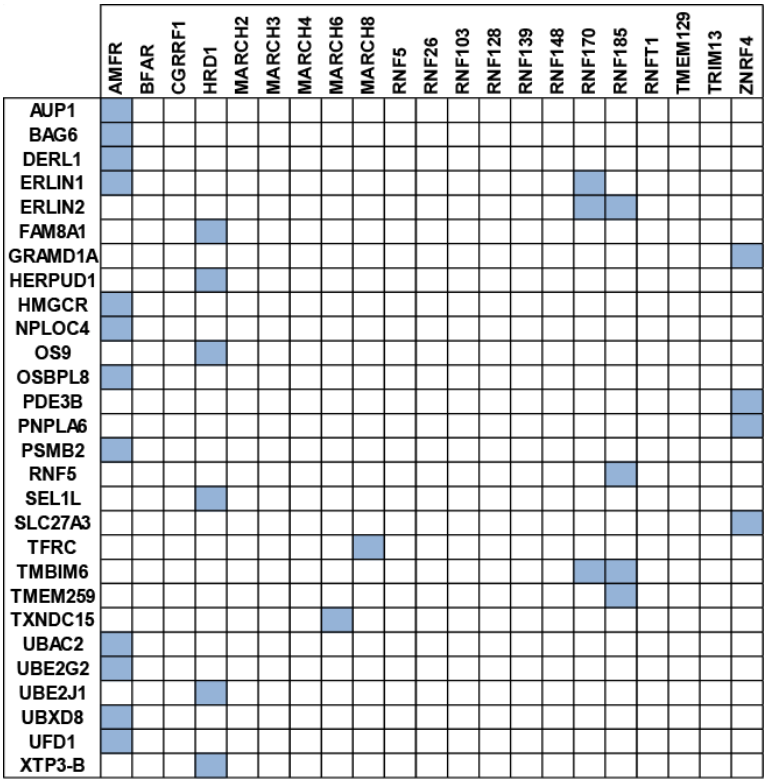

Figure 4.9: Interactions found in this study and reported on BioGRID. Blue squares indicate interactions identified as part of this study, which have been previously-reported.

To summarise, LC-MS/MS of immunoprecipitated FLAG-HA-tagged E3 complexes followed by comparative proteomic profiling identified 429 interactions between 21 E3s and 226 HCIPs. Nearly half of the HCIPs are unique to one E3, and 116 are shared between 2 or more E3s. This interaction landscape, enriched with ER-resident and transmembrane proteins, is the first comprehensive description of the candidate interactors of the ER-resident E3 family.

4.2.3 Placement of HCIPs within ER functional modules

To obtain an overview of the putative functions within this interaction landscape, Gene Ontology (GO) analysis was carried out on the HCIPs identified. This demonstrated a bias towards HCIPs involved primarily in different metabolic processes, followed by protein localization and transport (Figure 4.10).

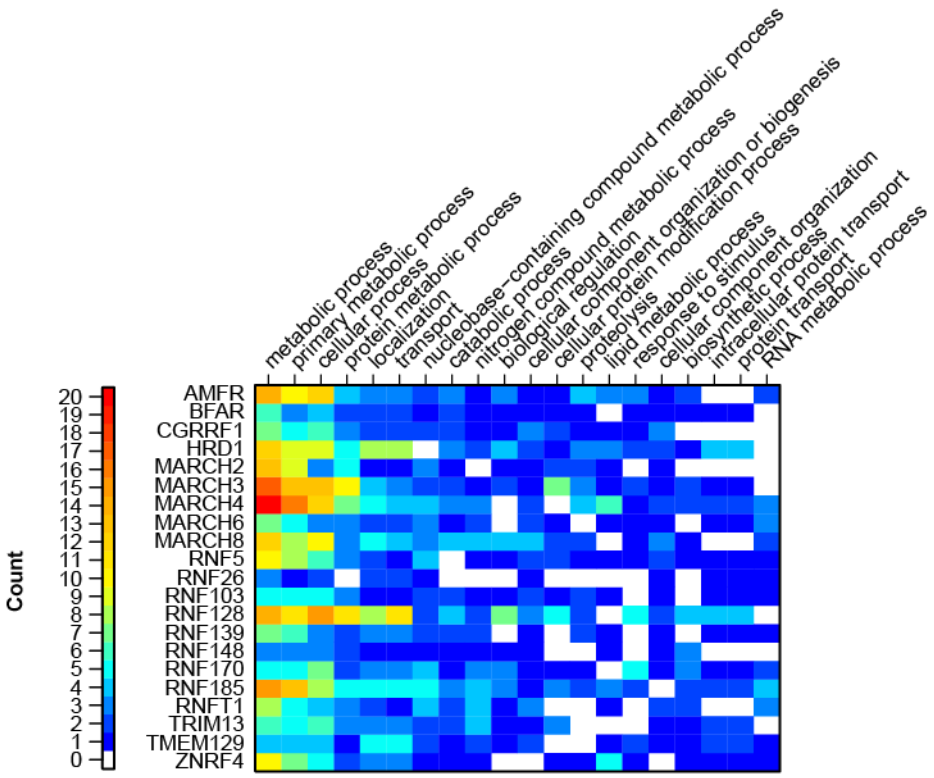

Figure 4.10: Heatmap of the Panther GO-Slim Biological Process terms associated with HCIPs and baits for the 21 WT E3 samples. The colour of square corresponds to the number of HCIPs assigned to a specific GO-category in each E3, as described in **(Sowa et al., 2009)**. Figure generated in R.

Although GO analysis is a useful tool for providing basic understanding in functions, processes and localisations of proteins within a large dataset, it ultimately offers a simplistic view largely based on observational data (Gaudet and Dessimoz, 2017). To gain a deeper insight into the putative function of these E3 complexes, we explored the HCIPs for ER-related functionalities, looking first at ER-associated degradation (ERAD) and protein quality control.

4.2.3.1 ERAD and protein quality control

ERAD cofactors identified as E3 HCIPs

ERAD is a multi-step process required for the degradation of misfolded proteins, as well as unassembled complex components (Olzmann et al., 2013a). It is also necessary for the degradation of proteins whose levels must be tightly regulated to maintain cellular homeostasis (Ruggiano et al., 2014). The process of ERAD is carried out by macromolecular complexes in the ER membrane, composed of E3 ligases and their respective cofactors (Mehnert et al., 2010). To discover E3s with a novel putative role in degradation, HCIPs were searched for known ERAD cofactors (see Chapter 1, section 1.3.4). This resulted in the identification of 16 proteins forming a total of 27 interactions involving nine E3s (Figure 4.11, top panel).

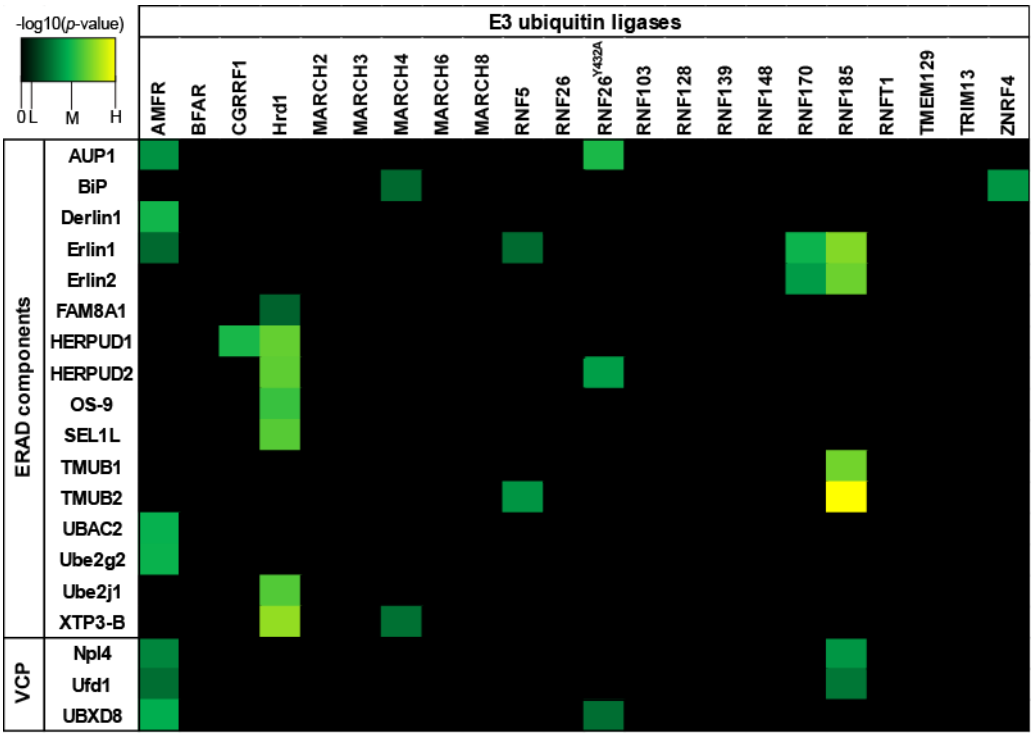

Figure 4.11: Heatmap of ERAD components identified as HCIPs from the FH-E3 LC-MS/MS screen. The scale used was based on the -log(*p*-value) of the HCIPs. If the HCIP was not present as a HCIP in a particular sample then it was scored as zero (black). The -log(*p*-value) of all the non-zero HCIPs was used to calculate the median (M), which was denoted as green. Any value lower than the median appears on the black-green side of the scale (L). The highest value (H) was set as yellow, and thus any value between the median and highest value appears on the green-yellow side of the scale.

Of the 27 interactions, 12 were associated with AMFR and Hrd1. These interactions have all been previously documented (Figure 4.9 and (Huang et al., 2014)), and since both ligases have well-established roles in degradation, it is not surprising that they form the majority of interactions with classical ERAD cofactors. Scaffold proteins Erlin1 and Erlin2 are known to be required for RNF170-mediated degradation of IP_3 receptors (Lu et al., 2011) and were positively identified as HCIPs for this ligase. Although Erlin2 has already been demonstrated to interact with RNF185 (Khouri et al., 2013), both Erlin proteins were present in the RNF185 interaction network. Additionally, Erlin1 was found with RNF5. TMUB1, previously identified as an Erlin2 interactor (Jo et al., 2011b), was captured with RNF185, and its related protein, TMUB2, was identified as a HCIP for both RNF185 and RNF5. MARCH4 and ZNRF4 were found to interact with the chaperone BiP, and MARCH4 also interacted with the lectin-binding protein XTP3-B. Interestingly, the mutant form of RNF26 formed putative interactions with AUP1, and Herp2. Herp1, on the other hand, was discovered as a CGRRF1 HCIP.

ERAD classically requires the activity of the AAA-ATPase VCP/p97 to extract polypeptides from the ER membrane (Meyer et al., 2012). Although VCP/p97 can interact with directly with AMFR (Ballar et al., 2006), it is also recruited to E3 membrane complexes via adaptor proteins containing VCP-binding motifs (Meyer et al., 2012). These motifs include UBX, UBX-like (UBX-L), peptide N-glycosidase/ubiquitin-associated (PUB), PLAA-Ufd3-Lub1 (PUL), VIM, VBM and SHP domains (Meyer et al., 2012). As an alternative method to assess the degradation potential of these E3 ligases, HCIPs were cross-referenced against data from Pfam, IntAct, and InterPro to scan for VCP-interacting domains. In addition to the ERAD cofactor Derlin1 which contains a SHP domain, only 3 HCIPs containing

VCP-binding elements were found: UBXD8, Npl4, and Ufd1, which contain UBX, UBX-L and SHP domains, respectively (Figure 4.11, bottom panel).

UBXD8, Npl4 and Ufd1 were identified as HCIPs for AMFR, and UBXD8 was also associated with the RNF26^{Y423A} mutant. Interestingly, Ufd1 and Npl4, which together form a complex with VCP/p97 (Ye et al., 2003), were also discovered as HCIPs for RNF185. This E3 was recently shown to be captured by a VCP/p97 trapping mutant (Hülsmann et al., 2018), and hence our data may lend insight into how RNF185 is recruited to VCP/p97. Therefore, combining ERAD cofactors together with VCP-adaptor proteins, a total of 19 HCIPs that play a role in degradation formed 33 interactions between nine E3 ligases: AMFR, CGRRF1, Hrd1, MARCH4, RNF5, RNF26 (mutant), RNF170, RNF185 and ZNRF4. Although several of these E3s are already implicated in ERAD (see Chapter 1, section 1.6), these findings suggest potential novel roles in ERAD for CGRRF1, MARCH4 and RNF26.

E3s in the resolution of ER stress

ER stress activates the UPR, which in turn upregulates components of the degradation machinery, with Hrd1 being a primary target (Travers et al., 2000). Transcriptional analysis was used to ascertain whether any other E3s are upregulated by protein misfolding stress. Nanostring™ technology was used to determine the changes in each E3 transcript level as well as 28 other ER-resident proteins known to play a role in ERAD and protein quality control. ER stress was induced either by Tunicamycin (Tm) or the cytotoxin SubtilaseAB$_5$ (SubAB$_5$) (Paton et al., 2006). Significant increases in *CGRRF1*, *Hrd1*, *RNF13*, *RNF170* and *RNFT1* were observed upon ER stress induction by either Tm (Figure 4.12) or SubAB$_5$ (Figure 4.13). *RNF5* was upregulated in response to Tm alone, whereas *RNF139* was uniquely upregulated by SubAB$_5$ treatment. Strikingly, *Hrd1* (shown in orange)

experienced the largest fold-change in transcript relative to any of the other upregulated E3s. *MARCH3*, *MARCH4*, *RNF148* and *TRIM59* were below the detection threshold required for quantitation, and a probe for *TMEM129* was not included in the original Nanostring™ chip, as this experiment was designed prior to the discovery of this E3. Therefore the transcriptional response of these five E3s unfortunately remains unknown.

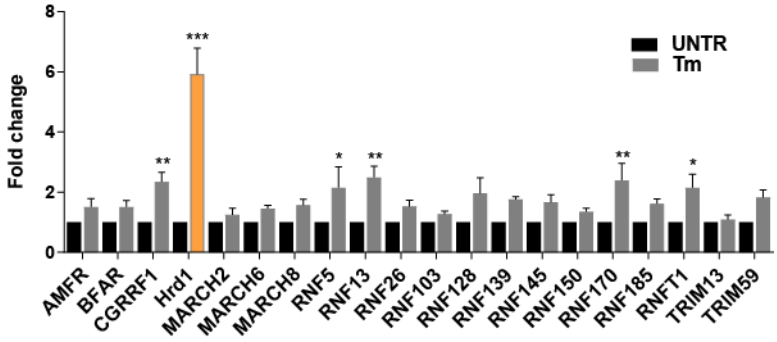

Figure 4.12: Fold-change of E3 transcripts upon Tunicamycin treatment. WT Flp-In293 cells were treated with 500 ng/ml Tm for 8 h. Error bars represent standard error of the mean (s.e.m.) from *n* = 3 biological repeats, **P* < 0.05, ***P* < 0.01, ****P* < 0.001. Hrd1 is shown in orange for reference.

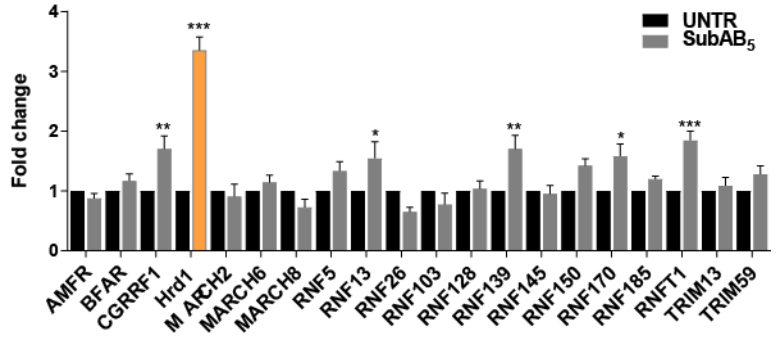

Figure 4.13: Fold-change of E3 transcripts upon SubtilaseAB$_5$ treatment. WT Flp-In293 cells were treated with 10 ng/ml SubAB$_5$ for 8 h. Error bars represent s.e.m. from *n* = 3 biological repeats, **P* < 0.05, ***P* < 0.01, ****P* < 0.001. Hrd1 is shown in orange for reference.

Furthermore, of the 28 PQC genes analysed (Supplementary data, Figure S4.1), 14 were identified as HCIPs in the E3 proteomic screen (Figure 4.14), six of which were components of the Hrd1 complex (shown in orange).

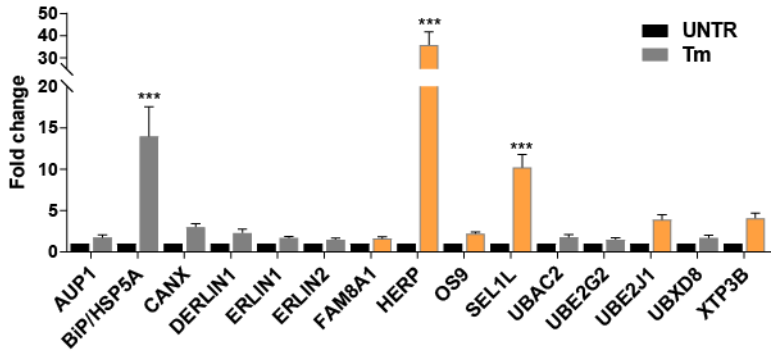

Figure 4.14: Transcriptional fold-change of ERAD components identified as HCIPs upon Tunicamycin treatment. WT Flp-In293 cells were treated with 500 ng/ml Tm for 8 h. Error bars represent s.e.m. from *n* = 3 biological repeats, ****P* < 0.001.

As anticipated, ER stress induced the upregulation of several Hrd1 cofactors (Sel1L, Herp, Ube2j1 and XTP3-B) (see Chapter 1). The combination of both proteomic and transcriptional analyses suggests that Hrd1 is uniquely positioned to mediate ERAD for the resolution of proteotoxic stress, as it is the most strongly upregulated E3 in response to UPR activation, and also forms a unique complex with components which are targets of this pathway. However, since CGRRF1 was modestly upregulated by UPR activation and formed a putative interaction with the stress-responsive gene, Herp1, it would be interesting to determine whether this E3 was able to contribute to alleviating ER stress through the degradation of misfolded proteins.

Other players in protein quality control identified as candidate E3 interactors

Alongside degradation machinery, PQC components such as UPR transducers, foldases and chaperones (see Chapter 1, section 1.3.2 and 1.3.3), were identified as interactors of different E3 ligases (Figure 4.15). Both isoforms of the mammalian ER stress transducer, ATF6, were classified as HCIPs. ATF6-α and ATF6-β were present in the RNF139 interaction network, and ATF6-β was additionally detected with MARCH3 and ZNRF4. The other mammalian stress transducer, PERK (annotated as EIF2AK3) was one of seven HCIPs associated with BFAR. TNFRSF10B (death receptor 5), a target of the PERK-CHOP branch (Yamaguchi and Wang, 2004), was identified to interact with MARCH3, MARCH8, and RNF128. Although Ire1 was not identified by LC-MS/MS, TMBIM6 (Bax inhibitor 1), an ER membrane calcium channel proposed to negatively regulate Ire1 activity (Bultynck et al., 2012; Lisbona et al., 2009), was discovered as a HCIP of six different E3s: MARCH4, RNF5, RNF170, RNF185, RNFT1 and TRIM13 (Figure 4.15, top panel).

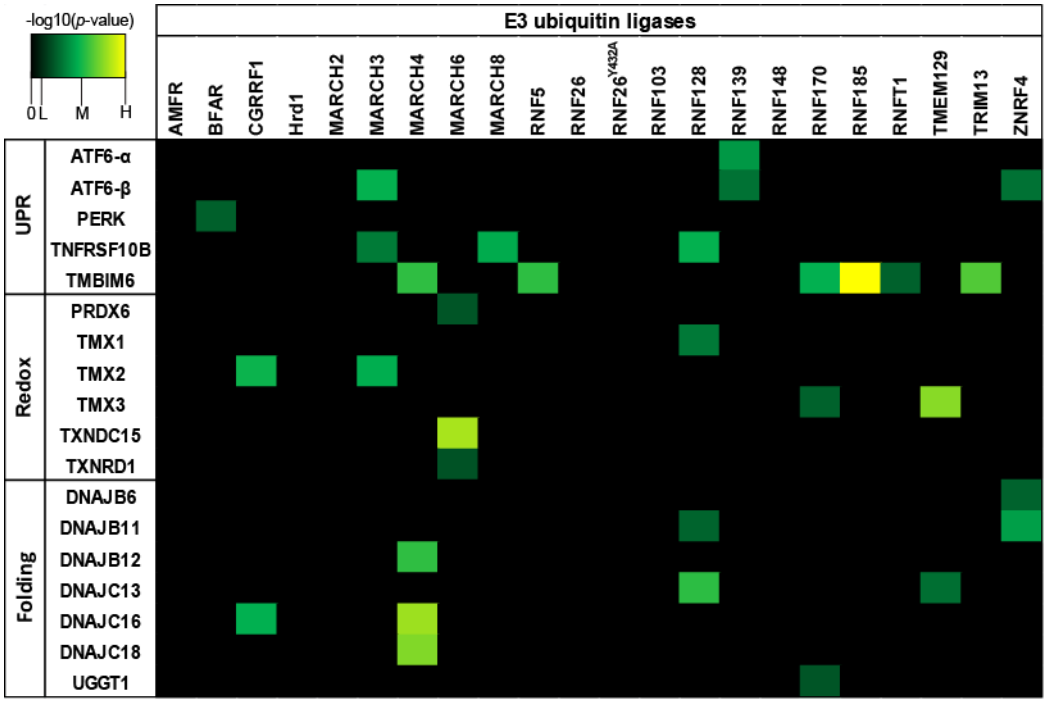

Figure 4.15: Heatmap of non-ERAD PQC components identified as HCIPs from the FH-E3 LC-MS/MS screen. The scale used is described in the legend of Figure 4.11.

Protein folding is catalyzed by oxidoreductases such as PDI (see Chapter 1, section 1.3.2). Three PDI family members were identified as HCIPs (Figure 4.15, middle panel). Thioredoxin-related transmembrane protein (TMX)1, an ER-resident oxidoreductase (Matsuo et al., 2001), was co-precipitated by RNF128. TMX2, an uncharacterised PDI member (Bulleid, 2012), was found with both CGRRF1 and MARCH3, whereas the ER-localised TMX3 (Haugstetter et al., 2005) interacted with RNF170 and TMEM129. The remaining identified proteins with redox capacity were strikingly all found in the MARCH6 interactome. These were peroxiredoxin-6 (PRDX6), thioredoxin reductase 1 (TXNRD1), and thioredoxin domain-containing protein 15 (TXNDC15), the latter already discovered as a MARCH6 HCIP from a previous screen (Figure 4.9, (Huttlin et al., 2017; Huttlin et al., 2015)).

DNAJ homologue proteins promote folding by acting as co-chaperones (see Chapter 1, section 1.3.2). Six different DNAJ proteins were found among E3 HCIPs. Interestingly, MARCH4 interacted with three DNAJ members: DNAJB12, an ER-resident co-chaperone involved in CFTR degradation (Yamamoto et al., 2010), DNAJC16, and DNAJC18, both of which are uncharacterised. The interaction with DNAJC16 was shared with CGRRF1. RNF128 was found to interact with DNAJB11 (ERDJ3), the co-chaperone for BiP (Shen and Hendershot, 2005) and endosomal DNAJC13 (Fujibayashi et al., 2008). DNAJB11 and DNAJC13 were also classified as HCIPs for ZNRF4 and TMEM129, respectively. Consistent with the role of DNAJB11 as a BiP co-chaperone, BiP was pulled-down with ZNRF4, which also interacted with DNAJB6, an Hsp70 co-chaperone (Chuang et al., 2002). Lastly, UGGT1, which recycles unfolded proteins back to the CNX/CRT pathway (Sousa and Parodi, 1995), was found to be a unique interactor of RNF170 (Figure 4.15, bottom panel).

In summary, classical ERAD cofactors interact primarily with AMFR and Hrd1, however novel putative interactions with CGRRF1, MARCH4, RNF26 and ZNRF4 are also described. Of note, Npl4 and Ufd1, which complex with VCP to dislocate proteins from the ER, were discovered as RNF185 HCIPs, implicating this E3 in VCP-dependent degradation. Although Hrd1 exhibits the strongest transcriptional upregulation in response to ER stress, the levels of four E3s (CGRRF1, RNF13, RNF170 and RNFT1) were also shown to increase independent of the stress-inducer used. Furthermore, several other E3s are associated with HCIPs that play a role in UPR signaling or protein folding, and thus may also contribute to maintaining ER homeostasis.

4.2.3.2 'Regulatory ERAD' – putative E3 substrates

Lipid regulatory proteins

The role of ERAD extends beyond misfolded protein degradation. 'Regulatory ERAD' is the term used to describe the degradation of proteins coordinated to meet the specific demands of a cell. The first reported example of this process was the degradation of the cholesterol biosynthetic enzyme Hmg2p by Hrd1p as part of a feedback mechanism to limit sterol generation in yeast (Gardner et al., 2001; Hampton et al., 1996). In mammals, HMGCR (homologue of Hmg2p) and squalene epoxidase (SQLE) both catalyse rate-limiting steps in *de novo* cholesterol biosynthesis, and are post-translationally regulated by ER-resident E3s (see Chapter 1, section 1.4.1). HMGCR levels are controlled by AMFR and RNF139 (Jo et al., 2011a), whereas SQLE is a substrate of MARCH6 (Foresti et al., 2013; Zelcer et al., 2014). Both substrates were detected by WB following pulldown of their respective ligases (Jo et al., 2011a; Zelcer et al., 2014). Since HMGCR was identified as a HCIP of AMFR, it was investigated whether other E3s associated with lipid regulatory proteins, as these could represent novel E3-substrate interactions with potential implications in regulating lipid homeostasis.

To classify HCIPs as 'lipid regulatory' proteins, the 'Retrieve/ID mapping' function on Uniprot was used to collect GO description terms and the results were subsequently combined with an extensive literature search. The 25 shortlisted HCIPs represent proteins involved in almost all aspects of lipid biology, including: fatty acid and phospholipid biosynthesis; cholesterol metabolism; transport; and lipid droplet regulation (Table 4.1). 11 of the HCIPs are localised exclusively to the ER, with the remaining 14 reportedly found at ER-mitochondria-associated membrane (MAM) sites, mitochondria, peroxisomes, and endosomal/Golgi compartments.

	Localisation	Function	Reference
ACSL4	ER	Phospholipid synthesis	(Golej et al., 2011)
ALDH3A2	ER/Peroxisome	Fatty acid synthesis	(Ashibe et al., 2007)
AUP1	ER/lipid droplets	ERQC/LD regulation	(Klemm et al., 2011)
DGKE	ER	Phospholipid synthesis	(Matsui et al., 2014)
DHCR24	ER	Sterol biosynthesis	(Luu et al., 2015)
DHCR7	ER	Sterol biosynthesis	(Prabhu et al., 2016)
EPHX1	ER	Epoxide hydrolysis	(Václavíková et al., 2015)
FAAH	ER/lipid droplets	Fatty acid degradation	(Oddi et al., 2008)
FADS2	ER	PUFA synthesis	(Guillou et al., 2004)
FAR1	Peroxisome	Fatty acyl-CoA reduction	(Honsho et al., 2010)
HADH	Mitochondrial	Fatty acid oxidation	(Houten and Wanders, 2010)
HMG-CoA	ER	Sterol biosynthesis	(Goldstein and Brown, 1990)
HSD17B12	ER	Fatty acid elongation	(Moon and Horton, 2003)
LPCAT1	ER/lipid droplets	Phospholipid synthesis	(Moessinger et al., 2011)
OSBPL8	ER/PM	Phospholipid transport	(Chung et al., 2015)
PI4K2A	Endosome/Golgi	PI(4)P generation	(Minogue, 2006; Minogue et al., 2010)
PTDSS2	ER MAMs	Phospholipid synthesis	(Stone and Vance, 2000)
SACM1L	ER	Phospholipid hydrolysis	(Mesmin et al., 2013)
SCD	ER	Fatty acid synthesis	(Paton and Ntambi, 2009)
SLC27A2	ER/Peroxisome	LCFA transport	(Mihalik et al., 2002)
SLC27A3	Mitochondrial	Transport	Predicted
SLC27A4	ER MAMs	LCFA transport	(Jia et al., 2007)
SOAT-1	ER MAMs	Cholesterol esterification	(Rusiñol et al., 1994)
SQLE	ER	Sterol biosynthesis	(Goldstein and Brown, 1990)
UBXD8	ER/lipid droplets	ERQC/LD regulation	(Olzmann et al., 2013b)

Table 4.1: Localisation and general function of lipid regulatory HCIPs identified from the FH-E3 LC-MS/MS screen. ERQC - ER quality control, LD- lipid droplets, PUFA - polyunsaturated fatty acid, LCFA - long-chain fatty acid. The references used provide evidence for both function and localisation of the HCIPs.

The 25 HCIPs identified to be involved in lipid regulation formed a total of 48 interactions between 16 E3s, as shown in the heatmap below (Figure 4.16). AMFR showed the strongest enrichment for this group of proteins, with 11 HCIPs associated with this ligase. Interestingly, the RNF26^{Y432A} mutant formed putative

interactions with seven of these HCIPs, however none were present with the WT form of RNF26 (see Discussion).

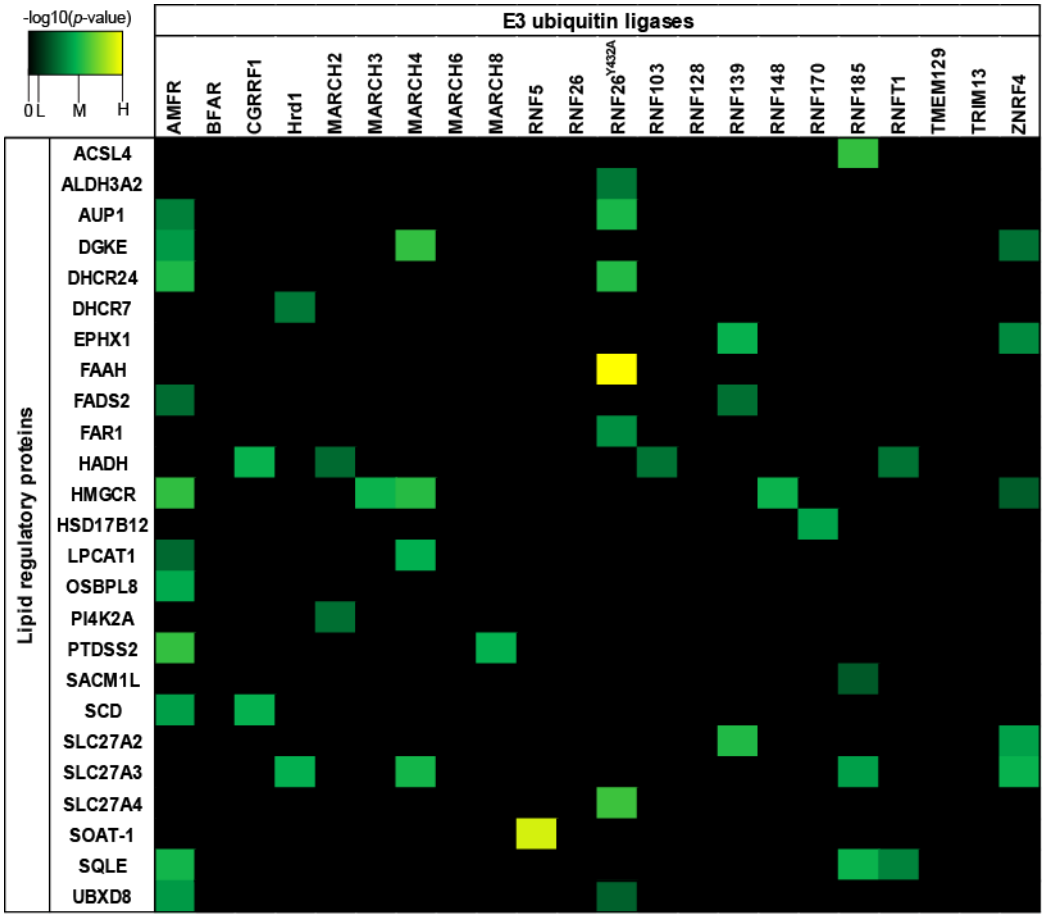

Figure 4.16: Heatmap of lipid regulatory proteins identified as HCIPs from the FH-E3 LC-MS/MS screen. The scale used is described in the legend of Figure 4.11.

Of the 16 E3s, nine were associated with two or more members of this lipid-related group of HCIPs, indicating that specific ligases may control lipid homeostasis by regulating the activity of multiple proteins. Alternatively, some HCIPs may be subject to regulation by several E3s. Evidence supporting this comes from the fact that 14 of the 25 HCIPs are associated with 2 or more ligases, with 3-hydroxyacyl-CoA dehydrogenase type-2 (HADH) and SLC27A3 both shared between four E3s, and HMGCR shared between five E3s (AMFR, MARCH3, MARCH4, RNF148 and ZNRF4). HMGCR has been shown to be mediated by AMFR and RNF139, however

the simultaneous depletion of both E3s did not completely abolish HMGCR turnover (Jo et al., 2011a). Therefore, it is plausible that other ligases may contribute to its regulation (see Discussion).

Although the ER accommodates enzymes which control several aspects of lipid regulation, ER-resident E3s are only currently implicated in the degradation of sterol-biosynthetic enzymes (see above and Section 1.4.1). Indeed, 7-dehydrocholesterol reductase (DHCR7) and DHCR24, whose activities are required in the terminal stages of cholesterol synthesis ((Luu et al., 2015) and Figure 1.5), were identified as HCIPs for Hrd1 and AMFR, which suggests a potential novel function for these ligases in fine-tuning cholesterol production. However, the information collected in Table 4.1 highlights the diversity of functions in the lipid-regulatory HCIPs and thus supports the hypothesis that ER-embedded E3s are likely to influence different pathways within the lipid homeostatic network.

Transporters and channels

Apart from controlling lipid metabolism, ERAD can also mediate the degradation of membrane channels and transporters. A prominent example of this process involves IP_3 receptors that are embedded in the ER membrane, which release calcium from the ER into the cytosol upon activation (see Chapter 1, section 1.5). IP_3Rs are rapidly inactivated through degradation by RNF170 to limit the increase of cytosolic calcium levels (Lu et al., 2011). Secretory pathway proteins destined for the plasma membrane are also under surveillance by ER-resident E3s. In yeast, upon nutrient depletion, the secretory zinc transporter, Zrt1, is first cleaved and then degraded by Doa10, allowing the cell to prepare and adapt to starvation (Avci et al., 2014). In mammalian cells, plasma membrane glutamine transporters, SLCA15 and SLC38A2 are targeted for degradation by RNF5 during ER stress. (Jeon et al., 2015). These

examples highlight the potential for the ER-resident E3s to regulate ion flux and nutrient uptake by controlling expression and turnover of membrane channels.

As for the lipid-regulatory proteins, 'Retrieve/ID mapping' (Uniprot) was used to screen HCIPs annotated by GO as either transporters or channels. This approach identified 16 proteins which were divided into three main subgroups: ion transporters; fatty acid channels; and amino acid transporters (Table 4.2). 12 HCIPs appear to be localised to secretory pathway organelles (ER, Golgi, and PM), and three are reportedly exclusive to the mitochondria.

		Localisation	Specificity	Reference
Divalent ions	**ATP13A1**	ER	Manganese ions	(Cohen et al., 2013)
	ITPR3	ER	Calcium ions	(Raffaello et al., 2016)
	SFXN1	Mitochondria	Iron ions	Predicted
	SLC30A5	Golgi	Zinc ions	(Kirschke and Huang, 2003)
	SLC30A6	Golgi	Zinc ions	Predicted
	SLC39A10	ND	Zinc ions	Predicted
	SLC39A14	PM	Zinc ions	(Taylor et al., 2004)
	TFRC	PM/endosome	Transferrin-Iron	Reviewed in (Morgan, 1981)
	TMBIM6	ER	Calcium ions	(Chang et al., 2014)
	TMCO1	ER	Calcium ions	(Wang et al., 2016)
	VDAC1	Mitochondria	Calcium ions	(GINCEL et al., 2001)
FA	**SLC27A2**	ER/Peroxisome	LCFA transport	(Mihalik et al., 2002)
	SLC27A4	ER MAMs	LCFA transport	(Jia et al., 2007)
AA	**SLC25A13**	Mitochondria	Aspartate/glutamate	(Palmieri et al., 2001)
	SLC7A2	PM	Cationic amino acids	(Closs et al., 1997)
	SLC3A2	PM	Neutral amino acids	(Mastroberardino et al., 1998)

Table 4.2: Localisation and general function of HCIPs identified as transporters or channels from the FH-E3 LC-MS/MS screen. FA - fatty acid, AA - amino acid, ND – not determined, LCFA - long-chain fatty acid. The references used provide evidence for both function and localisation of the HCIPs.

The 16 HCIPs were found across 17 E3 interaction networks, forming a total of 35 high-confidence interactions (Figure 4.17). Similar to observations made for the lipid-regulatory HCIPs, RNF26^{Y432A} captured five transporters despite none being

captured by WT RNF26, suggesting the RNF26 mutant may function as a substrate trap. Five transporter HCIPs were also identified for RNF128.

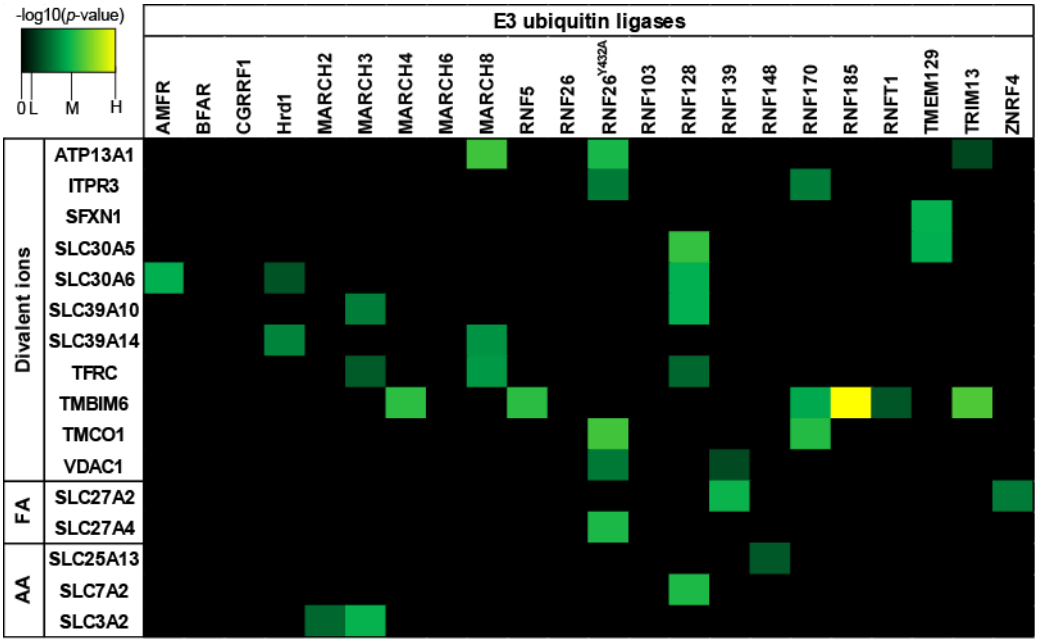

Figure 4.17: Heatmap of ion, fatty acid (FA) and amino acid (AA) transporters/channels identified as HCIPs from the FH-E3 LC-MS/MS screen. The scale used is described in the legend of Figure 4.11.

Most HCIPs in this group were associated with two or more E3s, with only four HCIPs specific to one ligase. Consistent with published data, the IP_3 receptor (ITPR3) was classified as a HCIP for RNF170 (Lu et al., 2011), and the plasma membrane-localised TFRC was captured by MARCH8 (Fujita et al., 2013). MARCH8 is reported to interact with and promote the lysosomal turnover of TFRC (Fujita et al., 2013), which in turn is required for the endocytic internalization of the extracellular iron-transferrin complex. Interestingly, TFRC was also present in the MARCH3 and RNF128 interaction networks, and IP_3R was additionally classified as an HCIP for the mutant form of RNF26. Collectively, these data emphasise the potential collaborative activity of this group of ER-resident E3s, and validate that the approach used to characterise E3 interactions was able to successfully discover substrates.

Wnt signalling

Wnt signaling is critical during development and for the maintenance of adult tissue homeostasis (Logan and Nusse, 2004). Wnt ligands are secretory proteins which are palmitoylated in the ER lumen, enabling interaction with the transmembrane Wnt cargo receptor, evenness interrupted homologue (Evi) (Herr and Basler, 2012). This interaction drives the delivery of the Wnt ligands to the plasma membrane, where they can be released (Bartscherer et al., 2006; Bänziger et al., 2006). Importantly, it was observed that Evi levels positively correlated with the amount of Wnt ligand (Voloshanenko et al., 2013), and with no change observed at the transcriptional level (Muzny et al., 2012), this lead to the hypothesis that Evi may be post-translationally regulated.

Evi was identified as a HCIP for CGRRF1, MARCH4 and RNF128. In collaboration with the Boutros group (DKFZ, Heidelberg), Evi was shown to be constitutively degraded by the proteasome in the absence of Wnt ligand. Knockdown of CGRRF1 by siRNA rescued Evi turnover, whilst co-IP assays demonstrated that endogenous Evi interacts with CGRRF1-FH, but not with control Hrd1-FH (Figure 4.18). These data confirmed Evi as a substrate of CGRRF1, which orchestrates Evi ubiquitination and turnover when it is surplus to requirement (i.e. under conditions of limited Wnt ligand) (Glaeser et al., 2018).

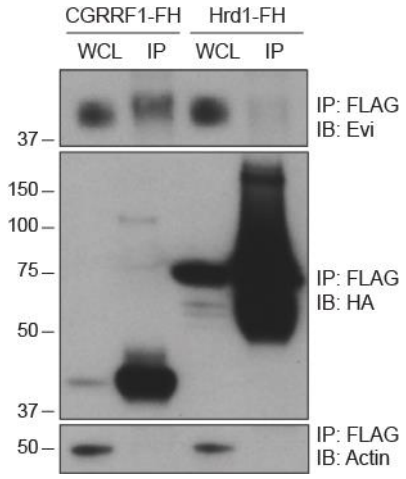

Figure 4.18: Endogenous Evi interacts with CGRRF1-FH. Flp-In293- cells expressing either CGRRF1-FH or Hrd1-FH were induced with DOX for 18 h and MG132 for 4 h. Harvested cells were solubilised in 1% LMNG and 5 mg WCL was used for anti-FLAG IP. 1% input (WCL) and IP samples were subject to SDS-PAGE and IB of endogenous Evi.

Other proteins involved in Wnt signaling were detected in distinct E3 complexes. Protein-tyrosine kinase 7 (PTK7), which complexes with β-Catenin and mediates its transcriptional program (Puppo et al., 2010), was found in both MARCH8 and RNF128 networks. Leucine-rich repeat flightless-interacting protein 2 (LRRFIP2) functions in Wnt signal transduction (Liu et al., 2005), and was identified as a HCIP of WT RNF26. On the other hand, the RNF26^{Y432A} mutant captured a different Wnt modulator, kelch-like protein 12 (KLHL12), which recruits the Cullin E3 ligase to promote Dishevelled ubiquitination and degradation (Angers et al., 2006).

The role verified for CGRRF1 in Evi degradation is another example of 'regulatory ERAD' and is also the first described function for this ligase. It is clear that apart from cofactors (see section 4.2.3.1), comparative proteomic profiling of the family of ER-resident E3s has discovered *bona fide* substrates. The HCIPs highlighted throughout section 4.2.3.2 therefore represent a collection of candidate substrates which have the potential to characterise novel functions for these E3 ubiquitin ligases.

4.2.3.3 A putative role for E3s in trafficking and at membrane contact sites

Several functions of the ER are dependent on its proximity and contact with other organelles. For example, contact sites between the ER and mitochondria can mediate both calcium and lipid transfer (Phillips and Voeltz, 2015), whilst the flux of secretory proteins from the ER to the Golgi relies on the formation of vesicles which bud off and fuse to the interfaces of these organelles (see Chapter 1, section 1.3.6). Protein exit from the ER is carried out by COPII vesicles, whilst COPI vesicles mediate the retrograde transport back to the ER (Gomez-Navarro and Miller, 2016). Proteins that escape the Golgi are either trafficked to the PM or sorted to the endosomal compartment. The endosomal pathway is also utilised by cell surface proteins, which upon internalisation are delivered to early endosomes, where they are either recycled back to the PM, shuttled to the trans-Golgi network (TGN), or sorted to late endosomes (LEs) which fuse to lysosomes to degrade their cargo (reviewed in (Foot et al., 2017)).

Protein trafficking

Spatial and temporal regulation of endosomal trafficking have long been understood to be regulated by ubiquitination of both cargo and machinery (Foot et al., 2017). Ubiquitin ligases have more recently been implicated in controlling ER export. KLHL12, an adaptor protein localised to ER-exit sites (ERES), recruits the Cullin-3 E3 ligase to promote the monoubiquitination of the Sec31 subunit of the COPII coat (Jin et al., 2012). This modification serves to enlarge COPII vesicles to accommodate bulky cargo such as collagen (Jin et al., 2012). Meanwhile, in fission yeast, the E3 activity of the Golgi-resident Dsc RING-ligase complex was found to be necessary for its exit from the ER (Raychaudhuri and Espenshade, 2015). Scanning HCIPs for known functions in trafficking discovered 13 proteins: 7 of which are linked

to ER export, and the remaining to endosomal transport, COPI vesicles, and exosomes (Table 4.3).

		Localisation	Trafficking function	Reference
ER export	**BCAP31**	ER	ER export	(Annaert et al., 1997)
	KLHL12	ERES	COPII coat formation	(Jin et al., 2012)
	LMAN2L	ER	Glycoprotein export	(Neve et al., 2003)
	SAR1A	ERES	COPII coat component	(Barlowe, 1994)
	SEC23IP	ERES	ERES organisation	(Shimoi et al., 2005)
	TMED1	ER	ER export	(Marzioch et al., 1999)
	TMED10	ERGIC	GPI-protein export	(Bonnon et al., 2010)
Endosome	**RAB11FIP1**	Early endosome	Endosome recycling	(Lindsay et al., 2002)
	RAB5C	Early endosome	Endocytosis	(Bucci et al., 2000)
	VAMP7	LE/lysosome	Endosome-lysosome fusion	(Advani et al., 1999)
Other	**AP3B1**	Tubular endosomal compartment	AP-3 complex component	(Peden et al., 2004)
	COPE	Golgi	COPI coat component	(Hara-Kuge, 1994)
	LMAN2	ERGIC, Golgi	Exosome trafficking	(Fullekrug et al., 1999; Kwon et al., 2016)

Table 4.3: Localisation and general function of HCIPs identified as trafficking components from the FH-E3 LC-MS/MS screen. ERES - ER exit site, ERGIC - ER-Golgi intermediate compartment, LE - late endosome. The references used provide evidence for both function and localisation of the HCIPs.

The 13 HCIPs involved in trafficking were found to form 22 interactions between 14 different E3s (Figure 4.19).

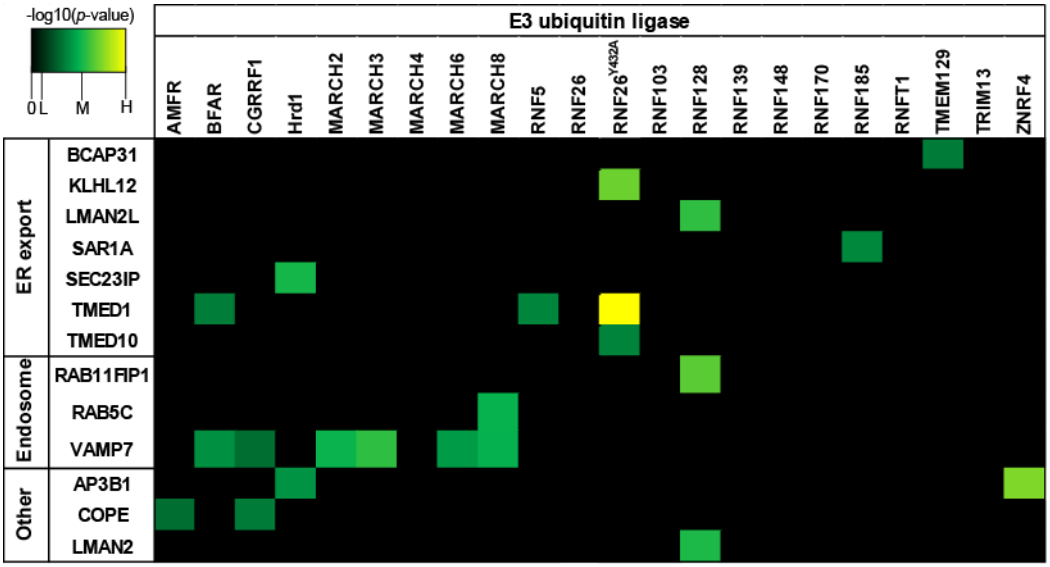

Figure 4.19: Heatmap of HCIPs involved in protein trafficking identified in the FH-E3 LC-MS/MS screen. The scale used is described in the legend of Figure 4.11.

With the exception of transmembrane emp24 domain-containing protein 1 (TMED1), which was a shared HCIP of three E3s, all ER-export HCIPs were uniquely associated with different E3s (Figure 4.19, top panel). This included the COPII coat protein SAR1A, which was found as a candidate interactor of RNF185. Whilst the four remaining COPII vesicle components (Sec23, Sec24, Sec13, and Sec31) were not identified as HCIPs, the Sec23-interacting protein (SEC23IP) was classified as a putative Hrd1 interactor. KLHL12 was associated with the RNF26^{Y432A} mutant, whilst B-cell receptor-associated protein 31 (BCAP31) and lectin mannose-binding 2-like (LMAN2L) were found with TMEM129 and RNF128, respectively.

The p24 family members are localised to the early secretory pathway and associate with both COPII and COPI vesicles. There are 11 family members in mammals, 8 of which have homologues in yeast (Strating and Martens, 2012). TMED10 and TMED1, whose yeast homologues have been shown to complex with one another

(Marzioch et al., 1999), were both identified as HCIPs of the RNF26^{Y432A} mutant. TMED1 was also associated with BFAR and RNF5.

Apart from ER export factors, other trafficking components were identified as HCIPs. A component of the COPI coat, epsilon-coat protein (COPE), was discovered as a HCIP of both AMFR and CGRRF1. The latter E3 was also associated with the late-endosomal/lysosomal vesicle-associated membrane protein 7 (VAMP7), however this HCIP was additionally shared between BFAR, MARCH2, MARCH3, MARCH6 and MARCH8. Early endosomal proteins Ras-related protein Rab-5C (RAB5C) and Rabb11 family-interacting protein 1 (RAB11FIP1) were determined as putative interactors of MARCH8 and RNF128, respectively. Only RNF128 pulled-down LMAN2, which plays a role in exosomal trafficking from the Golgi apparatus (Kwon et al., 2016). Lastly, AP3B1, the β-subunit of the protein-sorting AP-3 complex, featured as a HCIP in both Hrd1 and ZNRF4 interaction networks.

E3s at membrane contact sites

The ER interacts with other organelles via membrane contact sites (MCSs), which are determined by specific tethering proteins (listed in (Eisenberg-Bord et al., 2016)). Six MCS proteins were identified as HCIPs from the LC-MS/MS screen. Outer mitochondrial membrane (OMM) proteins, sorting and assembly machinery component 50 homologue (SAMM50) and metaxin-2 (MTX2), interact with the inner mitochondrial membrane (IMM) protein, MICOS complex subunit 60 (MIC60) (Xie et al., 2007). MIC60 is a component of the mitochondrial contact site and cristae organising system (MICOS) complex, which together with the sorting and assembly machinery (SAM) and ER-mitochondria encounter structure (ERMES) complexes, form the ER-mitochondrial organising network (ERMIONE) complex that spans the ER and both mitochondrial membranes. (M et al., 2012). Strikingly, SAMM50, MTX2 and MIC60 were all present in both RNF26 HCIP lists. MTX2 was also found in the TRIM13 interaction network. The mutant form of RNF26 also pulled-down the IP_3 receptor and VDAC1. The former is localised in the ER membrane, and the latter is embedded in the OMM, and they have been shown to bridge the two organelles (Szabadkai et al., 2006). IP_3 receptor was also identified with RNF170, and VDAC1 with RNF139. Lastly, one of the TMEM129 HCIPs was synaptotagmin-1 (ESYT1), which is an ER-plasma membrane tether (Giordano et al., 2013).

Collectively, these data might indicate that several E3s are recruited to particular ER sub-domains and/or MCSs to carry out specific functions. Given the fact that ubiquitin plays such an important role in coordinating endocytic protein transport, and the limited number of examples of ubiquitination in ER-Golgi trafficking, the role of the ER-resident E3s in this process is likely underestimated and warrants closer investigation.

4.2.4 Identification of unique interactors by Spectral Index Quantitation (SINQ)

The results in section 4.2.2 and 4.2.3 are based on the output from the cross-correlative, intensity-based analysis described by (Keilhauer et al., 2015) and detailed in section 4.2.1. However, there is one main disadvantage to this strategy: due to its comparative nature, if a protein is detected in only one bait sample and not any others, then it cannot be assigned a fold change and is thus excluded from classification as a HCIP. Therefore, to identify proteins unique to just one bait, which were simultaneously absent from the proteome of all remaining baits, we employed Spectral Index Quantitation (SINQ).

As highlighted in the introduction (section 4.1), LC-MS/MS generates both MS1 (peptide intensity) and MS2 (spectral count) data. MS1 data was used for the comparative analysis above. SINQ is a spectral count based method, which unlike classical spectral counting analysis, also takes into account the fragment ion intensity, thus generating a SINQ score (Trudgian et al., 2011).

SINQ analysis assigned a score to all proteins identified in each bait sample. The SINQ scores were sorted so as to select proteins only found in one E3 bait, and ranged from values of ~$8x10^{-5}$ to ~$2x10^{-9}$. SINQ-derived HCIPs were defined by imposing the following criteria on the dataset. First, a SINQ score cut-off of > $1x10^{-7}$ was applied. This cut-off was based on the SINQ scores of all Hrd1 interactors identified (SEL1L, OS-9, XTP3B, FAM8A1, Herp1, Herp2, Ube2j1), which were all > $1x10^{-7}$. Subsequently, proteins identified with only one spectral count were also removed, as these are unlikely to represent *bona fide* interactors (Sowa et al., 2009). Finally, common contaminants were removed (Supplementary data, Table S4.1). This approach successfully identified 28 unique HCIPs distributed between 13 different E3s (represented by dashed lines in Figure 4.20). Among the HCIPs

identified by SINQ were additional lipid regulatory, PQC, and trafficking components, all of which are annotated in the figures below.

In summary, combining HCIPs found by both analytical methods, over 450 putative interactions between 21 ER-resident E3s were identified. The HCIPs identified are linked to roles in ERAD, quality control, lipid regulation, trafficking, transport and signalling, suggesting these E3s are associated with numerous functions required for maintaining both ER and cellular homeostasis. Collectively, the HCIPs represent a diverse collection of candidate cofactors and substrates which will enable a more comprehensive characterisation of the ER-resident E3 family. The analysis of the interaction data is summarised in the individual E3 maps below (Figure 4.20).

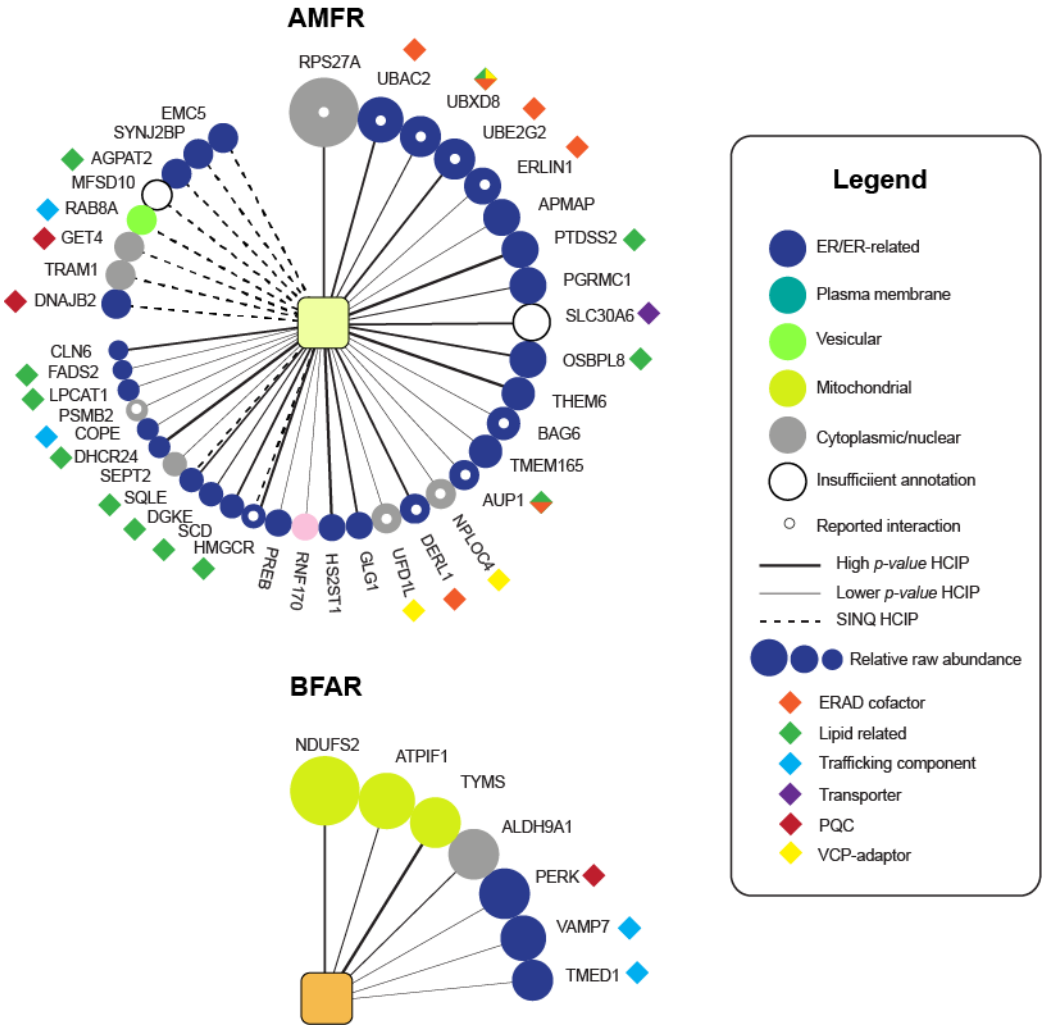

Figure 4.20: Interaction networks for AMFR and BFAR. The thickness of the line reflects the *p-value* of the interaction, and the size of the circle indicates raw abundance relative to the most abundant HCIP. ER/ER-related HCIPs are classified based on evidence from the literature, or in the case of uncharacterised proteins, the presence of a predicted signal sequence, glycosylation site, or disulphide bond. Diamonds represent functions referred to in Figures 4.11, 4.15, 4.16, 4.17 and 4.19. Previously reported HCIPs are marked with a central white dot. Dashed lines represent interactors found using the SINQ method.

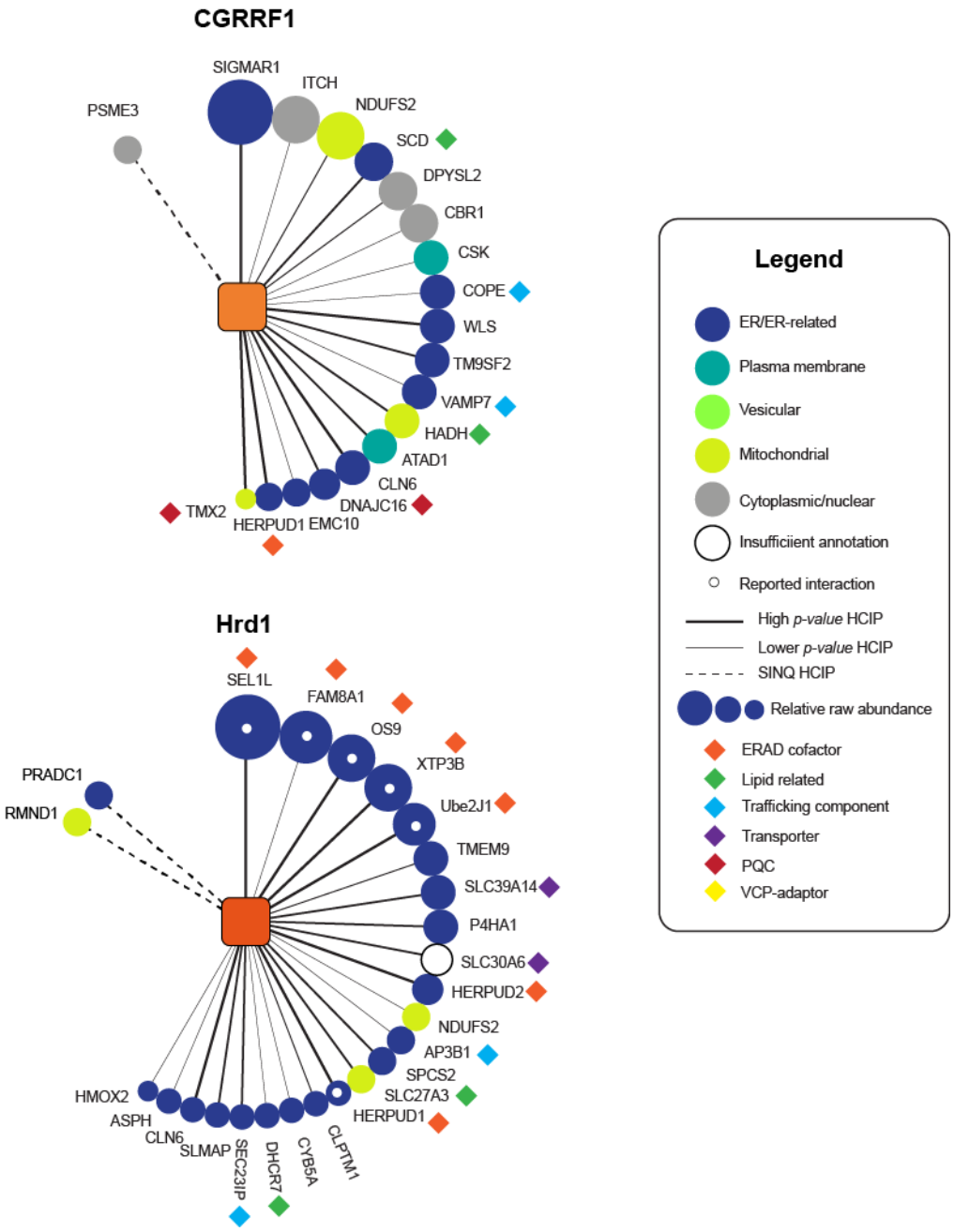

Figure 4.20 (continued): Legend as above but for CGRRF1 and Hrd1.

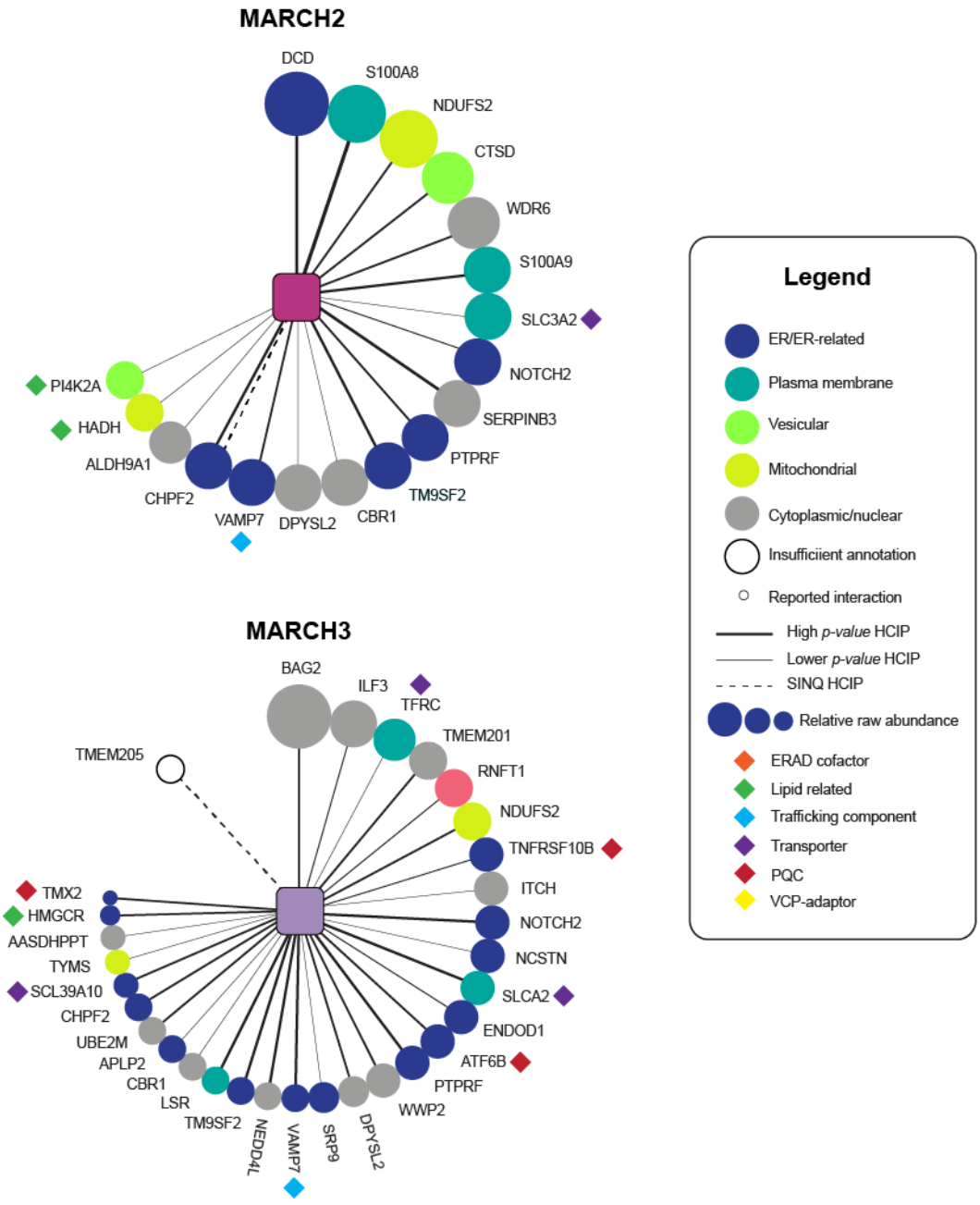

Figure 4.20 (continued): Legend as above but for MARCH2 and MARCH3.

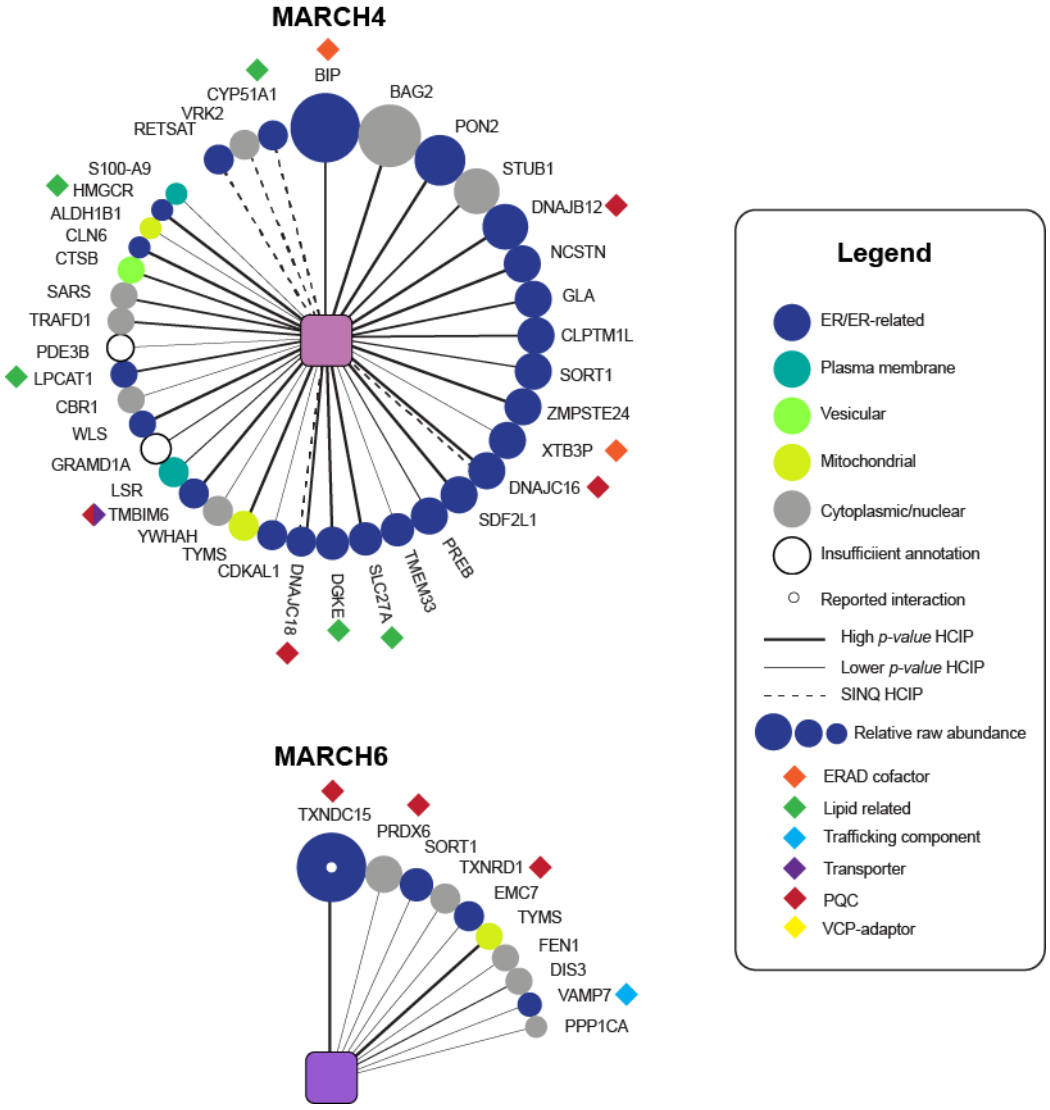

Figure 4.20 (continued): Legend as above but for MARCH4 and MARCH6.

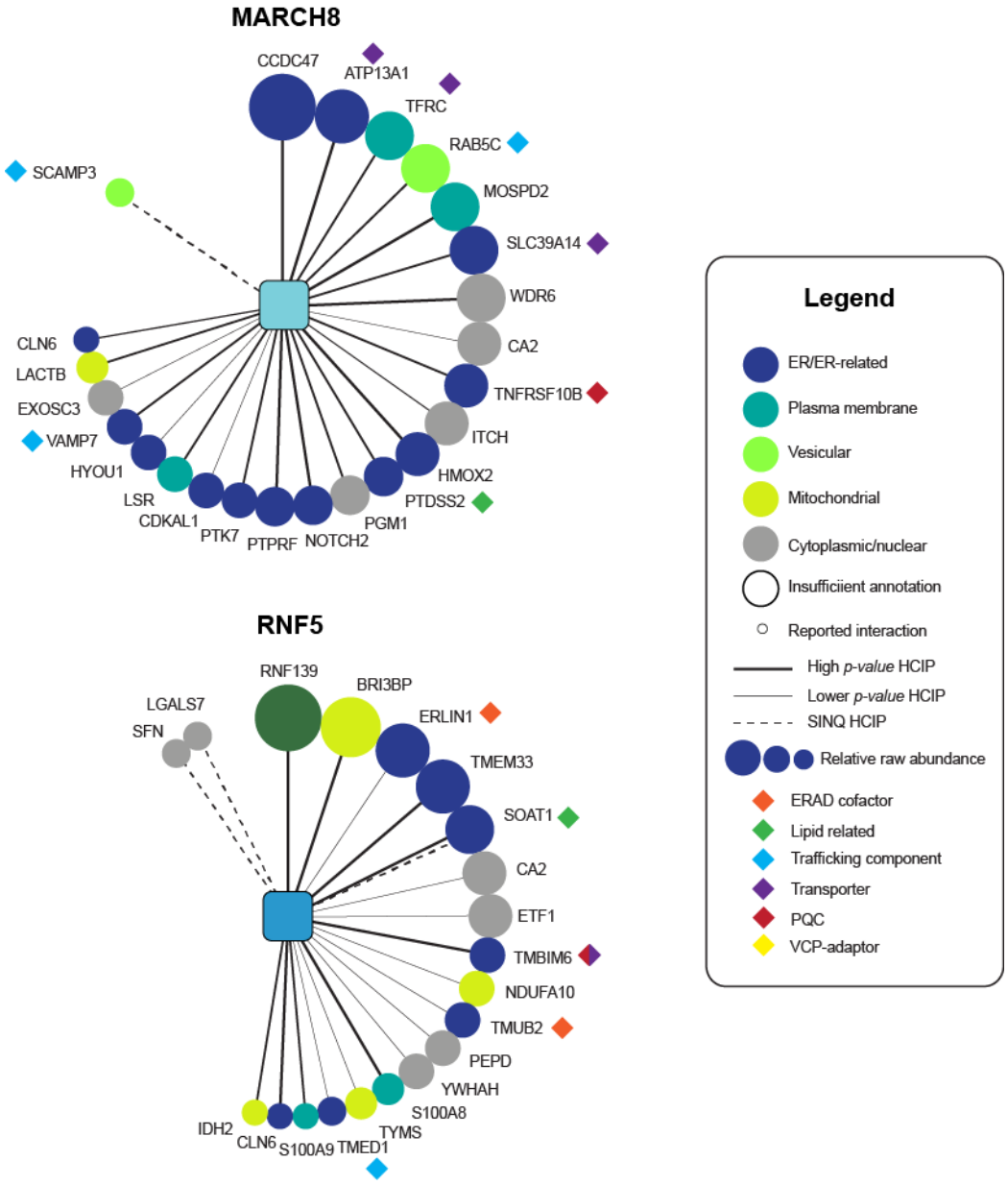

Figure 4.20 (continued): Legend as above but for MARCH8 and RNF5.

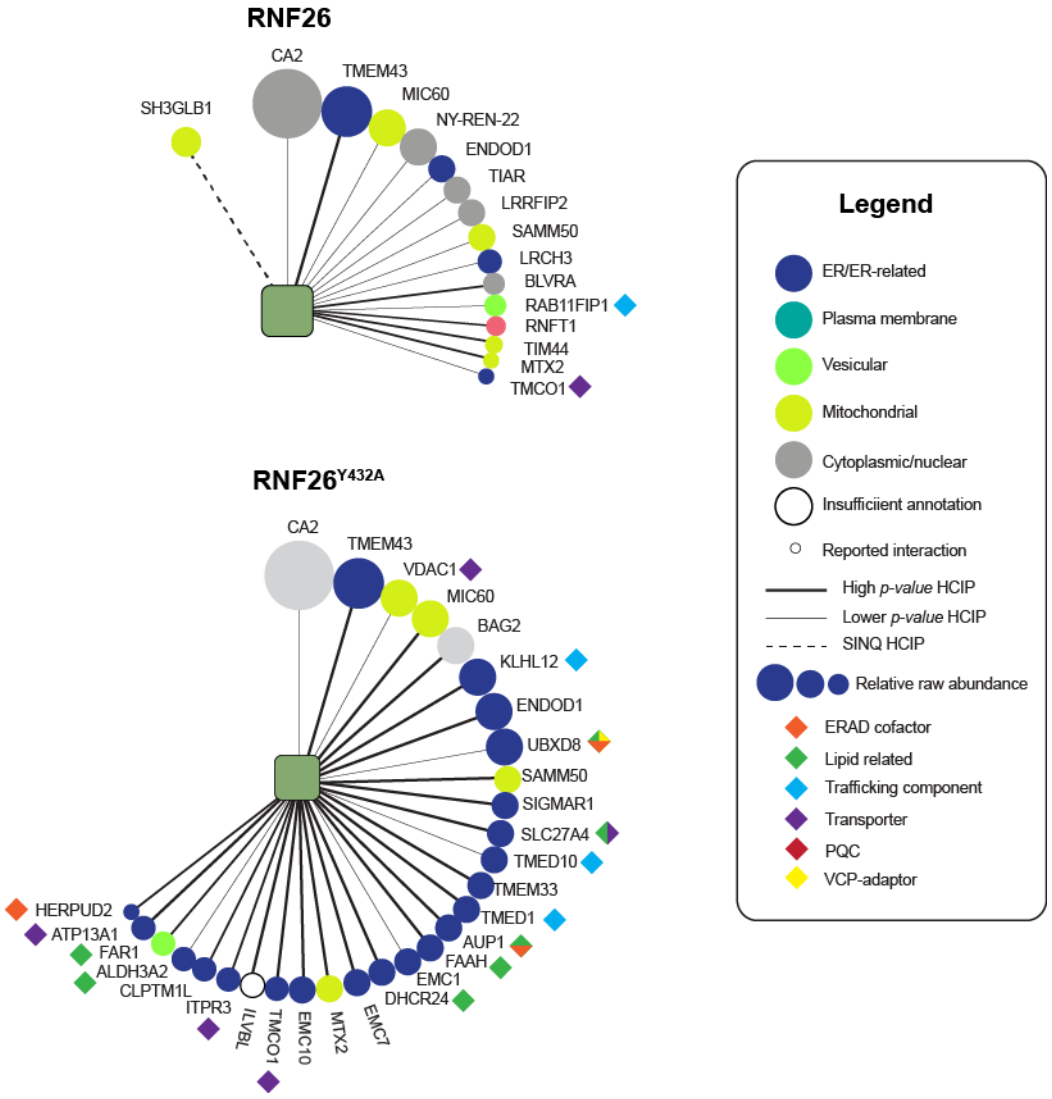

Figure 4.20 (continued): Legend as above but for WT RNF26 and RNF26^{Y432A}.

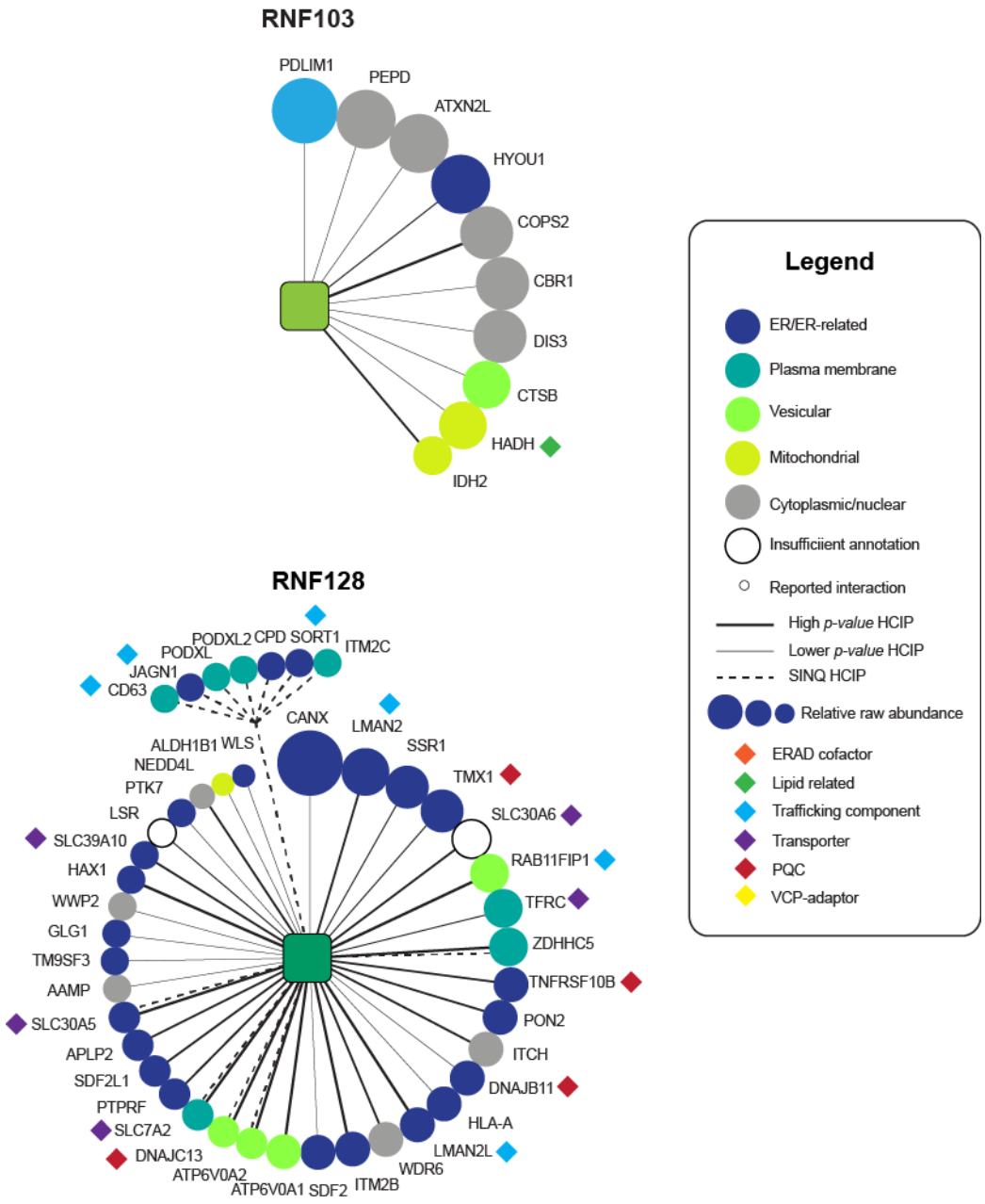

Figure 4.20 (continued): Legend as above but for RNF103 and RNF128.

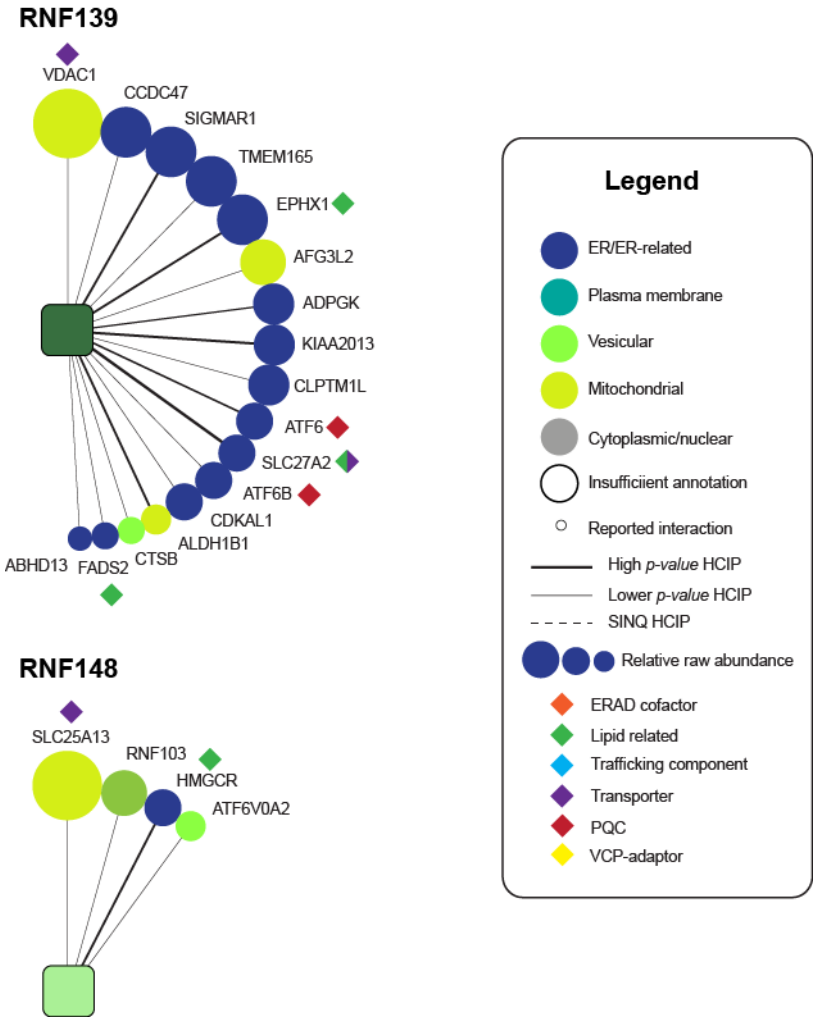

Figure 4.20 (continued): Legend as above but for RNF139 and RNF148.

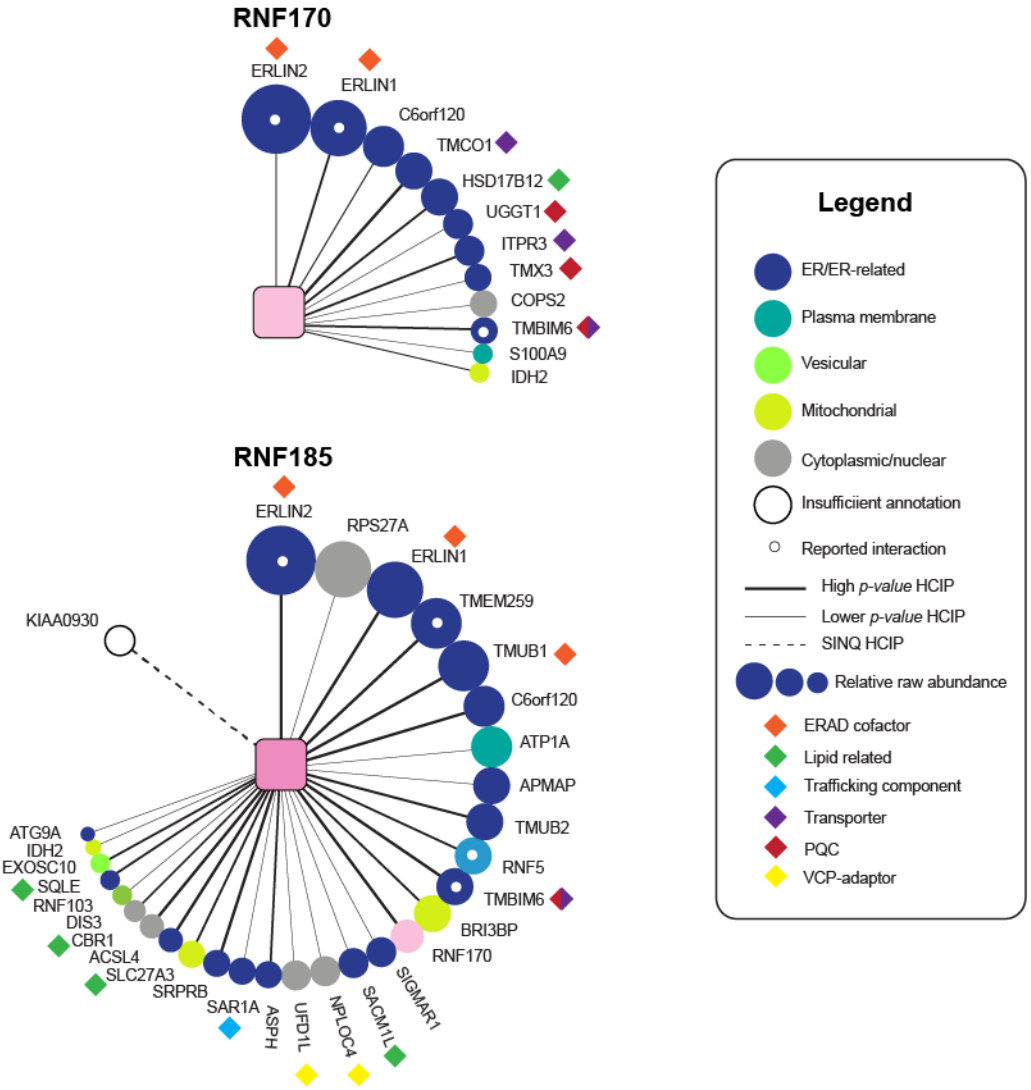

Figure 4.20 (continued): Legend as above but for RNF170 and RNF185.

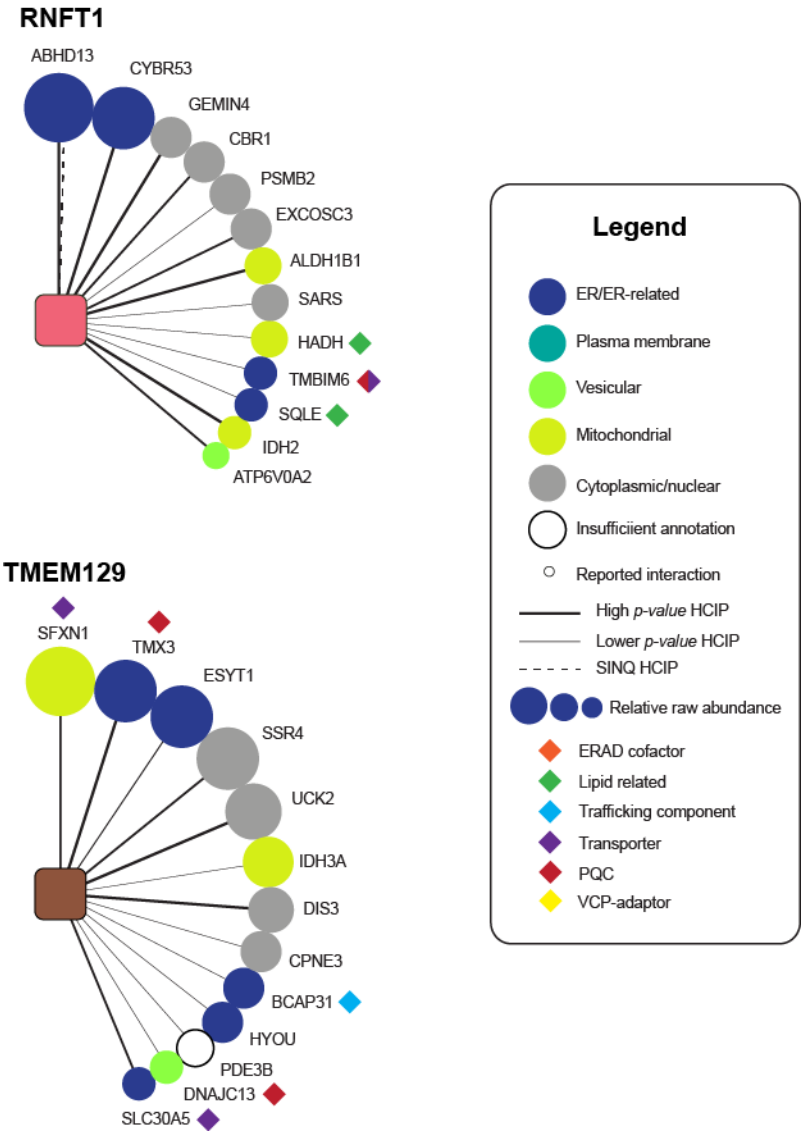

Figure 4.20 (continued): Legend as above but for RNFT1 and TMEM129.

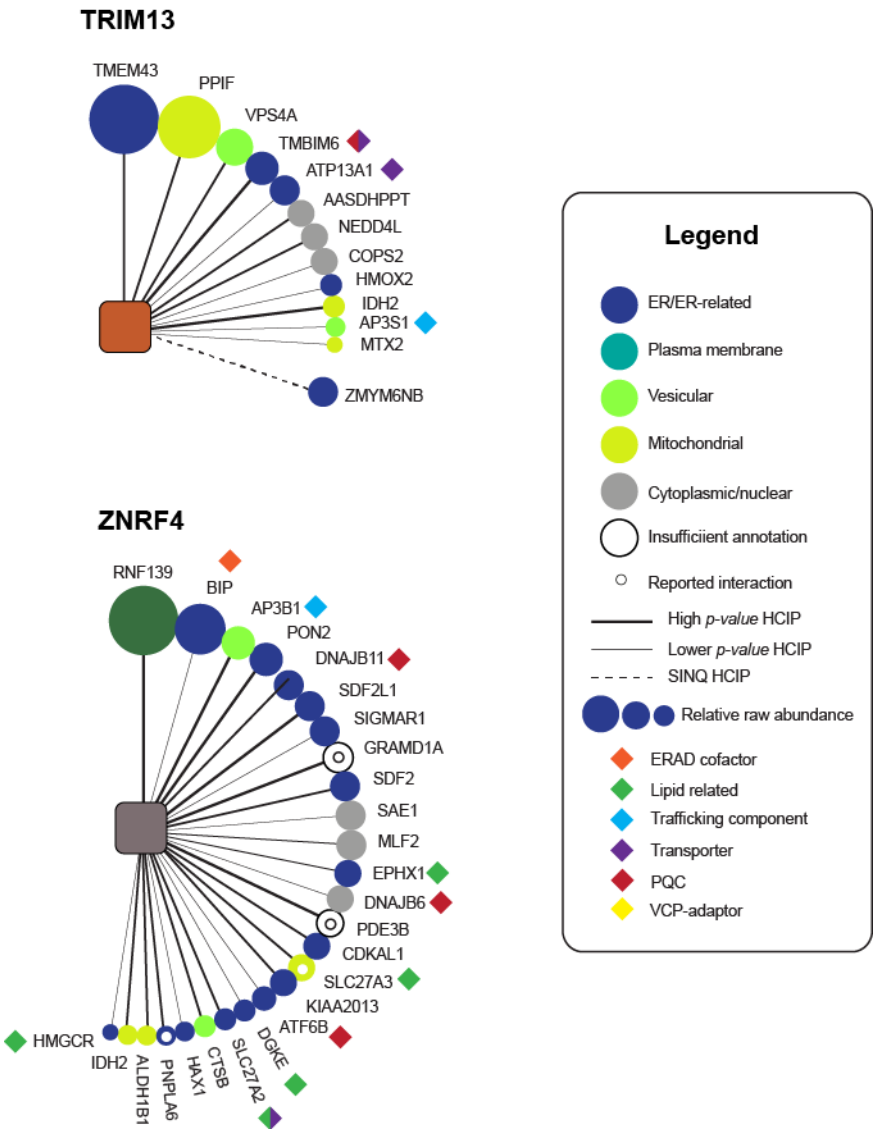

Figure 4.20 (continued): Legend as above but for TRIM13 and ZNRF4.

4.3 Discussion

Discovering E3 HCIPs - comparative proteomic profiling

To discover HCIPs for the ER-resident E3s, comparative proteomic profiling was adopted. This methodology was enabled by the fulfilment of several criteria. Firstly, samples were processed in parallel to reduce inter-sample variation. Secondly, the non-specific background interactors were maximized by solubilising cells with the non-stringent detergent LMNG, and effectively eluting all bead-bound material with SDS. Due to major advances in mass spectrometry sensitivity, peptides from several hundred proteins can be analysed, permitting the identification of both non-specific background 'binders' as well as specific interactors. Chromatograms from each LC-MS/MS sample run were aligned on Progenesis-QI, which compensates for variation between individual runs and hence allows comparative abundance profiling. The raw abundance of each identified protein is normalised against the background proteome allowing subsequent comparison between the samples. Each protein in a particular bait pull-down is compared to its 'bait-specific control group' (BSCG), which consists of all other bait pull-downs in which that protein was identified (Keilhauer et al., 2015). Therefore, the BSCG cross-correlative strategy essentially exploits the high number of samples, utilising the largest possible control group to generate fold changes for each identified protein (Figure 4.4). This is a much more powerful method relative to using 'empty bead' controls, which, due to the lack of specific antibody-antigen interactions do not necessarily yield a representative control group.

The fold-changes determined for each protein identified were used to derive individual *p-values*. This was performed using the MaxQuant Significance A algorithm (Cox and Mann, 2008) since the samples were run in technical duplicate, precluding them from standard *t*-test calculation. To distinguish HCIPs, a confidence

threshold of > 95% (*p-value* < 0.05) was applied to the data. This was combined with removing: significantly depleted proteins from each sample; proteins identified by less than two peptides; and common contaminants (Figure 4.5). Despite the fact that the cohort of significantly depleted proteins was not the focus of this study, it must be acknowledged that these proteins may represent substrates whose degradation kinetics have been increased by E3 overexpression, and therefore represent an interesting avenue for future research.

Proteins which satisfied the above-described thresholds were defined as HCIPs, with an average of 20 found per E3 bait. A total of 226 HCIPs were found between 22 bait samples (21 WT E3s and the RNF26^{Y432A} mutant, Figure 4.7). The number of HCIPs discovered relative to the number of bait samples was highly comparable to the ratio between HCIPs and baits in the DUB interactome study (Sowa et al., 2009), where 774 HCIPs were discovered for 75 DUB baits. Both the E3 and DUB interaction landscapes were compiled from the analysis of only one biological replicate of the LC-MS/MS experiment. However, the fact that each E3 was significantly enriched in its respective bait sample and that several known interactors of AMFR, Hrd1, RNF170 and RNF185 were identified as HCIPs (Figure 4.9), demonstrates that the pulldown and enrichment of the E3s and their *bona fide* interactors was successful.

There were inevitably some known interactions which were not identified as HCIPs from the E3 LC-MS/MS screen, most notably the Derlin and Insig members (See Chapter 1). Derlin1 is a known ERAD cofactor of AMFR, Hrd1 and TMEM129 (Lilley and Ploegh, 2005; van den Boomen et al., 2014; Ye et al., 2005), and although it was classified as an AMFR HCIP, it was absent from both Hrd1 and TMEM129 interaction networks (Figure 4.11). Derlin2, on the other hand, was not detected in any LC-MS/MS run, despite being a component of the Hrd1 and AMFR protein complexes (Christianson et al., 2012; Lilley and Ploegh, 2005). Similarly, Insig1 and

Insig2, functional interactors of AMFR and RNF139 (Lee et al., 2010; Song et al., 2005), were not detected by LC-MS/MS. The lack of detection may be attributed to discrepancies in experimental conditions compared to published studies, such as differences in sample preparation, and/or LC-MS/MS instrumentation.

Unique and shared features within the E3 interaction networks

One of the first observations from the global analysis of the comparative proteomic output, was that the unique HCIP was the most common type of candidate interactor (Figure 4.8a). This supports a model in which E3 complexes are largely distinct from one another and unique interactions are required to specify a diverse range of E3 functions. Shared interactions, on the other hand, may represent cofactors required for more general functions or could indicate E3 cooperativity. It is unlikely that common interactors are contaminants or background binders, as these would be expected to possess similar abundances in all or most samples and would therefore not be annotated with a large fold-change and high confidence score.

Both Erlin proteins were found shared between different E3s, with Erlin1 identified as a HCIP for AMFR, RNF5, RNF170 and RNF185, and Erlin2 present in the RNF170 and RNF185 interaction networks. Intriguingly, RNF5 and RNF170 were both discovered as HCIPs of RNF185, and RNF170 was additionally discovered as an AMFR HCIP (Figure 4.20). The Erlins were initially identified in lipid-raft-like domains within the ER membrane (Browman et al., 2006), and are required to degrade IP_3 receptors (Lu et al., 2011). However, despite their role in ERAD, their precise function remains unclear. It is tempting to speculate a role for the Erlins, and indeed other shared HCIPs, in bridging E3 complexes structurally and/or functionally.

Whilst the Erlins represent shared putative cofactors, several shared HCIPs were hypothesised to be potential E3 substrates (see next discussion section), such as TMBIM6, a calcium leak-channel (Bultynck et al., 2014) shared between six different E3s (Figure 4.17). Substrates whose turnover depends on two or more ligases are already documented, and include HMGCR (Jiang et al., 2018; Jo et al., 2011a) and CFTR (Khouri et al., 2013; Morito et al., 2008). In cases of substrates regulated by two or more E3, it would be necessary to distinguish whether the ligases involved worked cooperatively or if they were functionally redundant by assessing the outcome of individual and combined E3 knockdown.

Despite the fact that the BSCG method identified both unique and shared HCIPs, it is not able to classify a protein identified in only one sample as a HCIP. This comparative method is based on protein abundances derived from peptide intensities (MS1 data). The use of peak intensities for protein quantitation is a much more accurate method compared to spectral counting (Ahrné et al., 2013). However, spectral count-based quantitation is still reliable when large fold changes are involved, or if proteins are highly abundant in one sample but not present in another (Hutchinson et al., 2014). Therefore, spectral index quantitation (SINQ) was performed on the dataset and by selecting proteins with a high SINQ score, present only in one sample, an additional 28 unique HCIPs were found.

In summary, the advantages of intensity- and spectral count-based quantitation strategies were exploited to discover unique and shared HCIPs. Although SINQ was employed to overcome the shortcomings of the BSCG-based analysis by finding unique E3 candidate interactors, it can also be used to highlight the question of how to treat certain proteins identified in all samples.

If the SINQ data is sorted to list the proteins identified in all samples, the expected classic contaminants (keratins) and background binders (such as cytoskeletal components) are found. However VCP/p97 was also identified in this cohort, which is not necessarily surprising since it is one of the most abundant soluble proteins (Zeiler et al., 2012). Consistently, it was present in high abundance in all samples and was thus not identified as a HCIP of any E3 by the BSCG method. However, VCP/p97 is known to directly interact with the VIM domain of AMFR (Ballar et al., 2006). Indeed, ranking VCP/p97 SINQ scores from highest to lowest positioned AMFR as the strongest VCP interactor (Supplementary data, Figure S4.2). Interestingly, RNF185 was positioned third in list, consistent with the identification of the VCP cofactors, Npl4 and Ufd1, as two of its HCIPs (Figure 4.11). Whilst it is unlikely that VCP/p97 is a *bona fide* interactor of all ER-resident E3s, this observation does accentuate the difficulty in discovering interactions with proteins that appear to behave like common contaminants.

HCIPs - cofactors vs. substrates

HCIPs were scanned for known ERAD components to uncover novel roles in degradation for the less characterized E3s. This also included a bioinformatics search for VCP/p97 adaptor proteins, as they are known to bridge E3 complexes to the proteasome (Meyer et al., 2012). In total 16 ERAD cofactors and three VCP/p97 adaptor proteins were found, which included known cofactors of well-characterised E3s, and novel putative adaptors for CGRRF1, MARCH4, RNF26, RNF185 and ZNRF4 (Figure 4.11).

Based on the literature, these HCIPs are described as being E3 cofactors. However, it cannot be excluded that they may represent E3 substrates, and it is not possible to ascertain from the interaction alone whether a HCIP is more likely to be a cofactor or a substrate. Although PQC and degradation components are known to cooperate with ER-resident E3s to mediate substrate recognition, dislocation and ubiquitination (see Chapter 1), there is evidence from the literature to support the degradation of PQC machinery by E3s. For example, the ER stress transducer, Ire1, is a known substrate of Hrd1 (Sun et al., 2015), and ZNRF4 is proposed to degrade the chaperone, calnexin (Neutzner et al., 2011).

Notably, it is unlikely that the observed putative interactions with PQC machinery is due to E3 protein misfolding, since no *XBP1* splicing was observed upon overexpression (see Chapter 3). In addition, since Hrd1 is known to orchestrate ERAD of misfolded proteins (see Chapter 1) and is the most transcriptionally upregulated E3 in response to ER stress (Figure 4.12 and 4.13), one may expect misfolded E3s to be recognised by Hrd1. The lack of identification of Hrd1 as a HCIP for any E3s, together with the absence of detectable ER stress, strongly support that these overexpressed, tagged E3s are not substrates of the endogenous degradation machinery and that therefore their interactions with ERAD components and PQC factors are more likely to be of functional relevance.

PQC extends beyond misfolded protein degradation and includes ERAD of lipid metabolic and folded secretory proteins, such as transporters destined for the plasma membrane. The ‘Retrieve ID/mapping’ function on Uniprot was used to collect GO description terms to find lipid regulatory proteins and transporters, and the data was combined with a literature search to validate that the GO analysis matched the true function of the protein of interest.

This approach identified 26 lipid regulators and 16 transporters, which were proposed as putative substrates based on the evidence of E3 regulation of these protein types (see Chapter 1, section 1.4.1 and 1.5.1). The interactions between E3s and their substrates is often described as weak and/or transient (Iconomou and Saunders, 2016; O'Connor et al., 2015), however known substrates were successfully identified as HCIPs by LC-MS/MS of immunoprecipitated E3 complexes. Specifically, HMGCR was classified as a HCIP of AMFR (Jo et al., 2011b), the IP_3 receptor as a HCIP for RNF170 (Lu et al., 2011), and TFRC as a HCIP of MARCH8 (Fujita et al., 2013). Interestingly, these HCIPs were also associated with other E3s, suggesting their regulation may be controlled by the cooperative activity of different ligases. Despite these findings, it must be acknowledged that the approach used to characterise E3 interactions was not aimed specifically at enriching or 'trapping' substrates (see Chapter 6) and one would expect to predominantly identify cofactors which form more stable interactions. Indeed, several known E3-substrate interactions were not captured, such as that between MARCH6 and SQLE (Foresti et al., 2013; Zelcer et al., 2014) and RNF139 and HMGCR (Jo et al., 2011a).

The E3 LC-MS/MS screen did however discover the Wnt receptor, Evi, which follow-up studies confirmed as a substrate of the previously uncharacterised CGRRF1. In conditions of low Wnt ligand, Evi is ubiquitinated with K48-linked chains by CGRRF1 and targeted to the proteasome for degradation (Glaeser et al., 2018). Evidence of ubiquitination and/or protein stability can be used to help infer whether a HCIP is a likely E3 substrate or cognate cofactor. For example, stearol-CoA desaturase 1 (SCD1), an ER membrane embedded enzyme which synthesises monounsaturated fatty acids, has a half-life of 3 h and proteasome inhibition has been demonstrated to cause the accumulation of ubiquitinated SCD1 (Kato, 2006). It also known to interact with VCP/p97, however the mechanism through which it is degraded is unknown. Since it was detected as a HCIP of AMFR and CGRRF1, any stabilization upon

depletion of either or both ligases could indicate their participation in regulating its abundance.

Finally, it was also observed that several HCIPs classified as potential cofactors or substrates were found in the interaction network of the RNF26^{Y432A} mutant but not WT RNF26. The mutant is much more stable than its WT counterpart (see Chapter 5), and therefore any interactions with cofactors and substrates might be expected to be prolonged. The benefit of using E3 mutants to discover interactions, especially with substrates, is discussed further in Chapter 6.

E3 interactions - beyond the ER?

The ER is the entry-point of the secretory pathway, and therefore one of its primary functions is to mediate trafficking of secretory proteins to the Golgi apparatus and beyond. By scanning HCIPs for known functions in trafficking, 13 proteins required for either ER export or vesicle-mediate transport were discovered (Figure 4.19). The fact that the E3s are associated with HCIPs at ER-exit sites, raises the question whether E3s, or E3 sub-populations, could be localised to specific subdomains of the ER. Organelle subdomains include areas where membrane-contact sites (MCS) form and indeed, six contact site proteins were identified as HCIPs, including both ER-mitochondrial and ER-PM linkers. These data suggest that ubiquitination may occur at MCSs and it would be interesting to determine the recruitment and contribution of the E3s to these specialised membrane domains.

Furthermore, proteins not localised to the ER, and that have no current role in contact site formation, were discovered as HCIPs, supporting the evidence that some E3s used in this study are not exclusively localised to the ER membrane (Chapter 1, Table 1.2). HCIP localisation can be used to help construct hypotheses to assess E3 function. For example, VAMP7, which is localised to late endosomes and lysosomes, was found to interact with six different E3s (Figure 4.19). The interaction with MARCH2, MARCH3, and MARCH8 was not surprising, given that these E3s have also been shown to reside and function in endosomal compartments (Chapter 1, Table 1.2). Similarly, the PM-localised receptor TFRC, which is endocytosed upon binding the transferrin-iron complex, was discovered as a HCIP of MARCH3, MARCH8, and RNF128. RNF128 is known to traffic to the PM, and since ubiquitin can act as a signal for endocytic internalisation (Piper et al., 2014), then one could evaluate if RNF128 promoted ubiquitination and subsequent endocytosis of the TFRC-cargo complex.

To conclude, LC-MS/MS was successfully carried out for 21 ER-resident E3s. Intensity- and spectral count-based analyses of the LC-MS/MS data discovered 254 HCIPs which formed over 450 interactions. The HCIPs were biased towards ER-related and integral membrane proteins and approximately 50% were unique to just one E3. Known E3 cofactors and substrates were positively identified as HCIPs, demonstrating the capacity of this approach in finding both types of interaction. Over 80 HCIPs were mapped to ER functions, including quality control, lipid regulation and trafficking, ascribing putative novel roles for uncharacterised E3s in degradation and regulation at the ER membrane. The remaining HCIPs represent a rich pool of candidate interactors likely involved in a broad spectrum of functions beyond those specific to the ER membrane. Validation of HCIPs as true E3 interactors, and how this data can be used to characterise E3 complexes and function is the basis of the next chapter.

Chapter 5

Towards functional cofactors: the role of RNF26 and its interactors in regulating the innate immune response

5.1 An introduction to immune signalling at the ER membrane

Eukaryotic DNA is encapsulated within the nucleus and mitochondria, leaving the cytoplasm largely clear of DNA. This allows nucleic acid sensors to efficiently detect both microbial- and self-DNA, and elicit an innate immune response. DNA viruses, and retroviruses which rely on host reverse transcription machinery, are two common sources of cytoplasmic DNA. Self-DNA phagocytosed from neighbouring dead cells is also detected by cytosolic immuno-surveillance machinery (Chen et al., 2016).

Pathogenic nucleic acids have long been known to induce type I interferons (IFN-α and IFN-β). The transcriptional program orchestrated by these IFNs consists of the upregulation of a wide variety of genes, required for host defence and resistance, and activation of distinct immune response pathways (PERRY et al., 2005). However, until 2008, only the endosomal toll-like receptor, TLR9, had been characterised as a non-self DNA-sensor, with the response predominantly specific to unmethylated bacterial CpG DNA (Hemmi et al., 2000). To find novel immune effectors, a human embryonic kidney293 (HEK293T) system harbouring a luciferase gene downstream of the IFN-β promoter (IFN-β-Luc) was used to screen over 5,000 human ORFs (Ishikawa and Barber, 2008). ER-embedded STING (**St**imulator of **in**terferon **g**enes: named from this discovery) was identified for its capacity to induce luciferase upon overexpression. IFN-β is the primary target of the transcription factor interferon regulatory factor 3 (IRF3), and consistently STING drove luciferase expression controlled by an IRF3-responsive promoter (Ishikawa and Barber, 2008). IRF3 had previously been shown to be a substrate of TRAF family member-associated NFκB (TANK)-binding kinase 1 (TBK1), and in the absence of this kinase is unable to translocate to the nucleus to upregulate type I IFNs (McWhirter et al., 2004). It was therefore unsurprising that STING overexpression was unable to

induce IFN-β-Luc in *Tbk1*$^{-/-}$ mouse embryonic fibroblasts (MEFs) (Ishikawa and Barber, 2008).

Immediately after the discovery of STING, details of the pathway began to emerge. For example, it was demonstrated that STING, TBK1 and IRF3 formed a complex with one another (Zhong et al., 2008), and that STING dimerization through its transmembrane domains was necessary for signal transduction (Sun et al., 2009). Crucially, it was determined that the type I IFN response downstream of STING was specific to pathogenic DNA (Ishikawa et al., 2009). Compared to the almost complete loss of IFN signalling in *Sting*$^{-/-}$ MEFs upon treatment with viral or bacterial dsDNA, gene upregulation caused by activating melanoma differentiation associated protein 5 (MDA5, a cytosolic RNA-sensor) was unaffected in *STING* knockouts (Ishikawa et al., 2009). This work also revealed that after stimulation, STING translocates to perinuclear vesicles, a phenomenon blocked by the addition of Brefeldin A, which inhibits ER-to-Golgi trafficking. The identity of these vesicles was postulated to be autophagic given the colocalisation of STING-positive vesicles with autophagy-related protein 9a (Atg9a) (Saitoh et al., 2009). Indeed, it has recently been validated that activated STING is targeted for degradation by endolysosomes (Gonugunta et al., 2017).

It later emerged that STING could also respond to cyclic dinucleotides released by bacteria including *Listeria monocytogenes* (Sauer et al., 2011), and it was subsequently confirmed that radiolabelled cyclic-di-GMP directly bound STING (Burdette et al., 2011). However, there was no evidence that STING could bind dsDNA, despite the responses to cyclic dinucleotides and dsDNA being indistinguishable from one another (McWhirter et al., 2009). This discrepancy lead to the discovery of the cytosolic DNA-sensor, cyclic GMP-AMP synthase (cGAS), which

upon binding DNA, catalyses the formation of cyclic GMP-AMP (cGAMP), which subsequently binds STING (Sun et al., 2013; Wu et al., 2013).

Together, these findings have led to a model whereby DNA in the cytosol is sensed by cGAS, which synthesizes the secondary messenger, cGAMP (Sun et al., 2013). This binds STING (Wu et al., 2013), which then traffics from the ER to the ER-Golgi interface, before translocating to perinuclear vesicles (Dobbs et al., 2015; Ishikawa et al., 2009; Saitoh et al., 2009). During this translocation, TBK1 is recruited by STING to phosphorylate IFR3 (Tanaka and Chen, 2012), which is finally able to dimerise and enter the nucleus to induce type I IFN transcription (Figure 5.1). The ER membrane therefore provides a platform from which STING can be activated to signal. Additionally, STING is regulated by E3 ubiquitin ligases localised to the ER membrane, discussed in the next section.

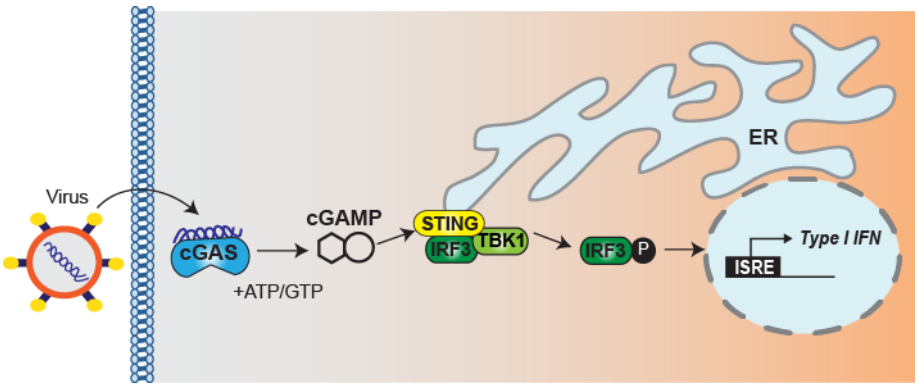

Figure 5.1: The cGAS-STING signalling cascade. Double-stranded DNA (dsDNA) binds cGAS, which generates cyclic dinucleotides (cGAMP). This secondary messenger is directly recognised by STING, which forms a complex with TBK1 and IRF3 and translocates to the Golgi apparatus. Phosphorylated IRF3 translocates to the nucleus to upregulate type I interferon (IFN) genes.

5.1.1 Modulation of the immune response by E3s

Innate immune signalling is dependent on ubiquitin's ability to assemble into different chains, allowing the appropriate protective response to be mounted against invading pathogens (Davis and Gack, 2015). Specifically, ubiquitination within the cGAS-STING pathway has been demonstrated to regulate downstream signalling events. Several E3 ligases have been reported to interact with and promote STING ubiquitination, including cytosolic members of the tripartite motif-containing protein (TRIM) E3 family, and ER-resident E3s (Chen et al., 2016).

Of the ER-resident E3s, RNF5 was the first identified to play a role in innate immune signalling modulation (Zhong et al., 2009). It was discovered as a STING-interacting protein by a yeast-two hybrid screen and subsequent analysis revealed that overexpression of RNF5, but not its inactive RING-mutant form, was sufficient to inhibit viral-induced type 1 IFN signalling (Zhong et al., 2009). Conversely, an increased signalling response was observed upon RNF5 knockdown. RNF5 was demonstrated to negatively regulate STING by promoting its K48-linked poly-ubiquitination and proteasomal degradation (Zhong et al., 2009). Although proteasome inhibition by MG132 rescues STING degradation following RNF5 overexpression (Zhong et al., 2009), it has recently been shown that MG132 treatment only rescued a small population of STING, which is degraded after activation (Gonugunta et al., 2017). These data hence raise questions about the precise contribution of RNF5 and the proteasome to this pathway.

The ER-embedded ligase, RNF26, has also been implicated in ubiquitination of STING (Qin et al., 2014). RNF26 was shown to interact with and promote K11-linked ubiquitination of STING at the K150 residue, which in turn protected it from premature K48-dependent degradation by RNF5. Consistent with a model where RNF26 antagonises RNF5 activity, it was demonstrated that RNF26 knockdown suppressed early viral-induced IFN signalling (Qin et al., 2014).

AMFR, an E3 ligase already associated with a range of different ER functions, was identified as a STING-interacting protein by mass spectrometry (Wang et al., 2014). Similar to RNF26, the depletion of AMFR caused IFN signalling attenuation after exposure to cytosolic DNA. This correlated with reduced translocation of the IRF3 transcription factor to the nucleus. It was elucidated that AMFR catalysed K27-linked ubiquitination of STING, which enabled effective recruitment of TBK1, previously determined to activate IRF3 through phosphorylation (Tanaka and Chen, 2012). Interestingly, the interaction between AMFR and STING was markedly strengthened by the AMFR cofactor Insig-1 (Wang et al., 2014), thus highlighting the functional relevance of E3 accessory factors.

Most recently, RNF185, a homologue of RNF5 (Khouri et al., 2013), was implicated in this immune response pathway (Wang et al., 2017b). IFN signalling triggered by infection with DNA virus (Herpes simplex virus 1, HSV-1) was reduced following knockdown of RNF185. This response was not observed when the pathway was activated with a STING ligand, indicating that RNF185 acts upstream of STING. Indeed, an interaction between cGAS and the cytosolic N-terminal domain of RNF185 was found and it was demonstrated that K27-poly-ubiquitination of cGAS by RNF185 was required for it to generate the 2’3’-cGAMP cyclic dinucleotide necessary for STING activation (Wang et al., 2017b).

These data collectively support a key role for ER membrane-localised E3s in controlling STING-dependent immune signalling. They also highlight the function of the ER membrane as a signalling platform, adding to the examples of non-K48-linked ubiquitination. The fact that the contribution of AMFR to this signalling pathway is reliant on its cofactor raises the interesting hypothesis that the other E3s involved in controlling this signalling event also depend on their functional interactions.

5.2 Rationale

Chapter 4 described how comparative proteomic analysis was used to successfully identify HCIPs for 21 of the 25 ER-resident E3s. All FH-tagged E3s used for LC-MS/MS profiling were WT E3s with the exception of RNF26. As mentioned in Chapter 3, RNF26 is a ubiquitin ligase with five transmembrane domains and a C-terminus which resembles that of the soluble dimeric E3, RNF4 (Supplementary data, Figure S3.1). The penultimate hydrophobic residue (Y193) of RNF4 resides at the interface of the dimers and mediates transfer of ubiquitin onto the substrate by activating the thioester bond in the E2-Ub intermediate (Plechanovová et al., 2011). Substitution of this tyrosine to a neutral alanine residue (Y193A) rendered the enzyme catalytically inactive (Plechanovová et al., 2011). The introduction of the equivalent mutation into RNF26 (Y423A) rendered it insensitive to proteasome inhibition (Chapter 3, Figure 3.11b). To characterise the FH-RNF26^{Y432A} mutant as catalytic-inactive, this chapter will begin with ubiquitin pulldowns and *in vitro* ubiquitination assays to compare both WT and mutant FH-RNF26 (section 5.3.1).

RNF26 activity is required for STING-dependent innate immune signalling (Qin et al., 2014) (see section 5.1.1) and endosomal sorting (Jongsma et al., 2016). The cGAS-STING pathway responds to cytosolic DNA by triggering IFN signaling (Chen et al., 2016). Qin and colleagues proposed that RNF26 regulated immune signaling by ubiquitinating STING and protecting it from K48-linked ubiquitination and subsequent degradation by RNF5 (Qin et al., 2014). Hence the knockdown of RNF26 was shown to abrogate IFN signaling downstream of viral-mediated STING activation (Qin et al., 2014). RNF26 was later demonstrated to recruit and ubiquitinate p62/SQSTM1, which in turn attracts ubiquitin-binding domains (UBDs) of different vesicle adaptor proteins, thus coordinating endosomal maturation and cargo trafficking (Jongsma et al., 2016).

Despite its associated functions, RNF26 was poorly characterised in terms of interactors prior to this study. Putative interactors (HCIPs) were discovered by LC-MS/MS performed on immunoprecipitated WT and mutant FH-RNF26 (Chapter 4). To determine whether the HCIPs identified by comparative proteomics are *bona fide* E3 interactors, a reciprocal-tagging strategy was employed to validate interactions between selected HCIPs and their respective E3s (section 5.3.2). Finally, to verify the utility of the LC-MS/MS screen in discovering functional E3 cofactors, a transcriptional-based readout was designed to test if the validated HCIPs contributed to the function of RNF26 in STING-dependent innate immune signaling (section 5.3.3).

5.3 Results

5.3.1 Characterisation of the catalytic-inactive RNF26^{Y432A} mutant

Based on its sequence similarity with RNF4, the Y432A mutation was introduced into RNF26 to disable its catalytic activity. Initial DOX titration experiments conducted on FH-RNF26^{Y432A} revealed it was insensitive to proteasome inhibition, in stark contrast to the acute sensitivity of WT FH-RNF26 to MG132 treatment (Chapter 3, Figure 3.11b). These data indicated that FH-RNF26 is a highly unstable enzyme. Therefore, to compare the degradation kinetics of both forms of RNF26, pulse-chase analysis was carried out on WT and mutant FH-RNF26-expressing cell lines (Figure 5.2).

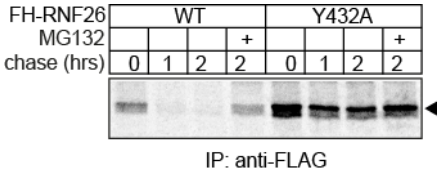

Figure 5.2: WT and mutant RNF26 pulse-chase. DOX-induced Flp-In293-FH-RNF26 and Flp-In293-FH-RNF26^{Y432A} cells were subject to pulse-chase analysis by S^{35} radiolabelling followed by anti-HA IP. Samples were subject SDS-PAGE and exposed to a phosphoimager.

These results clearly showed that WT FH-RNF26 has a very short half-life and that its degradation is rescued by MG132 addition. Conversely, FH-RNF26^{Y432A} appeared stable over the 2 h time-course. Several ubiquitin ligases have been reported to auto-ubiquitinate to control their turnover (Metzger et al., 2012). The above data suggest that WT RNF26 is degraded rapidly via auto-ubiquitination, whilst the mutant - which was generated to recapitulate the catalytic-inactivating effects of RNF4^{Y193A} - is unable to post-translationally auto-regulate. To test this hypothesis, ubiquitin pull-down experiments using tandem ubiquitin binding elements (TUBEs) (Hjerpe et al., 2009) were carried out to compare the ubiquitination profiles of both WT and mutant FH-RNF26 (Figure 5.3).

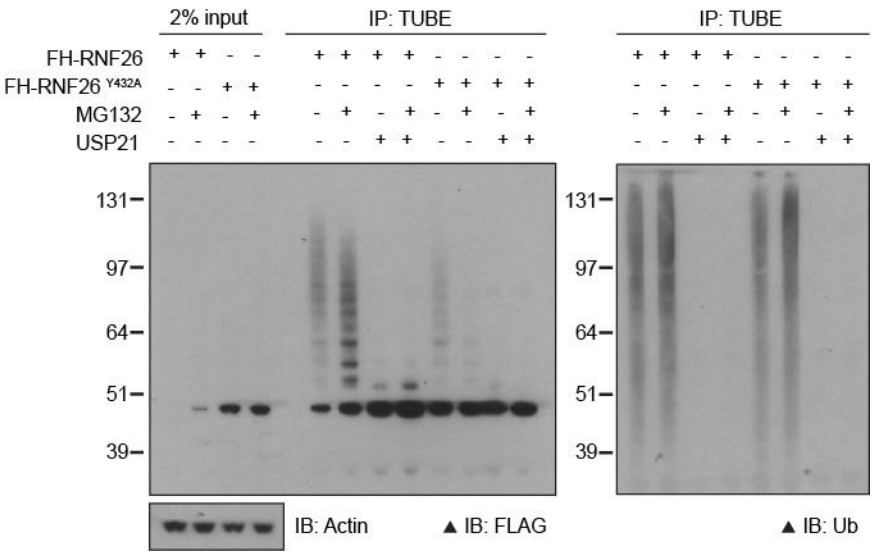

Figure 5.3: WT and mutant RNF26 TUBE pull-downs. WCL from DOX-induced Flp-In293-FH-RNF26 and Flp-In293-FH-RNF26^{Y432A} cells was subject to TUBE pulldown. MG132 treatment was for 2 h. DUB treatment (Usp21) was used to confirm the observed ubiquitin signal.

The high molecular weight FLAG-specific bands detected for FH-RNF26 are indicative of poly-ubiquitin. As expected, detection of this signal was enhanced upon MG132 treatment as proteasomal inhibition causes the ubiquitinated RNF26 to accumulate. Crucially, these bands were sensitive to de-ubiquitinating (DUB) enzyme (recombinant ubiquitin carboxyl-terminal hydrolase 21, USP21), confirming their identification as ubiquitin-positive species. Detection of poly-ubiquitinated FH-RNF26 was markedly reduced in the RNF26 mutant, consistent with the hypothesis that it is unable to auto-ubiquitinate. To confirm that the lack of poly-ubiquitin chains on FH-RNF26^{Y432A} is due to the catalytic inactivity of this enzyme, an *in vitro* ubiquitination assay was performed to compare ubiquitin chain formation by bead-bound FH-RNF26 and FH-RNF26^{Y432A} (Figure 5.4).

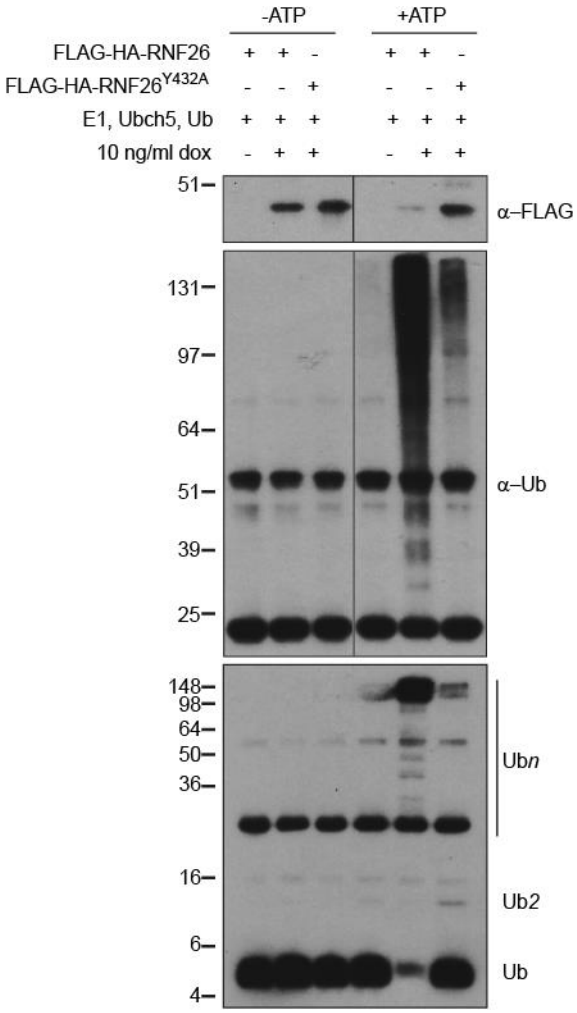

Figure 5.4: WT and mutant RNF26 *in vitro* ubiquitination assay. WCL from DMSO-treated and DOX-induced Flp-In293-FH-RNF26 and Flp-In293-FH-RNF26^{Y432A} cells was subject to anti-FLAG IP and used to carry out *in vitro* ubiquitination assays. Ub*n* - poly-ubiquitin, Ub*2* - di-ubiquitin, Ub - mono-ubiquitin.

Ubiquitination is an ATP-dependent process and therefore samples incubated without ATP serve as a negative control, along with the sample which was not treated with DOX. The ubiquitin blot (middle panel) reflects what was observed in Figure 5.3, with WT FH-RNF26 able to catalyse poly-ubiquitin chain formation and the mutant severely compromised in this activity. The ubiquitin blot in the bottom panel contains the same samples, but run on a high percentage SDS-PAGE gel so as to resolve mono- and di-ubiquitin (~7 and ~14 kDa, respectively). Significantly less mono-ubiquitin was detected with WT FH-RNF26, demonstrating that RNF26^{Y432A} has little remaining catalytic activity relative to WT RNF26.

Collectively, these results confirm that RNF26 is an active RING-domain E3 ubiquitin ligase, which auto-ubiquitinates to promote its rapid turnover by the 26S proteasome. RNF26 activity is dependent on the extreme C-terminal, hydrophobic tyrosine residue, which if substituted to a neutral amino acid, is rendered almost completely inactive.

5.3.2 Characterisation of an RNF26-containing protein complex

Both FH-RNF26 and FH-RNF26^{Y432A} were included in the LC-MS/MS interaction mapping. Given stability of the RNF26 mutant, it was expected to capture more HCIPs relative to the WT form. Indeed, 22 HCIPs were identified in the RNF26^{Y432A} sample, in addition to the seven HCIPs shared in common. Only eight HCIPs associated uniquely with WT RNF26 (Figure 5.5).

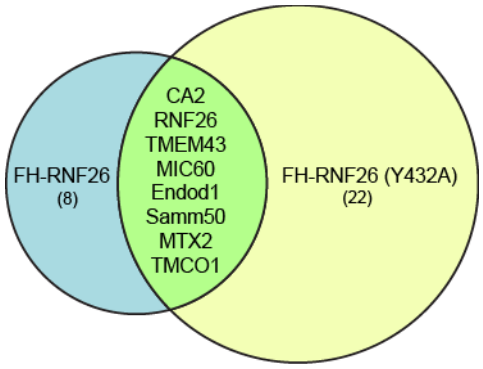

Figure 5.5: Venn diagram demonstrating the overlap between the WT FH-RNF26 and FH-RNF26^{Y432A} HCIPs.

To validate interactors of RNF26 and other E3s found by LC-MS/MS, a reciprocal-tagging method was employed. This method tests if the pulldown of an epitope-tagged HCIP is able to co-precipitate its respective E3. The HCIPs selected for validation were predicted/confirmed membrane proteins and displayed a wide range of *p-values* and raw abundances (Table 5.1 and Supplementary data, Table S5.1). For RNF26, putative interactors common to both WT and mutant, and unique to the mutant alone were chosen (Table 5.1).

	FH-RNF26		FH-RNF26^{Y432A}	
HCIP	**-log(*p-value*)**	**Raw abundance**	**-log(*p-value*)**	**Raw abundance**
ALDH3A2			1.78	1.76E+05
AUP1			4.40	1.08E+06
EMC1			1.45	1.02E+06
ENDOD1	1.61	1.81E+06	6.05	4.71E+06
SAMM50	1.81	1.05E+06	7.05	2.87E+06
TMED1			13.59	1.10E+06
TMED10			1.65	1.53E+06
TMEM33			7.05	1.24E+06
TMEM43	4.28	8.30E+07	12.03	1.39E+08
UBXD8			1.45	3.49E+06

Table 5.1: List of -log (*p-values*) and raw abundances for RNF26 HCIPs chosen for validation by reciprocal tagging.

ORFs of selected HCIPs were cloned to encode the S-peptide tag (S-tag) on either their N- or C-terminus. S-tagged HCIPs were subsequently transiently transfected into the appropriate FH-E3-expressing cell line and used for S-affinity purification (AP) followed by immunoblotting for the FH-tagged E3. Figure 5.6 shows the results from the pulldown of S-tagged HCIPs (listed in Table 5.1) transfected into FH-RNF26^{Y432A}-expressing cells. Unfortunately, S-tagged endonuclease domain-containing protein 1 (ENDOD1), SAMM50 and TMEM33 were not detectable by WB and are hence not presented. The interactions validated for other E3s by reciprocal tagging can be found in Supplementary data (Figure S5.1).

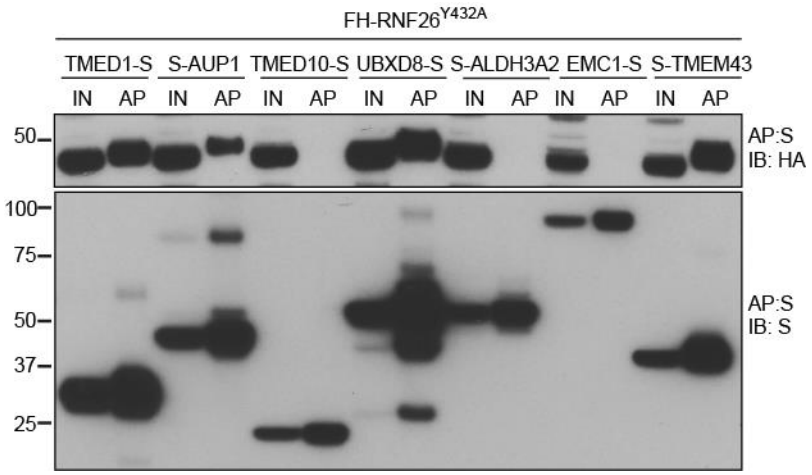

Figure 5.6: Validating FH-RNF26^{Y432A} HCIPs by reciprocal-tagging. S-tagged HCIPs were transiently expressed in the DOX-induced Flp-In293-FH-RNF26^{Y432A} cell line. Cell lysates were solubilized in 1% LMNG and 500 µg WCL were subject to S-AP followed by SDS-PAGE and S- and HA-immunoblotting. IN - 20% input, AP - affinity purification.

S-tagged TMED1, AUP1, UBDX8 and TMEM43 all efficiently captured FH-RNF26^{Y432A}, whilst TMED10-S, fatty aldehyde dehydrogenase (S-ALDH3A2) and ER membrane protein complex subunit 1 (EMC1-S) did not co-precipitate this E3, despite being identified as putative FH-RNF26^{Y432A} interactors (Figure 5.6). Interestingly, there was a positive correlation between HCIPs with stronger *p-values* and greater raw abundances being validated as interactors (Supplementary data, Figure S5.2).

As discussed in Chapter 3, the detergent used for preservation of E3 interactions, LMNG, forms large micelles and is often described as a mild detergent (Yang et al., 2014). By repeating the above experiment with the validated interactors and comparing the interaction profiles generated by solubilisation with LMNG, and a more stringent detergent, Triton-X-100, one can gain insight into the type of protein-protein interactions formed. This strategy was therefore used to help classify TMED1, AUP1, TMEM43, and UBXD8 into potential direct or indirect RNF26 interactors (Figure 5.7).

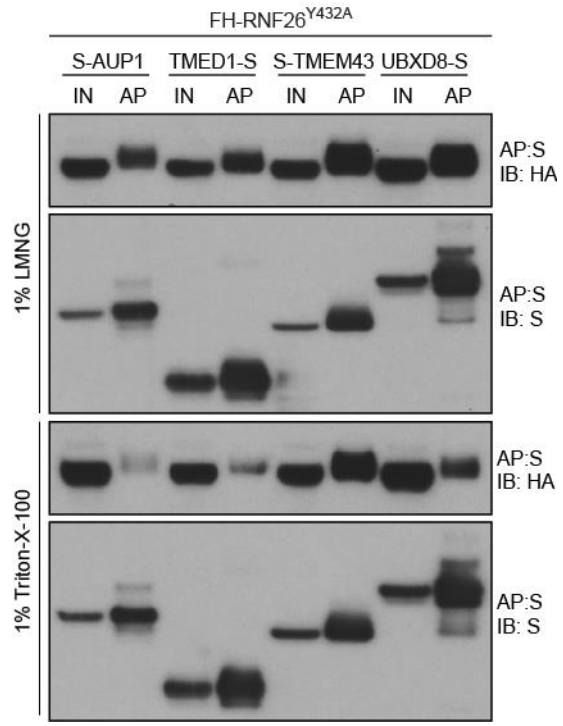

Figure 5.7: The effect of different solubilisation conditions on FH-RNF26^{Y432A} interactions. S-tagged HCIPs were transiently expressed in the DOX-induced Flp-In293-FH-RNF26^{Y432A} cell line. Cell lysates were solubilized in either 1% LMNG or 1% Triton-X-100 and 500 µg WCL were subject to S-AP followed by SDS-PAGE and S- and HA-immunoblotting. IN - 20% input, AP - affinity purification.

Strikingly, the interaction of both TMED1-S and S-AUP1 with FH-RNF26^{Y432A} was very sensitive to Triton-X-100 solubilisation. Relative to the amount of FH-RNF26^{Y432A} pulled down by these two S-tagged proteins in 1% LMNG, very little was co-precipitated from corresponding lysates solubilized in 1% Triton-X-100. The interaction between UBXD8-S and mutant FH-RNF26 was also sensitive to Triton-X-100 lysis, however more FH-RNF26^{Y432A} was co-precipitated by UBXD8-S relative to both TMED1-S and S-AUP1. Mutant FH-RNF26 was strongly enriched by S-TMEM43 pulldown, irrespective of the solubilisation conditions used. Collectively, these data suggest that TMEM43 forms a potential direct interaction with RNF26, whereas the interactions involving TMED1, AUP1 and UBXD8 are more labile and possibly mediated through interactions with other proteins.

The four S-tagged proteins shown in Figures 5.6 and 5.7 were validated to interact with the FH-RNF26 mutant, however TMEM43 was also identified as a HCIP of WT FH-RNF26 (see Table 5.1). Therefore, to determine if these S-tagged HCIPs were capable of interacting with the WT form of RNF26, transient transfections into the FH-RNF26-expressing cell line were also carried out, followed by S-AP in 1% LMNG and subsequent analysis by WB (Figure 5.8).

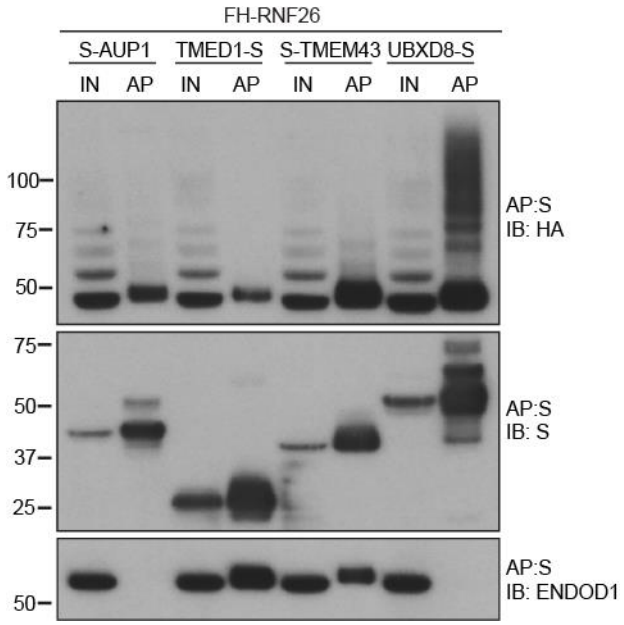

Figure 5.8: Recapitulating interactions using WT FH-RNF26. S-tagged HCIPs were transiently expressed in the DOX-induced Flp-In293-FH-RNF26 cell line. Cell lysates were solubilized in 1% LMNG and 500 µg WCL were subject to S-AP followed by SDS-PAGE and S- and HA-immunoblotting. IN - 20% input, AP - affinity purification.

The ability of these S-tagged HCIPs to co-precipitate either WT or mutant FH-RNF26 was essentially indistinguishable, with S-TMEM43 and UBXD8-S most efficiently enriching both forms of FH-RNF26. When blotting for WT FH-RNF26, the high-MW bands indicative of ubiquitinated species (see section 5.3.1) are clearly visible in the input lanes. Interestingly UBXD8-S co-precipitates both poly-ubiquitinated and unmodified WT FH-RNF26. This phenomenon may be due to the ubiquitin-associated (UBA) domain present in UBXD8, however this would have to be determined experimentally.

These results suggest that although HCIP discovery for WT RNF26 may have been restricted due to its instability, use of the catalytic-dead form of RNF26 compensated for this limitation. In addition, since S-tagged ENDOD1 had not been detectable by WB, immunoblotting for endogenous ENDOD1 was used to determine whether it was co-precipitated by any of the S-tagged proteins (Figure 5.8, bottom panel). Encouragingly, ENDOD1 was shown to interact with both TMED1-S and S-TMEM43, which confirms an interconnectivity between RNF26 interactors, indicative of a protein complex rather than a series of individual interactions. Intriguingly, ENDOD1 was not co-precipitated by UBXD8-S or S-AUP1, suggesting that different RNF26 populations might form independent complexes.

Components of complexes separated by density gradient sedimentation frequently co-migrate, as demonstrated for Hrd1 (Chapter 3, Figure 3.6). To verify if RNF26 and its validated interactors co-sediment, lysate from FH-RNF26-expressing cells was fractionated on 5-30% sucrose gradients. Precipitated fractions were subject to SDS-PAGE and immunoblotting of endogenous RNF26 interactors (Figure 5.9).

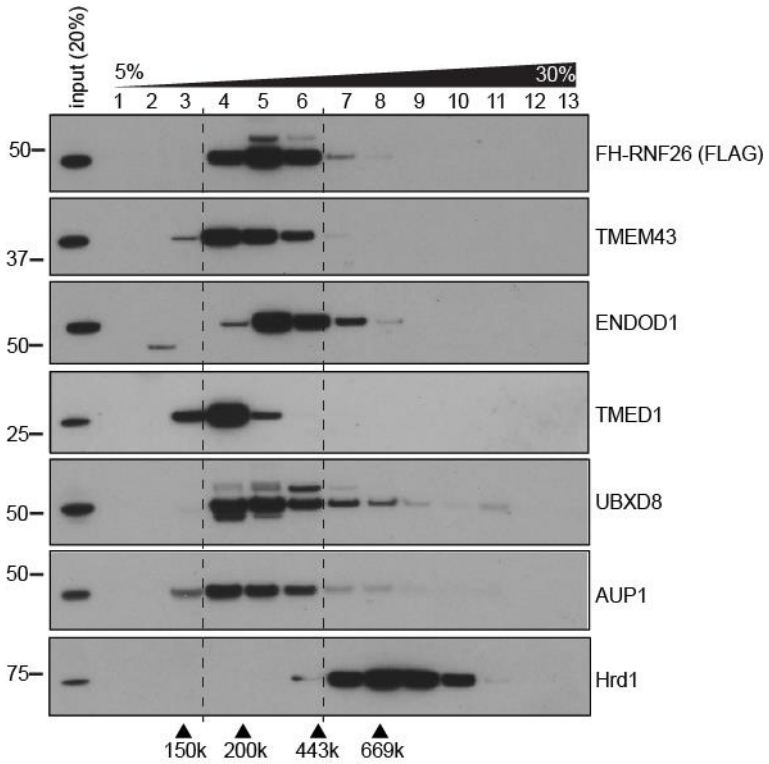

Figure 5.9: Sucrose gradient sedimentation profile of FH-RNF26 and its endogenous interactors. DOX-induced Flp-In293-FH-RNF26 cells were solubilised in 1% LMNG. 500 µg WCL was loaded onto 5-30% sucrose gradients and subject to ultra-centrifugation. Precipitated fractions and input (WCL) were subject to SDS-PAGE and immunoblotting.

WT FH-RNF26 clearly co-sediments with endogenous TMEM43, ENDOD1, TMED1, UBXD8 and AUP1 between fractions 4-6. This corresponds to a molecular weight of ~300 kDa (Supplementary data, Figure S5.3), which is approximately the sum of the MWs of these six proteins. Notably, the sedimentation profiles of some proteins do not completely overlap and extend beyond fractions 4-6. This does not preclude these proteins from being in the same complex, as demonstrated by the sedimentation pattern of Ube2j1, which migrates in fractions lower than Hrd1, despite both being components of the same complex (Chapter 3, Figure 3.6). Hrd1 was used as a negative control in Figure 5.9 as it migrates in higher fractions relative to FH-RNF26 and its interactors. Whilst co-sedimentation is a characteristic feature of proteins which interact to form complexes, this data does not confirm these proteins form a complex with each other, as each protein may be a component of an unrelated complex of the same MW.

The sedimentation pattern of TMEM43 was very similar to that of FH-RNF26 (Figure 5.9). Earlier it was shown that the TMEM43-RNF26 interaction was insensitive to stringent solubilisation conditions (Figure 5.7), indicative of a robust protein-protein interaction. Interestingly however, TMEM43 has previously been shown to be enriched in the nuclear envelope (NE), with its TMDs embedded in the inner nuclear membrane (INM) and its first hydrophilic loop extending into the ER lumen (Bengtsson and Otto, 2008).

The NE is continuous with the ER, and some proteins can be present in both subcellular environments. Therefore, to test if TMEM43 co-localised with RNF26, immunofluorescence (IF) was performed (Figure 5.10). The endogenous TMEM43 antibody was not suitable for IF, and therefore the S-tagged version was used. Additionally, FH-RNF26^{Y432A} was utilised for this method as WT FH-RNF26 did not produce a signal sufficient for detection above background, most likely due to its lower steady-state levels.

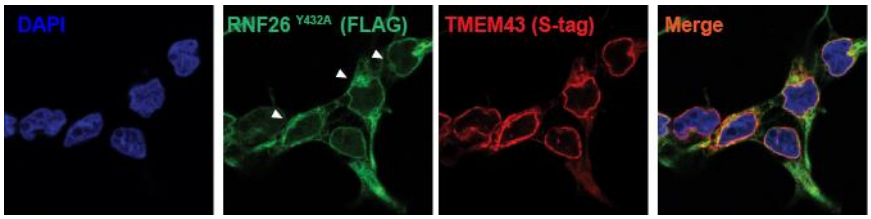

Figure 5.10: Perinuclear co-localisation between FH-RNF26^{Y432A} and S-TMEM43. Immunofluorescence of DOX-induced Flp-In293-FH-RNF26^{Y432A} cells. Anti-FLAG (Rb), anti-S-peptide (ms) and the corresponding Alexa-Fluor® secondary antibodies were used to stain FH-RNF26^{Y432A} and TMEM43-S, respectively. Nuclei were stained using DAPI.

As expected, TMEM43-S was predominantly organized in a clear perinuclear pattern. Strikingly, FH-RNF26^{Y432A} produced a distinct ER staining as well as colocalising with TMEM43 around the NE, suggesting a subpopulation of RNF26 may reside in the perinuclear compartment.

Given this observation, it would be interesting to determine how the subceullar localisation of RNF26 might impact its function. The localisation of its validated interactors is also intriguing. TMED1 (also known as Tp24) is a member of the p24 family of proteins and is proposed to be involved in secretory protein trafficking between the ER and Golgi (Marzioch et al., 1999). Unsurprisingly, therefore, it was found to localize to both organelles (Jenne et al., 2002). Both AUP1 and UBXD8 were originally identified as ER-resident proteins and play a role in ERAD (Mueller et al., 2008), however it later emerged that UBDX8 could migrate to lipid droplets (LDs) (Zehmer et al., 2009), where a small proportion of AUP1 was also present (Klemm et al., 2011). The uncharacterized protein ENDOD1 is anticipated to be an ER membrane-embedded protein as it is predicted to have a signal peptide (SignalP Server 4.1) and 3 TMDs (TMHMM Server v. 2.0).

It is possible that RNF26 forms complexes with these interactors in distinct ER subdomains. Nonetheless, the above data substantiates the use of proteomics in discovering novel E3 interactors, and the utility of including catalytic-inactive versions of E3s which are normally rapidly degraded through an auto-regulatory process. The fact that validated interactors, TMED1-S and S-TMEM43, were able to co-precipitate endogenous ENDOD1, a protein identified as a HCIP for both WT and mutant FH-RNF26, determines an association between the interactors. This in turn is indicative of a protein complex, which is further supported by the co-migration of these proteins by sucrose gradient sedimentation.

5.3.3 The role of RNF26 interactors in innate immune signaling regulation

As discussed in Chapter 4, substrates targeted for ubiquitination tend to interact transiently with their cognate E3 (Iconomou and Saunders, 2016). Consequently, one might expect their interaction with catalytic-inactive E3 mutants to be enriched as their 'docking time' on the E3 is likely to be prolonged. However, S-tagged AUP1, TMED1, TMEM43 and UBXD8 each co-precipitated comparable amounts of both WT and mutant RNF26 (compare Figures 5.7 and 5.8) suggesting that these interactors could be cofactors, rather than substrates, of this E3. Cofactors are not intrinsically active and instead coordinate to regulate the function of their cognate enzyme, as described earlier for Hrd1 and other ER-resident E3s (see Chapter 1, sections 1.3.5, 1.4.1 and 1.5.1). RNF26 is proposed to modulate the innate immune response downstream of STING activation (Qin et al., 2014) (see section 5.1.1). STING is activated by cyclic dinucleotide, 2'3'-cGAMP, generated by cGAS upon detection of cytosolic DNA (reviewed in (Chen et al., 2016) and section 5.1). Therefore, in an attempt to determine if the validated interactors are indeed cofactors of RNF26, a functional readout was designed based on the role described for RNF26 in STING-dependent signaling (Qin et al., 2014).

To activate this signaling pathway, the commercially available STING ligand, 2'3'-cGAMP (henceforth referred to as cGAMP), was transfected into WT Flp-In293 cells. Activated STING triggers the type I IFN response, which includes the upregulation of a plethora of IFN-stimulated genes (ISGs), one of which is *IFIT1* (Schoggins and Rice, 2011). Transfection of WT Flp-In293 with cGAMP caused a dose-dependent increase in expression of the *IFIT1* target gene, which was not induced by exposure to transfection reagent alone (Supplementary data, Figure S5.4).

Using two independent siRNA sequences targeting *RNF26* it was observed that the increase in *IFIT1* levels upon cGAMP transfection was attenuated relative to control knockdown cells (Figure 5.11a). Knockdown efficiencies are reported in Supplementary data (Figure S5.5). This result recapitulated the data presented by Qin and colleagues and is consistent with the role of RNF26 in supporting signaling downstream of STING activation (Qin et al., 2014). Interestingly, expression of the catalytic-inactive mutant of RNF26 caused a similar reduction in *IFIT1* upregulation, demonstrating the Y432A mutation has a dominant negative effect (Figure 5.11b).

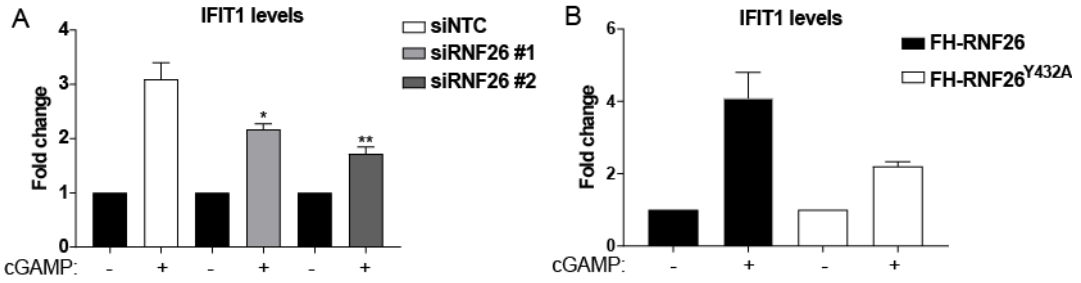

Figure 5.11: Reduced cGAMP-induced *IFIT1* upregulation upon RNF26 knockdown or expression of FH-RNF26^{Y432A}. (a) siNTC and siRNF26-transfected Flp-In293 cells were treated with cGAMP (5 µg/ml, 6 h) and analysed by Taqman qRT-PCR to determine *IFIT1* and *GAPDH* levels. Error bars represent s.e.m. from $n = 6$ biological replicates. *$P < 0.05$, **$P < 0.01$. (b) DOX-induced Flp-In293-FH-RNF26 and Flp-In293-FH-RNF26^{Y432A} cells were treated with cGAMP (5 µg/ml, 6 h) and analysed as described for (a). Data representative of two biological replicates.

The established readout was subsequently used to screen whether the validated interactors of RNF26 also played a role in modulating signaling downstream of STING activation. Knockdown of either TMED1 or ENDOD1 phenocopied the inhibited *IFIT1* upregulation observed upon cGAMP treatment in RNF26-depleted cells (Figure 5.12a). In constrast, cGAMP transfection in cells knocked-down for TMEM43 led to increased *IFIT1* signaling compared to control cells (Figure 5.12b). The same effect was observed for TMEM33 (Figure 5.12b), which was identified as a HCIP of FH-RNF26^{Y432A} (Table 5.1). Unfortunately, neither S-tagged nor endogenous TMEM33 were detectable from WCL, and hence it requires validation as a *bona fide* interactor of RNF26.

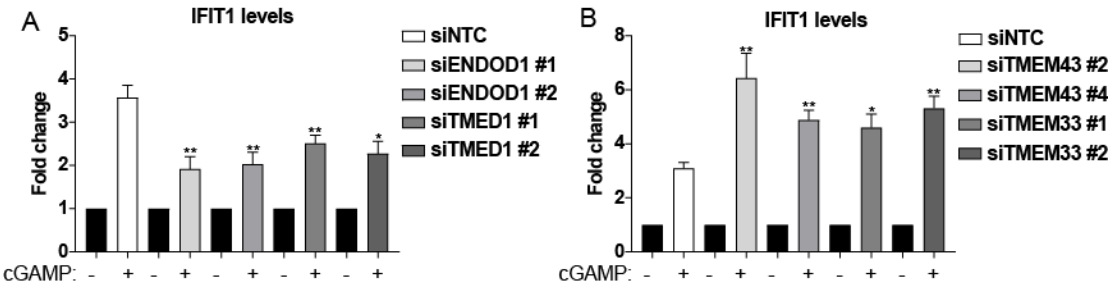

Figure 5.12: The effect on cGAMP-induced *IFIT1* upregulation upon depletion of RNF26 interactors. (a) siNTC, siENDOD1 and siTMED1-transfected Flp-In293 cells were treated and analysed as described in Figure 5.11. Error bars represent s.e.m. from *n* = 4 biological replicates. (b) siNTC, siTMEM43 and siTMEM33-transfected Flp-In293 cells were treated and analysed as described in Figure 5.11. Error bars represent s.e.m. from *n* = 8, 4, 8, 6 (reading from left to right) biological replicates. **P* < 0.05, ***P* < 0.01, ns is not significant.

Intriguingly, knocking down UBXD8 or AUP1 caused no significant changes in *IFIT1* upregulation in response to STING activation (Figure 5.13) and therefore served as negative controls for this assay. Earlier it was shown that S-AUP1 and UBXD8-S were not able to co-precipitate ENDOD1 despite pulling down FH-RNF26 (Figure 5.8). Together these data support a hypothesis whereby distinct RNF26 interactions (and possibly complexes) are required to carry out unique functions, with the interactions between UBXD8, AUP1 and RNF26 potentially involved in processes independent of STING signaling.

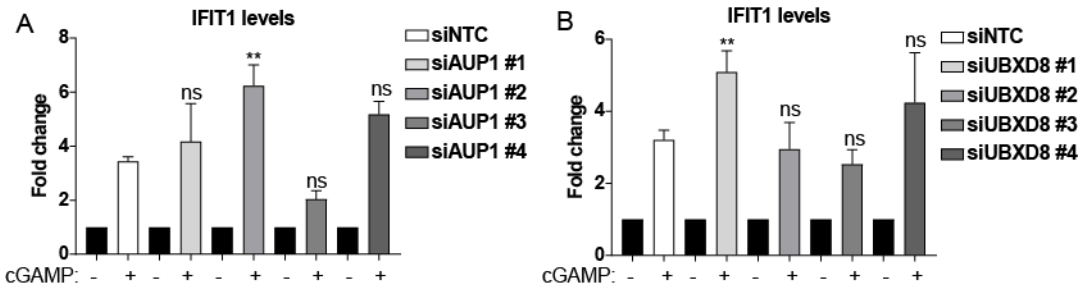

Figure 5.13: Knockdown of AUP1 and UBXD8 has no effect on cGAMP-induced *IFIT1* upregulation. (a) siNTC and siAUP-transfected Flp-In293 cells were treated and analysed as described in Figure 5.11. Error bars represent s.e.m. from *n* = 8, 5, 4, 4 (reading from left to right) biological replicates. (b) siNTC and siUBXD8-transfected Flp-In293 cells were treated and analysed as described in Figure 5.11. Error bars represent s.e.m. from *n* = 6, 9, 3, 3 (reading from left to right) biological replicates. **P* < 0.05, ***P* < 0.01, ns is not significant.

Collectively, the above data describes four novel regulators of STING-dependent immune signalling and segregates the RNF26 interactors into two categories: those which positively contribute to the function of RNF26 and potentiate innate immune signalling (TMED1 and ENDOD1); and those which antagonize its function (TMEM43 and TMEM33). Subsequent experiments were carried out in an attempt to understand the mechanism through which these interactors function. Given the short half-life of RNF26, it was initially investigated whether the depletion of selected interactors significantly altered its degradation kinetics, by performing cyclohexamide (CHX) chase analysis. Control knockdown samples were subject to both proteasomal inhibition (MG132) and VCP/p97 inhibition (NMS873). The Hrd1-dependent ERAD substrate, CD147, (Tyler et al., 2012) was used as a negative control (Figure 5.14).

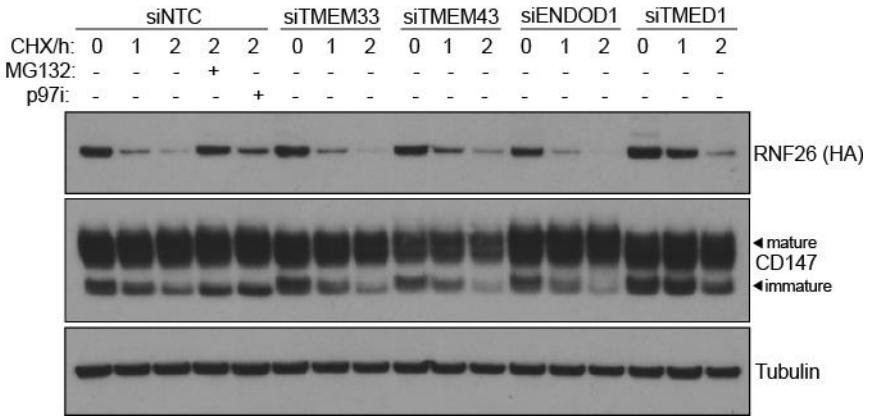

Figure 5.14: RNF26 interactor depletion does not effect FH-RNF26 turnover. siRNA-transfected Flp-In293-FH-RNF26 cells were treated with 1 µg/ml DOX for 18 h and subsequently with cyclohexamide (CHX, 100 µg/ml) for the indicated time-points. MG132 (10 µM, 2 h) and NMS-873 (10 µM, 2 h) treatments were included in the siNTC samples. Data representative of three biological replicates.

Interestingly, although proteasome inhibition completely rescued RNF26 degradation, VCP/p97 inhibition only prevented a small fraction of the RNF26 population from being degraded, suggesting that RNF26 is degraded by the proteasome in a VCP/p97-independent manner. This observation is not due to differences in drug efficacy, as CD147, which is dependent on VCP/p97 for its proteasomal degradation, was equally sensitive to both MG132 and NMS873 treatments. Importantly however, the depletion of TMEM43, TMEM33, ENDOD1 or TMED1 did not cause any striking changes to RNF26 stability relative to the CD147 control. Therefore, the differences in STING-dependent *IFIT1* upregulation caused by knockdown of these transcripts cannot be explained by changes in the stability of RNF26.

RNF26 is reported to regulate innate immune signaling by K11-ubiquitinating STING, which is proposed to protect it from RNF5-mediated K48-linked ubiquitination and subsequent proteasomal degradation (Qin et al., 2014). Therefore, investigating STING ubiquitination would ideally be used to help determine the role of the RNF26 interactors in modulating the downstream response. Unfortunately however, detecting ubiquitinated STING proved challenging, with little or no signal detected from multiple attempts (data not shown). Instead, since RNF26 is suggested to reduce the rate of STING degradation (Qin et al., 2014), one could use STING levels as a proxy for ubiquitination to infer interactor function. STING is degraded following dsDNA or cGAMP treatment to limit proinflammatory signaling (Prabakaran et al., 2018). Indeed, STING levels decreased over time upon treatment with the DNA-virus, HSV-1, and a greater decrease was observed in cells depleted for RNF26 (Qin et al., 2014).

Interestingly, upon knockdown of RNF26 the basal levels of STING in untreated cells were found to be significantly reduced (Figure 5.15). A similar reduction was observed in cells depleted for TMED1, however reduction of TMEM33, TMEM43 or ENDOD1 had no effect on basal STING levels (Figure 5.15).

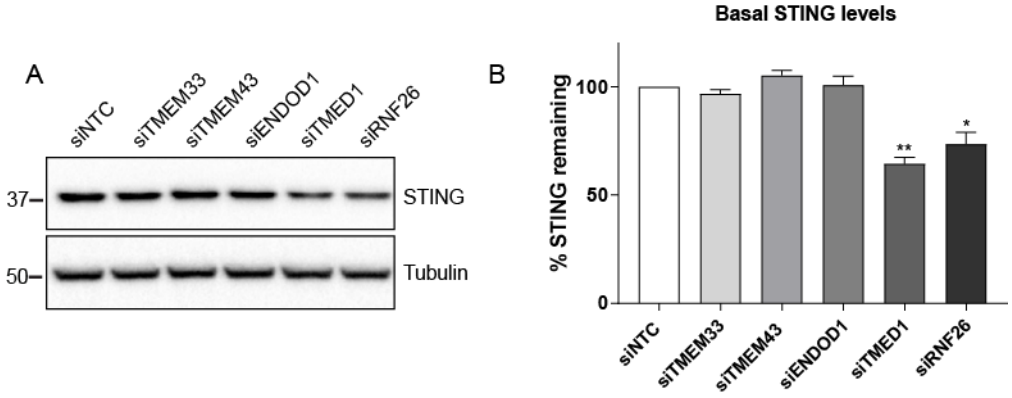

Figure 5.15: Changes in basal STING levels upon RNF26 interactor knockdown. (a) Anti-STING WB on siRNA transfected Flp-In293 cells. (b) Quantitation of (a) by densitometry. Error bars represent s.e.m. from *n* = 3 biological repeats.

The decrease in STING levels following knockdown of RNF26 was further enhanced upon STING activation by cGAMP (Figure 5.16), recapitulating published data (Qin et al., 2014). Again, siTMED1-transfected cells showed the same effect, correlating with the attenuated *IFIT1* upregulation observed earlier (Figure 5.12a). Counter-intuitively, knockdown of ENDOD1, which produced the same *IFIT1* phenotype as TMED1 knockdown, seemed to increase STING levels after activation, although this was not significant. A small but significant increase in activated STING levels was observed in TMEM43 depleted cells (Figure 5.16), which is consistent with the increase in *IFIT1* upregulation (Figure 5.12b). Interestingly, despite the fact that knockdown of TMEM33 generated a comparable increase in *IFIT1* compared to the knockdown of TMEM43, levels of activated STING were consistently decreased, albeit by a very small margin (Figure 5.16).

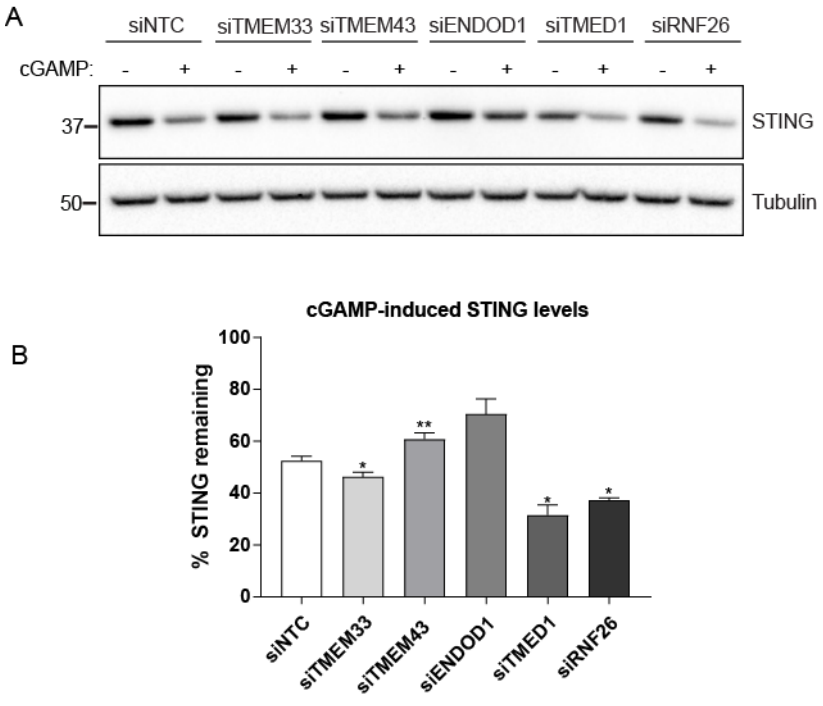

Figure 5.16: Changes in cGAMP-induced STING levels following depletion of RNF26 interactors. (a) Anti-STING WB on siRNA-transfected Flp-In293 cells treated with cGAMP (6 h, 10 µg/ml). (b) Quantitation of (a) by densitometry. Error bars represent s.e.m. from *n* = 3 biological repeats.

In summary, using a assay to test whether RNF26 interactors were involved in regulating STING-dependent innate immune signaling uncovered four proteins with a novel role in this pathway. Three of these proteins, TMED1, ENDOD1 and TMEM43, were validated as RNF26 interactors, and one HCIP, TMEM33, is awaiting validation. Knockdown of TMED1 and ENDOD1 phenocopied the reduced IFN signaling downstream of STING activation observed in RNF26-depleted cells. Therefore, RNF26 together with its interactors, TMED1 and ENDOD1, are required to potentiate this signaling pathway. Conversely, the depletion of TMEM43 and TMEM33 resulted in increased cGAMP-induced *IFIT1* upregulation, and hence these interactors antagonise the response to STING activation. It also seems clear that RNF26 and TMED1 reduce the levels of both basal and engaged STING. How this may occur, and the role of the other interactors in this process, remains unknown.

Together however, these data indicate that RNF26 nucleates a complex (or complexes) with functional interactors which collectively work to balance the signaling outcome to STING activation. The combined effect of both ‘potentiators’ and ‘inhibitors’ would ensure a sufficient yet controlled response to pathogenic invasion.

5.4 Discussion

WT and catalytic-inactive FH-RNF26

ER-resident RNF26 is implicated in both STING-mediated signaling and endosomal trafficking (Jongsma et al., 2016; Qin et al., 2014). Despite this, it has remained poorly characterised in terms of the protein-protein interactions it forms. A previous study used a tagged version of the RNF26 RING-domain to identify interacting proteins by immunoprecipitation followed by LC-MS/MS (Jongsma et al., 2016). Although the interactors discovered from this study were used to describe the role of RNF26 in regulating endosomal cargo transport, the RING-domain only represents 42 amino acids at the C-terminus of this 433 amino acid-length protein. Therefore, any interactions which are mediated through TMDs or luminal/cytosolic loops will have failed to be identified by this approach.

Here, full-length WT and mutant FH-tagged RNF26 were used in the E3 LC-MS/MS screen to identify putative interactors of this ligase. Based on the predictions made from the cytosolic ligase RNF4 (Plechanovová et al., 2011), the RNF26^{Y432A} mutant was expected to be catalytic-inactive, and this was indeed demonstrated to be the case (Figures 5.3 and 5.4). The dimeric interface between the two monomers of RNF4 is required for activation of the thioester bond between the E2-conjugating enzyme and ubiquitin, thus enabling ubiquitin transfer onto its substrate (Plechanovová et al., 2011). There are currently no examples of this mechanism of ubiquitination among the ER-resident E3s, so although an E2-conjugating enzyme has not been found for RNF26, it would be interesting to determine whether RNF26 functions as a dimeric RING E3.

It was additionally observed that overexpression of FH-RNF26^{Y432A} phenocopied the *IFIT1* phenotype of RNF26-depleted cells, and thus this mutant has a dominant-negative effect over endogenous RNF26 (Figure 5.11b). This was further shown qualitatively by the pattern of endosome localisation in Flp-InU2OS cells expressing either WT or mutant RNF26 (Supplementary data, Figure S5.6). In the endosomal study, it was demonstrated that RNF26 is required to maintain the perinuclear pattern of late endosomes (LEs), and in cells expressing RNF26-ΔRING the distance between nucleus and LEs significantly increased (Jongsma et al., 2016). In agreement with this data, the overexpression of FH-RNF26^{Y432A} resulted in the mislocalisation of LEs away from the nucleus, relative to cells overexpressing WT FH-RNF26 (Supplementary data, Figure S5.6).

Validating interactors

Reciprocal-tagging of specific proteins identified as HCIPs of WT and/or mutant FH-RNF26 was used to validate these interactions. HCIPs of other E3s, including AMFR, CGRRF1, Hrd1 and RNF185, were also selected for validation (Table 5.1 and Supplementary table S5.1). In total, 20 HCIPs were selected for S-tagging, of which only three (SAMM50, ENDOD1, TMEM33) were undetectable by WB. Of the 17 interactions tested, 11 were successfully validated. The remaining six S-tagged HCIPs did not co-precipitate their respective E3 and serve as negative controls for the AB-WB procedure (Figure 5.6 and Supplementary data, Figure S5.1). However, these results do not necessarily mean that these six proteins do not interact with their respective E3. It is possible that the S-tag on the HCIP precludes it from interacting with the FH-tagged E3, and therefore the experiment could be repeated with the HCIP tag on the opposite terminus (see Chapter 2, Table 2.1.3.3 for information on which HCIP terminus was tagged). Of course, the possibility that these HCIPs represent false-positives cannot be excluded and this highlights the

necessity of validating interactions identified by mass spectrometry. Interestingly HCIPs with combined higher *p-values* and raw abundances were more likely to be validated as E3 interactors by the reciprocal-tagging method (Supplementary data, Figure S5.2). This suggests that one may be able to prioritise future validation of HCIP-E3 interactions based on the magnitude of these values.

Although reciprocal-tagging is a useful strategy for validating interactors, ideally one would confirm interactions between endogenous proteins. However, this option may not always be available due to the lack of specific antibodies, as demonstrated for TMEM33. Exogenously expressed S-tagged TMEM33 was not detectable by WB, irrespective of whether the tag was located on the N- or C-terminus. An antibody reportedly validated for detection by WB was also not suitable for recognizing endogenous TMEM33, and therefore this interaction remains unconfirmed. Similarly, endogenous RNF26 was not detectable, likely due to its fast turnover rate.

In addition to the 11 positively confirmed interactions, endogenous ENDOD1, which was identified as a HCIP of both WT and mutant RNF26, was shown to be co-precipitated by S-tagged TMED1 and TMEM43 (Figure 5.8). As TMED1-S and S-TMEM43 were able to co-precipitate both FH-RNF26 and ENDOD1, this suggests that RNF26 does not participate in a series of individual interactions with each validated HCIP, but rather forms a complex of interconnected proteins. Although this hypothesis is supported by the alignment of the sucrose sedimentation profiles of each of the endogenous validated interactors (Figure 5.9), the formation of a protein complex has not been empirically determined. One could confirm the formation of a protein complex by performing sequential pulldowns of tagged interactors and FH-RNF26, followed by WB of a validated interactor not used for IP.

It is likely that RNF26 does not form a single complex with the all the proteins confirmed as interactors. This idea is supported by the observation that S-tagged UBXD8 and AUP1 did not co-precipitate ENDOD1 (Figure 5.8). Given depletion of either of these interactors did not cause a change in *IFIT1* upregulation relative to the control knockdown (Figure 5.13), this suggests different interactions with RNF26 may be required for regulating different functions. Notably, both AUP1 and UBXD8 pulled-down less FH-RNF26 in the presence of Triton-X-100, compared to LMNG (Figure 5.7). Triton-X-100 is a comparatively stringent detergent, and therefore indicates the interactions between these proteins and RNF26 may be indirect. TMED1 showed a similar behavior to AUP1 and UBXD8 in this regard, however the interaction between TMEM43 and RNF26 was unperturbed by Triton-X-100 (Figure 5.7). Based on this data, a model can be proposed in which TMEM43 is a direct interactor of RNF26, whilst the remaining validated HCIPs may interact with RNF26 through direct interactors. Indirect recruitment is supported by the interaction mapping of UBX-domain-containing proteins, which reports TMEM43 as a HCIP of UBXD8 (Raman et al., 2015), and also work from the Ploegh lab, which shows AUP1 is co-precipitated by UBXD8 (Klemm et al., 2011).

Towards functional cofactors

Having validated select HCIPs as RNF26 interactors, an assay was designed to test the contribution of these proteins to RNF26 function. As previously mentioned, RNF26 is known to play a role in both innate immune signaling and endosomal positioning (Jongsma et al., 2016; Qin et al., 2014). In the Supplementary data, a qualitative difference in the localization of CD63-positve LEs was observed for Flp-InU2OS cells expressing either WT or mutant FH-RNF26 (Figure S5.6). However, this data proved more challenging to quantify compared to changes in gene expression downstream of STING activation.

Therefore, a functional readout was created to screen the response of HEK293 cells depleted for RNF26 interactors to cGAMP treatment, by measuring changes in the IFN-stimulated gene, *IFIT1*. Although not immune cells, HEK293 are one of the few transformed cell lines which express endogenous STING (Burdette and Vance, 2013) and thus elicit an IFN response upon STING activation by cGAMP (Bridgeman et al., 2015). Initially, *IFIT1* upregulation downstream of cGAMP transfection was quantified in WT Flp-In293 cells depleted for RNF26. Consistent with published data (Qin et al., 2014), there was a significant decrease in *IFIT1* transcription, compared to control knockdown cells. Interestingly, TMEM43 and TMEM33 knockdown resulted in a larger increase in *IFIT1* upregulation (Figure 5.12b), whereas depletion of ENDOD1 and TMED1 phenocopied the attenuated response observed with RNF26 silencing (Figure 5.12a). These data suggest that RNF26 and its interactors collectively fine-tune the downstream response to STING activation (Figure 5.17).

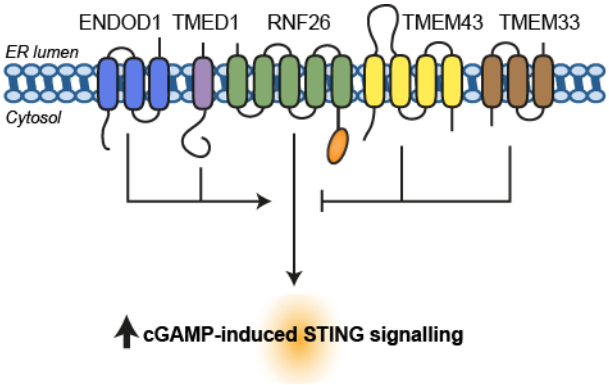

Figure 5.17: A summary of the influence of RNF26 interactors on STING signalling downstream of its activation by cGAMP.

If these interactors are indeed cofactors of RNF26, it would be interesting to determine how they influence the function of RNF26 in innate immune signaling. It was initially demonstrated that RNF26 stability was not altered by the depletion of TMEM43, TMEM33, TMED1 or ENDOD1 (Figure 5.14). Since RNF26 degradation is likely controlled by auto-ubiquitination, this data would suggest that the activity of RNF26 in cells depleted for its interactors is intact, however this would require experimental confirmation.

The current model is that upon viral infection, RNF26 catalyses K11-linked ubiquitination of STING, protecting it from K48-mediated proteasomal degradation by RNF5 (Qin et al., 2014; Zhong et al., 2009). However, one must consider that these experiments were performed using overexpressed and tagged forms of E3s, substrate (STING) and ubiquitin, and therefore this highly artificial system may not reflect the endogenous cellular processes. Nonetheless, the addition of cGAMP to cells depleted for RNF26 did result in a larger reduction in STING protein levels relative to control knockdown cells (Figure 5.16). This observation recapitulates the published data and the above model proposed by the Shu group (Qin et al., 2014).

Interestingly, knockdown of TMED1 resulted in a comparable cGAMP-dependent decrease in STING (Figure 5.16), although basal (inactive) STING levels were also reduced in siRNF26- and siTMED1-transfected cells (Figure 5.15). This could mean that RNF26, and possibly TMED1, prevent STING turnover prior to its activation. The hypothesis that inactive STING could be proteasomally degraded is supported by published data, although it was not directly discussed by the authors (Zhong et al., 2009). In this publication, RNF5 was postulated to mediate degradation of STING by the proteasome following viral infection (Zhong et al., 2009). Upon overexpression of RNF5, STING levels decreased, and this was rescued by proteasome inhibition (Zhong et al., 2009). However, this experiment was carried out in uninfected cells, suggesting that RNF5-mediated degradation may not require STING activation.

According to recent data, the contribution of the proteasome to the degradation of activated STING appears to be rather minimal (Gonugunta et al., 2017). It was demonstrated that the reduction in STING protein levels in response to viral DNA was barely rescued by MG132 treatment, in stark contrast to the near-complete rescue observed by treating cells with bafilomycin A1 (BafA1) (Gonugunta et al., 2017), a chemical inhibitor of autophagic degradation (Yoshimori et al., 1991). This group proposed that STING degradation required it to be sorted to acidified endolysosomes, which subsequently fuse with lysosomes, degrading their cargo (Gonugunta et al., 2017). This conclusion was supported by the finding that p62/SQSTM1-dependent autophagy was required to degrade ubiquitinated STING following its activation, thus providing a negative feedback loop to prevent an excessive inflammatory response (Prabakaran et al., 2018). Interestingly, the role of RNF26 in endosomal trafficking is dependent on its ability to recruit and ubiquitinate p62/SQSTM1 (Jongsma et al., 2016). In addition to controlling the position of endosomal vesicles, RNF26 also regulates their dynamics by restricting fast microtubule-based transport (Jongsma et al., 2016). It is therefore possible that

RNF26 plays a role in trafficking STING-loaded endolysosomes, or in the p62/SQSTM1-mediated degradation of ubiquitinated STING.

STING trafficking is crucial for downstream IFN-signalling. Prior to being sorted into vesicles destined for degradation, STING exits the ER upon stimulation, and translocates to the ERGIC/Golgi interface (Dobbs et al., 2015; Ishikawa et al., 2009). Blocking ER to Golgi transport was sufficient to attenuate DNA-dependent STING signaling (Dobbs et al., 2015). TMED1 is one of 11 members of the human p24 family (Strating and Martens, 2012) which is implicated in the ER-export of GPI-anchored proteins (Takida et al., 2008). The yeast homolog of TMED1 is proposed to be involved in trafficking of the GPI-anchored Gas1p protein (Marzioch et al., 1999), although its function in mammals remains uncharacterised. Given the fact that STING translocation from the ER to the Golgi is necessary for its signalling (Dobbs et al., 2015), it would be interesting to test whether TMED1 is required for ER-export of activated STING, and whether this is the reason for the reduced *IFIT1* upregulation observed upon TMED1 depletion.

Although this is the first functional description of a p24 protein in STING-dependent signaling, TMED1 has previously been implicated in immune signaling (Connolly et al., 2013). Interleukin (IL)-33, which is released as a ‘danger signal’ from dying and damaged cells, triggers a pro-inflammatory response in neighbouring cells (Kakkar and Lee, 2008). In cells depleted for TMED1, the response to IL-33 stimulation (measured by the increase in IL-6 and IL-8) was attenuated (Connolly et al., 2013), in agreement with the data presented earlier (Figure 5.12a). It is hence possible that TMED1 plays a more general role in immune signaling, and this should be the subject of future investigation (see Chapter 6).

The knockdown of ENDOD1 resulted in the same *IFTI1* phenotype as TMED1 and RNF26 depletion (Figure 5.12a). ENDOD1 is a functionally uncharacterized protein, predicted to be resident in the ER membrane. It was found to be transcriptionally upregulated in astrocytes overexpressing IL-6, suggesting a potential involvement in the immune response (Quintana et al., 2008). The results above support this hypothesis and it is therefore important to establish the role of ENDOD1 in regulating this pathway.

Contrary to the results obtained for ENDOD1 and TMED1 knockdown, the depletion of either TMEM43 or TMEM33 caused an increase in cGAMP-induced *IFIT1* transcription relative to control cells (Figure 5.12b). TMEM33 has previously not been associated with immune signaling. However, one study showed an increase in NF-κB luciferase activity upon overexpression of TMEM43 (Jiang et al., 2016), although this result was not expanded upon and the context in which TMEM43 would be required for NF-κB activation is unclear.

Missense mutations in TMEM43 are known to cause Arrhythmogenic Right Ventricular Cardiomyopathy Type 5 (ARVD5) (Merner et al., 2008) and the nuclear laminopathy Emery-Dreifuss Muscular Dystrophy 7 (EDMD7) (Liang et al., 2011). TMEM43 is a highly conserved tetraspannin and through a series of microscopy-based and biochemical studies, it was concluded that it is an ER-resident protein enriched at the INM (Bengtsson and Otto, 2008). Overexpression of mutant TMEM43 correlated with the appearance of deformed nuclear phenotypes associated with laminopathies such as EDMD (Liang et al., 2011). Interestingly, although both yeast and human TMEM33 are known to localize to the ER (Sakabe et al., 2015; Zhang and Oliferenko, 2014), it was demonstrated to be required for mitotic nuclear remodeling in yeast (Zhang and Oliferenko, 2014). Since activated

STING is trafficked to perinuclear vesicles (Ishikawa et al., 2009), it is tempting to speculate that TMEM43 and TMEM33 may regulate the positioning of STING-loaded vesicles given their proposed roles in NE organisation.

In summary, the data presented in this chapter demonstrate that RNF26 is an auto-regulatory ubiquitin ligase. It forms a ~300 kD complex, interacting with membrane proteins which also play a role in regulating STING-dependent innate immune signaling. Besides ascribing novel roles for TMEM43, TMEM33, TMED1 and ENDOD1, these results highlight the utility of the ER E3 network mapping in discovering functional E3 interactors.

RNF26 and its interactors collectively fine-tune the downstream response to STING activation, which needs to be sufficient to mount an effective response against the invading pathogen, but limited to prevent prolonged proinflammation. However, it has not strictly been demonstrated that these four proteins are cofactors of RNF26, as it was not determined if and how they control STING signaling through RNF26. The cGAS-STING pathway is regulated at several different levels, with STING subject to conformational change, trafficking, complex formation, post-translational modification, and degradation. As will be discussed in the next chapter, future experiments should focus on elucidating the mechanism of how RNF26 and its interactors modulate this pathway, and indeed whether any other ER-resident E3s play a role in regulating innate immune signaling.

Chapter 6

Concluding remarks and future perspectives

Interactions formed by E3 ubiquitin ligases define their function. Therefore the principal aim of this project was to discover putative interactors of the ER-resident E3 family by LC-MS/MS. To enable immunoprecipitation of E3s and their associated interactors, stable, DOX-inducible Flp-In293 cell lines encoding FH-tagged E3s were generated. A series of quality control experiments were used to confirm that overexpression did not result in E3 mislocalisation or ER-stress induction. In addition, the well-characterised Hrd1 complex was used to verify that complexes composed of endogenous interactions could assemble upon expression of tagged Hrd1 (Chapter 3).

Despite the positive outcome of these results, tagged E3s are still expressed in excess over their endogenous counterparts. Overexpression can be associated with the formation of non-native interactions and competition for interactors between endogenous and exogenous components. To reduce these risks, a short hairpin RNA (shRNA) sequence targeting the 3' untranslated region (UTR) of the endogenous E3 could have been fused to the FLAG-HA-tagged ORF of the same E3, so that upon doxycycline induction the endogenous E3 would have been depleted and 'replaced' with the exogenous form. This strategy could be tested for future comparative LC-MS/MS studies. However, since RNAi can produce off-target effects, at least two different shRNA sequences would have to be used, making parallel processing of all samples much more labour-intensive. Alternatively, advances in CRISPR (clusters of regularly interspaced short palindromic repeats)-mediated knock-in will enable epitope-tagging of a large number of endogenous genes in a reasonable time-frame in the near future, which would abate any concerns related to protein overexpression and identification of native interactors. One caveat with this approach would be that the expression levels of some E3s might be too low to obtain sufficient material for LC-MS/MS.

The sample preparation workflow for LC-MS/MS was developed to preserve interactions within E3 complexes and simultaneously maximise the non-specific background interactions thus facilitating comparative proteomic analysis. Two key features of the pipeline were the use of LMNG for solubilisation, and SDS for elution of proteinaceous material captured by FLAG-agarose immunoprecipitation (Chapter 3). Following optimisation of this protocol, LC-MS/MS of the purified eluates from each E3 sample was carried out, identifying over 2,000 unique protein signatures.

The background proteome was defined as the cohort of proteins which were present in all samples and displayed the least variation in abundance. This proteome was used to perform median-normalisation on the dataset, allowing each sample to be compared against all others in a process termed BSCG analysis (Chapter 4, (Keilhauer et al., 2015)). Significantly enriched proteins were classified as HCIPs, of which 226 were discovered across 21 of the 25 ER-resident E3s. Most HCIPs were ER/membrane resident and nearly half were unique to one E3. The remaining HCIPs were shared between two or more baits and therefore a total of 429 putative interactions were identified by this technique. An additional 31 unique HCIPs were characterised by SINQ analysis, which was primarily employed to address the shortcomings of the comparative proteomic profiling (Chapter 4). The HCIPs represent potential cofactors which could contribute to E3 function, or substrates regulated by E3-mediated ubiquitination, and therefore provide a foundation to characterise the roles of these enzymes and the processes they are involved in.

The comparative analysis annotated the E3 baits, as well as known E3 cofactors, with very high *p-values*. This demonstrates that both the FH-tagged E3s were significantly enriched in their appropriate sample, and that the approach was able to positively identify E3 interactors. In this study, the *p-value* is directly related to relative fold-change of the identified protein, and not the reproducibility of the fold-change, since the results were obtained from technical LC-MS/MS duplicates from one biological sample. Despite the fact that other published interaction networks have been generated without the use of biological repeats (such as the DUB interactome (Sowa et al., 2009)), replicates would undoubtedly increase the confidence in identified HCIPs. Furthermore, the largest source of variation in the raw data was due to 'batch effects' between the first and second LC-MS/MS experiments (data not shown). Although the batch effects were computationally removed using the Limma package in R, future experiments would ideally run each biological replicate as a single batch.

It is possible to use the sample preparation and analytical workflow established in this project to help further characterise HCIPs and broaden the current understanding of E3 functionality. For example, the LC-MS/MS experiment could be repeated to categorise likely direct and indirect E3 interactors by comparing HCIPs identified by immunoprecipitation in different solubilisation conditions (as carried out for RNF26 HCIPs in Chapter 4). Furthermore, if cells lines were generated to express E3 catalytic-inactive RING-domain mutants, the LC-MS/MS workflow could be used to assess the changes in the HCIP profiles between WT and mutant E3s. Since RING-mutants lack substrate processivity, this approach should theoretically enrich for substrates as the dissociation rate of the substrate from the E3 should be reduced, thus increasing the probability of substrate detection (Iconomou and Saunders, 2016). As with any technique, each candidate substrate would require validating by pulse-chase or ubiquitination assays.

Whilst it is not possible to distinguish HCIPs as cofactors or substrates from the LC-MS/MS data alone, certain HCIPs were tentatively suggested to be substrates based on the established functions of the ER (Chapter 4). For example, regulatory ERAD is known to degrade cholesterol-biosynthetic machinery (Foresti et al., 2013; Jo et al., 2011a; Zelcer et al., 2014), and therefore HCIPs with a function in cholesterol and fatty acid regulation were proposed to be potential E3 substrates. Of the 226 HCIPs identified, approximately 90 mapped to different ER functions, including ERAD, PQC, lipid regulation, and trafficking. Interestingly, degradation machinery which is upregulated by ER stress was mainly associated with Hrd1. In addition to monitoring fold changes of classic UPR targets, NanoString™ technology was used to measure transcriptional changes of the E3s upon ER stress induction. Hrd1 experienced the largest transcriptional increase, and therefore the data collectively indicate that this E3 is likely to be principally involved in the clearance of misfolded proteins and the resolution of ER stress (Chapter 4). Notably, the NanoString™ experiment was designed prior to obtaining the LC-MS/MS results and therefore the response of the HCIPs to ER stress remains unknown and would be interesting to determine in the future.

CGRRF1 was modestly but significantly upregulated in response to ER stress, and so its putative interaction with Herp1, a principal UPR target (Ma and Hendershot, 2004), should be validated and investigated. The interaction between CGRRF1 and another of its HCIPs, Evi, was validated and shown to be required for constitutive proteasomal turnover of Evi (Glaeser et al., 2018). Although the LC-MS/MS did capture several known E3 interactors of AMFR, Hrd1 and RNF185, validating interactors increases confidence in the ability of this approach to discover novel *bona fide* interactions. One method commonly used to validate putative interactions is reciprocal-tagging (Christianson et al., 2012; Raman et al., 2015; Sowa et al., 2009),

where a tagged version of the HCIP is used to pulldown the appropriate bait protein (Chapter 5).

Of 17 detectable S-tagged HCIPs, 11 interactions involving AMFR, Hrd1, RNF26 and RNF185 were validated by reciprocal-tagging. In addition to validating its HCIPs, RNF26 was characterised as a highly unstable protein degraded by the proteasome. Its degradation was shown to be dependent on its auto-ubiquitination, which was severely compromised in the $RNF26^{Y432A}$ mutant. Furthermore, the Y432A substitution was determined to be a dominant negative mutation (Chapter 5).

Having already verified that the E3 LC-MS/MS was able to find novel substrates (CGRRF1-Evi), the validated RNF26 interactors were used to demonstrate that uncharacterised E3s form complexes with functional cofactors. Working on the premise that cofactors would contribute to E3 function, an assay based on the known role of RNF26 in regulating innate immune signalling (Qin et al., 2014) was designed to screen validated HCIPs. Indeed, knockdown of both ENDOD1 and TMED1 phenocopied the attenuated IFN signalling downstream of STING activation in RNF26-depleted cells. Surprisingly, knockdown of another two interactors, TMEM43 and TMEM33, resulted in an increase in STING-dependent signalling (Chapter 5). Finding novel regulators of the STING-signalling pathway is of particular interest given the growing evidence that targeted STING activation promotes anti-tumour immunity and tumour regression (Corrales et al., 2015; Fu et al., 2015; Gonugunta et al., 2017).

Although it is clear that RNF26 forms interactions with proteins that participate in modulating immune signalling, it remains to be determined how these interactors influence RNF26 function. If these interactors function uniquely through RNF26, one would anticipate that the combined knockdown of RNF26 with each of the four interactors would replicate the cGAMP-induced *IFIT1* phenotype caused by depletion of RNF26 alone. Additionally, although ENDOD1 was found to interact with TMEM43 and TMED1, sequential pulldown would have to be performed to determine the presence of a protein complex containing RNF26 and its functional interactors.

RNF26 is proposed to regulate innate immune signalling by K11-ubiquitinating STING and thus preventing it from K48-mediated degradation by RNF5 (Qin et al., 2014). Recapitulating published data, STING protein levels following treatment with cGAMP were consistently decreased in RNF26-depleted cells, relative to control knockdown cells. Knockdown of TMED1 had the same effect. However, basal levels of STING were also found to be reduced in siRNF26- and siTMED1-transfected cells. It is therefore possible that RNF26 (and TMED1) protect inactive STING from constitutive proteasomal degradation (see Chapter 5, discussion).

To elucidate how RNF26 and its cofactors regulate the cGAS-STING pathway, it would be necessary to first clarify STING ubiquitination. As mentioned in Chapter 5, ubiquitination of STING by RNF26 was determined using a relatively artificial system consisting of overexpressed substrate, E3, and different ubiquitin constructs (Qin et al., 2014). A recent study used specific TUBEs to detect endogenous K48 and K63 poly-ubiquitination of STING upon stimulation with dsDNA (Prabakaran et al., 2018). This methodology could be used to detect changes in STING ubiquitination and turnover upon knockdown of RNF26 and its validated interactors, in both untreated (basal) and cGAMP-treated (induced) conditions.

Importantly, IFN signalling downstream of STING activation is not solely controlled by STING turnover, but also by its dimerization, trafficking, and protein-protein interactions (Chen et al., 2016), all of which require regulation. While the interactors of RNF26 may not directly influence its catalytic-activity (and hence STING ubiquitination), they may be required to facilitate or inhibit RNF26-STING interaction, which could easily be tested by IP-WB. One must also consider the possibility that RNF26 and its interactors may play a more general role in immune signalling and are not unique to the cGAS-STING pathway. Activation of other nucleic acid-sensing pathways, such as RNA-specific RIG-I and MDA5 (Barral et al., 2009), triggers the same IFN signalling response. Therefore, changes in signalling upon activation of these pathways should also be monitored in cells knocked down for RNF26 and its associated proteins. The idea that RNF26 might be a master regulator of innate immune signalling is supported by published data, as an attenuated IFN response was observed when stimulating RNF26-deficient monocytes with either DNA or RNA virus (Qin et al., 2014).

The functional interactors of RNF26 were also discovered as HCIPs of other E3s. In particular, TMED1 was annotated as a HCIP of BFAR and RNF5, whilst TMEM33 was also associated with RNF5 as well as MARCH4. ENDOD1 was found as a HCIP of MARCH3, and TMEM43 was described as a putative interactor of TRIM13. Interestingly, TRIM13 has recently been proposed as a negative regulator of the RNA sensor, MDA5 (Narayan et al., 2014). Since it is clear that ER-resident E3 ligases are required to regulate different nucleic-acid sensing pathways, the LC-MS/MS data generated from this study could be used to screen for novel E3s and cofactors which modulate innate immune signalling. This would provide the foundation for a new project to determine the role of ubiquitination at the ER membrane in regulating responses downstream of viral nucleic acid detection.

To conclude, a workflow based on the LC-MS/MS of immunoprecipitated E3s to discover novel interactors was developed and optimised, and successfully used to annotate over 250 HCIPs which formed ~450 interactions across 21 E3s. The HCIPs are associated with a variety of ER and cellular processes. These data have already proved valuable in finding E3 substrates (Evi), hence describing a role for the previously-uncharacterised CGRRF1 in regulating Wnt signalling (Glaeser et al., 2018). Furthermore, RNF26 was revealed to be an unstable, auto-regulatory E3, whose catalytic activity is dependent on its C-terminal tyrosine residue. Validated interactors TMEM43, ENDOD1 and TMED1 are likely to form a functional complex with RNF26, and together with the HCIP TMEM33, were found to modulate STING-mediated innate immune signalling. In addition to determining novel functions for these four interactor proteins, this data collectively suggests that RNF26 nucleates an immuno-regulatory complex which fine-tunes the signalling outcome of this pathway. The information contained within this interaction landscape is therefore a comprehensive resource for discovering novel E3 functional interactors and substrates necessary for characterising the role of ER-resident E3s in the cell.

Supplementary data

		p-value	Fold change	Average unique peptides
1st batch	AMFR-FH	1.16E-13	1.08E+01	35.0
	FH-BFAR	1.58E-11	6.12E+00	11.0
	CGRRF1-FH	1.32E-31	7.60E+00	13.0
	Hrd1-FH	3.57E-06	5.23E+00	30.0
	MARCH2-FH	5.46E-17	7.01E+00	4.0
	MARCH3-FH	6.28E-38	8.83E+00	5.5
	MARCH4-FH	3.62E-32	7.96E+00	9.0
	FH-MARCH6	2.37E-26	6.77E+00	10.0
	MARCH8-FH	3.57E-19	7.05E+00	8.0
	FH-RNF5	3.78E-13	6.04E+00	5.0
	RNF13-FH	5.00E-01	-1.31E-02	7.5
	RNF26-FH	2.73E-06	8.84E+00	20.0
	RNF103-FH	7.08E-35	8.10E+00	4.0
	RNF128-FH	2.14E-19	8.96E+00	8.0
	RNF139-FH	3.76E-31	1.10E+01	10.5
	RNF148-FH	7.96E-15	8.56E+00	4.0
	RNF170-FH	3.61E-13	7.31E+00	5.0
	RNF185-FH	2.83E-24	7.82E+00	3.5
	FH-RNFT1	1.29E-21	7.26E+00	5.5
	TMEM129-FH	3.17E-27	7.45E+00	6.0
	TRIM13-FH	1.30E-22	8.12E+00	14.0
	TRIM59-FH	2.14E-30	9.77E+00	2.0
	ZNRF4-FH	9.43E-13	7.11E+00	9.0
2nd batch	RNF13-FH	4.96E-01	-6.08E-01	7.5
	FH-RNF26	1.88E-03	4.26E+00	20.0
	FH-RNF26^{Y432A}	4.00E-12	5.54E+00	20.0
	RNF145-FH	1.10E-17	6.20E+00	1.0
	FH-RNF150	7.62E-02	2.47E+00	1.0
	TRIM59-FH	4.87E-10	4.23E+00	2.0

Table S3.1: Table of *p-values,* fold changes and number of unique peptides for each of the E3 baits in their corresponding samples. Figures were not exportable from Progenesis-QI, however, the *p-values* and fold-changes derived from the comparative analysis (see Chapter 4) can be used to infer enrichment of the E3 baits. The rows highlighted in grey show the E3s which were not enriched (RNF13) or insufficiently expressed (RNF145, RNF150, TRIM59).

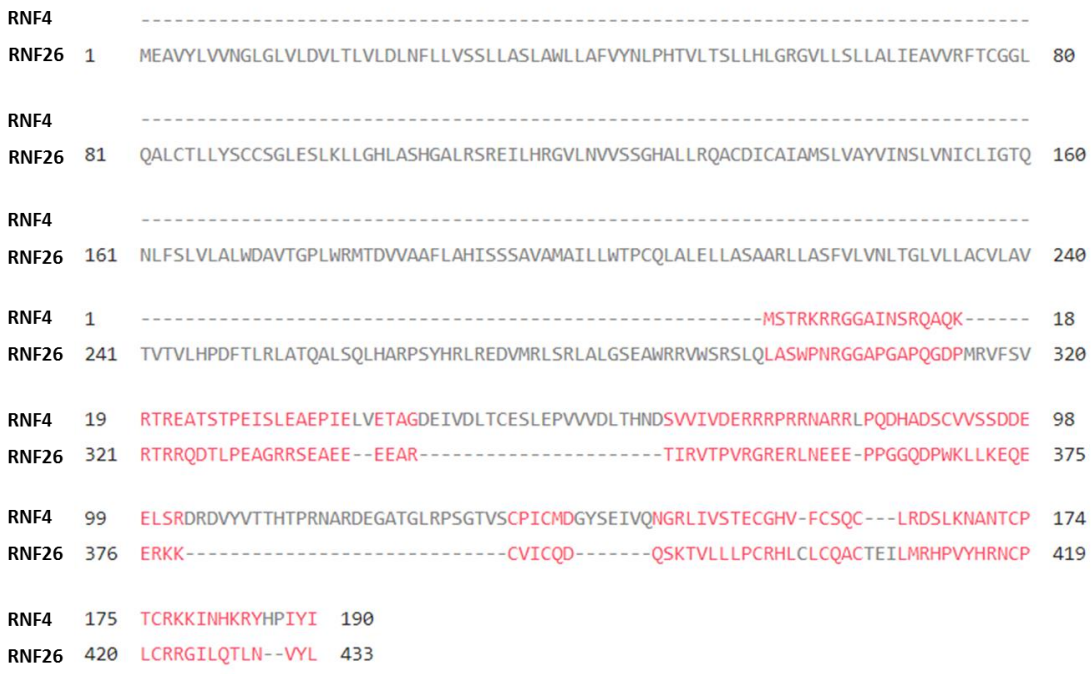

Figure S3.1: Sequence alignment of RNF4 and RNF26 (COBALT: Multiple Alignment Tool, NCBI).

Uniprot ID	Entry name	Uniprot ID	Entry name	Uniprot ID	Entry name	Uniprot ID	Entry name
P06753	TPM3	Q8TEM1	PO210	Q14166	TTL12	Q7L576	CYFP1
Q9BPX3	CND3	Q9P0K7	RAI14	O43795	MYO1B	O43790	KRT86
P67936	TPM4	P14649	MYL6B	P49643	PRI2	Q9BWJ5	SF3B5
P61927	RL37	Q7L2J0	MEPCE	O76013	KRT36	Q969T9	WBP2
Q9H254	SPTN4	Q6UN15	FIP1	P62304	RUXE	O14529	CUX2
Q9NRH3	TBG2	P15927	RFA2	Q9BTX1	NDC1	Q9NTK5	OLA1
Q16181	SEPT7	Q9NZR1	TMOD2	Q9BSJ2	GCP2	Q6PI48	SYDM
Q9Y2U8	MAN1	P28289	TMOD1	P18615	NELFE	O60237	MYPT2
Q01105	SET	P29692	EF1D	P82673	RT35	O95684	FR1OP
P35579	MYH9	Q15393	SF3B3	Q7L014	DDX46	Q9BUQ8	DDX23
P52701	MSH6	A7E2Y1	MYH7B	P19387	RPB3	Q9Y3A5	SBDS
Q9NYL9	TMOD3	Q9UM54	MYO6	Q2NL82	TSR1	Q96EA4	SPDLY
Q8WXH0	SYNE2	Q66K74	MAP1S	Q53GS9	SNUT2	Q9NRG9	AAAS
O14929	HAT1	Q92804	RBP56	P10155	RO60	Q9NWZ8	GEMI8
Q08554	DSC1	P17480	UBF1	P08754	GNAI3	Q9UIA9	XPO7
Q02413	DSG1	Q9UH99	SUN2	P50570	DYN2	O95071	UBR5
Q5D862	FILA2	Q14186	TFDP1	Q07065	CKAP4	P17096	HMGA1
Q92734	TFG	Q96P70	IPO9	P36954	RPB9	Q9NZ72	STMN3
O95232	LC7L3	O94901	SUN1	Q7Z333	SETX	Q8N5G2	MACOI
P02533	K1C14	Q8TEX9	IPO4	Q86YZ3	HORN	O60548	FOXD2
Q15813	TBCE	Q92621	NU205	P13646	K1C13	Q9NUU7	DD19A
Q92541	RTF1	Q9NVI1	FANCI	Q9NVJ2	ARL8B	O14530	TXND9
P60228	EIF3E	P42695	CNDD3	Q2TAY7	SMU1	Q9P1Z2	CACO1
Q9BQ67	GRWD1	O95793	STAU1	P18754	RCC1	Q16342	PDCD2
P49321	NASP	O75122	CLAP2	P0C0S8	H2A1	Q9UJC5	SH3L2
P20700	LMNB1	Q9GZS3	WDR61	Q71DI3	H32	Q9Y5B9	SP16H
O95347	SMC2	Q96K17	BT3L4	P11532	DMD	Q9BRK4	LZTS2
Q29RF7	PDS5A	P35609	ACTN2	P62805	H4	Q08945	SSRP1
O96019	ACL6A	P00491	PNPH	P16401	H15	O60610	DIAP1
P42766	RL35	P13796	PLSL	P16403	H12		

Table S4.1: List of contaminant proteins identified by LC-MS/MS. Contaminants were defined as cytoskeletal and nuclear proteins, and included chromatin-associated proteins, components of the spliceosome and DNA-binding proteins. Contaminants were cross-referenced against the CRAPome repository **(Mellacheruvu et al., 2013)**.

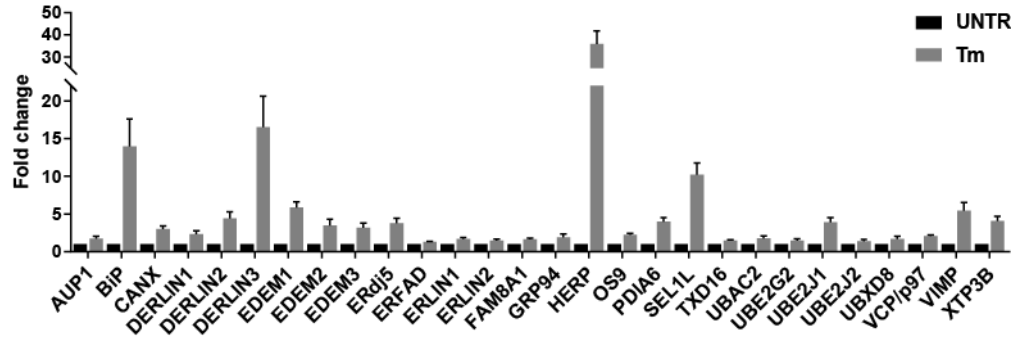

Figure S4.1: Fold-change of all ERAD component transcripts upon Tunicamycin treatment. WT Flp-In293 cells were treated with 500 ng/ml Tm for 8 h. Error bars represent s.e.m. from *n* = 3 biological repeats.

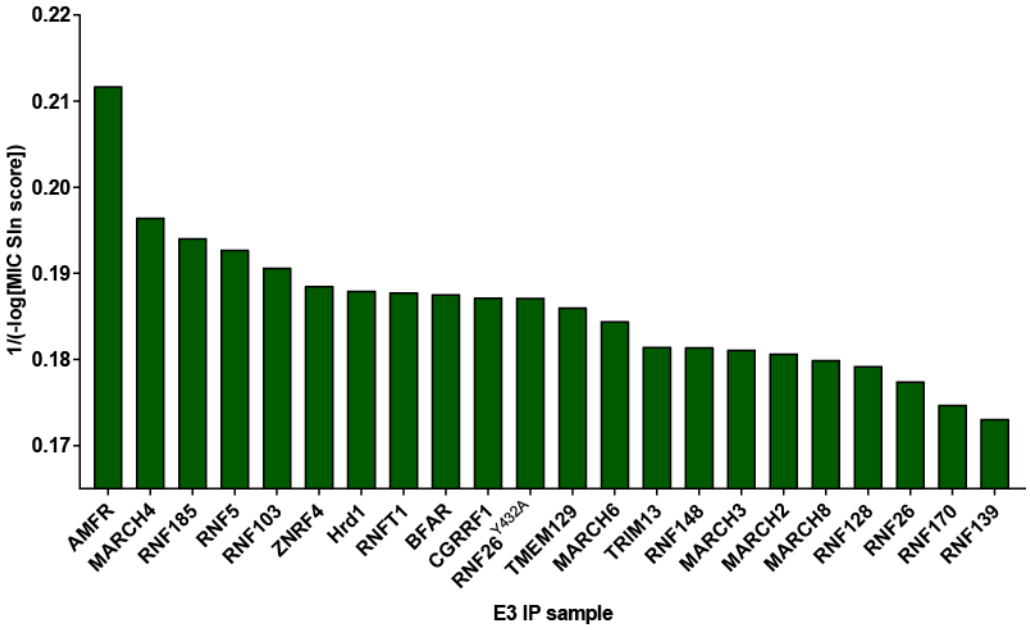

Figure S4.2: Graph of the ranked VCP/p97 1/(-log[MIC SIn score]) values in each bait sample.

	AMFR-FH		CGRRF1-FH		Hrd1-FH		RNF185-FH	
HCIP	-log(p-value)	Raw abundance	-log(p-value)	Raw abundance	-log(p-value)	Raw abundance	-log(p-value)	Raw abundance
OSBPL8	2.52	2.59E+06						
PGRMC1	2.30	3.46E+06						
DNAJC16			3.24	8.41E+03				
SCD1			3.03	6.59E+04				
TMEM9					2.14	8.32E+05		
ERLIN2							11.02	1.20E+08
SACM1L							1.33	7.49E+05
TMUB1							11.53	1.28E+07
TMUB2							22.80	3.33E+06
TMEM259							13.58	3.57E+07

Table S5.1: List of -log (*p-values*) and raw abundances for E3 HCIPs selected for validation by reciprocal tagging.

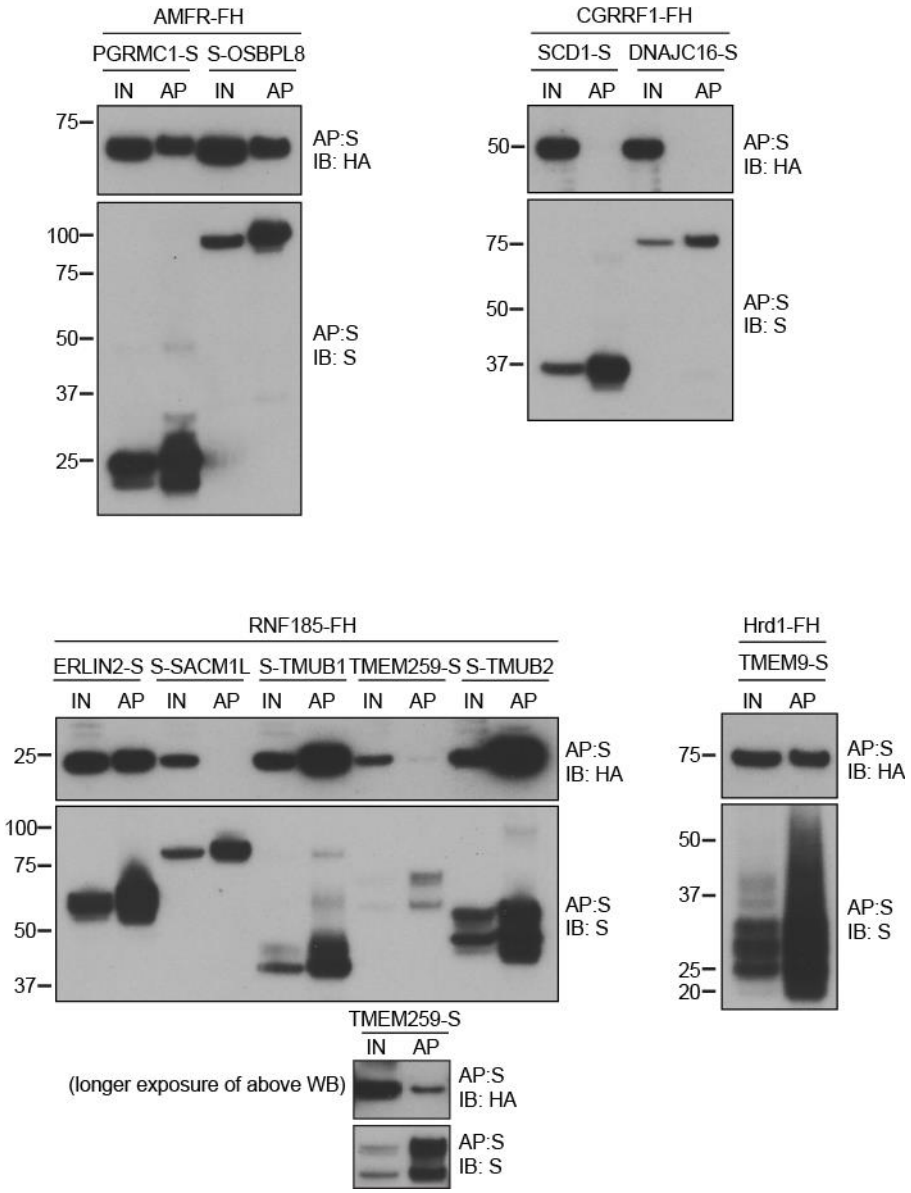

Figure S5.1: Validating AMFR, CGRRF1, RNF185 and Hrd1 HCIPs by reciprocal-tagging. S-tagged HCIPs were transiently expressed in their respective DOX-induced Flp-In293-FH-E3 cell line (see Table S5.1). Cell lysates were solubilized in 1% LMNG and 500 µg WCL were subject to S-AP followed by SDS-PAGE and S- and HA-immunoblotting. IN - 20% input, AP - affinity purification.

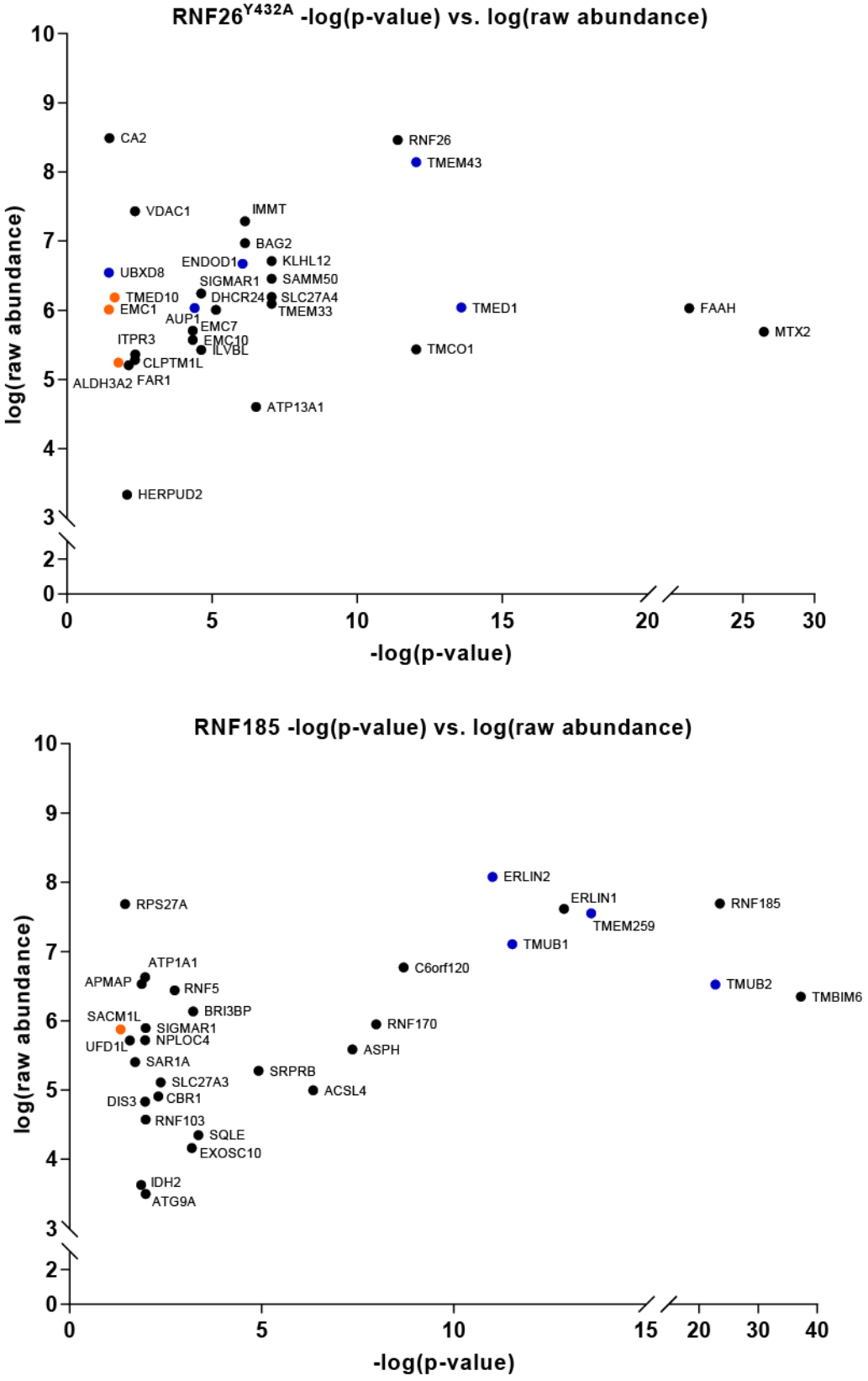

Figure S5.2: Graphs of $-\log_{10}$(*p-value*) against log(raw abundance) for RNF185 and RNF26^{Y432A} HCIPs. Blue and orange points represent HCIPs selected for reciprocal-tagging. Blue points were HCIPs validated as interactors, whereas orange points were not.

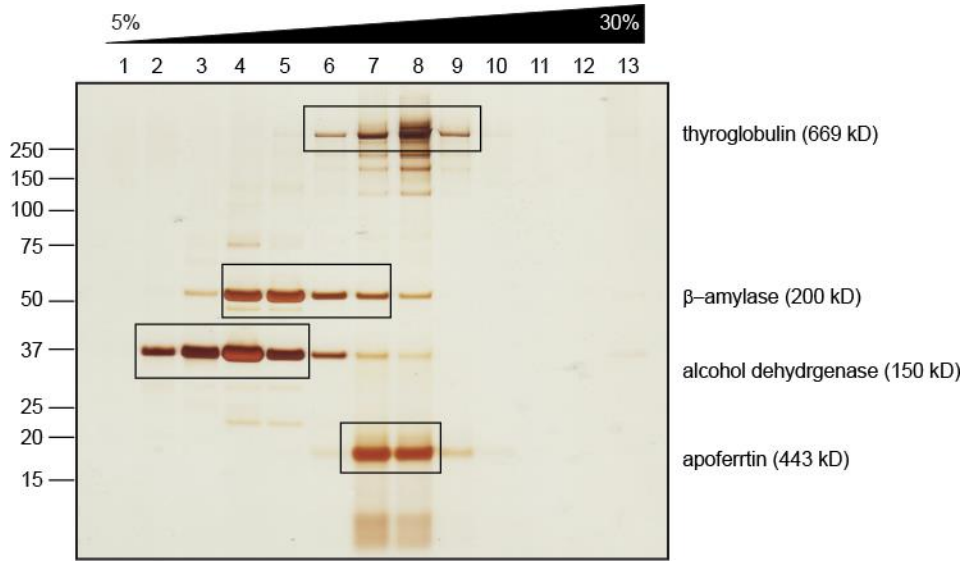

Figure S5.3: 5-30% sucrose gradient sedimentation profile of molecular weight markers. Gel filtration makers (boxed) were resuspended in 1% LMNG, loaded onto 5-30% sucrose gradients and subject to ultra-centrifugation. Precipitated fractions were separated by SDS-PAGE and visualised by silver staining.

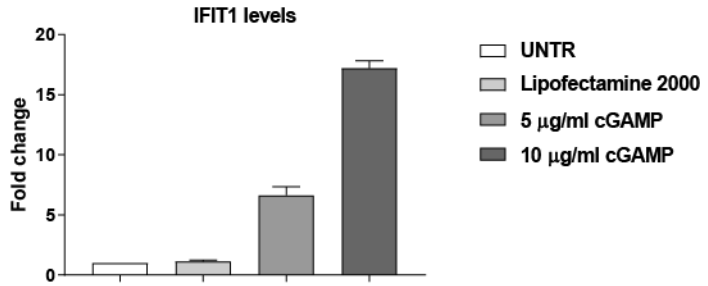

Figure S5.4: Effect of Lipofectamine2000 and cGAMP on *IFIT1* upregulation. WT Flp-In293 cells were treated with Lipefectamine2000, 5 μg/ml cGAMP or 10 μg/ml cGAMP and analysed by Taqman qRT-PCR to determine *IFIT1* and *GAPDH* levels. Error bars represent s.e.m. from *n* = 3 biological repeats.

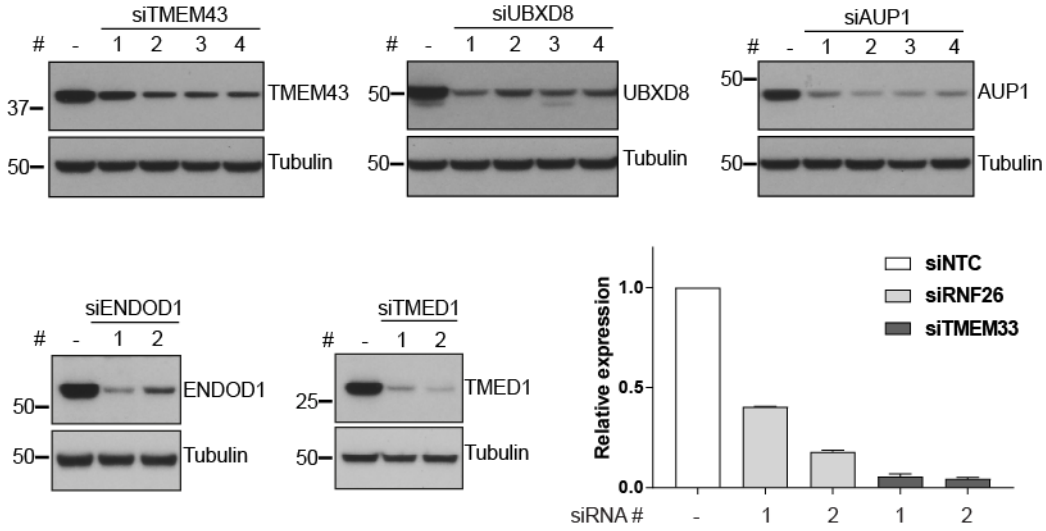

Figure S5.5: Knockdown efficiencies of RNF26 and selected HCIPs. Knockdown efficiencies of TMEM43, UBXD8, AUP1, ENDOD1 and TMED1 by WB, and RNF26 and TMEM33 by qRT-PCR.

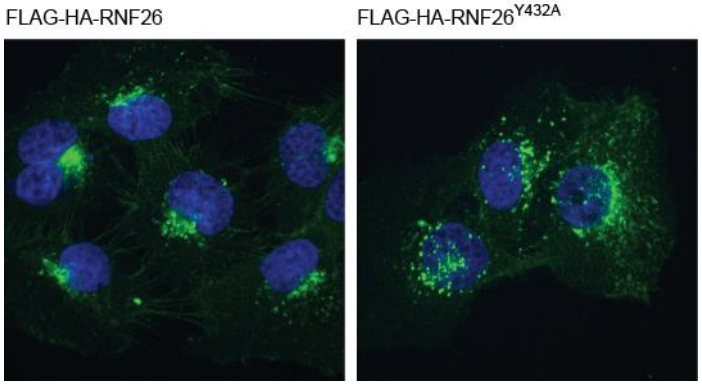

Figure S5.6: Localisation of CD63-positive late endosomes upon expression of either WT or mutant RNF26. Immunofluorescence of DOX-induced Flp-U2OS-FH-RNF26 and Flp-U2OS-FH-RNF26^{Y432A} cells. Anti-CD63 (Rb) and the corresponding Alexa-Fluor® secondary antibodies were used to stain late endosomes. Nuclei were stained using DAPI.

Bibliography

Ablack, J. N. G., Metz, P. J., Chang, J. T., Cantor, J. M. and Ginsberg, M. H. (2015). Ubiquitylation of CD98 limits cell proliferation and clonal expansion. *Journal of Cell Science* **128**, 4273–4278.

Adachi, Y., Yamamoto, K., Okada, T., Yoshida, H., Harada, A. and Mori, K. (2008). ATF6 Is a Transcription Factor Specializing in the Regulation of Quality Control Proteins in the Endoplasmic Reticulum TI . *Cell Structure and Function* **33**, 75–89.

Advani, R. J., Yang, B., Prekeris, R., Lee, K. C., Klumperman, J. and Scheller, R. H. (1999). Vamp-7 Mediates Vesicular Transport from Endosomes to Lysosomes. *J Cell Biol* **146**, 765–776.

Ahrné, E., Molzahn, L., Glatter, T. and Schmidt, A. (2013). Critical assessment of proteome-wide label-free absolute abundance estimation strategies. *Proteomics* **13**, 2567–2578.

Alzayady, K. J., Panning, M. M., Kelley, G. G. and Wojcikiewicz, R. J. H. (2005). Involvement of the p97-Ufd1-Npl4 Complex in the Regulated Endoplasmic Reticulum-associated Degradation of Inositol 1,4,5-Trisphosphate Receptors. *J. Biol. Chem.* **280**, 34530–34537.

Amano, T., Yamasaki, S., Yagishita, N., Tsuchimochi, K., Shin, H., Kawahara, K.-I., Aratani, S., Fujita, H., Zhang, L., Ikeda, R., et al. (2003). Synoviolin/Hrd1, an E3 ubiquitin ligase, as a novel pathogenic factor for arthropathy. *Genes & Development* **17**, 2436–2449.

Amemiya-Kudo, M., Shimano, H., Hasty, A. H., Yahagi, N., Yoshikawa, T., Matsuzaka, T., Okazaki, H., Tamura, Y., Iizuka, Y., Ohashi, K., et al. (2002). Transcriptional activities of nuclear SREBP-1a, -1c, and -2 to different target promoters of lipogenic and cholesterogenic genes. *Journal of Lipid Research* **43**, 1220–1235.

Angers, S., Thorpe, C. J., Biechele, T. L., Goldenberg, S. J., Zheng, N., MacCoss, M. J. and Moon, R. T. (2006). The KLHL12–Cullin-3 ubiquitin ligase negatively regulates the Wnt–β-catenin pathway by targeting Dishevelled for degradation. *Nature Cell Biology* **8**, 348–357.

Annaert, W. G., Becker, B., Kistner, U., Reth, M. and Jahn, R. (1997). Export of Cellubrevin from the Endoplasmic Reticulum Is Controlled by BAP31. *J Cell Biol* **139**, 1397–1410.

Appenzeller, C., Andersson, H., Kappeler, F. and Hauri, H.-P. (1999). The lectin ERGIC-53 is a cargo transport receptor for glycoproteins. *Nature Cell Biology* **1**, 330–334.

Arshad, M., Ye, Z., Gu, X., Wong, C. K., Liu, Y., Li, D., Zhou, L., Zhang, Y., Bay, W. P., Yu, V. C., et al. (2013). RNF13, a RING Finger Protein, Mediates Endoplasmic Reticulum Stress-induced Apoptosis through the Inositol-requiring Enzyme (IRE1α)/c-Jun NH2-terminal Kinase Pathway. *J. Biol. Chem.* **288**, 8726–8736.

Ashibe, B., Hirai, T., Higashi, K., Sekimizu, K. and Motojima, K. (2007). Dual Subcellular Localization in the Endoplasmic Reticulum and Peroxisomes and a Vital Role in Protecting against Oxidative Stress of Fatty Aldehyde Dehydrogenase Are Achieved by Alternative Splicing. *J. Biol. Chem.* **282**, 20763–20773.

Avci, D., Fuchs, S., Schrul, B., Fukumori, A., Breker, M., Frumkin, I., Chen, C.-Y., Biniossek, M. L., Kremmer, E., Schilling, O., et al. (2014). The Yeast ER-Intramembrane Protease Ypf1 Refines Nutrient Sensing by Regulating Transporter Abundance. *Molecular Cell* **56**, 630–640.

Baldridge, R. D. and Rapoport, T. A. (2016). Autoubiquitination of the Hrd1 Ligase Triggers Protein Retrotranslocation in ERAD. *Cell* **166**, 394–407.

Ballar, P., Shen, Y., Yang, H. and Fang, S. (2006). The Role of a Novel p97/Valosin-containing Protein-interacting Motif of gp78 in Endoplasmic Reticulum-associated Degradation. *J. Biol. Chem.* **281**, 35359–35368.

Barlowe, C. (1994). COPII: A membrane coat formed by Sec proteins that drive vesicle budding from the endoplasmic reticulum. *Cell* **77**, 895–907.

Barlowe, C. K. and Miller, E. A. (2013). Secretory Protein Biogenesis and Traffic in the Early Secretory Pathway. *Genetics* **193**, 383–410.

Barral, P. M., Sarkar, D., Su, Z.-Z., Barber, G. N., DeSalle, R., Racaniello, V. R. and Fisher, P. B. (2009). Functions of the cytoplasmic RNA sensors RIG-I and MDA-5: Key regulators of innate immunity. *Pharmacology & therapeutics* **124**, 219–234.

Bartee, E., Mansouri, M., Hovey Nerenberg, B. T., Gouveia, K. and Früh, K. (2004). Downregulation of Major Histocompatibility Complex Class I by Human Ubiquitin Ligases Related to Viral Immune Evasion Proteins. *Journal of Virology* **78**, 1109–1120.

Bartscherer, K., Pelte, N., Ingelfinger, D. and Boutros, M. (2006). Secretion of Wnt Ligands Requires Evi, a Conserved Transmembrane Protein. *Cell* **125**, 523–533.

Bänziger, C., Soldini, D., Schütt, C., Zipperlen, P., Hausmann, G. and Basler, K. (2006). Wntless, a Conserved Membrane Protein Dedicated to the Secretion of Wnt Proteins from Signaling Cells. *Cell* **125**, 509–522.

Behnke, J., Mann, M. J., Scruggs, F.-L., Feige, M. J. and Hendershot, L. M. (2016). Members of the Hsp70 Family Recognize Distinct Types of Sequences to Execute ER Quality Control. *Molecular Cell* **63**, 739–752.

Bengtsson, L. and Otto, H. (2008). LUMA interacts with emerin and influences its distribution at the inner nuclear membrane. *Journal of Cell Science* **121**, 536–548.

Bernasconi, R., Galli, C., Calanca, V., Nakajima, T. and Molinari, M. (2010). Stringent requirement for HRD1, SEL1L, and OS-9/XTP3-B for disposal of ERAD-L Ssubstrates. *J Cell Biol* **188**, 223–235.

Bernasconi, R., Pertel, T., Luban, J. and Molinari, M. (2008). A Dual Task for the Xbp1-responsive OS-9 Variants in the Mammalian Endoplasmic Reticulum: INHIBITING SECRETION OF MISFOLDED PROTEIN CONFORMERS AND ENHANCING THEIR DISPOSAL. *J. Biol. Chem.* **283**, 16446–16454.

Berndsen, C. E. and Wolberger, C. (2014). New insights into ubiquitin E3 ligase mechanism. *Nat Struct Mol Biol* **21**, 301–307.

Berridge, M. J., Lipp, P. and Bootman, M. D. (2000). The versatility and universality of calcium signalling. *Nat Rev Mol Cell Biol* **1**, 11–21.

Biederer, T., Volkwein, C. and Sommer, T. (1997). Role of Cue1p in Ubiquitination and Degradation at the ER Surface. *Science* **278**, 1806–1809.

Blobel, G. (1975). Transfer of proteins across membranes. I. Presence of proteolytically processed and unprocessed nascent immunoglobulin light chains on membrane-bound ribosomes of murine myeloma. *J Cell Biol* **67**, 835–851.

Blom, D., Hirsch, C., Stern, P., Tortorella, D. and Ploegh, H. L. (2004). A glycosylated type I membrane protein becomes cytosolic when peptide: N-glycanase is compromised. *EMBO J.* **23**, 650–658.

Blom, T., Somerharju, P. and Ikonen, E. (2011). Synthesis and Biosynthetic Trafficking of Membrane Lipids. *Cold Spring Harbor Perspectives in Biology* **3**, a004713.

Blond-Elguindi, S. (1993). Affinity panning of a library of peptides displayed on bacteriophages reveals the binding specificity of BiP. *Cell* **75**, 717–728.

Bodnar, N. O. and Rapoport, T. A. (2017). Molecular Mechanism of Substrate Processing by the Cdc48 ATPase Complex. *Cell* **169**, 722–735.e9.

Bonifacino, J. S., Cosson, P., Shah, N. and Klausner, R. D. (1991). Role of potentially charged transmembrane residues in targeting proteins for retention and degradation within the endoplasmic reticulum. *The EMBO Journal* **10**, 2783–2793.

Bonnon, C., Wendeler, M. W., Paccaud, J. P. and Hauri, H. P. (2010). Selective export of human GPI-anchored proteins from the endoplasmic reticulum. *Journal of Cell Science* **123**, 1705–1715.

Bordallo, J., Plemper, R. K., Finger, A. and Wolf, D. H. (1998). Der3p/Hrd1p Is Required for Endoplasmic Reticulum-associated Degradation of Misfolded Lumenal and Integral Membrane Proteins. *Molecular Biology of the Cell* **9**, 209–222.

Braakman, I. and Hebert, D. N. (2013). Protein Folding in the Endoplasmic Reticulum. *Cold Spring Harbor Perspectives in Biology* **5**.

Breitling, J. and Aebi, M. (2013). N-Linked Protein Glycosylation in the Endoplasmic Reticulum. *Cold Spring Harbor Perspectives in Biology* **5**, a013359.

Bridgeman, A., Maelfait, J., Davenne, T., Partridge, T., Peng, Y., Mayer, A., Dong, T., Kaever, V., Borrow, P. and Rehwinkel, J. (2015). Viruses transfer the antiviral second messenger cGAMP between cells. *Science* **349**, 1228–1232.

Browman, D. T., Resek, M. E., Zajchowski, L. D. and Robbins, S. M. (2006). Erlin-1 and erlin-2 are novel members of the prohibitin family of proteins that define lipid-raft-like domains of the ER. *Journal of Cell Science* **119**, 3149–3160.

Brown, A. J., Sun, L., Feramisco, J. D., Brown, M. S. and Goldstein, J. L. (2002). Cholesterol Addition to ER Membranes Alters Conformation of SCAP, the SREBP Escort Protein that Regulates Cholesterol Metabolism. *Molecular Cell* **10**, 237–245.

Bucci, C., Lütcke, A., Steele-Mortimer, O., Olkkonen, V. M., Dupree, P., Chiariello, M., Bruni, C. B., Simons, K. and Zerial, M. (2000). Co-operative regulation of endocytosis by three RAB5 isoforms. *FEBS Letters* **366**, 65–71.

Bulleid, N. J. (2012). Disulfide Bond Formation in the Mammalian Endoplasmic Reticulum. *Cold Spring Harbor Perspectives in Biology* **4**, a013219.

Bultynck, G., Kiviluoto, S. and Methner, A. (2014). Bax Inhibitor-1 Is Likely a pH-Sensitive Calcium Leak Channel, Not a H+/Ca2+ Exchanger. *Science Signaling* **7**, pe22–pe22.

Bultynck, G., Kiviluoto, S., Henke, N., Ivanova, H., Schneider, L., Rybalchenko, V., Luyten, T., Nuyts, K., De Borggraeve, W., Bezprozvanny, I., et al. (2012). The C Terminus of Bax Inhibitor-1 Forms a Ca2+-permeable Channel Pore. *J. Biol. Chem.* **287**, 2544–2557.

Burdette, D. L. and Vance, R. E. (2013). STING and the innate immune response to nucleic acids in the cytosol. *Nature Immunology* **14**, 19–26.

Burdette, D. L., Monroe, K. M., Sotelo-Troha, K., Iwig, J. S., Eckert, B., Hyodo, M., Hayakawa, Y. and Vance, R. E. (2011). STING is a direct innate immune sensor of cyclic di-GMP. *Nature* **478**, 515–518.

Burg, J. S. and Espenshade, P. J. (2011). Regulation of HMG-CoA reductase in mammals and yeast. *Progress in lipid research* **50**, 403–410.

Burr, M. L., Cano, F., Svobodova, S., Boyle, L. H., Boname, J. M. and Lehner, P. J. (2011). HRD1 and UBE2J1 target misfolded MHC class I heavy chains for endoplasmic reticulum-associated degradation. *Proc. Natl. Acad. Sci. U.S.A.* **108**, 2034–2039.

Carreras-Sureda, A., Pihán, P. and Hetz, C. (2018). Calcium signaling at the endoplasmic reticulum: fine-tuning stress responses. *The role of Ca2+ signals in the regulation of cell death & survival processes in health, disease and therapy* **70**, 24–31.

Carvalho, P., Goder, V. and Rapoport, T. A. (2006). Distinct Ubiquitin-Ligase Complexes Define Convergent Pathways for the Degradation of ER Proteins. *Cell* **126**, 361–373.

Carvalho, P., Stanley, A. M. and Rapoport, T. A. (2010). Retrotranslocation of a Misfolded Luminal ER Protein by the Ubiquitin-Ligase Hrd1p. *Cell* **143**, 579–591.

Chae, P. S., Rasmussen, S. G. F., Rana, R. R., Gotfryd, K., Chandra, R., Goren, M. A., Kruse, A. C., Nurva, S., Loland, C. J., Pierre, Y., et al. (2010). Maltose-neopentyl glycol (MNG) amphiphiles for solubilization, stabilization and crystallization of membrane proteins. *Nat Meth* **7**, 1003–1008.

Chang, Y., Bruni, R., Kloss, B., Assur, Z., Kloppmann, E., Rost, B., Hendrickson, W. A. and Liu, Q. (2014). Structural basis for a pH-sensitive calcium leak across membranes. *Science* **344**, 1131–1135.

Chau, V., Tobias, J. W., Bachmair, A., Marriott, D., Ecker, D. J., Gonda, D. K. and Varshavsky, A. (1989). A multiubiquitin chain is confined to specific lysine in a targeted short-lived protein. *Science* **243**, 1576–1583.

Chen, C.-Y., Malchus, N. S., Hehn, B., Stelzer, W., Avci, D., Langosch, D. and Lemberg, M. K. (2014). Signal peptide peptidase functions in ERAD to cleave the unfolded protein response regulator XBP1u. *The EMBO Journal* **33**, 2492–2506.

Chen, Q., Sun, L. and Chen, Z. J. (2016). Regulation and function of the cGAS–STING pathway of cytosolic DNA sensing. *Nature Immunology* **17**, 1142–1149.

Chen, R., Li, M., Zhang, Y., Zhou, Q. and Shu, H. B. (2012). The E3 ubiquitin ligase MARCH8 negatively regulates IL-1 -induced NF- B activation by targeting the IL1RAP coreceptor for ubiquitination and degradation. *Proceedings of the National Academy of Sciences* **109**, 14128–14133.

Christianson, J. C. and Green, W. N. (2004). Regulation of nicotinic receptor expression by the ubiquitin–proteasome system. *The EMBO Journal* **23**, 4156–4165.

Christianson, J. C., Olzmann, J. A., Shaler, T. A., Sowa, M. E., Bennett, E. J., Richter, C. M., Tyler, R. E., Greenblatt, E. J., Harper, J. W. and Kopito, R. R. (2012). Defining human ERAD networks through an integrative mapping strategy. *Nature Cell Biology* **14**, 93–105.

Christianson, J. C., Shaler, T. A., Tyler, R. E. and Kopito, R. R. (2008). OS-9 and GRP94 deliver mutant α1-antitrypsin to the Hrd1–SEL1L ubiquitin ligase complex for ERAD. *Nature Cell Biology* **10**, 272–282.

Chuang, J.-Z., Zhou, H., Zhu, M., Li, S.-H., Li, X.-J. and Sung, C.-H. (2002). Characterization of a Brain-enriched Chaperone, MRJ, That Inhibits Huntingtin Aggregation and Toxicity Independently. *J. Biol. Chem.* **277**, 19831–19838.

Chung, J., Torta, F., Masai, K., Lucast, L., Czapla, H., Tanner, L. B., Narayanaswamy, P., Wenk, M. R., Nakatsu, F. and De Camilli, P. (2015). PI4P/phosphatidylserine countertransport at ORP5- and ORP8-mediated ER-plasma membrane contacts. *Science* **349**, 428–432.

Closs, E. I., Gräf, P., Habermeier, A., Cunningham, J. M. and Förstermann, U. (1997). Human Cationic Amino Acid Transporters hCAT-1, hCAT-2A, and hCAT-2B: Three Related Carriers with Distinct Transport Properties †,‡. *Biochemistry* **36**, 6462–6468.

Cohen, Y., Megyeri, M., Chen, O. C. W., Condomitti, G., Riezman, I., Loizides-Mangold, U., Abdul-Sada, A., Rimon, N., Riezman, H., Platt, F. M., et al. (2013). The Yeast P5 Type ATPase, Spf1, Regulates Manganese Transport into the Endoplasmic Reticulum. *PLoS ONE* **8**, e85519.

Connolly, D. J., O'Neill, L. A. J. and McGettrick, A. F. (2013). The GOLD Domain-containing Protein TMED1 Is Involved in Interleukin-33 Signaling. *J. Biol. Chem.* **288**, 5616–5623.

Cormier, J. H., Tamura, T., Sunryd, J. C. and Hebert, D. N. (2009). EDEM1 recognition and delivery of misfolded proteins to the SEL1L-containing ERAD complex. *Molecular Cell* **34**, 627–633.

Corrales, L., Glickman, L. H., McWhirter, S. M., Kanne, D. B., Sivick, K. E., Katibah, G. E., Woo, S.-R., Lemmens, E., Banda, T., Leong, J. J., et al. (2015). Direct Activation of STING in the Tumor Microenvironment Leads to Potent and Systemic Tumor Regression and Immunity. *Cell Reports* **11**, 1018–1030.

Cox, J. and Mann, M. (2008). MaxQuant enables high peptide identification rates, individualized p.p.b.-range mass accuracies and proteome-wide protein quantification. *Nat Biotechnol* **26**, 1367–1372.

Davis, M. E. and Gack, M. U. (2015). Ubiquitination in the Antiviral Immune Response. *Virology* **0**, 52–65.

DeLaBarre, B. and Brunger, A. T. (2003). Complete structure of p97/valosin-containing protein reveals communication between nucleotide domains. *Nat Struct Mol Biol* **10**, 856–863.

DeLaBarre, B., Christianson, J. C., Kopito, R. R. and Brunger, A. T. (2006). Central Pore Residues Mediate the p97/VCP Activity Required for ERAD. *Molecular Cell* **22**, 451–462.

Dersh, D., Jones, S. M., Eletto, D., Christianson, J. C. and Argon, Y. (2014). OS-9 facilitates turnover of nonnative GRP94 marked by hyperglycosylation. *Molecular Biology of the Cell* **25**, 2220–2234.

Didier, C., Broday, L., Bhoumik, A., Israeli, S., Takahashi, S., Nakayama, K., Thomas, S. M., Turner, C. E., Henderson, S., Sabe, H., et al. (2003). RNF5, a RING Finger Protein That Regulates Cell Motility by Targeting Paxillin Ubiquitination and Altered Localization. *Molecular and Cellular Biology* **23**, 5331–5345.

Dimcheff, D. E., Faasse, M. A., McAtee, F. J. and Portis, J. L. (2004). Endoplasmic Reticulum (ER) Stress Induced by a Neurovirulent Mouse Retrovirus Is Associated with Prolonged BiP Binding and Retention of a Viral Protein in the ER. *J. Biol. Chem.* **279**, 33782–33790.

Ding, W.-X., Ni, H.-M., Gao, W., Yoshimori, T., Stolz, D. B., Ron, D. and Yin, X.-M. (2007). Linking of Autophagy to Ubiquitin-Proteasome System Is Important for the Regulation of Endoplasmic Reticulum Stress and Cell Viability. *The American Journal of Pathology* **171**, 513–524.

Dobbs, N., Burnaevskiy, N., Chen, D., Gonugunta, V. K., Alto, N. M. and Yan, N. (2015). STING Activation by Translocation from the ER Is Associated with Infection and Autoinflammatory Disease. *Cell Host & Microbe* **18**, 157–168.

Dong, M., Bridges, J. P., Apsley, K., Xu, Y. and Weaver, T. E. (2008). ERdj4 and ERdj5 Are Required for Endoplasmic Reticulum-associated Protein Degradation of Misfolded Surfactant Protein C. *Molecular Biology of the Cell* **19**, 2620–2630.

Dougan, S. K., Hu, C.-C. A., Paquet, M.-E., Greenblatt, M. B., Kim, J., Lilley, B. N., Watson, N. and Ploegh, H. L. (2011). Derlin-2-Deficient Mice Reveal an Essential Role for Protein Dislocation in Chondrocytes. *Molecular and Cellular Biology* **31**, 1145–1159.

Dudek, J. (2002). A novel type of co-chaperone mediates transmembrane recruitment of DnaK-like chaperones to ribosomes. *The EMBO Journal* **21**, 2958–2967.

Eisenberg-Bord, M., Shai, N., Schuldiner, M. and Bohnert, M. (2016). A Tether Is a Tether Is a Tether: Tethering at Membrane Contact Sites. *Developmental Cell* **39**, 395–409.

Eletto, D., Dersh, D. and Argon, Y. (2010). GRP94 in ER Quality Control and Stress Responses. *Seminars in cell & developmental biology* **21**, 479–485.

Ellgaard, L. and Ruddock, L. W. (2005). The human protein disulphide isomerase family: substrate interactions and functional properties. *EMBO rep* **6**, 28–32.

English, A. R. and Voeltz, G. K. (2013). Endoplasmic Reticulum Structure and Interconnections with Other Organelles. *Cold Spring Harbor Perspectives in Biology* **5**.

Erzberger, J. P. and Berger, J. M. (2006). EVOLUTIONARY RELATIONSHIPS AND STRUCTURAL MECHANISMS OF AAA+ PROTEINS. *Annu. Rev. Biophys. Biomol. Struct.* **35**, 93–114.

Fang, S., Ferrone, M., Yang, C., Jensen, J. P., Tiwari, S. and Weissman, A. M. (2001). The tumor autocrine motility factor receptor, gp78, is a ubiquitin protein ligase implicated in degradation from the endoplasmic reticulum. *Proceedings of the National Academy of Sciences* **98**, 14422–14427.

Ferreira, L. R., Norris, K., Smith, T., Hebert, C. and Sauk, J. J. (1994). Association of Hsp47, Grp78, and Grp94 with procollagen supports the successive or coupled action of molecular chaperones. *J. Cell. Biochem.* **56**, 518–526.

Ferris, S. P., Kodali, V. K. and Kaufman, R. J. (2014). Glycoprotein folding and quality-control mechanisms in protein-folding diseases. *Disease Models & Mechanisms* **7**, 331–341.

Feske, S., Gwack, Y., Prakriya, M., Srikanth, S., Puppel, S.-H., Tanasa, B., Hogan, P. G., Lewis, R. S., Daly, M. and Rao, A. (2006). A mutation in Orai1 causes immune deficiency by abrogating CRAC channel function. *Nature* **441**, 179–185.

Foot, N., Henshall, T. and Kumar, S. (2017). Ubiquitination and the Regulation of Membrane Proteins. *Physiological Reviews* **97**, 253–281.

Foresti, O., Ruggiano, A., Hannibal-Bach, H. K., Ejsing, C. S. and Carvalho, P. (2013). Sterol homeostasis requires regulated degradation of squalene monooxygenase by the ubiquitin ligase Doa10/Teb4. *eLife* **2**, e00953.

Francisco, A. B., Singh, R., Li, S., Vani, A. K., Yang, L., Munroe, R. J., Diaferia, G., Cardano, M., Biunno, I., Qi, L., et al. (2010). Deficiency of Suppressor Enhancer Lin12 1 Like (SEL1L) in Mice Leads to Systemic Endoplasmic Reticulum Stress and Embryonic Lethality. *J. Biol. Chem.* **285**, 13694–13703.

Fu, H., Sadis, S., Rubin, D. M., Glickman, M., van Nocker, S., Finley, D. and Vierstra, R. D. (1998). Multiubiquitin Chain Binding and Protein Degradation Are Mediated by Distinct Domains within the 26 S Proteasome Subunit Mcb1. *J. Biol. Chem.* **273**, 1970–1981.

Fu, J., Kanne, D. B., Leong, M., Glickman, L. H., McWhirter, S. M., Lemmens, E., Mechette, K., Leong, J. J., Lauer, P., Liu, W., et al. (2015). STING agonist formulated cancer vaccines can cure established tumors resistant to PD-1 blockade. *Sci. Transl. Med.* **7**, 283ra52–283ra52.

Fujibayashi, A., Taguchi, T., Misaki, R., Ohtani, M., Dohmae, N., Takio, K., Yamada, M., Gu, J., Yamakami, M., Fukuda, M., et al. (2008). Human RME-8 Is Involved in Membrane Trafficking through Early Endosomes TI . *Cell Structure and Function* **33**, 35–50.

Fujita, H., Iwabu, Y., Tokunaga, K. and Tanaka, Y. (2013). Membrane-associated RING-CH (MARCH) 8 mediates the ubiquitination and lysosomal degradation of the transferrin receptor. *Journal of Cell Science* **126**, 2798–2809.

Fukuda, H., Nakamura, N. and Hirose, S. (2006). MARCH-III Is a Novel Component of Endosomes with Properties Similar to Those of MARCH-II. *The Journal of Biochemistry* **139**, 137–145.

Fullekrug, J., Scheiffele, P. and Simons, K. (1999). VIP36 localisation to the early secretory pathway. *J. Cell Sci.* **112**, 2813.

Garavito, R. M. and Ferguson-Miller, S. (2001). Detergents as Tools in Membrane Biochemistry. *J. Biol. Chem.* **276**, 32403–32406.

Gardner, B. M. and Walter, P. (2011). Unfolded Proteins Are Ire1-Activating Ligands That Directly Induce the Unfolded Protein Response. *Science* **333**, 1891–1894.

Gardner, B. M., Pincus, D., Gotthardt, K., Gallagher, C. M. and Walter, P. (2013). Endoplasmic Reticulum Stress Sensing in the Unfolded Protein Response. *Cold Spring Harbor Perspectives in Biology* **5**, a013169.

Gardner, R. G., Shearer, A. G. and Hampton, R. Y. (2001). In Vivo Action of the HRD Ubiquitin Ligase Complex: Mechanisms of Endoplasmic Reticulum Quality Control and Sterol Regulation. *Molecular and Cellular Biology* **21**, 4276–4291.

Gaudet, P. and Dessimoz, C. (2017). Gene Ontology: Pitfalls, Biases, and Remedies. In *The Gene Ontology Handbook* (eds. Dessimoz, C. and Škunca, N., pp. 189–205. New York, NY: Springer New York.

Gemmill, R. M., Bemis, L. T., Lee, J. P., Sozen, M. A., Baron, A., Zeng, C., Erickson, P. F., Hooper, J. E. and Drabkin, H. A. (2002). The TRC8 hereditary kidney cancer gene suppresses growth and functions with VHL in a common pathway. *Oncogene* **21**, 3507–3516.

Ghaemmaghami, S., Huh, W.-K., Bower, K., Howson, R. W., Belle, A., Dephoure, N., O'Shea, E. K. and Weissman, J. S. (2003). Global analysis of protein expression in yeast. *Nature* **425**, 737–741.

Gilmore, R. (1982a). Protein translocation across the endoplasmic reticulum. I. Detection in the microsomal membrane of a receptor for the signal recognition particle. *J Cell Biol* **95**, 463–469.

Gilmore, R. (1982b). Protein translocation across the endoplasmic reticulum. II. Isolation and characterization of the signal recognition particle receptor. *J Cell Biol* **95**, 470–477.

GINCEL, D., ZAID, H. and SHOSHAN-BARMATZ, V. (2001). Calcium binding and translocation by the voltage-dependent anion channel: a possible regulatory mechanism in mitochondrial function. *Biochem. J.* **358**, 147–155.

Giordano, F., Saheki, Y., Idevall-Hagren, O., Colombo, S. F., Pirruccello, M., Milosevic, I., Gracheva, E. O., Bagriantsev, S. N., Borgese, N. and De Camilli, P. (2013). PI(4,5)P2-Dependent and Ca2+-Regulated ER-PM Interactions Mediated by the Extended Synaptotagmins. *Cell* **153**, 1494–1509.

Glaeser, K., Urban, M., Fenech, E., Voloshanenko, O., Kranz, D., Lari, F., Christianson, J. C. and Boutros, M. (2018). ERAD-dependent control of the Wnt secretory factor Evi. *EMBO J.* **37**, e97311.

Goldstein, J. L. and Brown, M. S. (1990). Regulation of the mevalonate pathway. *Nature* **343**, 425–430.

Golej, D. L., Askari, B., Kramer, F., Barnhart, S., Vivekanandan-Giri, A., Pennathur, S. and Bornfeldt, K. E. (2011). Long-chain acyl-CoA synthetase 4 modulates prostaglandin E2 release from human arterial smooth muscle cells. *Journal of Lipid Research* **52**, 782–793.

Gomez-Navarro, N. and Miller, E. (2016). Protein sorting at the ER–Golgi interface. *J Cell Biol* **3**, jcb.201610031.

Gonugunta, V. K., Sakai, T., Pokatayev, V., Yang, K., Wu, J., Dobbs, N. and Yan, N. (2017). Trafficking-Mediated STING Degradation Requires Sorting to Acidified Endolysosomes and Can Be Targeted to Enhance Anti-tumor Response. *Cell Reports* **21**, 3234–3242.

Gonzalez, D. S., Karaveg, K., Vandersall-Nairn, A. S., Lal, A. and Moremen, K. W. (1999). Identification, Expression, and Characterization of a cDNA Encoding Human Endoplasmic Reticulum Mannosidase I, the Enzyme That Catalyzes the First Mannose Trimming Step in Mammalian Asn-linked Oligosaccharide Biosynthesis. *J. Biol. Chem.* **274**, 21375–21386.

Graham, D. B., Becker, C. E., Doan, A., Goel, G., Villablanca, E. J., Knights, D., Mok, A., Ng, A. C. Y., Doench, J. G., Root, D. E., et al. (2015). Functional genomics identifies negative regulatory nodes controlling phagocyte oxidative burst. *Nat Comms* **6**, 1576.

Greenblatt, E. J., Olzmann, J. A. and Kopito, R. R. (2011). Derlin-1 is a rhomboid pseudoprotease required for the dislocation of mutant α-1 antitrypsin from the endoplasmic reticulum. *Nat Struct Mol Biol* **18**, 1147–1152.

Guillou, H., D'Andrea, S., Rioux, V., Barnouin, R., Dalaine, S., Pedrono, F., Jan, S. and Legrand, P. (2004). Distinct roles of endoplasmic reticulum cytochrome b5 and fused cytochrome b5-like domain for rat Δ6-desaturase activity. *Journal of Lipid Research* **45**, 32–40.

Hainzl, O., Lapina, M. C., Buchner, J. and Richter, K. (2009). The Charged Linker Region Is an Important Regulator of Hsp90 Function. *J. Biol. Chem.* **284**, 22559–22567.

Halic, M., Becker, T., Pool, M. R., Spahn, C. M. T., Grassucci, R. A., Frank, J. and Beckmann, R. (2004). Structure of the signal recognition particle interacting with the elongation-arrested ribosome. *Nature* **427**, 808–814.

Hammond, C., Braakman, I. and Helenius, A. (1994). Role of N-linked oligosaccharide recognition, glucose trimming, and calnexin in glycoprotein folding and quality control. *Proceedings of the National Academy of Sciences* **91**, 913–917.

Hampton, R. Y., Gardner, R. G. and Rine, J. (1996). Role of 26S proteasome and HRD genes in the degradation of 3-hydroxy-3-methylglutaryl-CoA reductase, an integral endoplasmic reticulum membrane protein. *Molecular Biology of the Cell* **7**, 2029–2044.

Han, S.-O., Xiao, K., Kim, J., Wu, J.-H., Wisler, J. W., Nakamura, N., Freedman, N. J. and Shenoy, S. K. (2012). MARCH2 promotes endocytosis and lysosomal sorting of carvedilol-bound β(2)-adrenergic receptors. *J Cell Biol* **199**, 817–830.

Hanson, S. R., Culyba, E. K., Hsu, T. L., Wong, C. H., Kelly, J. W. and Powers, E. T. (2009). The core trisaccharide of an N-linked glycoprotein intrinsically accelerates folding and enhances stability. *Proceedings of the National Academy of Sciences* **106**, 3131–3136.

Hara-Kuge, S. (1994). En bloc incorporation of coatomer subunits during the assembly of COP- coated vesicles [published erratum appears in J Cell Biol 1994 Jul;126(2):589]. *J Cell Biol* **124**, 883–892.

Harding, H. P., Novoa, I., Zhang, Y., Zeng, H., Wek, R., Schapira, M. and Ron, D. (2000). Regulated Translation Initiation Controls Stress-Induced Gene Expression in Mammalian Cells. *Molecular Cell* **6**, 1099–1108.

Harding, H. P., Zhang, Y. and Ron, D. (1999). Protein translation and folding are coupled by an endoplasmic-reticulum-resident kinase. *Nature* **397**, 271–274.

Harding, H. P., Zhang, Y., Zeng, H., Novoa, I., Lu, P. D., Calfon, M., Sadri, N., Yun, C., Popko, B., Paules, R., et al. (2003). An Integrated Stress Response Regulates Amino Acid Metabolism and Resistance to Oxidative Stress. *Molecular Cell* **11**, 619–633.

Hassink, G., Kikkert, M., VOORDEN, S. V., Lee, S.-J., Spaapen, R., LAAR, T. V., Coleman, C. S., Bartee, E., Früh, K., Chau, V., et al. (2005). TEB4 is a C4HC3 RING finger-containing ubiquitin ligase of the endoplasmic reticulum. *Biochem. J.* **388**, 647–655.

Hauer, F., Gerle, C., Fischer, N., Oshima, A., Shinzawa-Itoh, K., Shimada, S., Yokoyama, K., Fujiyoshi, Y. and Stark, H. (2015). GraDeR: Membrane Protein Complex Preparation for Single-Particle Cryo-EM. *Structure* **23**, 1769–1775.

Haugstetter, J., Blicher, T. and Ellgaard, L. (2005). Identification and Characterization of a Novel Thioredoxin-related Transmembrane Protein of the Endoplasmic Reticulum. *J. Biol. Chem.* **280**, 8371–8380.

Haze, K., Yoshida, H., Yanagi, H., Yura, T. and Mori, K. (1999). Mammalian Transcription Factor ATF6 Is Synthesized as a Transmembrane Protein and Activated by Proteolysis in Response to Endoplasmic Reticulum Stress. *Molecular Biology of the Cell* **10**, 3787–3799.

Hebert, D. N., Foellmer, B. and Helenius, A. (1996). Calnexin and calreticulin promote folding, delay oligomerization and suppress degradation of influenza hemagglutinin in microsomes. *The EMBO Journal* **15**, 2961–2968.

Hebert, D. N., Foellmer, B. and Helenius, A. (1995). Glucose trimming and reglucosylation determine glycoprotein association with calnexin in the endoplasmic reticulum. *Cell* **81**, 425–433.

Hemmi, H., Takeuchi, O., Kawai, T., Kaisho, T., Sato, S., Sanjo, H., Matsumoto, M., Hoshino, K., Wagner, H., Takeda, K., et al. (2000). A Toll-like receptor recognizes bacterial DNA. *Nature* **408**, 740–745.

Hermansson, M., Hokynar, K. and Somerharju, P. (2011). Mechanisms of glycerophospholipid homeostasis in mammalian cells. *Progress in lipid research* **50**, 240–257.

Herr, P. and Basler, K. (2012). Porcupine-mediated lipidation is required for Wnt recognition by Wls. *Developmental Biology* **361**, 392–402.

Hirao, K., Natsuka, Y., Tamura, T., Wada, I., Morito, D., Natsuka, S., Romero, P., Sleno, B., Tremblay, L. O., Herscovics, A., et al. (2006). EDEM3, a Soluble EDEM Homolog, Enhances Glycoprotein Endoplasmic Reticulum-associated Degradation and Mannose Trimming. *J. Biol. Chem.* **281**, 9650–9658.

Hjerpe, R., Aillet, F., Lopitz-Otsoa, F., Lang, V., England, P. and Rodriguez, M. S. (2009). Efficient protection and isolation of ubiquitylated proteins using tandem ubiquitin-binding entities. *EMBO rep* **10**, 1250–1258.

Hollien, J., Lin, J. H., Li, H., Stevens, N., Walter, P. and Weissman, J. S. (2009). Regulated Ire1-dependent decay of messenger RNAs in mammalian cells. *J Cell Biol* **186**, 323–331.

Honsho, M., Asaoku, S. and Fujiki, Y. (2010). Posttranslational Regulation of Fatty Acyl-CoA Reductase 1, Far1, Controls Ether Glycerophospholipid Synthesis. *J. Biol. Chem.* **285**, 8537–8542.

Hosokawa, N., Wada, I., Nagasawa, K., Moriyama, T., Okawa, K. and Nagata, K. (2008a). Human XTP3-B Forms an Endoplasmic Reticulum Quality Control Scaffold with the HRD1-SEL1L Ubiquitin Ligase Complex and BiP. *J. Biol. Chem.* **283**, 20914–20924.

Hosokawa, N., Wada, I., Nagasawa, K., Moriyama, T., Okawa, K. and Nagata, K. (2008b). Human XTP3-B Forms an Endoplasmic Reticulum Quality Control Scaffold with the HRD1-SEL1L Ubiquitin Ligase Complex and BiP. **283**, 20914–20924.

Hosokawa, N., You, Z., Tremblay, L. O., Nagata, K. and Herscovics, A. (2007). Stimulation of ERAD of misfolded null Hong Kong α1-antitrypsin by Golgi α1,2-mannosidases. *Biochemical and Biophysical Research Communications* **362**, 626–632.

Houten, S. M. and Wanders, R. J. A. (2010). A general introduction to the biochemistry of mitochondrial fatty acid β-oxidation. *Journal of Inherited Metabolic Disease* **33**, 469–477.

Hua, X., Nohturfft, A., Goldstein, J. L. and Brown, M. S. (1996). Sterol Resistance in CHO Cells Traced to Point Mutation in SREBP Cleavage–Activating Protein. *Cell* **87**, 415–426.

Huang, B. and Baek, S.-H. (2017). Trim13 Potentiates Toll-Like Receptor 2-Mediated Nuclear FactorκB Activation via K29-Linked Polyubiquitination of Tumor Necrosis Factor Receptor-Associated Factor 6. *Mol Pharmacol* **91**, 307–316.

Huang, C.-H., Chu, Y.-R., Ye, Y. and Chen, X. (2014). Role of HERP and a HERP-related Protein in HRD1-dependent Protein Degradation at the Endoplasmic Reticulum. *J. Biol. Chem.* **289**, 4444–4454.

Huang, C.-H., Hsiao, H.-T., Chu, Y.-R., Ye, Y. and Chen, X. (2013). Derlin2 Protein Facilitates HRD1-mediated Retro-translocation of Sonic Hedgehog at the Endoplasmic Reticulum. *J. Biol. Chem.* **288**, 25330–25339.

Huang, E. Y., To, M., Tran, E., Dionisio, L. T. A., Cho, H. J., Baney, K. L. M., Pataki, C. I. and Olzmann, J. A. (2018). A VCP inhibitor substrate trapping approach (VISTA) enables proteomic profiling of endogenous ERAD substrates. *Molecular Biology of the Cell* mbc.E17–08–0514.

Husnjak, K., Elsasser, S., Zhang, N., Chen, X., Randles, L., Shi, Y., Hofmann, K., Walters, K. J., Finley, D. and Dikic, I. (2008). Proteasome subunit Rpn13 is a novel ubiquitin receptor. *Nature* **453**, 481–488.

Hutchinson, E. C., Charles, P. D., Hester, S. S., Thomas, B., Trudgian, D., Martínez-Alonso, M. and Fodor, E. (2014). Conserved and host-specific features of influenza virion architecture. *Nat Comms* **5**, 4816.

Huttlin, E. L., Bruckner, R. J., Paulo, J. A., Cannon, J. R., Ting, L., Baltier, K., Colby, G., Gebreab, F., Gygi, M. P., Parzen, H., et al. (2017). Architecture of the human interactome defines protein communities and disease networks. *Nature* **545**, 505–509.

Huttlin, E. L., Ting, L., Bruckner, R. J., Gebreab, F., Gygi, M. P., Szpyt, J., Tam, S., Zarraga, G., Colby, G., Baltier, K., et al. (2015). The BioPlex Network: A Systematic Exploration of the Human Interactome. *Cell* **162**, 425–440.

Hülsmann, J., Kravic, B., Weith, M., Gstaiger, M., Aebersold, R. H., Collins, B. C. and Meyer, H. (2018). AP-SWATH reveals direct involvement of VCP/p97 in integrated stress response signaling through facilitating CReP/PPP1R15B degradation. *Molecular & Cellular Proteomics*.

Hwang, J., Walczak, C. P., Shaler, T. A., Olzmann, J. A., Zhang, L., Elias, J. E. and Kopito, R. R. (2017). Characterization of protein complexes of the endoplasmic reticulum-associated degradation E3 ubiquitin ligase Hrd1. *J. Biol. Chem.* **292**, 9104–9116.

Ichikawa, D., Mizuno, M., Yamamura, T. and Miyake, S. (2011). GRAIL (Gene Related to Anergy in Lymphocytes) Regulates Cytoskeletal Reorganization through Ubiquitination and Degradation of Arp2/3 Subunit 5 and Coronin 1A. *J. Biol. Chem.* **286**, 43465–43474.

Iconomou, M. and Saunders, D. N. (2016). Systematic approaches to identify E3 ligase substrates. *Biochemical Journal* **473**, 4083–4101.

Iida, Y., Fujimori, T., Okawa, K., Nagata, K., Wada, I. and Hosokawa, N. (2011). SEL1L Protein Critically Determines the Stability of the HRD1-SEL1L Endoplasmic Reticulum-associated Degradation (ERAD) Complex to Optimize the Degradation Kinetics of ERAD Substrates. *J. Biol. Chem.* **286**, 16929–16939.

Ishikawa, H. and Barber, G. N. (2008). STING is an endoplasmic reticulum adaptor that facilitates innate immune signalling. *Nature* **455**, 674–678.

Ishikawa, H., Ma, Z. and Barber, G. N. (2009). STING regulates intracellular DNA-mediated, type I interferon-dependent innate immunity. *Nature* **461**, 788–792.

Jackson, R. J., Hellen, C. U. T. and Pestova, T. V. (2010). The mechanism of eukaryotic translation initiation and principles of its regulation. *Nat Rev Mol Cell Biol* **11**, 113–127.

Jacquemyn, J., Cascalho, A. and Goodchild, R. E. (2017). The ins and outs of endoplasmic reticulum-controlled lipid biosynthesis. *EMBO rep* **18**, 1905–1921.

Jansens, A. (2002). Coordinated Nonvectorial Folding in a Newly Synthesized Multidomain Protein. *Science* **298**, 2401–2403.

Jenne, N., Frey, K., Brügger, B. and Wieland, F. T. (2002). Oligomeric State and Stoichiometry of p24 Proteins in the Early Secretory Pathway. *J. Biol. Chem.* **277**, 46504–46511.

Jeon, Y. J., Khelifa, S., Ratnikov, B., Scott, D. A., Feng, Y., Parisi, F., Ruller, C., Lau, E., Kim, H., Brill, L. M., et al. (2015). Regulation of Glutamine Carrier Proteins by RNF5 Determines Breast Cancer Response to ER Stress-Inducing Chemotherapies. *Cancer Cell* **27**, 354–369.

Jia, Z., Moulson, C. L., Pei, Z., Miner, J. H. and Watkins, P. A. (2007). Fatty Acid Transport Protein 4 Is the Principal Very Long Chain Fatty Acyl-CoA Synthetase in Skin Fibroblasts. *J. Biol. Chem.* **282**, 20573–20583.

Jiang, C., Zhu, Y., Zhou, Z., Gumin, J., Bengtsson, L., Wu, W., Songyang, Z., Lang, F. F. and Lin, X. (2016). TMEM43/LUMA is a key signaling component mediating EGFR-induced NF-κB activation and tumor progression. *Oncogene* **36**, 2813–2823.

Jiang, L.-Y., Jiang, W., Tian, N., Xiong, Y.-N., Liu, J., Wei, J., Wu, K.-Y., Luo, J., Shi, X.-J. and Song, B.-L. (2018). Ring finger protein 145 (RNF145) is a ubiquitin ligase for sterol-induced degradation of HMG-CoA reductase. *J. Biol. Chem.*

Jin, L., Pahuja, K. B., Wickliffe, K. E., Gorur, A., Baumgärtel, C., Schekman, R. and Rape, M. (2012). Ubiquitin-dependent regulation of COPII coat size and function. *Nature* **482**, 495–500.

Jo, Y., Lee, P. C. W., Sguigna, P. V. and DeBose-Boyd, R. A. (2011a). Sterol-induced degradation of HMG CoA reductase depends on interplay of two Insigs and two ubiquitin ligases, gp78 and Trc8. *Proceedings of the National Academy of Sciences* **108**, 20503–20508.

Jo, Y., Sguigna, P. V. and DeBose-Boyd, R. A. (2011b). Membrane-associated Ubiquitin Ligase Complex Containing gp78 Mediates Sterol-accelerated Degradation of 3-Hydroxy-3-methylglutaryl-coenzyme A Reductase. *J. Biol. Chem.* **286**, 15022–15031.

Jongsma, M. L. M., Berlin, I., Wijdeven, R. H. M., Janssen, L., Janssen, G. M. C., Garstka, M. A., Janssen, H., Mensink, M., van Veelen, P. A., Spaapen, R. M., et al. (2016). An ER-Associated Pathway Defines Endosomal Architecture for Controlled Cargo Transport. *Cell* **166**, 152–166.

Joo, H. M., Kim, J. Y., Jeong, J. B., Seong, K. M., Nam, S. Y., Yang, K. H., Kim, C. S., Kim, H. S., Jeong, M., An, S., et al. (2011). Ret finger protein 2 enhances ionizing radiation-induced apoptosis via degradation of AKT and MDM2. *European Journal of Cell Biology* **90**, 420–431.

Kakkar, R. and Lee, R. T. (2008). The IL-33/ST2 pathway: therapeutic target and novel biomarker. *Nature reviews. Drug discovery* **7**, 827–840.

Kaneko, M., Ishiguro, M., Niinuma, Y., Uesugi, M. and Nomura, Y. (2002). Human HRD1 protects against ER stress-induced apoptosis through ER-associated degradation11The nucleotide sequence data reported are available in the DDBJ/EMBL/GenBank databases under the accession number AB085847. *FEBS Letters* **532**, 147–152.

Kaneko, M., Iwase, I., Yamasaki, Y., Takai, T., Wu, Y., Kanemoto, S., Matsuhisa, K., Asada, R., Okuma, Y., Watanabe, T., et al. (2016). Genome-wide identification and gene expression profiling of ubiquitin ligases for endoplasmic reticulum protein degradation. *Sci Rep* **6**, 425.

Kaneko, M., Koike, H., Saito, R., Kitamura, Y., Okuma, Y. and Nomura, Y. (2010). Loss of HRD1-Mediated Protein Degradation Causes Amyloid Precursor Protein Accumulation and Amyloid- Generation. *Journal of Neuroscience* **30**, 3924–3932.

Kappeler, F., Klopfenstein, D. R. C., Foguet, M., Paccaud, J.-P. and Hauri, H.-P. (1997). The Recycling of ERGIC-53 in the Early Secretory Pathway: ERGIC-53 CARRIES A CYTOSOLIC ENDOPLASMIC RETICULUM-EXIT DETERMINANT INTERACTING WITH COPII. *J. Biol. Chem.* **272**, 31801–31808.

Kato, H. (2006). Ubiquitin-proteasome-dependent degradation of mammalian ER stearoyl-CoA desaturase. *Journal of Cell Science* **119**, 2342–2353.

Keilhauer, E. C., Hein, M. Y. and Mann, M. (2015). Accurate Protein Complex Retrieval by Affinity Enrichment Mass Spectrometry (AE-MS) Rather than Affinity Purification Mass Spectrometry (AP-MS). *Molecular & Cellular Proteomics* **14**, 120–135.

Kelleher, D. J., Karaoglu, D., Mandon, E. C. and Gilmore, R. (2003). Oligosaccharyltransferase Isoforms that Contain Different Catalytic STT3 Subunits Have Distinct Enzymatic Properties. *Molecular Cell* **12**, 101–111.

Khouri, El, E., Le Pavec, G., Toledano, M. B. and Delaunay-Moisan, A. (2013). RNF185 Is a Novel E3 Ligase of Endoplasmic Reticulum-associated Degradation (ERAD) That Targets Cystic Fibrosis Transmembrane Conductance Regulator (CFTR). **288**, 31177–31191.

Kikkert, M., Doolman, R., Dai, M., Avner, R., Hassink, G., van Voorden, S., Thanedar, S., Roitelman, J., Chau, V. and Wiertz, E. (2004). Human HRD1 is an E3 ubiquitin ligase involved in degradation of proteins from the endoplasmic reticulum. *J. Biol. Chem.* **279**, 3525–3534.

Kim, I., Ahn, J., Liu, C., Tanabe, K., Apodaca, J., Suzuki, T. and Rao, H. (2006). The Png1–Rad23 complex regulates glycoprotein turnover. *J Cell Biol* **172**, 211–219.

Kirschke, C. P. and Huang, L. (2003). ZnT7, a Novel Mammalian Zinc Transporter, Accumulates Zinc in the Golgi Apparatus. *J. Biol. Chem.* **278**, 4096–4102.

Klappa, P., Freedman, R. B. and Zimmermann, R. (1995). Protein Disulphide Isomerase and a Lumenal Cyclophilin-Type Peptidyl Prolyl Cis-Trans Isomerase are in Transient Contact with Secretory Proteins During Late Stages of Translocation. *European Journal of Biochemistry* **232**, 755–764.

Klemm, E. J., Spooner, E. and Ploegh, H. L. (2011). Dual Role of Ancient Ubiquitous Protein 1 (AUP1) in Lipid Droplet Accumulation and Endoplasmic Reticulum (ER) Protein Quality Control. *J. Biol. Chem.* **286**, 37602–37614.

Kondo, T., Watanabe, M. and Hatakeyama, S. (2012). TRIM59 interacts with ECSIT and negatively regulates NF-κB and IRF-3/7-mediated signal pathways. *Biochemical and Biophysical Research Communications* **422**, 501–507.

Korennykh, A. V., Egea, P. F., Korostelev, A. A., Finer-Moore, J., Zhang, C., Shokat, K. M., Stroud, R. M. and Walter, P. (2008). The unfolded protein response signals through high-order assembly of Ire1. *Nature* **457**, 687–693.

Kuang, E., Okumura, C. Y. M., Sheffy-Levin, S., Varsano, T., Shu, V. C.-W., Qi, J., Niesman, I. R., Yang, H.-J., López-Otín, C., Yang, W. Y., et al. (2012). Regulation of ATG4B Stability by RNF5 Limits Basal Levels of Autophagy and Influences Susceptibility to Bacterial Infection. *PLOS Genetics* **8**, e1003007.

Kwon, S.-H., Oh, S., Nacke, M., Mostov, K. E. and Lipschutz, J. H. (2016). Adaptor Protein CD2AP and L-type Lectin LMAN2 Regulate Exosome Cargo Protein Trafficking through the Golgi Complex. *J. Biol. Chem.* **291**, 25462–25475.

Lederkremer, G. Z. (2009). Glycoprotein folding, quality control and ER-associated degradation. *Carbohydradtes and glycoconjugates / Biophysical methods* **19**, 515–523.

Lee, A.-H., Iwakoshi, N. N. and Glimcher, L. H. (2003). XBP-1 Regulates a Subset of Endoplasmic Reticulum Resident Chaperone Genes in the Unfolded Protein Response. *Molecular and Cellular Biology* **23**, 7448–7459.

Lee, J. N., Song, B., DeBose-Boyd, R. A. and Ye, J. (2006). Sterol-regulated Degradation of Insig-1 Mediated by the Membrane-bound Ubiquitin Ligase gp78. *J. Biol. Chem.* **281**, 39308–39315.

Lee, J. P., Brauweiler, A., Rudolph, M., Hooper, J. E., Drabkin, H. A. and Gemmill, R. M. (2010). TRC8, A KIDNEY CANCER-ASSOCIATED UBIQUITIN LIGASE, IS STEROL-REGULATED AND INTERACTS WITH LIPID AND PROTEIN BIOSYNTHETIC PATHWAYS. *Molecular cancer research : MCR* **8**, 93–106.

Lee, K. P. K., Dey, M., Neculai, D., Cao, C., Dever, T. E. and Sicheri, F. (2008). Structure of the Dual Enzyme Ire1 Reveals the Basis for Catalysis and Regulation in Nonconventional RNA Splicing. *Cell* **132**, 89–100.

Lerner, M., Corcoran, M., Cepeda, D., Nielsen, M. L., Zubarev, R., Ponten, F., Uhlen, M., Hober, S., Grander, D. and Sangfelt, O. (2007). The RBCC Gene RFP2 (Leu5) Encodes a Novel Transmembrane E3 Ubiquitin Ligase Involved in ERAD. *Molecular Biology of the Cell* **18**, 1670–1682.

Li, G., Zhao, G., Zhou, X., Schindelin, H. and Lennarz, W. J. (2006). The AAA ATPase p97 links peptide N-glycanase to the endoplasmic reticulum-associated E3 ligase autocrine motility factor receptor. *Proceedings of the National Academy of Sciences* **103**, 8348–8353.

Li, W., Bengtson, M. H., Ulbrich, A., Matsuda, A., Reddy, V. A., Orth, A., Chanda, S. K., Batalov, S. and Joazeiro, C. A. P. (2008). Genome-Wide and Functional Annotation of Human E3 Ubiquitin Ligases Identifies MULAN, a Mitochondrial E3 that Regulates the Organelle's Dynamics and Signaling. *PLoS ONE* **3**, e1487.

Liang, J.-S., Kim, T., Fang, S., Yamaguchi, J., Weissman, A. M., Fisher, E. A. and Ginsberg, H. N. (2003). Overexpression of the Tumor Autocrine Motility Factor Receptor Gp78, a Ubiquitin Protein Ligase, Results in Increased Ubiquitinylation and Decreased Secretion of Apolipoprotein B100 in HepG2 Cells. *J. Biol. Chem.* **278**, 23984–23988.

Liang, W.-C., Mitsuhashi, H., Keduka, E., Nonaka, I., Noguchi, S., Nishino, I. and Hayashi, Y. K. (2011). TMEM43 mutations in emery-dreifuss muscular dystrophy-related myopathy. *Ann Neurol.* **69**, 1005–1013.

Lièvremont, J.-P., Rizzuto, R., Hendershot, L. and Meldolesi, J. (1997). BiP, a Major Chaperone Protein of the Endoplasmic Reticulum Lumen, Plays a Direct and Important Role in the Storage of the Rapidly Exchanging Pool of Ca2. *J. Biol. Chem.* **272**, 30873–30879.

Lilley, B. N. and Ploegh, H. L. (2005). Multiprotein complexes that link dislocation, ubiquitination, and extraction of misfolded proteins from the endoplasmic reticulum membrane. *Proceedings of the National Academy of Sciences* **102**, 14296–14301.

Lilley, B. N. and Ploegh, H. L. (2004). A membrane protein required for dislocation of misfolded proteins from the ER. *Nature* **429**, 834–840.

Lin, J. H., Li, H., Yasumura, D., Cohen, H. R., Zhang, C., Panning, B., Shokat, K. M., LaVail, M. M. and Walter, P. (2007). IRE1 Signaling Affects Cell Fate During the Unfolded Protein Response. *Science* **318**, 944–949.

Lindsay, A. J., Hendrick, A. G., Cantalupo, G., Senic-Matuglia, F., Goud, B., Bucci, C. and McCaffrey, M. W. (2002). Rab Coupling Protein (RCP), a Novel Rab4 and Rab11 Effector Protein. *J. Biol. Chem.* **277**, 12190–12199.

Lineberry, N., Su, L., Soares, L. and Fathman, C. G. (2008). The Single Subunit Transmembrane E3 Ligase Gene Related to Anergy in Lymphocytes (GRAIL) Captures and Then Ubiquitinates Transmembrane Proteins across the Cell Membrane. *The Journal of Biological Chemistry* **283**, 28497–28505.

Lisbona, F., Rojas-Rivera, D., Thielen, P., Zamorano, S., Todd, D., Martinon, F., Glavic, A., Kress, C., Lin, J. H., Walter, P., et al. (2009). BAX Inhibitor-1 Is a Negative Regulator of the ER Stress Sensor IRE1α. *Molecular Cell* **33**, 679–691.

Liu, H., Sadygov, R. G. and Yates, J. R. (2004). A Model for Random Sampling and Estimation of Relative Protein Abundance in Shotgun Proteomics. *Anal. Chem.* **76**, 4193–4201.

Liu, J., Bang, A. G., Kintner, C., Orth, A. P., Chanda, S. K., Ding, S. and Schultz, P. G. (2005). Identification of the Wnt signaling activator leucine-rich repeat in Flightless interaction protein 2 by a genome-wide functional analysis. *Proceedings of the National Academy of Sciences* **102**, 1927–1932.

Liu, Y. and Ye, Y. (2012). Roles of p97-associated deubiquitinases in protein quality control at the endoplasmic reticulum. *Current protein & peptide science* **13**, 436–446.

Livneh, I., Cohen-Kaplan, V., Cohen-Rosenzweig, C., Avni, N. and Ciechanover, A. (2016). The life cycle of the 26S proteasome: from birth, through regulation and function and onto its death. *Cell Res* **26**, 869–885.

Logan, C. Y. and Nusse, R. (2004). THE WNT SIGNALING PATHWAY IN DEVELOPMENT AND DISEASE. *Annu. Rev. Cell Dev. Biol.* **20**, 781–810.

Lu, J. P., Wang, Y., Sliter, D. A., Pearce, M. M. P. and Wojcikiewicz, R. J. H. (2011). RNF170 Protein, an Endoplasmic Reticulum Membrane Ubiquitin Ligase, Mediates Inositol 1,4,5-Trisphosphate Receptor Ubiquitination and Degradation. *J. Biol. Chem.* **286**, 24426–24433.

Luu, W., Hart-Smith, G., Sharpe, L. J. and Brown, A. J. (2015). The terminal enzymes of cholesterol synthesis, DHCR24 and DHCR7, interact physically and functionally. *Journal of Lipid Research* **56**, 888–897.

M, Z. R., van der Klei Ida J, Marten, V., Nikolaus, P., van der Laan Martin and Maria, B. (2012). Mitofilin complexes: conserved organizers of mitochondrial membrane architecture T2 . *bchm* **393**, 1247.

Ma, K., Vattem, K. M. and Wek, R. C. (2002). Dimerization and Release of Molecular Chaperone Inhibition Facilitate Activation of Eukaryotic Initiation Factor-2 Kinase in Response to Endoplasmic Reticulum Stress. *J. Biol. Chem.* **277**, 18728–18735.

Ma, Y. and Hendershot, L. M. (2004). Herp Is Dually Regulated by Both the Endoplasmic Reticulum Stress-specific Branch of the Unfolded Protein Response and a Branch That Is Shared with Other Cellular Stress Pathways. *J. Biol. Chem.* **279**, 13792–13799.

Marciniak, S. J., Yun, C. Y., Oyadomari, S., Novoa, I., Zhang, Y., Jungreis, R., Nagata, K., Harding, H. P. and Ron, D. (2004). CHOP induces death by promoting protein synthesis and oxidation in the stressed endoplasmic reticulum. *Genes & Development* **18**, 3066–3077.

Maruyama, Y., Yamada, M., Takahashi, K. and Yamada, M. (2008). Ubiquitin ligase Kf-1 is involved in the endoplasmic reticulum-associated degradation pathway. *Biochemical and Biophysical Research Communications* **374**, 737–741.

Marzec, M., Eletto, D. and Argon, Y. (2012). GRP94: an HSP90-like protein specialized for protein folding and quality control in the Endoplasmic Reticulum. *Biochimica et biophysica acta* **1823**, 774–787.

Marzioch, M., Henthorn, D. C., Herrmann, J. M., Wilson, R., Thomas, D. Y., Bergeron, J. J. M., Solari, R. C. E. and Rowley, A. (1999). Erp1p and Erp2p, Partners for Emp24p and Erv25p in a Yeast p24 Complex. *Molecular Biology of the Cell* **10**, 1923–1938.

Mastroberardino, L., Spindler, B., Pfeiffer, R., Skelly, P. J., Loffing, J., Shoemaker, C. B. and Verrey, F. (1998). Amino-acid transport by heterodimers of 4F2hc/CD98 and members of a permease family. *Nature* **395**, 288–291.

Matsui, H., Hozumi, Y., Tanaka, T., Okada, M., Nakano, T., Suzuki, Y., Iseki, K., Kakehata, S., Topham, M. K. and Goto, K. (2014). Role of the N-terminal hydrophobic residues of DGKε in targeting the endoplasmic reticulum. *Biochimica et Biophysica Acta (BBA) - Molecular and Cell Biology of Lipids* **1841**, 1440–1450.

Matsuo, Y., Akiyama, N., Nakamura, H., Yodoi, J., Noda, M. and Kizaka-Kondoh, S. (2001). Identification of a Novel Thioredoxin-related Transmembrane Protein. *J. Biol. Chem.* **276**, 10032–10038.

Mayer, M. P. and Bukau, B. (2005). Hsp70 chaperones: Cellular functions and molecular mechanism. *Cellular and Molecular Life Sciences* **62**, 670.

McWhirter, S. M., Barbalat, R., Monroe, K. M., Fontana, M. F., Hyodo, M., Joncker, N. T., Ishii, K. J., Akira, S., Colonna, M., Chen, Z. J., et al. (2009). A host type I interferon response is induced by cytosolic sensing of the bacterial second messenger cyclic-di-GMP. *J Exp Med* **206**, 1899–1911.

McWhirter, S. M., Fitzgerald, K. A., Rosains, J., Rowe, D. C., Golenbock, D. T. and Maniatis, T. (2004). IFN-regulatory factor 3-dependent gene expression is defective in Tbk1-deficient mouse embryonic fibroblasts. *Proceedings of the National Academy of Sciences* **101**, 233–238.

Mehnert, M., Sommer, T. and Jarosch, E. (2010). ERAD ubiquitin ligases. *Bioessays* **32**, 905–913.

Mellacheruvu, D., Wright, Z., Couzens, A. L., Lambert, J.-P., St-Denis, N. A., Li, T., Miteva, Y. V., Hauri, S., Sardiu, M. E., Low, T. Y., et al. (2013). The CRAPome: a contaminant repository for affinity purification–mass spectrometry data. *Nat Meth* **10**, 730–736.

Merlie, J. P., Sebbane, R., Tzartos, S. and Lindstrom, J. (1982). Inhibition of glycosylation with tunicamycin blocks assembly of newly synthesized acetylcholine receptor subunits in muscle cells. *J. Biol. Chem.* **257**, 2694–2701.

Merner, N. D., Hodgkinson, K. A., Haywood, A. F. M., Connors, S., French, V. M., Drenckhahn, J.-D., Kupprion, C., Ramadanova, K., Thierfelder, L., McKenna, W., et al. (2008). Arrhythmogenic Right Ventricular Cardiomyopathy Type 5 Is a Fully Penetrant, Lethal Arrhythmic Disorder Caused by a Missense Mutation in the TMEM43 Gene. *The American Journal of Human Genetics* **82**, 809–821.

Mesmin, B., Bigay, J., Moser von Filseck, J., Lacas-Gervais, S., Drin, G. and Antonny, B. (2013). A Four-Step Cycle Driven by PI(4)P Hydrolysis Directs Sterol/PI(4)P Exchange by the ER-Golgi Tether OSBP. *Cell* **155**, 830–843.

Metzger, M. B., Metzger, M. B., Hristova, V. A., Hristova, V. A., Weissman, A. M. and Weissman, A. M. (2012). HECT and RING finger families of E3 ubiquitin ligases at a glance. *Journal of Cell Science* **125**, 531–537.

Metzger, M. B., Pruneda, J. N., Klevit, R. E. and Weissman, A. M. (2014). RING-type E3 ligases: Master manipulators of E2 ubiquitin-conjugating enzymes and ubiquitination. *Ubiquitin-Proteasome System* **1843**, 47–60.

Meyer, H., Bug, M. and Bremer, S. (2012). Emerging functions of the VCP/p97 AAA-ATPase in the ubiquitin system. *Nature Cell Biology* **14**, 117–123.

Mihalik, S. J., Steinberg, S. J., Pei, Z., Park, J., Kim, D. G., Heinzer, A. K., Dacremont, G., Wanders, R. J. A., Cuebas, D. A., Smith, K. D., et al. (2002). Participation of Two Members of the Very Long-chain Acyl-CoA Synthetase Family in Bile Acid Synthesis and Recycling. *J. Biol. Chem.* **277**, 24771–24779.

Miller, E. A., Beilharz, T. H., Malkus, P. N., Lee, M. C. S., Hamamoto, S., Orci, L. and Schekman, R. (2003). Multiple Cargo Binding Sites on the COPII Subunit Sec24p Ensure Capture of Diverse Membrane Proteins into Transport Vesicles. *Cell* **114**, 497–509.

Minogue, S. (2006). Phosphatidylinositol 4-kinase is required for endosomal trafficking and degradation of the EGF receptor. *Journal of Cell Science* **119**, 571–581.

Minogue, S., Chu, K. M. E., Westover, E. J., Covey, D. F., Hsuan, J. J. and Waugh, M. G. (2010). Relationship between phosphatidylinositol 4-phosphate synthesis, membrane organization, and lateral diffusion of PI4KIIα at the trans-Golgi network. *Journal of Lipid Research* **51**, 2314–2324.

Moessinger, C., Kuerschner, L., Spandl, J., Shevchenko, A. and Thiele, C. (2011). Human Lysophosphatidylcholine Acyltransferases 1 and 2 Are Located in Lipid Droplets Where They Catalyze the Formation of Phosphatidylcholine. *J. Biol. Chem.* **286**, 21330–21339.

Moon, Y.-A. and Horton, J. D. (2003). Identification of Two Mammalian Reductases Involved in the Two-carbon Fatty Acyl Elongation Cascade. *J. Biol. Chem.* **278**, 7335–7343.

Morgan, E. H. (1981). Transferrin, biochemistry, physiology and clinical significance. *Molecular Aspects of Medicine* **4**, 1–123.

Morito, D., Hirao, K., Oda, Y., Hosokawa, N., Tokunaga, F., Cyr, D. M., Tanaka, K., Iwai, K. and Nagata, K. (2008). Gp78 Cooperates with RMA1 in Endoplasmic Reticulum-associated Degradation of CFTRΔF508. *Molecular Biology of the Cell* **19**, 1328–1336.

Morreale, G., Conforti, L., Coadwell, J., Wilbrey, A. L. and Coleman, M. P. (2009). Evolutionary divergence of valosin-containing protein/cell division cycle protein 48 binding interactions among endoplasmic reticulum-associated degradation proteins. *FEBS Journal* **276**, 1208–1220.

Mueller, B., Lilley, B. N. and Ploegh, H. L. (2006). SEL1L, the homologue of yeast Hrd3p, is involved in protein dislocation from the mammalian ER. *J Cell Biol* **175**, 261–270.

Mueller, B., Mueller, B., Klemm, E. J., Klemm, E. J., Spooner, E., Spooner, E., Claessen, J. H., Claessen, J. H., Ploegh, H. L. and Ploegh, H. L. (2008). SEL1L nucleates a protein complex required for dislocation of misfolded glycoproteins. *Proceedings of the National Academy of Sciences* **105**, 12325–12330.

Muzny, D. M., Bainbridge, M. N., Chang, K., Dinh, H. H., Drummond, J. A., Fowler, G., Kovar, C. L., Lewis, L. R., Morgan, M. B., Newsham, I. F., et al. (2012). Comprehensive molecular characterization of human colon and rectal cancer. *Nature* **487**, 330–337.

Nadav, E., Shmueli, A., Barr, H., Gonen, H., Ciechanover, A. and Reiss, Y. (2003). A novel mammalian endoplasmic reticulum ubiquitin ligase homologous to the yeast Hrd1. *Biochemical and Biophysical Research Communications* **303**, 91–97.

Nahnsen, S., Bielow, C., Reinert, K. and Kohlbacher, O. (2013). Tools for Label-free Peptide Quantification. *Molecular & Cellular Proteomics* **12**, 549–556.

Nakamura, N. (2011). The Role of the Transmembrane RING Finger Proteins in Cellular and Organelle Function. *Membranes* **1**, 354–393.

Nakamura, N., Fukuda, H., Kato, A. and Hirose, S. (2005). MARCH-II Is a Syntaxin-6–binding Protein Involved in Endosomal Trafficking. *Molecular Biology of the Cell* **16**, 1696–1710.

Narayan, K., Waggoner, L., Pham, S. T., Hendricks, G. L., Waggoner, S. N., Conlon, J., Wang, J. P., Fitzgerald, K. A. and Kang, J. (2014). TRIM13 Is a Negative Regulator of MDA5-Mediated Type I Interferon Production. *Journal of Virology* **88**, 10748–10757.

Neal, S., Jaeger, P. A., Duttke, S. H., Benner, C., K Glass, C., Ideker, T. and Hampton, R. Y. (2018). The Dfm1 Derlin Is Required for ERAD Retrotranslocation of Integral Membrane Proteins. *Molecular Cell* **69**, 306–320.e4.

Neutzner, A., Neutzner, M., Benischke, A.-S., Ryu, S.-W., Frank, S., Youle, R. J. and Karbowski, M. (2011). A systematic search for ER membrane-associated RING finger proteins identifies Nixin/ZNRF4 as a regulator of calnexin stability and ER homeostasis. *J. Biol. Chem.*

Neve, E. P. A., Svensson, K., Fuxe, J. and Pettersson, R. F. (2003). VIPL, a VIP36-like membrane protein with a putative function in the export of glycoproteins from the endoplasmic reticulum☆. *Special Review Issue on Intracellular Trafficking* **288**, 70–83.

Nilsson, I. M. and Heijne, von, G. (1993). Determination of the distance between the oligosaccharyltransferase active site and the endoplasmic reticulum membrane. *J. Biol. Chem.* **268**, 5798–5801.

Ninagawa, S., Okada, T., Sumitomo, Y., Horimoto, S., Sugimoto, T., Ishikawa, T., Takeda, S., Yamamoto, T., Suzuki, T., Kamiya, Y., et al. (2015). Forcible destruction of severely misfolded mammalian glycoproteins by the non-glycoprotein ERAD pathway. *J Cell Biol* **211**, 775–784.

Ninagawa, S., Okada, T., Sumitomo, Y., Kamiya, Y., Kato, K., Horimoto, S., Ishikawa, T., Takeda, S., Sakuma, T., Yamamoto, T., et al. (2014). EDEM2 initiates mammalian glycoprotein ERAD by catalyzing the first mannose trimming step. *J Cell Biol* **206**, 347–356.

Novoa, I., Zeng, H., Harding, H. P. and Ron, D. (2001). Feedback Inhibition of the Unfolded Protein Response by GADD34-Mediated Dephosphorylation of eIF2α. *J Cell Biol* **153**, 1011–1022.

Nurieva, R. I., Zheng, S., Jin, W., Chung, Y., Zhang, Y., Martinez, G. J., Reynolds, J. M., Wang, S.-L., Lin, X., Sun, S.-C., et al. (2010). The E3 ubiquitin ligase GRAIL regulates T cell tolerance and regulatory T cell function by mediating T cell receptor-CD3 degradation. *Immunity* **32**, 670–680.

O'Connor, H. F., Lyon, N., Leung, J. W., Agarwal, P., Swaim, C. D., Miller, K. M. and Huibregtse, J. M. (2015). Ubiquitin-Activated Interaction Traps (UBAITs) identify E3 ligase binding partners. *EMBO rep* **16**, 1699–1712.

Oberdorf, J., Webster, J. M., Zhu, C. C., Luo, S. G. and Wojcikiewicz, R. J. (1999). Down-regulation of types I, II and III inositol 1,4,5-trisphosphate receptors is mediated by the ubiquitin/proteasome pathway. *Biochem. J.* **339 (Pt 2)**, 453–461.

Oddi, S., Fezza, F., Pasquariello, N., De Simone, C., Rapino, C., Dainese, E., Finazzi-Agrò, A. and Maccarrone, M. (2008). Evidence for the intracellular accumulation of anandamide in adiposomes. *Cellular and Molecular Life Sciences* **65**, 840.

Ohmura-Hoshino, M., Matsuki, Y., Aoki, M., Goto, E., Mito, M., Uematsu, M., Kakiuchi, T., Hotta, H. and Ishido, S. (2006). Inhibition of MHC class II expression and immune responses by c-MIR. *The Journal of Immunology* **177**, 341–354.

Okuda-Shimizu, Y. and Hendershot, L. M. (2007). Characterization of an ERAD pathway for non-glycosylated BiP substrates which requires Herp. *Molecular Cell* **28**, 544–554.

Olivari, S., Cali, T., Salo, K. E. H., Paganetti, P., Ruddock, L. W. and Molinari, M. (2006). EDEM1 regulates ER-associated degradation by accelerating de-mannosylation of folding-defective polypeptides and by inhibiting their covalent aggregation. *Biochemical and Biophysical Research Communications* **349**, 1278–1284.

Oliver, J. D. (1997). Interaction of the Thiol-Dependent Reductase ERp57 with Nascent Glycoproteins. *Science* **275**, 86–88.

Olzmann, J. A., Olzmann, J. A., Kopito, R. R., Kopito, R. R., Christianson, J. C. and Christianson, J. C. (2013a). The Mammalian Endoplasmic Reticulum-Associated Degradation System. *Cold Spring Harbor Perspectives in Biology* **5**, a013185–a013185.

Olzmann, J. A., Richter, C. M. and Kopito, R. R. (2013b). Spatial regulation of UBXD8 and p97/VCP controls ATGL-mediated lipid droplet turnover. *Proceedings of the National Academy of Sciences* **110**, 1345–1350.

Omura, T., Kaneko, M., Okuma, Y., Orba, Y., Nagashima, K., Takahashi, R., Fujitani, N., Matsumura, S., Hata, A., Kubota, K., et al. (2006). A ubiquitin ligase HRD1 promotes the degradation of Pael receptor, a substrate of Parkin. *J Neurochem* **99**, 1456–1469.

Palmieri, L., Pardo, B., Lasorsa, F. M., del Arco, A., Kobayashi, K., Iijima, M., Runswick, M. J., Walker, J. E., Saheki, T., Satrústegui, J., et al. (2001). Citrin and aralar1 are Ca2+-stimulated aspartate/glutamate transporters in mitochondria. *EMBO J.* **20**, 5060–5069.

Patil, A., Chan, C. T., Dyavaiah, M., Rooney, J. P., Dedon, P. C. and Begley, T. J. (2012). Translational infidelity-induced protein stress results from a deficiency in Trm9-catalyzed tRNA modifications. *RNA Biology* **9**, 990–1001.

Paton, A. W., Beddoe, T., Thorpe, C. M., Whisstock, J. C., Wilce, M. C. J., Rossjohn, J., Talbot, U. M. and Paton, J. C. (2006). AB5 subtilase cytotoxin inactivates the endoplasmic reticulum chaperone BiP. *Nature* **443**, 548–552.

Paton, C. M. and Ntambi, J. M. (2009). Biochemical and physiological function of stearoyl-CoA desaturase. *American Journal of Physiology - Endocrinology and Metabolism* **297**, E28–E37.

Pearce, M. M. P., Wang, Y., Kelley, G. G. and Wojcikiewicz, R. J. H. (2007). SPFH2 Mediates the Endoplasmic Reticulum-associated Degradation of Inositol 1,4,5-Trisphosphate Receptors and Other Substrates in Mammalian Cells. *J. Biol. Chem.* **282**, 20104–20115.

Pearce, M. M. P., Wormer, D. B., Wilkens, S. and Wojcikiewicz, R. J. H. (2009). An Endoplasmic Reticulum (ER) Membrane Complex Composed of SPFH1 and SPFH2 Mediates the ER-associated Degradation of Inositol 1,4,5-Trisphosphate Receptors. *J. Biol. Chem.* **284**, 10433–10445.

Peden, A. A., Oorschot, V., Hesser, B. A., Austin, C. D., Scheller, R. H. and Klumperman, J. (2004). Localization of the AP-3 adaptor complex defines a novel endosomal exit site for lysosomal membrane proteins. *J Cell Biol* **164**, 1065–1076.

PERRY, A. K., CHEN, G., ZHENG, D., TANG, H. and CHENG, G. (2005). The host type I interferon response to viral and bacterial infections. *Cell Res* **15**, 407–422.

Peterson, J. R., Ora, A., Van, P. N. and Helenius, A. (1995). Transient, lectin-like association of calreticulin with folding intermediates of cellular and viral glycoproteins. *Molecular Biology of the Cell* **6**, 1173–1184.

Petrova, K., Oyadomari, S., Hendershot, L. M. and Ron, D. (2008). Regulated association of misfolded endoplasmic reticulum lumenal proteins with P58/DNAJc3. *The EMBO Journal* **27**, 2862–2872.

Phillips, M. J. and Voeltz, G. K. (2015). Structure and function of ER membrane contact sites with other organelles. *Nat Rev Mol Cell Biol* **17**, 69–82.

Piper, R. C., Dikic, I. and Lukacs, G. L. (2014). Ubiquitin-Dependent Sorting in Endocytosis. *Cold Spring Harbor Perspectives in Biology* **6**.

Plechanovová, A., Jaffray, E. G., McMahon, S. A., Johnson, K. A., Navrátilová, I., Naismith, J. H. and Hay, R. T. (2011). Mechanism of ubiquitylation by dimeric RING ligase RNF4. *Nat Struct Mol Biol* **18**, 1052–1059.

Plemper, R. K., Böhmler, S., Bordallo, J., Sommer, T. and Wolf, D. H. (1997). Mutant analysis links the translocon and BiP to retrograde protein transport for ER degradation. *Nature* **388**, 891–895.

Prabakaran, T., Bodda, C., Krapp, C., Zhang, B. C., Christensen, M. H., Sun, C., Reinert, L., Cai, Y., Jensen, S. B., Skouboe, M. K., et al. (2018). Attenuation of cGAS‐STING signaling is mediated by a p62/SQSTM1‐dependent autophagy pathway activated by TBK1. *EMBO J.* **37**, e97858.

Prabhu, A. V., Luu, W., Sharpe, L. J. and Brown, A. J. (2016). Cholesterol-mediated Degradation of 7-Dehydrocholesterol Reductase Switches the Balance from Cholesterol to Vitamin D Synthesis. *J. Biol. Chem.* **291**, 8363–8373.

Puppo, F., Thomé, V., Lhoumeau, A. C., Cibois, M., Gangar, A., Lembo, F., Belotti, E., Marchetto, S., Lécine, P., Prébet, T., et al. (2010). Protein tyrosine kinase 7 has a conserved role in Wnt/β-catenin canonical signalling. *EMBO rep* **12**, 43–49.

Qin, Y., Zhou, M.-T., Hu, M.-M., Hu, Y.-H., Zhang, J., Guo, L., Zhong, B. and Shu, H.-B. (2014). RNF26 Temporally Regulates Virus-Triggered Type I Interferon Induction by Two Distinct Mechanisms. *PLOS Pathogens* **10**, e1004358.

Quintana, A., Molinero, A., Borup, R., Nielsen, F. C., Campbell, I. L., Penkowa, M. and Hidalgo, J. (2008). Effect of astrocyte-targeted production of IL-6 on traumatic brain injury and its impact on the cortical transcriptome. *Devel Neurobio* **68**, 195–208.

Raffaello, A., Mammucari, C., Gherardi, G. and Rizzuto, R. (2016). Calcium at the Center of Cell Signaling: Interplay between Endoplasmic Reticulum, Mitochondria, and Lysosomes. *Trends in Biochemical Sciences* **41**, 1035–1049.

Raman, M., Sergeev, M., Garnaas, M., Lydeard, J. R., Huttlin, E. L., Goessling, W., Shah, J. V. and Harper, J. W. (2015). Systematic proteomics of the VCP–UBXD adaptor network identifies a role for UBXN10 in regulating ciliogenesis. *Nature Cell Biology* **17**, 1356–1369.

Randow, F. and Seed, B. (2001). Endoplasmic reticulum chaperone gp96 is required for innate immunity but not cell viability. *Nature Cell Biology* **3**, 891–896.

Rao, R. V. and Bredesen, D. E. (2004). Misfolded proteins, endoplasmic reticulum stress and neurodegeneration. *Current Opinion in Cell Biology* **16**, 653–662.

Rawson, R. B. (2003). The SREBP pathway — insights from insigs and insects. *Nat Rev Mol Cell Biol* **4**, 631–640.

Raychaudhuri, S. and Espenshade, P. J. (2015). Endoplasmic Reticulum Exit of Golgi-resident Defective for SREBP Cleavage (Dsc) E3 Ligase Complex Requires Its Activity. *J. Biol. Chem.* **290**, 14430–14440.

Riemer, J., Appenzeller-Herzog, C., Johansson, L., Bodenmiller, B., Hartmann-Petersen, R. and Ellgaard, L. (2009). A luminal flavoprotein in endoplasmic reticulum-associated degradation. *Proceedings of the National Academy of Sciences* **106**, 14831–14836.

Riemer, J., Hansen, H. G., Appenzeller-Herzog, C., Johansson, L. and Ellgaard, L. (2011). Identification of the PDI-Family Member ERp90 as an Interaction Partner of ERFAD. *PLoS ONE* **6**, e17037.

Ritchie, M. E., Phipson, B., Wu, D., Hu, Y., Law, C. W., Shi, W. and Smyth, G. K. (2015). limma powers differential expression analyses for RNA-sequencing and microarray studies. *Nucleic Acids Research* **43**, e47–e47.

Rong, J., Chen, L., Toth, J. I., Tcherpakov, M., Petroski, M. D. and Reed, J. C. (2011). Bifunctional Apoptosis Regulator (BAR), an Endoplasmic Reticulum (ER)-associated E3 Ubiquitin Ligase, Modulates BI-1 Protein Stability and Function in ER Stress. *J. Biol. Chem.* **286**, 1453–1463.

Roth, W., Kermer, P., Krajewska, M., Welsh, K., Davis, S., Krajewski, S. and Reed, J. C. (2003). Bifunctional apoptosis inhibitor (BAR) protects neurons from diverse cell death pathways. *Cell Death Differ* **10**, 1178–1187.

Rubio, C., Pincus, D., Korennykh, A., Schuck, S., El-Samad, H. and Walter, P. (2011). Homeostatic adaptation to endoplasmic reticulum stress depends on Ire1 kinase activity. *J Cell Biol* **193**, 171–184.

Ruggiano, A., Foresti, O. and Carvalho, P. (2014). ER-associated degradation: Protein quality control and beyond. *J Cell Biol* **204**, 869–879.

Ruiz-Canada, C., Kelleher, D. J. and Gilmore, R. (2009). Cotranslational and Posttranslational N-Glycosylation of Polypeptides by Distinct Mammalian OST Isoforms. *Cell* **136**, 272–283.

Rusiñol, A. E., Cui, Z., Chen, M. H. and Vance, J. E. (1994). A unique mitochondria-associated membrane fraction from rat liver has a high capacity for lipid synthesis and contains pre-Golgi secretory proteins including nascent lipoproteins. *J. Biol. Chem.* **269**, 27494–27502.

Saitoh, T., Fujita, N., Hayashi, T., Takahara, K., Satoh, T., Lee, H., Matsunaga, K., Kageyama, S., Omori, H., Noda, T., et al. (2009). Atg9a controls dsDNA-driven dynamic translocation of STING and the innate immune response. *Proceedings of the National Academy of Sciences* **106**, 20842–20846.

Sakabe, I., Hu, R., Jin, L., Clarke, R. and Kasid, U. N. (2015). TMEM33: a new stress-inducible endoplasmic reticulum transmembrane protein and modulator of the unfolded protein response signaling. *Breast Cancer Research and Treatment* **153**, 285–297.

Sato, B. K., Schulz, D., Do, P. H. and Hampton, R. Y. (2009). Misfolded Membrane Proteins Are Specifically Recognized by the Transmembrane Domain of the Hrd1p Ubiquitin Ligase. *Molecular Cell* **34**, 212–222.

Sato, T., Sako, Y., Sho, M., Momohara, M., Suico, M. A., Shuto, T., Nishitoh, H., Okiyoneda, T., Kokame, K., Kaneko, M., et al. (2012). STT3B-Dependent Posttranslational N-Glycosylation as a Surveillance System for Secretory Protein. *Molecular Cell* **47**, 99–110.

Sauer, J.-D., Sotelo-Troha, K., Moltke, von, J., Monroe, K. M., Rae, C. S., Brubaker, S. W., Hyodo, M., Hayakawa, Y., Woodward, J. J., Portnoy, D. A., et al. (2011). The N-Ethyl-N-Nitrosourea-Induced Goldenticket Mouse Mutant Reveals an Essential Function of Sting in the In Vivo Interferon Response to Listeria monocytogenes and Cyclic Dinucleotides. *Infection and Immunity* **79**, 688–694.

Schallus, T., Jaeckh, C., Fehér, K., Palma, A. S., Liu, Y., Simpson, J. C., Mackeen, M., Stier, G., Gibson, T. J., Feizi, T., et al. (2008). Malectin: A Novel Carbohydrate-binding Protein of the Endoplasmic Reticulum and a Candidate Player in the Early Steps of Protein N-Glycosylation. *Molecular Biology of the Cell* **19**, 3404–3414.

Schoebel, S., Mi, W., Stein, A., Ovchinnikov, S., Pavlovicz, R., DiMaio, F., Baker, D., Chambers, M. G., Su, H., Li, D., et al. (2017). Cryo-EM structure of the protein-conducting ERAD channel Hrd1 in complex with Hrd3. *Nature* **548**, 352–355.

Schoggins, J. W. and Rice, C. M. (2011). Interferon-stimulated genes and their antiviral effector functions. *Current opinion in virology* **1**, 519–525.

Schröder, M. and Kaufman, R. J. (2005). THE MAMMALIAN UNFOLDED PROTEIN RESPONSE. *Annu. Rev. Biochem.* **74**, 739–789.

Schulz, J., Avci, D., Queisser, M. A., Gutschmidt, A., Dreher, L.-S., Fenech, E. J., Volkmar, N., Hayashi, Y., Hoppe, T. and Christianson, J. C. (2017). Conserved cytoplasmic domains promote Hrd1 ubiquitin ligase complex formation for ER-associated degradation (ERAD). *Journal of Cell Science* **130**, 3322–3335.

Schulze, A., Standera, S., Buerger, E., Kikkert, M., van Voorden, S., Wiertz, E., Koning, F., Kloetzel, P.-M. and Seeger, M. (2005). The Ubiquitin-domain Protein HERP forms a Complex with Components of the Endoplasmic Reticulum Associated Degradation Pathway. *Journal of Molecular Biology* **354**, 1021–1027.

Schwarz, D. S. and Blower, M. D. (2016). The endoplasmic reticulum: structure, function and response to cellular signaling. *Cellular and Molecular Life Sciences* **73**, 79–94.

Schweizer, A. (1988). Identification, by a monoclonal antibody, of a 53-kD protein associated with a tubulo-vesicular compartment at the cis-side of the Golgi apparatus. *J Cell Biol* **107**, 1643–1653.

Sever, N., Song, B.-L., Yabe, D., Goldstein, J. L., Brown, M. S. and DeBose-Boyd, R. A. (2003). Insig-dependent Ubiquitination and Degradation of Mammalian 3-Hydroxy-3-methylglutaryl-CoA Reductase Stimulated by Sterols and Geranylgeraniol. *J. Biol. Chem.* **278**, 52479–52490.

Shen, J., Chen, X., Hendershot, L. and Prywes, R. (2002). ER Stress Regulation of ATF6 Localization by Dissociation of BiP/GRP78 Binding and Unmasking of Golgi Localization Signals. *Developmental Cell* **3**, 99–111.

Shen, Y. and Hendershot, L. M. (2005). ERdj3, a Stress-inducible Endoplasmic Reticulum DnaJ Homologue, Serves as a CoFactor for BiP's Interactions with Unfolded Substrates. *Molecular Biology of the Cell* **16**, 40–50.

Shen, Y., Ballar, P. and Fang, S. (2006). Ubiquitin ligase gp78 increases solubility and facilitates degradation of the Z variant of α-1-antitrypsin. *Biochemical and Biophysical Research Communications* **349**, 1285–1293.

Shi, Y., Chen, X., Elsasser, S., Stocks, B. B., Tian, G., Lee, B.-H., Shi, Y., Zhang, N., de Poot, S. A. H., Tuebing, F., et al. (2016). Rpn1 provides adjacent receptor sites for substrate binding and deubiquitination by the proteasome. *Science* **351**, aad9421–aad9421.

Shibata, Y., Voeltz, G. K. and Rapoport, T. A. (2006). Rough Sheets and Smooth Tubules. *Cell* **126**, 435–439.

Shimoi, W., Ezawa, I., Nakamoto, K., Uesaki, S., Gabreski, G., Aridor, M., Yamamoto, A., Nagahama, M., Tagaya, M. and Tani, K. (2005). p125 Is Localized in Endoplasmic Reticulum Exit Sites and Involved in Their Organization. *J. Biol. Chem.* **280**, 10141–10148.

Shoulders, M. D., Ryno, L. M., Genereux, J. C., Moresco, J. J., Tu, P. G., Wu, C., Yates, J. R., III, Su, A. I., Kelly, J. W. and Wiseman, R. L. (2013). Stress-Independent Activation of XBP1s and/or ATF6 Reveals Three Functionally Diverse ER Proteostasis Environments. *Cell Reports* **3**, 1279–1292.

Silverman, G. A., Pak, S. C. and Perlmutter, D. H. (2013). Disorders of Protein Misfolding: Alpha-1-antitrypsin Deficiency as Prototype. *The Journal of pediatrics* **163**, 320–326.

Sokołowska, I., Piłka, E. S., Sandvig, K., Węgrzyn, G. and Słomińska-Wojewódzka, M. (2015). Hydrophobicity of protein determinants influences the recognition of substrates by EDEM1 and EDEM2 in human cells. *BMC Cell Biology* **16**, 1.

Song, B.-L., Sever, N. and DeBose-Boyd, R. A. (2005). Gp78, a Membrane-Anchored Ubiquitin Ligase, Associates with Insig-1 and Couples Sterol-Regulated Ubiquitination to Degradation of HMG CoA Reductase. *Molecular Cell* **19**, 829–840.

Sousa, M. and Parodi, A. J. (1995). The molecular basis for the recognition of misfolded glycoproteins by the UDP-Glc:glycoprotein glucosyltransferase. *The EMBO Journal* **14**, 4196–4203.

Sowa, M. E., Bennett, E. J., Gygi, S. P. and Harper, J. W. (2009). Defining the Human Deubiquitinating Enzyme Interaction Landscape. *Cell* **138**, 389–403.

Stagg, H. R., Thomas, M., van den Boomen, D., Wiertz, E. J., Drabkin, H. A., Gemmill, R. M. and Lehner, P. J. (2009). The TRC8 E3 ligase ubiquitinates MHC class I molecules before dislocation from the ER. *J Cell Biol* **186**, 685–692.

Stark, C. (2006). BioGRID: a general repository for interaction datasets. *Nucleic Acids Research* **34**, D535–D539.

Steffen, J., Seeger, M., Koch, A. and Krüger, E. (2010). Proteasomal Degradation Is Transcriptionally Controlled by TCF11 via an ERAD-Dependent Feedback Loop. *Molecular Cell* **40**, 147–158.

Stone, S. J. and Vance, J. E. (2000). Phosphatidylserine Synthase-1 and -2 Are Localized to Mitochondria-associated Membranes. *J. Biol. Chem.* **275**, 34534–34540.

Strating, J. R. P. M. and Martens, G. J. M. (2012). The p24 family and selective transport processes at the ER-Golgi interface. *Biology of the Cell* **101**, 495–509.

Sun, F., Zhang, R., Gong, X., Geng, X., Drain, P. F. and Frizzell, R. A. (2006). Derlin-1 Promotes the Efficient Degradation of the Cystic Fibrosis Transmembrane Conductance Regulator (CFTR) and CFTR Folding Mutants. *J. Biol. Chem.* **281**, 36856–36863.

Sun, L., Wu, J., Du, F., Chen, X. and Chen, Z. J. (2013). Cyclic GMP-AMP Synthase Is a Cytosolic DNA Sensor That Activates the Type I Interferon Pathway. *Science* **339**, 786–791.

Sun, S., Shi, G., Sha, H., Ji, Y., Han, X., Shu, X., Ma, H., Inoue, T., Gao, B., Kim, H., et al. (2015). IRE1α is an endogenous substrate of endoplasmic-reticulum-associated degradation. *Nature Cell Biology* **17**, 1546–1555.

Sun, W., Li, Y., Chen, L., Chen, H., You, F., Zhou, X., Zhou, Y., Zhai, Z., Chen, D. and Jiang, Z. (2009). ERIS, an endoplasmic reticulum IFN stimulator, activates innate immune signaling through dimerization. *Proceedings of the National Academy of Sciences* **106**, 8653–8658.

Suzuki, M., Otsuka, T., Ohsaki, Y., Cheng, J., Taniguchi, T., Hashimoto, H., Taniguchi, H. and Fujimoto, T. (2012). Derlin-1 and UBXD8 are engaged in dislocation and degradation of lipidated ApoB-100 at lipid droplets. *Molecular Biology of the Cell* **23**, 800–810.

Swanson, R., Locher, M. and Hochstrasser, M. (2001). A conserved ubiquitin ligase of the nuclear envelope/endoplasmic reticulum that functions in both ER-associated and Matα2 repressor degradation. *Genes & Development* **15**, 2660–2674.

Swatek, K. N. and Komander, D. (2016). Ubiquitin modifications. *Cell Res* **26**, 399–422.

Szabadkai, G., Bianchi, K., Várnai, P., De Stefani, D., Wieckowski, M. R., Cavagna, D., Nagy, A. I., Balla, T. and Rizzuto, R. (2006). Chaperone-mediated coupling of endoplasmic reticulum and mitochondrial Ca 2+channels. *J Cell Biol* **175**, 901–911.

Takida, S., Maeda, Y. and Kinoshita, T. (2008). Mammalian GPI-anchored proteins require p24 proteins for their efficient transport from the ER to the plasma membrane. *Biochem. J.* **409**, 555–562.

Tanaka, Y. and Chen, Z. J. (2012). STING Specifies IRF3 Phosphorylation by TBK1 in the Cytosolic DNA Signaling Pathway. *Science Signaling* **5**, ra20–ra20.

Tang, F., Bin Wang, Li, N., Wu, Y., Jia, J., Suo, T., Chen, Q., Liu, Y.-J. and Tang, J. (2011). RNF185, a Novel Mitochondrial Ubiquitin E3 Ligase, Regulates Autophagy through Interaction with BNIP1. **6**, e24367.

Tang, H.-Y., Huang, C.-H., Zhuang, Y.-H., Christianson, J. C. and Chen, X. (2014). EDEM2 and OS-9 Are Required for ER-Associated Degradation of Non-Glycosylated Sonic Hedgehog. *PLoS ONE* **9**, e92164.

Taylor, K. M., Morgan, H. E., Johnson, A. and Nicholson, R. I. (2004). Structure-function analysis of a novel member of the LIV-1 subfamily of zinc transporters, ZIP14. *FEBS Letters* **579**, 427–432.

Tcherpakov, M., Delaunay, A., Toth, J., Kadoya, T., Petroski, M. D. and Ronai, Z. A. (2009). Regulation of Endoplasmic Reticulum-associated Degradation by RNF5-dependent Ubiquitination of JNK-associated Membrane Protein (JAMP). *J. Biol. Chem.* **284**, 12099–12109.

Thrower, J. S. (2000). Recognition of the polyubiquitin proteolytic signal. *The EMBO Journal* **19**, 94–102.

Tirosh, B., Furman, M. H., Tortorella, D. and Ploegh, H. L. (2003). Protein Unfolding Is Not a Prerequisite for Endoplasmic Reticulum-to-Cytosol Dislocation. *J. Biol. Chem.* **278**, 6664–6672.

Todd-Corlett, A., Jones, E., Seghers, C. and Gething, M.-J. (2007). Lobe IB of the ATPase Domain of Kar2p/BiP Interacts with Ire1p to Negatively Regulate the Unfolded Protein Response in Saccharomyces cerevisiae. *Journal of Molecular Biology* **367**, 770–787.

Travers, K. J., Patil, C. K., Wodicka, L., Lockhart, D. J., Weissman, J. S. and Walter, P. (2000). Functional and Genomic Analyses Reveal an Essential Coordination between the Unfolded Protein Response and ER-Associated Degradation. *Cell* **101**, 249–258.

Trudgian, D. C., Ridlova, G., Fischer, R., Mackeen, M. M., Ternette, N., Acuto, O., Kessler, B. M. and Thomas, B. (2011). Comparative evaluation of label-free SINQ normalized spectral index quantitation in the central proteomics facilities pipeline. *Proteomics* **11**, 2790–2797.

Tsai, Y. C., Leichner, G. S., Pearce, M. M. P., Wilson, G. L., Wojcikiewicz, R. J. H., Roitelman, J. and Weissman, A. M. (2012). Differential regulation of HMG-CoA reductase and Insig-1 by enzymes of the ubiquitin-proteasome system. *MBoC* **23**, 4484–4494.

Tyedmers, J., Lerner, M., Bies, C., Dudek, J., Skowronek, M. H., Haas, I. G., Heim, N., Nastainczyk, W., Volkmer, J. and Zimmermann, R. (2000). Homologs of the yeast Sec complex subunits Sec62p and Sec63p are abundant proteins in dog pancreas microsomes. *Proceedings of the National Academy of Sciences* **97**, 7214–7219.

Tyler, R. E., Pearce, M. M. P., Shaler, T. A., Olzmann, J. A., Greenblatt, E. J. and Kopito, R. R. (2012). Unassembled CD147 is an endogenous endoplasmic reticulum–associated degradation substrate. *Molecular Biology of the Cell* **23**, 4668–4678.

Urano, F., Wang, X., Bertolotti, A., Zhang, Y., Chung, P., Harding, H. P. and Ron, D. (2000). Coupling of stress in the ER to activation of JNK protein kinases by transmembrane protein kinase IRE1. *Science* **287**, 664–666.

Urra, H., Dufey, E., Avril, T., Chevet, E. and Hetz, C. (2016). Endoplasmic Reticulum Stress and the Hallmarks of Cancer. *Trends in Cancer* **2**, 252–262.

Ushioda, R., Hoseki, J., Araki, K., Jansen, G., Thomas, D. Y. and Nagata, K. (2008). ERdj5 Is Required as a Disulfide Reductase for Degradation of Misfolded Proteins in the ER. *Science* **321**, 569–572.

van de Kooij, B., Verbrugge, I., de Vries, E., Gijsen, M., Montserrat, V., Maas, C., Neefjes, J. and Borst, J. (2013). Ubiquitination by the Membrane-associated RING-CH-8 (MARCH-8) Ligase Controls Steady-state Cell Surface Expression of Tumor Necrosis Factor-related Apoptosis Inducing Ligand (TRAIL) Receptor 1. *J. Biol. Chem.* **288**, 6617–6628.

van de Weijer, M. L., Bassik, M. C., Luteijn, R. D., Voorburg, C. M., Lohuis, M. A. M., Kremmer, E., Hoeben, R. C., LeProust, E. M., Chen, S., Hoelen, H., et al. (2014). A high-coverage shRNA screen identifies TMEM129 as an E3 ligase involved in ER-associated protein degradation. *Nat Comms* **5**, 3007.

van den Boomen, D. J. H., Timms, R. T., Grice, G. L., Stagg, H. R., Skodt, K., Dougan, G., Nathan, J. A. and Lehner, P. J. (2014). TMEM129 is a Derlin-1 associated ERAD E3 ligase essential for virus-induced degradation of MHC-I. *Proceedings of the National Academy of Sciences* **111**, 11425–11430.

Vandecaetsbeek, I., Vangheluwe, P., Raeymaekers, L., Wuytack, F. and Vanoevelen, J. (2011). The Ca(2+) Pumps of the Endoplasmic Reticulum and Golgi Apparatus. *Cold Spring Harbor Perspectives in Biology* **3**, a004184.

Vattem, K. M. and Wek, R. C. (2004). Reinitiation involving upstream ORFs regulates ATF4 mRNA translation in mammalian cells. *Proceedings of the National Academy of Sciences* **101**, 11269–11274.

Václavíková, R., Hughes, D. J. and Souček, P. (2015). Microsomal epoxide hydrolase 1 (EPHX1): Gene, structure, function, and role in human disease. *Gene* **571**, 1–8.

Vig, M., Beck, A., Billingsley, J. M., Lis, A., Parvez, S., Peinelt, C., Koomoa, D. L., Soboloff, J., Gill, D. L., Fleig, A., et al. (2006). CRACM1 Multimers Form the Ion-Selective Pore of the CRAC Channel. *Current Biology* **16**, 2073–2079.

Voloshanenko, O., Erdmann, G., Dubash, T. D., Augustin, I., Metzig, M., Moffa, G., Hundsrucker, C., Kerr, G., Sandmann, T., Anchang, B., et al. (2013). Wnt secretion is required to maintain high levels of Wnt activity in colon cancer cells. *Nat Comms* **4**, 1130.

Walter, P. and Blobel, G. (1980). Purification of a membrane-associated protein complex required for protein translocation across the endoplasmic reticulum. *Proc Natl Acad Sci USA* **77**, 7112.

Walter, P. and Ron, D. (2011). The Unfolded Protein Response: From Stress Pathway to Homeostatic Regulation. *Science* **334**, 1081–1086.

Wang, F., Olson, E. M. and Shyng, S.-L. (2012). Role of Derlin-1 Protein in Proteostasis Regulation of ATP-sensitive Potassium Channels. *J. Biol. Chem.* **287**, 10482–10493.

Wang, H., Li, Q., Shen, Y., Sun, A., Zhu, X., Fang, S. and Shen, Y. (2011). The ubiquitin ligase Hrd1 promotes degradation of the Z variant alpha 1-antitrypsin and increases its solubility. *Molecular and Cellular Biochemistry* **346**, 137–145.

Wang, M. and Kaufman, R. J. (2016). Protein misfolding in the endoplasmic reticulum as a conduit to human disease. *Nature* **529**, 326–335.

Wang, Q., Chen, Q., Zhu, L., Chen, M., Xu, W., Panday, S., Wang, Z., Li, A., Røe, O. D., Chen, R., et al. (2017a). JWA regulates TRAIL-induced apoptosis via MARCH8-mediated DR4 ubiquitination in cisplatin-resistant gastric cancer cells. *Oncogenesis* **6**, e353 EP –.

Wang, Q., Huang, L., Hong, Z., Lv, Z., Mao, Z., Tang, Y., Kong, X., Li, S., Cui, Y., Liu, H., et al. (2017b). The E3 ubiquitin ligase RNF185 facilitates the cGAS-mediated innate immune response. *PLOS Pathogens* **13**, e1006264.

Wang, Q., Liu, X., Cui, Y., Tang, Y., Chen, W., Li, S., Yu, H., Pan, Y. and Wang, C. (2014). The E3 Ubiquitin Ligase AMFR and INSIG1 Bridge the Activation of TBK1 Kinase by Modifying the Adaptor STING. *Immunity* **41**, 919–933.

Wang, Q.-C., Zheng, Q., Tan, H., Zhang, B., Li, X., Yang, Y., Yu, J., Liu, Y., Chai, H., Wang, X., et al. (2016). TMCO1 Is an ER Ca 2+ Load-Activated Ca 2+ Channel. *Cell* **165**, 1454–1466.

Webster, J. M., Tiwari, S., Weissman, A. M. and Wojcikiewicz, R. J. H. (2003). Inositol 1,4,5-Trisphosphate Receptor Ubiquitination Is Mediated by Mammalian Ubc7, a Component of the Endoplasmic Reticulum-associated Degradation Pathway, and Is Inhibited by Chelation of Intracellular Zn2. *J. Biol. Chem.* **278**, 38238–38246.

Wiertz, E. J. H. J., Tortorella, D., Bogyo, M., Yu, J., Mothes, W., Jones, T. R., Rapoport, T. A. and Ploegh, H. L. (1996). Sec6l-mediated transfer of a membrane protein from the endoplasmic reticulum to the proteasome for destruction. *Nature* **384**, 432–438.

Wojcikiewicz, R. J. H. (2004). Regulated ubiquitination of proteins in GPCR-initiated signaling pathways. *Trends in Pharmacological Sciences* **25**, 35–41.

Wojcikiewicz, R. J. H., Xu, Q., Webster, J. M., Alzayady, K. and Gao, C. (2003). Ubiquitination and Proteasomal Degradation of Endogenous and Exogenous Inositol 1,4,5-Trisphosphate Receptors in αT3-1 Anterior Pituitary Cells. *J. Biol. Chem.* **278**, 940–947.

Wright, F. A., Lu, J. P., Sliter, D. A., Dupré, N., Rouleau, G. A. and Wojcikiewicz, R. J. H. (2015). A Point Mutation in the Ubiquitin Ligase RNF170 That Causes Autosomal Dominant Sensory Ataxia Destabilizes the Protein and Impairs Inositol 1,4,5-Trisphosphate Receptor-mediated Ca(2+) Signaling. *The Journal of Biological Chemistry* **290**, 13948–13957.

Wu, J., Sun, L., Chen, X., Du, F., Shi, H., Chen, C. and Chen, Z. J. (2013). Cyclic GMP-AMP Is an Endogenous Second Messenger in Innate Immune Signaling by Cytosolic DNA. *Science* **339**, 826–830.

Xie, J., Marusich, M. F., Souda, P., Whitelegge, J. and Capaldi, R. A. (2007). The mitochondrial inner membrane protein Mitofilin exists as a complex with SAM50, metaxins 1 and 2, coiled-coil-helix coiled-coil-helix domain-containing protein 3 and 6 and DnaJC11. *FEBS Letters* **581**, 3545–3549.

Xu, P., Duong, D. M., Seyfried, N. T., Cheng, D., Xie, Y., Robert, J., Rush, J., Hochstrasser, M., Finley, D. and Peng, J. (2009). Quantitative Proteomics Reveals the Function of Unconventional Ubiquitin Chains in Proteasomal Degradation. *Cell* **137**, 133–145.

Yabe, D., Brown, M. S. and Goldstein, J. L. (2002). Insig-2, a second endoplasmic reticulum protein that binds SCAP and blocks export of sterol regulatory element-binding proteins. *Proceedings of the National Academy of Sciences* **99**, 12753–12758.

Yagishita, N., Ohneda, K., Amano, T., Yamasaki, S., Sugiura, A., Tsuchimochi, K., Shin, H., Kawahara, K.-I., Ohneda, O., Ohta, T., et al. (2005). Essential Role of Synoviolin in Embryogenesis. *J. Biol. Chem.* **280**, 7909–7916.

Yamaguchi, H. and Wang, H.-G. (2004). CHOP Is Involved in Endoplasmic Reticulum Stress-induced Apoptosis by Enhancing DR5 Expression in Human Carcinoma Cells. *J. Biol. Chem.* **279**, 45495–45502.

Yamamoto, Y.-H., Kimura, T., Momohara, S., Takeuchi, M., Tani, T., Kimata, Y., Kadokura, H. and Kohno, K. (2010). A Novel ER J-protein DNAJB12 Accelerates ER-associated Degradation of Membrane Proteins Including CFTR TI . *Cell Structure and Function* **35**, 107–116.

Yan, L., Liu, W., Zhang, H., Liu, C., Shang, Y., Ye, Y., Zhang, X. and Li, W. (2014). Ube2g2–gp78-mediated HERP polyubiquitylation is involved in ER stress recovery. *Journal of Cell Science* **127**, 1417–1427.

Yang, H., Zhong, X., Ballar, P., Luo, S., Shen, Y., Rubinsztein, D. C., Monteiro, M. J. and Fang, S. (2007). Ubiquitin ligase Hrd1 enhances the degradation and suppresses the toxicity of polyglutamine-expanded huntingtin. *Special Review Issue on Intracellular Trafficking* **313**, 538–550.

Yang, T., Espenshade, P. J., Wright, M. E., Yabe, D., Gong, Y., Aebersold, R., Goldstein, J. L. and Brown, M. S. (2002). Crucial Step in Cholesterol Homeostasis. *Cell* **110**, 489–500.

Yang, Z., Wang, C., Zhou, Q., An, J., Hildebrandt, E., Aleksandrov, L. A., Kappes, J. C., DeLucas, L. J., Riordan, J. R., Urbatsch, I. L., et al. (2014). Membrane protein stability can be compromised by detergent interactions with the extramembranous soluble domains. *Protein Science : A Publication of the Protein Society* **23**, 769–789.

Ye, Y., Meyer, H. H. and Rapoport, T. A. (2001). The AAA ATPase Cdc48/p97 and its partners transport proteins from the ER into the cytosol. *Nature* **414**, 652–656.

Ye, Y., Meyer, H. H. and Rapoport, T. A. (2003). Function of the p97–Ufd1–Npl4 complex in retrotranslocation from the ER to the cytosol. *J Cell Biol* **162**, 71–84.

Ye, Y., Shibata, Y., Kikkert, M., van Voorden, S., Wiertz, E. and Rapoport, T. A. (2005). Recruitment of the p97 ATPase and ubiquitin ligases to the site of retrotranslocation at the endoplasmic reticulum membrane. *Proceedings of the National Academy of Sciences* **102**, 14132–14138.

Ye, Y., Shibata, Y., Yun, C., Ron, D. and Rapoport, T. A. (2004). A membrane protein complex mediates retro-translocation from the ER lumen into the cytosol. *Nature* **429**, 841–847.

Ying, Z., Wang, H., Fan, H., Zhu, X., Zhou, J., Fei, E. and Wang, G. (2009). Gp78, an ER associated E3, promotes SOD1 and ataxin-3 degradation. *Human Molecular Genetics* **18**, 4268–4281.

Yoshida, H. (2007). ER stress and diseases. *FEBS Journal* **274**, 630–658.

Yoshida, H., Matsui, T., Yamamoto, A., Okada, T. and Mori, K. (2001). XBP1 mRNA Is Induced by ATF6 and Spliced by IRE1 in Response to ER Stress to Produce a Highly Active Transcription Factor. *Cell* **107**, 881–891.

Yoshimori, T., Yamamoto, A., Moriyama, Y., Futai, M. and Tashiro, Y. (1991). Bafilomycin A1, a specific inhibitor of vacuolar-type H(+)-ATPase, inhibits acidification and protein degradation in lysosomes of cultured cells. *J. Biol. Chem.* **266**, 17707–17712.

You, H., Ge, Y., Zhang, J., Cao, Y., Xing, J., Su, D., Huang, Y., Li, M., Qu, S., Sun, F., et al. (2017). Derlin-1 promotes ubiquitination and degradation of epithelial sodium channel (ENaC). *Journal of Cell Science* **269**, jcs.198242.

Younger, J. M., Chen, L., Ren, H.-Y., Rosser, M. F. N., Turnbull, E. L., Fan, C.-Y., Patterson, C. and Cyr, D. M. (2006). Sequential Quality-Control Checkpoints Triage Misfolded Cystic Fibrosis Transmembrane Conductance Regulator. *Cell* **126**, 571–582.

Zavacki, A. M., Arrojo E Drigo, R., Freitas, B. C. G., Chung, M., Harney, J. W., Egri, P., Wittmann, G., Fekete, C., Gereben, B. and Bianco, A. C. (2009). The E3 ubiquitin ligase TEB4 mediates degradation of type 2 iodothyronine deiodinase. *Molecular and Cellular Biology* **29**, 5339–5347.

Zehmer, J. K., Bartz, R., Bisel, B., Liu, P., Seemann, J. and Anderson, R. G. W. (2009). Targeting sequences of UBXD8 and AAM-B reveal that the ER has a direct role in the emergence and regression of lipid droplets. *Journal of Cell Science* **122**, 3694–3702.

Zeiler, M., Straube, W. L., Lundberg, E., Uhlén, M. and Mann, M. (2012). A Protein Epitope Signature Tag (PrEST) Library Allows SILAC-based Absolute Quantification and Multiplexed Determination of Protein Copy Numbers in Cell Lines. *Molecular & Cellular Proteomics* **11**.

Zelcer, N., Sharpe, L. J., Loregger, A., Kristiana, I., Cook, E. C. L., Phan, L., Stevenson, J. and Brown, A. J. (2014). The E3 ubiquitin ligase MARCH6 degrades squalene monooxygenase and affects 3-hydroxy-3-methyl-glutaryl coenzyme A reductase and the cholesterol synthesis pathway. *Molecular and Cellular Biology* **34**, 1262–1270.

Zhang, D. and Oliferenko, S. (2014). Tts1, the fission yeast homologue of the TMEM33 family, functions in NE remodeling during mitosis. *Molecular Biology of the Cell* **25**, 2970–2983.

Zhang, L., Rajbhandari, P., Priest, C., Sandhu, J., Wu, X., Temel, R., Castrillo, A., de Aguiar Vallim, T. Q., Sallam, T. and Tontonoz, P. (2017). Inhibition of cholesterol biosynthesis through RNF145-dependent ubiquitination of SCAP. *eLife* **6**, e28766.

Zhang, Q., Meng, Y., Zhang, L., Chen, J. and Zhu, D. (2008). RNF13: a novel RING-type ubiquitin ligase over-expressed in pancreatic cancer. *Cell Res* **19**, 348–357.

Zhang, Y., Higashide, W., Dai, S., Sherman, D. M. and Zhou, D. (2005). Recognition and Ubiquitination of Salmonella Type III Effector SopA by a Ubiquitin E3 Ligase, HsRMA1. *J. Biol. Chem.* **280**, 38682–38688.

Zhong, B., Yang, Y., Li, S., Wang, Y.-Y., Li, Y., Diao, F., Lei, C., He, X., Zhang, L., Tien, P., et al. (2008). The Adaptor Protein MITA Links Virus-Sensing Receptors to IRF3 Transcription Factor Activation. *Immunity* **29**, 538–550.

Zhong, B., Zhang, L., Lei, C., Li, Y., Mao, A.-P., Yang, Y., Wang, Y.-Y., Zhang, X.-L. and Shu, H.-B. (2009). The Ubiquitin Ligase RNF5 Regulates Antiviral Responses by Mediating Degradation of the Adaptor Protein MITA. *Immunity* **30**, 397–407.

Zhou, Y., Shang, H., Zhang, C., Liu, Y., Zhao, Y., Shuang, F., Zhong, H., Tang, J. and Hou, S. (2014). The E3 ligase RNF185 negatively regulates osteogenic differentiation by targeting Dvl2 for degradation. *Biochemical and Biophysical Research Communications* **447**, 431–436.

Zordan, R. E., Beliveau, B. J., Trow, J. A., Craig, N. L. and Cormack, B. P. (2015). Avoiding the Ends: Internal Epitope Tagging of Proteins Using Transposon Tn7. *Genetics* **200**, 47–58.